

Investigate the Effect of Stiffness Degradation near Intermediate Support on Load Distribution of Continuous Prestressed Concrete Girder

Vincent Ponson 4270827

Student report Civil Engineering | Structural Engineering  
Delft University of Technology



## Abstract

---

This thesis focuses on the structural behaviour of prestressed concrete girder beams with a particular emphasis on stiffness degradation near intermediate supports due to cracking, in inverted-T girders. Despite advancements in bridge engineering, there is still a lack of understanding regarding crack development along the length of the beam and its impact on stiffness, including the redistribution of forces. The thesis aims to analyse the implications of these structural changes by utilizing methodologies such as the moment-curvature diagram and Finite Element Method (FEM) models. The unique properties of the moment-curvature diagram are leveraged to accurately reproduce changes in stiffness caused by cracking. Two case studies are conducted to achieve these objectives. Case Study 1 involves comparing actual tests with FEM models, it revealed a disparity between the FEM models and actual test results. Particularly in load-deformation behaviour and stiffness variation due to crack development, this case study highlights the necessity to accurately calculate the moment regions, especially the cracking moment, which defines the moment-curvature diagram. While Case Study 2 evaluates the performance of FEM models to realistic loading conditions, including traffic loads, with some models surpassing expected performance while others failed to withstand traffic loads. Overall, the study underscores the importance of a proper methodology to accurately translate the material parameters and complex behaviours into a FEM environment.

## Table of Contents

---

Introduction .....	1
Chapter 1 – Analysis of the inverted T-beam girder system .....	3
Chapter 1.1 – Test Setup .....	3
Chapter 1.2 – Test Beam, S10H1A.....	4
Chapter 1.3 – Material properties of the Test Beam.....	5
Chapter 2 – Establishing of the Moment-curvature Diagram .....	7
Chapter 2.1 – Moment-curvature Relationship .....	7
Chapter 2.2 – Python Code .....	7
Chapter 2.3 – Moment-Curvature Diagrams.....	10
Chapter 3 – Case Study 1 .....	14
Chapter 3.1 – Case Study, Description .....	14
Chapter 3.2 – FEM Models.....	14
Chapter 3.3 – FEM Analysis.....	17
Chapter 4 – Case Study 2 .....	29
Chapter 4.1 – Case Study, Description .....	29
Chapter 4.2 – FEM Models.....	29
Chapter 4.3 – FEM Analysis.....	31
Discussion.....	45
Conclusion.....	49
References.....	51
Appendix .....	I
Appendix I – Additional information Chapter 1 .....	I
Appendix II – Additional information Chapter 2 .....	VII
Appendix III – Additional information Chapter 3 .....	XIV
Appendix IV – Additional information Chapter 4.....	XLI

## Introduction

---

Currently, Rijkswaterstaat is conducting multiple concurrent research projects aimed at re-evaluating the strength of inverted-T girders with the goal of better understanding the behaviour of the girders and eventually adjusting the National guidelines accordingly. In addition to these projects, Rijkswaterstaat is also focused on developing a suitable structural analysis procedure to enable a reassessment of existing inverted-T girder bridges with the aim of identifying which bridges need further examination.

In the past, these girders were mostly used as simply supported beams, meaning that they were supported only at their two ends. With advancements in bridge engineering, continuous prestressed girders have become a more popular option for longer spans. In a continuous girder, the deck is supported by multiple supports along the span of the bridge. Inverted-T girders have also undergone similar changes in their design, with the development of the continuous deck becoming the standard design. This re-design brought about several improvements, such as a decrease in moment at mid-span and an increase in the span of the girder bridge. However, it also brought some unfavourable consequences, which in turn brought new challenges in the design and maintenance of these bridges.

One of the challenges facing Rijkswaterstaat, is reassessing the stiffness of these inverted-T girder bridges. To accurately determine the bending moment distribution and shear forces in the cross section of the individual girders. As seen in older research project (Sliedrecht, Smith, & Roosen), the moment does not follow the linear elastic theory, likely due to the redistribution of the load caused by crack development.

Crack development over the length of a beam has many origins, including loading, material defects, or even environmental conditions. All these factors play a part in determining the structural integrity and mechanical behaviour of a beam system. It is, therefore, important to understand the effect of cracks on beams. One such negative effect is on stiffness degradation of an element, along its length. A method to encompass this change in stiffness is a moment-curvature diagram.

The moment-curvature diagram is a crucial tool for understanding material behaviour. This diagram allows us to examine and comprehend the strength, ductility, energy dissipation capacity, and safety of an element. The moment-curvature diagram illustrates how the internal bending moment varies with the curvature of an element, whether imposed or self-inflicted.

This thesis is a case study into the structural behaviour of a prestressed concrete girder beam, employing methods such as the moment-curvature diagram and Finite Element Modelling. It aims to analyse the effects of stiffness degradation near intermediate support due to crack formation of inverted-T girders. Two case studies will be examined in this thesis, with each case study having its own objectives and goals. In summary, Case Study 1 will look to translate the actual test from the Report to a FEM model, whereas Case Study 2 will evaluate its model set on its performance when a traffic load is applied.

### Problem Statement

#### *Crack Development in Inverted T-Beam:*

Despite advancements in the understanding of inverted T-beam girder systems, there is a lack of comprehensive exploration into the factors influencing crack development.

#### *Crack Effect on Stiffness:*

The influence of cracks on the stiffness of structural elements, particularly inverted T-beams, remains an area that demands further investigation.

#### *Modelling Stiffness using Moment-Curvature Diagrams:*

The accuracy of stiffness depicted in Moment-Curvature diagrams, and its subsequent application, is a critical aspect that warrants a more in-depth examination.

## Research Question and Sub-Questions

### *Main Question:*

How does the stiffness degradation affect the structural behaviour of a continuous prestressed girder beam around the intermediate supports?

### *Sub-Questions:*

- I. How closely does the structural behaviour of beam S10H1A, as depicted by the  $M_n-\kappa$  diagram, align with the outcomes obtained from actual testing?
- II. How does the structural integrity of a bridge model, as depicted by the  $M_n-\kappa$  diagram, hold up when subjected to traffic loads?
- III. Are there specific areas within the bridge model exhibiting significant alterations in curvature and moment development during the application of traffic loads?
- IV. Can the FEM models accurately identify and replicate the occurrence of cracking regions based on changes in curvature and moment regions during simulations?

## Methodology

### Case Studies

In this report, two case studies will be examined, with each case study having its own set of FEM models, properties, and objectives. Several base assumptions and simplifications will be the same, and the two model sets will be a continuation of one another. In summary, Case Study 1 will look to translate the actual test from the Report to a FEM model, whereas Case Study 2 will evaluate its model set on their performance when a traffic load is applied.

### Approach

#### *Analysis of the inverted T-beam girder system*

In this phase of the report, a comprehensive analysis of the inverted T-beam girder system, and the beam S10H1A will be conducted. Two distinct cross-sections will be examined over the length of the girder system. A data set will be made for each cross section and will be used in later steps to calculate the moment-curvature diagram in Python and to recreate the girder system in the Finite Element Method (FEM) program Diana.

Each data set will contain information on the material and cross-sectional properties, dimensions, and structural characteristics of two distinct cross-sections of the girder system. This process will be repeated for each Case Study, based on their own unique requirements. This provides a total of four individual data sets.

#### *Establishing of the Moment-curvature Diagram*

Subsequently, a Moment-Curvature ( $M_n-\kappa$ ) diagram will be generated for each of the four data sets. This process involves the calculation of moments using the equilibrium method, in conjunction with the layer method for a set curvature range. A standalone function in Python will be created and employed to facilitate the calculation and plotting of moment-curvature diagrams.

#### *Execution and Analysis of Case Studie 1*

The next step involves the creation of the FEM model sets, based on the requirements setup of Case Study 1. Sets of models are established to compare results with the Report, these models will be used for Case Study 1. This set of models comprises of 2D beam elements to recreate the test beam, allowing for a verification of the calculated moment-curvature diagram.

#### *Execution and Analysis of Case Studie 2*

This step involves the creation of the second set of FEM models. This entails creating 3D models representing a full bridge deck, with traffic loads applied based on traffic norms. The crack development of this bridge deck will be examined and analysed.

## Chapter 1 – Analysis of the inverted T-beam girder system

Before any calculations, models or analyses can be done. One must have a basic understanding of the bridge system and the inverted Test Beam girder which play a central role in this thesis, with both taken from the Report (Experiment on precast continuous girders, 2023).

The bridge system is a continuous support girder bridge, this means that the deck is supported by multiple supports along the span of the bridge. This design has an impact on several different aspects throughout the thesis, the most important are the unique moment distribution and the implementation of the construction phases.

The inverted T-beam girder is the Test Beam S10H1a, this girder will be the basis on which the moment-curvature diagram as well as the models for the Case Studies. Therefore, an analysis of the inverted T-beam girder system as seen in the Report is needed, an overview of the Test girder and system can be seen in Figure here below.

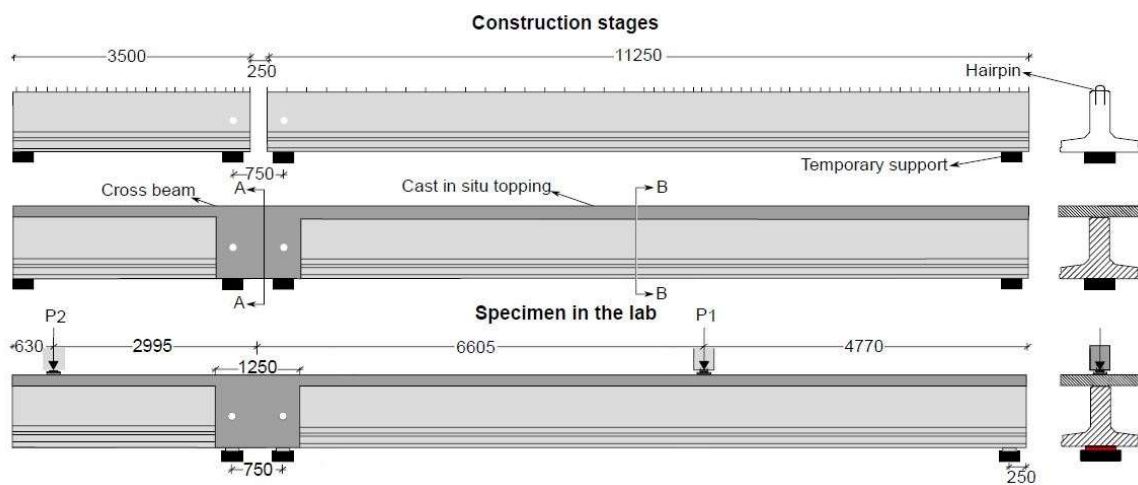


Figure 1, overview Test Beam S10H1A, element, construction phases & cross-sections locations [5]

In this Chapter, the dimensions, cross-sections of the Test Beam setup, materials properties of the individual elements, and construction phases will all be examined and discussed. With the aim to calculate the moment-curvature diagram and understand the setup of the test system.

### Chapter 1.1 – Test Setup

The test system consists of several different unique parts, from left to right a half-combined beam, the crossbeam section and lastly a whole combined beam. The combined beams consist of a prefabricated inverted T-beam and a cast in-situ top layer. Whereas the cross beam is a square cast in-situ beam.

Inverted T-beam girder systems are generally constructed in several phases, the girder used for the Test is no different. To summarise, firstly the prefabricated inverted T-beam girder is made, and its prestress load is applied during fabrication. It's then brought to the construction site, where the top layer is poured in situ, and lastly, any additional layers are added after this phase, e.g., the road deck. These multiple phases come with two main issues. First off, a difference in initial stress over the height of the beam, more on this in Appendix Ic. And secondly, the construction phases must be accounted for in the Models, more on this in Appendix Id

Construction Phases.

Lastly Figure 1, overview Test Beam S10H1A, element, construction phases & cross-sections locations also shows the following: the location of the applied loads P1 and P2, the support locations throughout all the construction phases and the change in support setup. An overview of the lateral dimensions or locations of the Test Setup can be found in the Table here below.

Table 1, Overview longitudinal dimension Test Beam S10H1A [5]

Element	Length [mm]	Point	Distance* [mm]
Left Beam	3500	Left Force (P2)	630
Cross Beam	1250	Left Support	3250
Right Beam	11250	Middle Support	3750
		Right Force (P1)	9940
		Right Support	14500

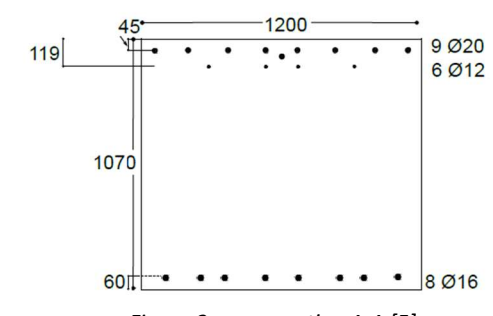
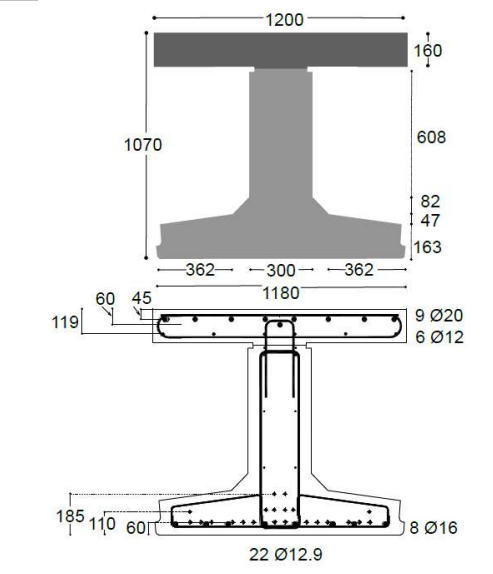
Distance\*, denotes the distance from left to right.

### Chapter 1.2 – Test Beam, S10H1A

In this paragraph, two cross-sections will be examined, one for the cross beam (A-A) and one for the combined beam (B-B). The half beam and whole beam will be assumed to be the same. Each part in turn consists of different elements, such as concrete and steel rebar.

Figured below, and in the Tables here below the individual elements from cross-section A-A and B-B can be found. As each cross-section has multiple different elements, it is important to distinguish between them. For example, the combined beam as seen in cross-section B-B consists of two different concrete materials and four distinct steel materials. To simplify the process, an overview of the abbreviations of the distinct elements can also be found in Figure 2, cross-section A-A and Figure 3, cross-section B-B.

Table 2, overview cross-section dimension, for cross-section A-A and B-B [5]

 <p>Figure 2, cross-section A-A [5]</p>	<b>Elements</b>	<b>Dimensions [mm]</b>	<b>Abbreviation</b>
	Cross Beam	1070 x 1200	CB
	Longitudinal reinforcement (top flange 2)	9 Ø20	t2
	Longitudinal reinforcement (top flange 1)	6 Ø12	t1
	Longitudinal reinforcement (bottom flange)	8 Ø16	b
 <p>Figure 3, cross-section B-B [5]</p>	<b>Elements</b>	<b>Dimensions [mm]</b>	<b>Abbreviation</b>
	Cast in-situ topping (Top layer)	160 x 1200	dl
	Precast Beam (Inverted T-beam Girder)	HRP - 900	T
	Longitudinal reinforcement (top flange 2)	9 Ø20	t2
	Longitudinal reinforcement (top flange 1)	6 Ø12	t1
	Longitudinal reinforcement (bottom flange)	8 Ø16	b
Longitudinal Prestressing strands	22 Ø12.9	P	

With the use of HRP/HIP-ligger folder (Beton, 2021) and the Report, the remaining dimensions for the inverted T-beam and the combined beam were found, an overview of the parameters can be seen in Appendix Ia.

An important thing to note is that each Case Study will have its own unique set of values. The values used for each Case study must therefore with its assumptions. Therefore, two sets of values for the material properties—the actual tested values and the characteristic values will be calculated in this chapter. The tested values for Case Study 1 and the characteristic values for Case Study 2.

### Chapter 1.3 – Material properties of the Test Beam

This paragraph provides an overview of the characteristic values of the individual elements for both cross-sections. Using the NEN-EN 1992-1-1 (NEN-EN 1992-1-1+C2; Eurocode 2: Design of concrete structures – Part 1-1: General rules and rules for buildings, 2011) and the RTD (Hendriks & Roosen, 2020), together with the given characteristic values from the Report, stress-strain relationships will be calculated and graphed.

For the stress-strain diagram, a bi-linear relationship was taken as seen in Figure 3.4 from the NEN-EN 1992-1-1 chapter 3.1.7 and Figure 5 from the RTD chapter 2.4.1.4, for the compressive zone. For the tensile zone, an ideal brittle behaviour was taken with no softening effect. This also accounts for both value sets, their calculations, and their diagram.

Another important aspect of the material properties is the construction phases, in which the test beam is constructed. To summarize the phases: first, the prefabricated inverted T-beam girder is made, and its prestress load is applied during fabrication. Then the T-beam girder is brought on site and the top layer is added in situ. These multiple construction phases have the unforeseen consequence that the materials in the T-beam girder will have a different initial stress compared to the top layer. This difference must be accounted for in the stress-strain diagrams.

In the figures (Figure 4, Figure 5, Figure 6, Figure 7) below the stress-strain relationship for the concrete and steel materials can be seen, for both case studies. In Appendix Ie, a complete overview of the material properties can be found, and additional information on the material's initial stresses can be found in Appendix Id.

#### Chapter 1.3.1 – Tested Values, Concrete and Steel

The tested values for the two concrete and 4 steel materials were taken from the Report, the stress-strain diagrams can be seen in the figures below.

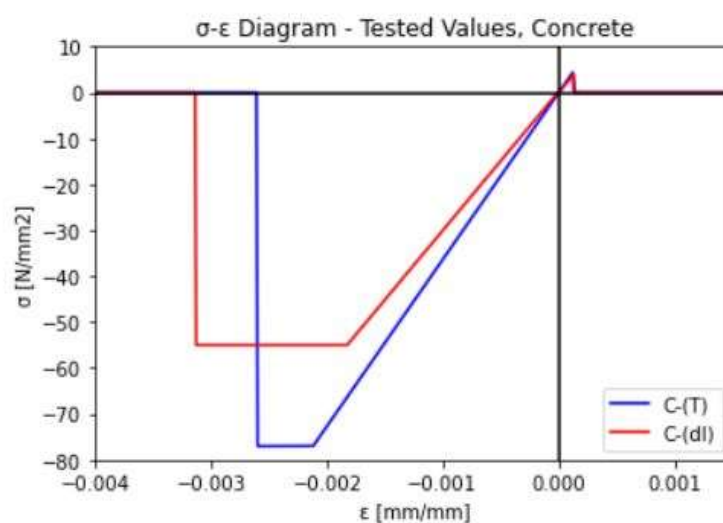


Figure 4, stress-strain diagram, tested value - inverted T-beam (T) and top layer (dl) Concrete

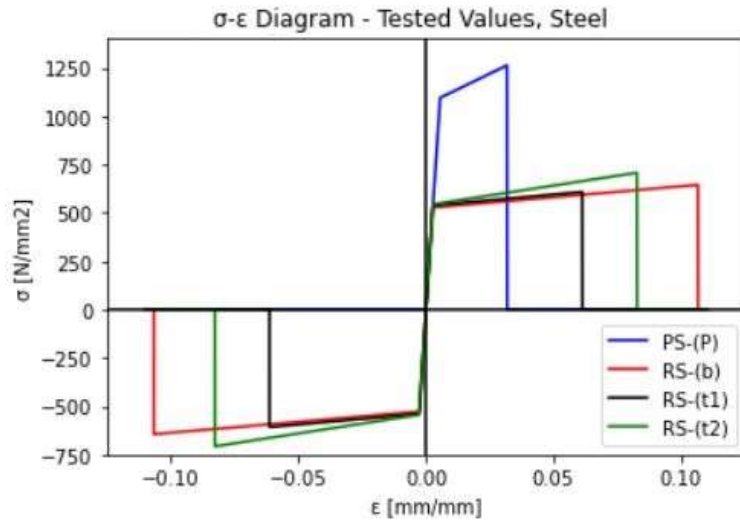


Figure 5, stress-strain diagram, tested value -reinforcement steel (b, t1 & t2) and prestress (P) steel

Chapter 1.3.2 – Characteristic Values, Concrete and Steel

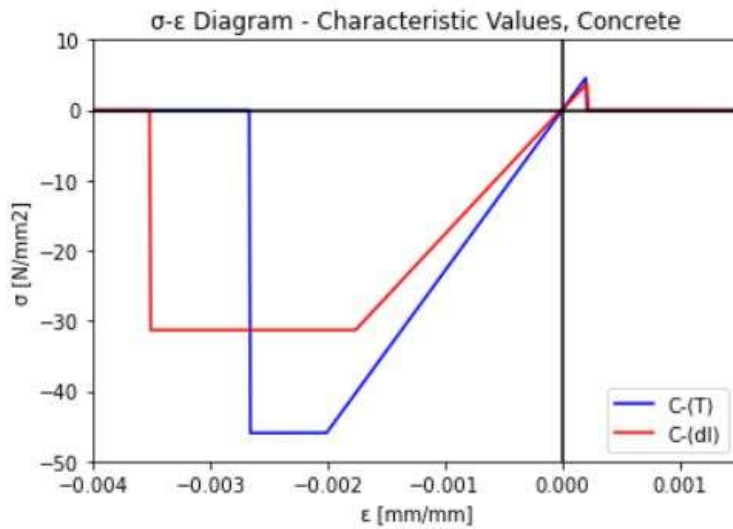


Figure 6, stress-strain diagram, characteristic value – inverted T-beam (T) and top layer (dl) Concrete

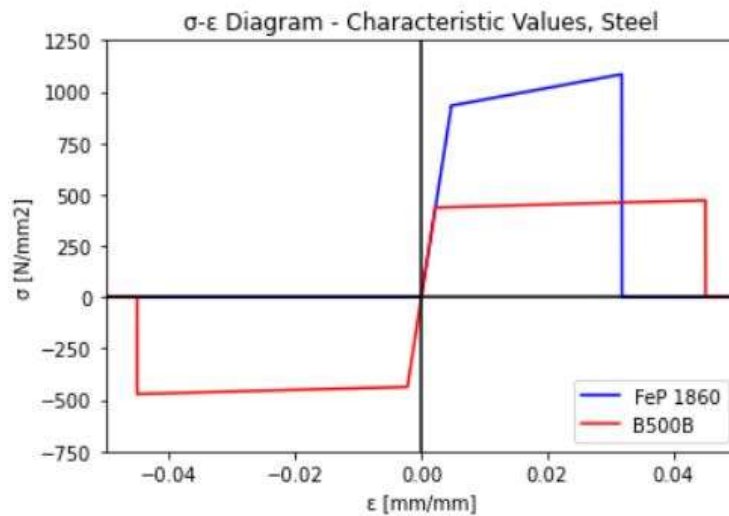


Figure 7, stress-strain diagram, characteristic values – reinforcement (B500) and prestress (FeP 1860) steel

## Chapter 2 – Establishing of the Moment-curvature Diagram

A key step in this report is to calculate a moment-curvature ( $M_n$ - $\kappa$ ) Diagram for any combination of cross-sections and material properties. By employing the equilibrium method alongside a layered method approach, the aim is to develop a set of codes for calculating and graphing the moment ( $M_n$ ) at different curvatures ( $\kappa$ ). In essence, the code will slice a cross-section into  $n$  number of layers in the vertical direction, then examine each layer individually and calculate the necessary values (e.g., stress and strain) to establish a horizontal equilibrium over the hole height. The equilibrium will be found using a bisectional function, and once found the code can then determine the moment at the given curvature.

Python will be used to calculate and plot an  $M_n$ - $\kappa$  Diagram, the code will have three distinct sets of calculations. Namely:

1. A matrix containing all the cross-sectional and material parameters, this set of codes will be referred to as the cross-sectional parameter matrix (PM).
2. Three sets of calculation functions: one for calculating the stresses, one for calculating the Normal forces and Moment, and the other for implementing a bisectional method.
3. The final set of codes will involve moment calculations, verifications and graph plotting.

### Chapter 2.1 – Moment-curvature Relationship

This moment-curvature relationship is based on curvature ( $\kappa$ ), material property Young's modulus ( $E$ ), and cross-sectional property moment of inertia ( $I$ ), as depicted in the formula below. This relationship yields the  $M_n$ - $\kappa$  diagram, enabling us to assess the strength, ductility, energy dissipation capacity, and safety of an element.

$$M_n = EI * \kappa \quad (1)$$

$E = \text{Young's Modulus}$   
 $I = \text{Moment of Inertia}$   
 $\kappa = \text{curvature}$

To construct the  $M_n$ - $\kappa$  diagram, comprehensive knowledge of an element's properties and dimensions is required, with none more critical than the elastic behaviour of the individual materials and their constitutive relationship. At the heart of the  $M_n$ - $\kappa$  diagram lies Hooke's law, which states that the force required to deform a material is directly proportional to the deformation within the material's elastic range. Understanding the elastic and plastic ranges of a material are vital aspect to understand and is graphically represented in the  $M_n$ - $\kappa$  diagram. Elasticity denotes a material's ability to return to its original shape and size after being deformed within the elastic limit. Plasticity, on the other hand, signifies the permanent deformation of a material when subjected to a force.

In this analysis three moments will be identified; the cracking moment, the yielding moment, and the ultimate moment capacity, each of which might have multiple occurrences. The cracking moment marks the onset of tensile stress in a reinforced concrete structure, indicating the initiation of cracking. The yielding moment occurs when a material surpasses its elastic limit and enters the plastic range, in this report the yielding of the prestress and reinforcements steel will be examined. Finally, the ultimate moment capacity denotes the maximum moment an element can withstand before failure. Between these points, variations in stiffness are observable, manifested in the differing slopes among the three points of interest.

### Chapter 2.2 – Python Code

#### Chapter 2.2.1 – Cross-sectional Parameter Matrix.

This part of the code is dedicated to generating a dataset for the cross-sections, encompassing all its properties and dimensions along its height. A function will be written that splits the cross-section into multiple layers over its height, each layer possessing its own unique set of dimensions and material properties. Ultimately, the function will combine all the individual datasets into one main set, thereby

creating a final matrix array called the Parameter Matrix (PM). This PM will serve as input for the main calculation in the final part of the Python code.

A goal for the code was to make a universal set of functions, ensuring that the calculations or the code remained independent of any specific cross-section or material combination. While the functions that calculate individual properties or dimensions are universal, the cross-sectional PM is tailored to any one beam. An overview of this process can be seen in the figure below, and a detailed explanation of the individual parameters can be found in Appendix IIa.

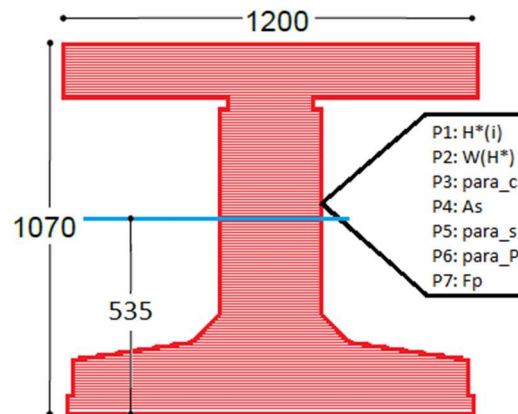


Figure 8, overview layered cross-section, showcasing all the properties within PM for each layer

Numerous properties and dimensions are needed to properly create the PM array; parameters such as heights, widths, and material properties must all be specified within the Python code prior to generating the PM array. Datasets and parameter arrays will be created before any of the main calculations.

Furthermore, several intermediate calculations must be done before the PM array is setup. For example, the initial prestress force needs to be calculated at  $t=0$  and at  $t=\infty$  along with their respective forces, moments, stresses, and strains in the beam at those times.

#### Chapter 2.2.2 – Calculations Functions.

Several essential calculation functions must be coded, these functions include those for computing the stress-strain relationship, a function which implements the bisectional method and a function which calculates the normal force ( $N_x$ ) and the moment ( $M_k$ ).

The first set of functions will focus on the stress-strain relationship, it takes an array of material properties and calculates the stress at a given strain. Three versions of this function are necessary: one for concrete, another for steel reinforcement, and the last one for prestress steel. Each material requires distinct properties to determine its stress-strain relationship. These functions will be named  $\text{sig}_c$  (concrete),  $\text{sig}_s$  (steel) and  $\text{sig}_{sp}$  (prestress).

The second function will implement the bisectional method function (BMF), a bisectional method used to find an approximate solution to an equation within an interval. The method requires initial inputs, including the two initial values ( $x_0$  &  $x_1$ ), and a condition (accuracy condition, ac) that must be met—this condition can be anything. The function then evaluates if the initial values satisfy the condition. If neither does, then the function calculates a new input value ( $x_2$ ):  $x_2 = (x_0 - x_1)/2$ , and check if this value meets the conditions. This process continues, recalculating new input values and checking whether they meet the conditions. The function concludes and returns a value ( $x_n$ ) which satisfies the condition. It is essential to provide a well-defined initial interval and a reasonable condition, as the function it is prone to entering an endless loop.



These graphs will be used in the final calculation case, the specific calculation. The specific curvature and moments corresponding to certain conditions, these conditions can be seen in the tables below. By using the different graphs and checks, these specific curvatures, and moments can be found.

Table 3, strain conditions - combined beam

Moment	Condition	Description
$M_u^-$	$\epsilon_{3uk,dl}$	Ultimate compressive strain top layer
$M_y^-$	$\epsilon_{y,P}$	Yielding strain reinforcement prestress Tendon
	$\epsilon_{y,b}$	Yielding strain reinforcement steel b
$M_{cr}^-$	$\epsilon_{ctm,T}$	Ultimate tensile strain inv. T-Beam
$M_0$	$K_0$	Moment at $\kappa=0$
$M_{cr}^+$	$\epsilon_{ctm,dl}$	Ultimate tensile strain top layer
$M_y^+$	$\epsilon_{y,t2}$	Yielding strain reinforcement steel t2
$M_u^+$	$\epsilon_{3uk,T}$	Ultimate compressive strain inv. T-Beam

Table 4, strain conditions - cross beam

Moment	Condition	Description
$M_u^-$	$\epsilon_{3uk,dl}$	Ultimate compressive strain top layer
$M_y^-$	$\epsilon_{y,b}$	Yielding strain reinforcement steel b
$M_{cr}^-$	$\epsilon_{ctm,dl}$	Ultimate tensile strain top layer
$M_0$	$K_0$	Moment at $\kappa=0$
$M_{cr}^+$	$\epsilon_{ctm,dl}$	Ultimate tensile strain top layer
$M_y^+$	$\epsilon_{y,t2}$	Yielding strain reinforcement steel t2
$M_u^+$	$\epsilon_{3uk,dl}$	Ultimate compressive strain top layer

### Chapter 2.3 – Moment-Curvature Diagrams

With the calculation scheme in place and the Python script written, the final step will be to compute and graph the  $M_n-\kappa$  diagrams. The script will run for all four data sets for each of the two case studies. Each diagram will be examined and the 6 unique moment points will be highlighted in the  $M_n-\kappa$  diagram, the conditions for each point can be seen in Table 3 & Table 4.

Before any graph was made, a comprehensive analysis and verification of the Python code was conducted, this can be found in Appendix IIc.

#### Chapter 2.3.1 – Moment-Curvature Diagrams, Python

The figures and tables here below, show all 4  $M_n-\kappa$  diagrams, note the differences in curvature ranges and the presence of blue dots. These dots signify the unique moment points where then moment-curvature diagrams transition from one state to another. As explained in Chapter 2.2.3, each point corresponds to a specific strain within the entire bending of the beam.

Table 5, overview  $M_n$ - $\kappa$  Diagram - combined beam with tested values (CB-t)

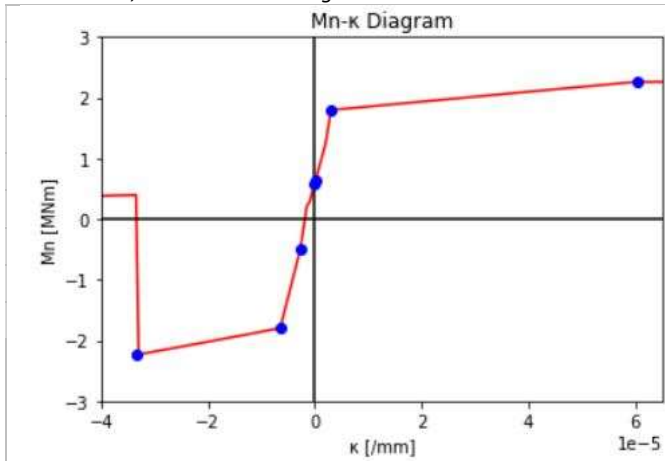


Figure 11,  $M_n$ - $\kappa$  diagram – combined beam with tested values (CB-t)

Moment	Condition	$\kappa$ [ $\text{mm}^{-1}$ ]	$M_n$ [Nmm]
$M_u^-$	$\epsilon_{3uk,dl}$	-3.33e-05	-2.24e+09
$M_y^-$	$\epsilon_{y,p}$	-6.29e-06	-1.79e+09
	$\epsilon_{y,b}$	-2.72e-06	-4.93e+08
$M_{cr}^-$	$\epsilon_{ctm,T}$	-1.00e-07	5.71e+08
$M_0$	$K_0$	0.00	6.06e+08
$M_{cr}^+$	$\epsilon_{ctm,dl}$	1.00e-07	6.35e+08
$M_y^+$	$\epsilon_{y,t2}$	2.93e-06	1.78e+09
$M_u^+$	$\epsilon_{3uk,T}$	6.04e-05	2.26e+09

Table 6, overview  $M_n$ - $\kappa$  Diagram - combined beam with characteristic values (CB-c)

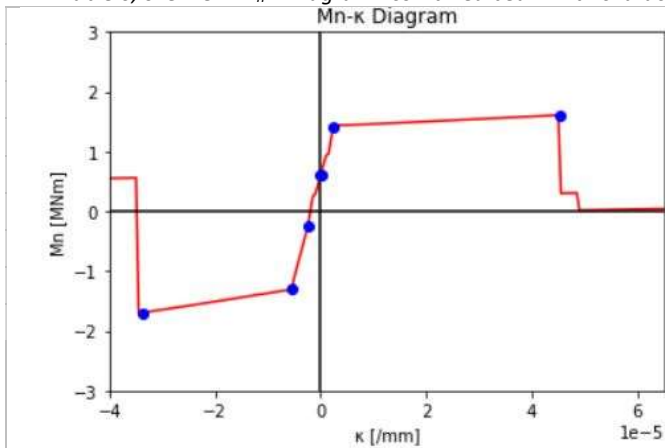


Figure 12,  $M_n$ - $\kappa$  diagram – combined beam with char. values (CB-c)

Moment	Condition	$\kappa$ [ $\text{mm}^{-1}$ ]	$M_n$ [Nmm]
$M_u^-$	$\epsilon_{3uk,dl}$	-3.38e-05	-1.70e+09
$M_y^-$	$\epsilon_{y,p}$	-5.49e-06	-1.30e+09
	$\epsilon_{y,b}$	-2.41e-06	-2.41e+08
$M_{cr}^-$	$\epsilon_{ctm,T}$	-1.00e-07	5.82e+08
$M_0$	$K_0$	0.00	6.06e+08
$M_{cr}^+$	$\epsilon_{ctm,dl}$	1.00e-07	6.46e+08
$M_y^+$	$\epsilon_{y,t2}$	2.32e-06	1.41e+09
$M_u^+$	$\epsilon_{3uk,T}$	4.54e-05	1.61e+09

Table 7, overview  $M_n$ - $\kappa$  Diagram - cross beam with tested values (TB-t)

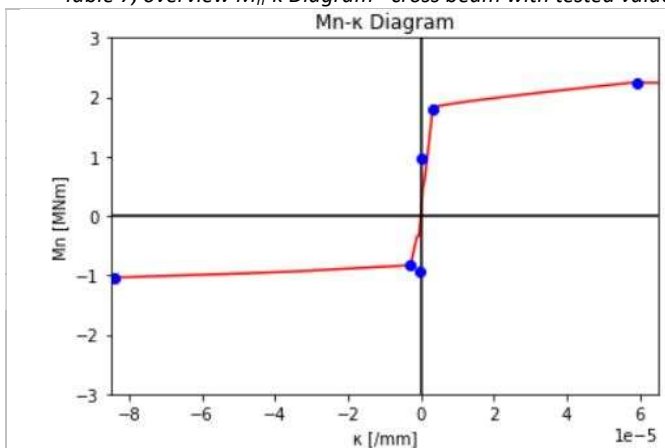


Figure 13,  $M_n$ - $\kappa$  diagram – cross beam with tested values (TB-t)

Moment	Condition	$\kappa$ [ $\text{mm}^{-1}$ ]	$M_n$ [Nmm]
$M_u^-$	$\epsilon_{3uk,dl}$	-8.42e-05	-1.03e+09
$M_y^-$	$\epsilon_{y,b}$	-2.79e-06	-8.32e+08
$M_{cr}^-$	$\epsilon_{ctm,dl}$	-2.44e-07	-8.42e+08
$M_0$	$K_0$	0.00	0.00
$M_{cr}^+$	$\epsilon_{ctm,dl}$	2.48e-07	8.68e+08
$M_y^+$	$\epsilon_{y,t2}$	3.22e-06	1.81e+09
$M_u^+$	$\epsilon_{3uk,dl}$	5.93e-05	2.25e+09

Table 8, overview  $M_n$ - $\kappa$  Diagram - cross beam with characteristic values (TB-t)

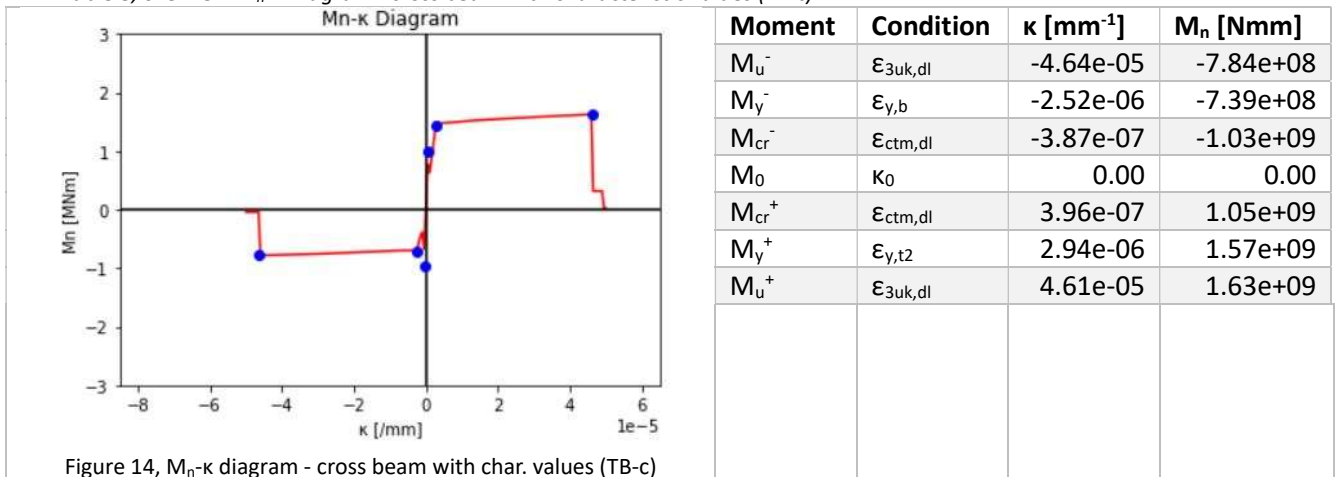


Figure 14,  $M_n$ - $\kappa$  diagram - cross beam with char. values (TB-c)

### Chapter 2.3.2 – Moment-Curvature Diagrams, Diana

Diana requires further simplification of the diagrams; it runs best with as few points as possible. This necessitated a re-examination of the most crucial points. Ultimately, the moment at  $\kappa=0$  and, for the combined beam diagrams, the yielding of the bottom reinforcement steel ( $\epsilon_{y,b}$ ) were removed. Additionally, adjustments were made to the range of the diagrams; all diagrams were adjusted to have a version with a curvature with the range  $[-5.00e-5; 5.00e-5]$  or  $[-5.00e-5; 10.00e-5]$ . The first range is for the diagrams using the mean values, and the second range is for the diagrams using the characteristic values. The final diagrams are depicted in the figures below.

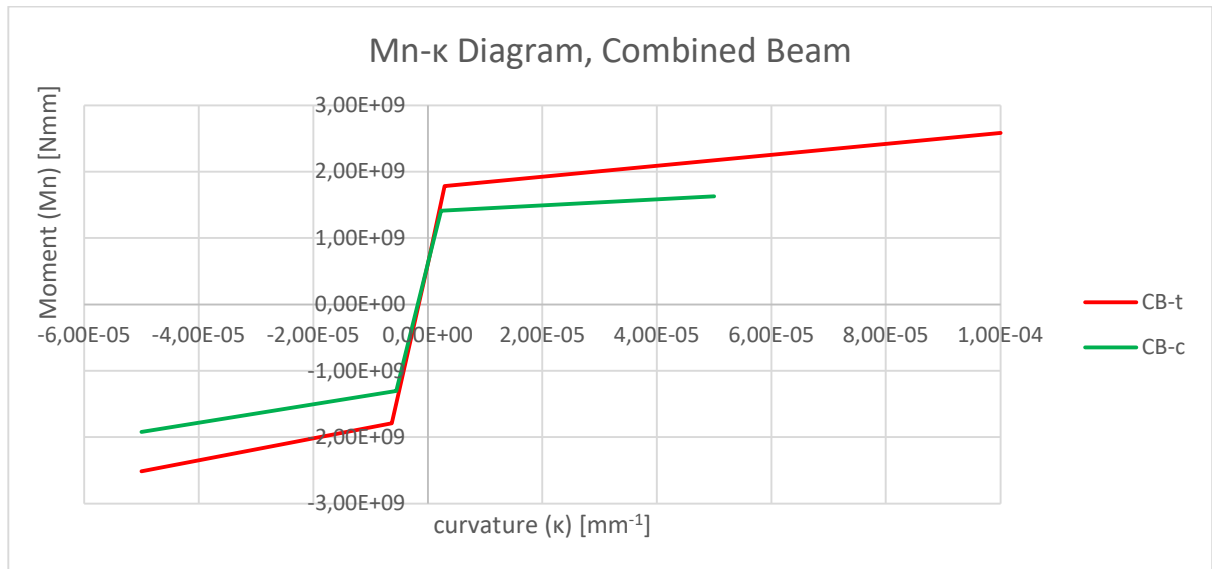


Figure 15,  $M_n$ - $\kappa$  diagram - combined beams (CB), idealised for Diana

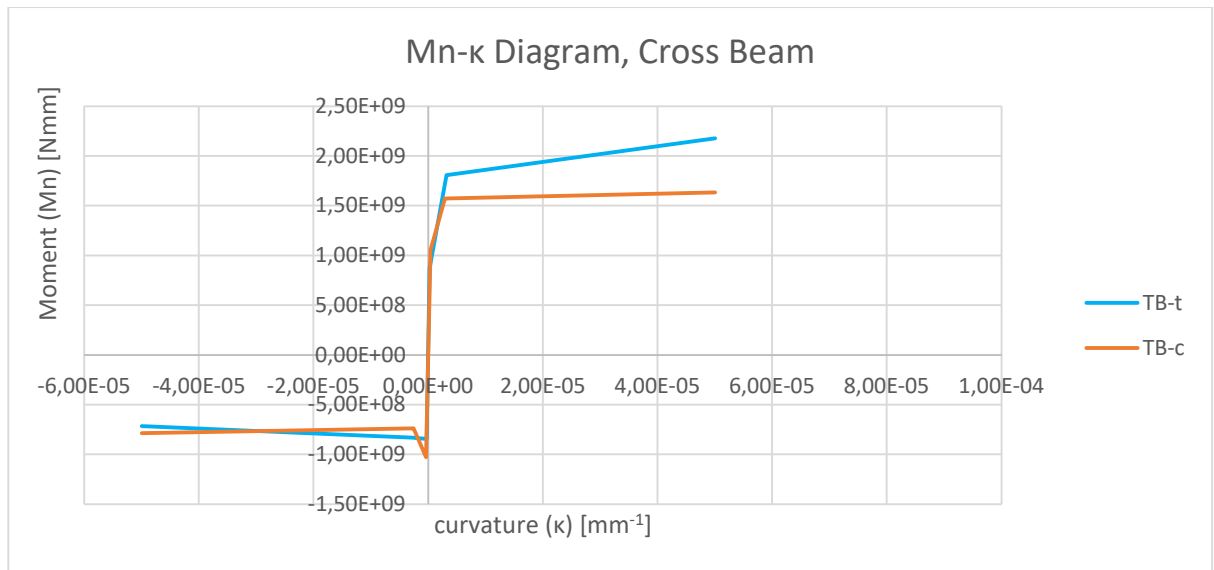


Figure 16,  $M_n$ - $\kappa$  diagram - cross beams (TB), idealised for Diana

## Chapter 3 – Case Study 1

---

Case study 1 aims to reconstruct the actual Test beam S10H1A into a Finite Element Method (FEM) model, using the FEM program Diana. First off, two 2D beam models will be created, with loads will be applied like the Test beam setup. Subsequently, linear and non-linear analyses will be conducted, and the results of these analyses will be compared with those of the Test beam. Following the examination of the 2D models, a third 3D model will be developed. Similar to the 2D models, this 3D model will be loaded and examined to compare results.

### *Chapter 3.1 – Case Study, Description*

The primary objective of this case study will be to compare the results of the FEM model analyses with those of the Test beams experiment. Additionally, the objectives include fine-tuning the FEM model's elements and analyses, exploring, and determining the optimal combination of settings for accurate analyses, and implementing the examination results into subsequent models to prepare for Case Study 2.

A significant challenge of this case study lies in the translation of the material and structural properties of the multiple elements of the Test beam setup into a FEM space. This involves simplifying the actual beam for smoother and faster operation, while still ensuring accurate modelling and practical results. This has an impact on the translation of the cross sections, supports and applied loads. Other challenges will be in the application of the calculated moment-curvature diagrams, and the implementation of the multiple construction phases and their respective loads.

As previously mentioned in Chapter 1, this case study uses the tested material values for all the materials in the combined beam and cross beam element. It is essential to use actual material values rather than characteristic values from the NEN or RBK to facilitate an accurate comparison between FEM model results and those of the Test beam.

### *Chapter 3.2 – FEM Models*

Case Study 1 will itself be split into three models; Model 1 (Figure 17) is a recreation of the test beam, comprising one full beam connected to a half-beam with a support section, this model will have a force-controlled load applied to it. Model 2 (Figure 18) consists of two full beams connected with a support section; however, this model will be loaded using a displacement-controlled load. Lastly, Model 3 (Figure 19) will be a replica of the Model 1 in a 3D environment.

The outcomes of Model 1 will be used to scrutinize the similarities between the FEM model and the actual results, while the results for the second model will be employed to examine the behaviour of the beams under load. Model 2 will be used to examine the effect of a displacement-controlled load compared to a force-controlled load. Model 3 will be used to further examine and assist in the recreation of models for Case Study 2, and its results will be compared to those of Model 1.

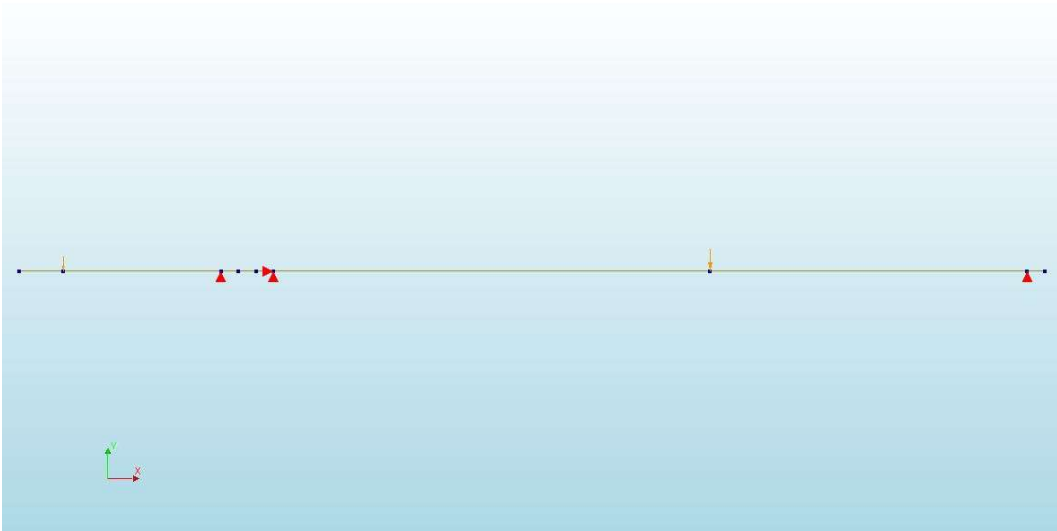


Figure 17, FEM Model 1

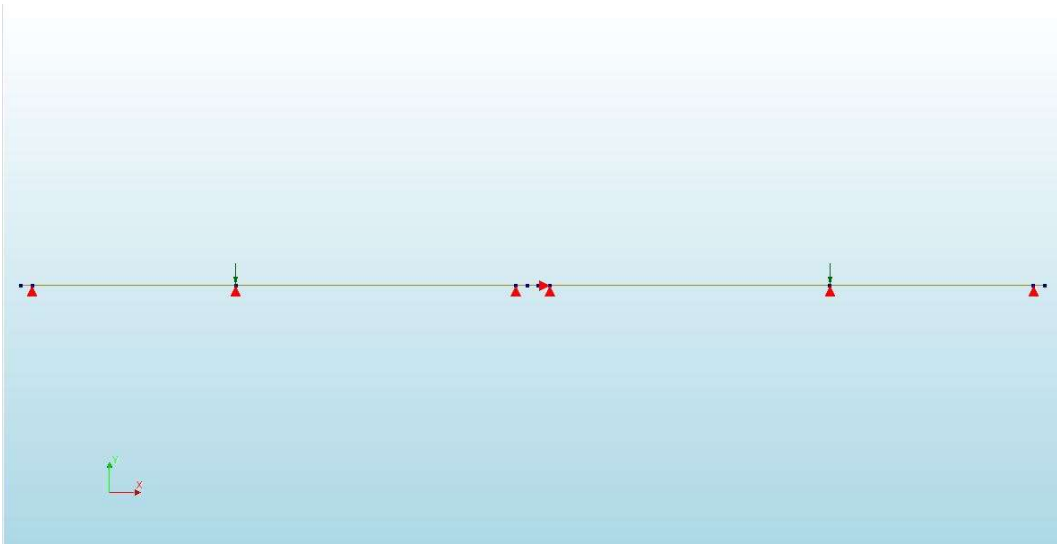


Figure 18, FEM Model 2

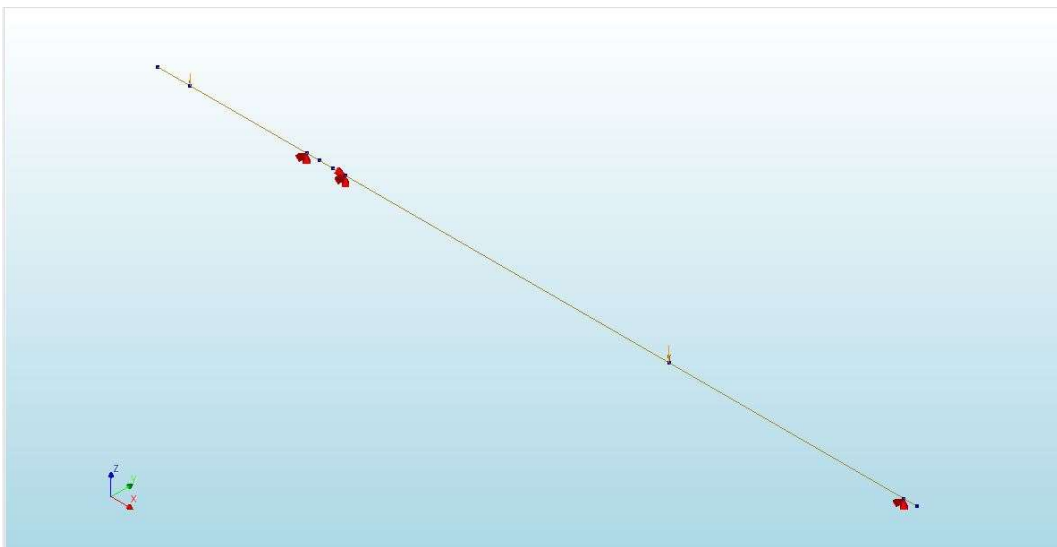


Figure 19, FEM Model 3

### Chapter 3.2.1 – FEM Models, Description

The 2D model will utilize the "Class-I beams 2D" element class, providing a simplified approach to modelling the complex beam described in the Report. While this method simplifies the model, it effectively allows for an examination of the behaviour of the calculated Mn- $\kappa$  diagram. Some further simplifications have been applied to the beam models and the model setup to facilitate ease of construction and execution:

- In the cross section of the combined beam
  - Actual: complex I-shape cross-section, with multiple materials over its height.
  - Models: standard I-shape, with 1 material property with the dimensions adjusted accordingly.
- In the support & loads area
  - Actual: the supports and load are on steel plates, spread over an area
  - Model: the supports and load are on 1 point (node).
- In the applied load
  - Actual: the Test beam was loaded over a duration of time, with intermediate steps. Secondary effects (such as fatigue) could be present in the Beam.
  - Model: the models were only subject to their applied loads, and secondary displacement effects.

Model 3, like its 2D counterpart (Model 1) will use "Class-I Beams 3D". However, the additional dimension in the model space necessitates adjustments to supports and material properties to align them correctly. Applied loads and further simplifications will remain consistent with Model 1.

For Models 1 & 3, force-controlled load will be applied in the same manner as reported in the Report, maintaining the same ratio between the two loads and maximum value. In contrast, for Model 2, the displacement-controlled load will reach an arbitrarily high value, and both loads will have the same magnitude.

As previously mentioned, the construction of the inverted T-beam occurs in two phases, with changes in supports and loads. The model must account for these phases in the model. Diana has a function to easily add these phases to the analysis steps. By adjusting which elements, support sets, and load cases are active during each phase, the analyses can be tailored to reflect the actual behaviour of the construction and load phases.

- In the first phase, the model only consists of the inverted T-beam elements (BL & BR), and the cross beam element (M-Sup.) is not active in this phase. Both models 1 & 2 will be supported such that they are simply supported beams; therefore, the support set 'Initial Support' will be active. Load Cases '01 – Prestress' will be applied to simulate the prestress forces being applied to the beams.
- In the second phase, the cross beam element (M-Sup.) is added, changing the support set to 'Combined Supports.' Now the beam will act as one continuous beam, and load case '02 – Global Loads' will be applied to simulate the self-weight of all elements.
- In the last phase, the load case '03 – Applied load' is applied to the model. For Model 2, additional support must be added to apply a displacement-controlled load. Therefore, the 'Displacement Supports' will be active in this phase.

### Chapter 3.2.2 – FEM Models, Analysis

Two main analyses will be conducted: a structural linear static analysis and a nonlinear static analysis. The linear analysis will be used to examine whether the loads are applied correctly and to see whether the beam behaves as expected. For example, it will help verify whether the displacement and moment are indeed in the correct direction or axis. The second analysis, the nonlinear static analysis, is more complex, involving three phases and multiple load steps. Model 3 will undergo the same analyses as its 2D counterpart: a structural linear static analysis and a nonlinear static analysis.

### Chapter 3.2.3 – FEM Models, Output

There are three main outputs which are important to examine: displacement, curvature, and moments. These outputs allow for a proper examination of the prestress forces and applied loads, to determine if their application was done correctly. Additionally, they facilitate further examination of how the moment and curvature develop in the beam elements. For Model 2, it is also important to observe how the reaction force at the displacement-controlled supports develops. Furthermore, an examination of the force output for Model 2 must be made.

In Appendix IIIa and Appendix IIIb, an overview of the properties of the models can be found, including Diana model characteristics, general dimensions of the beams, material and cross-sectional properties, support types, the applied loads values, and mesh properties and a detailed outline of the Analysis setting for all three models.

### Chapter 3.3 – FEM Analysis

#### Chapter 3.3.1 – FEM Analysis, Model 1

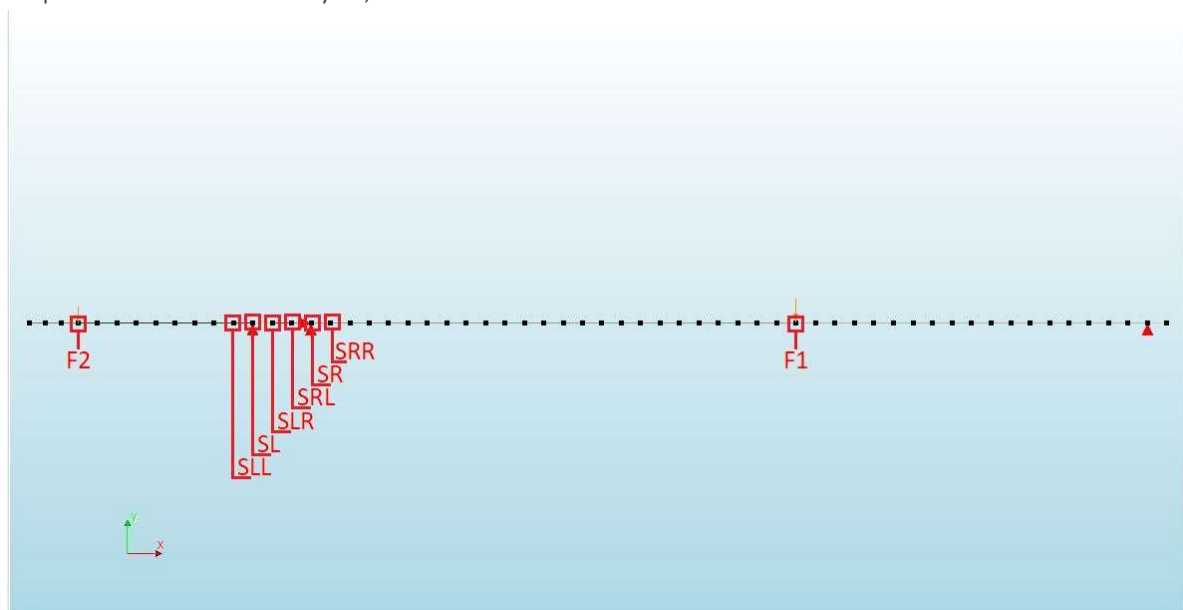


Figure 20, Model 1 with point (nodes) of interest

<b>F2</b>	location of F2		<b>SRL</b>	Right Support, left
<b>SLL</b>	Left Support, left		<b>SR</b>	Right Support
<b>SL</b>	Left Support, left		<b>SRR</b>	Right Support, right
<b>SLR</b>	Left Support, right		<b>F1</b>	location of F1

An overview of 8 points of interest in Model 1 can be seen in the Figures and Table above. For each point, the moment and curvature development were calculated and taken from Diana. The resulting  $M_n-\kappa$  diagram for each point can be seen in the figures below. Note the calculated  $M_n-\kappa$  diagram in the background of the figure, referred to as TB-c. It's important to note that Diana calculates curvature and moment on the left and right sides of each node. Therefore, the values represented in the figures are averaged values over the two sides.

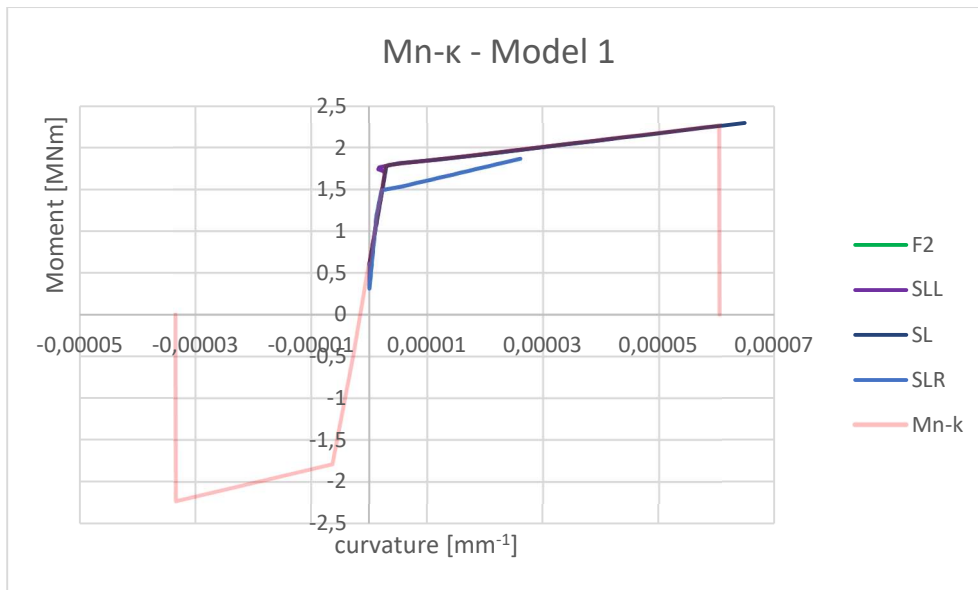


Figure 21, moment development, Model 1 (p1)

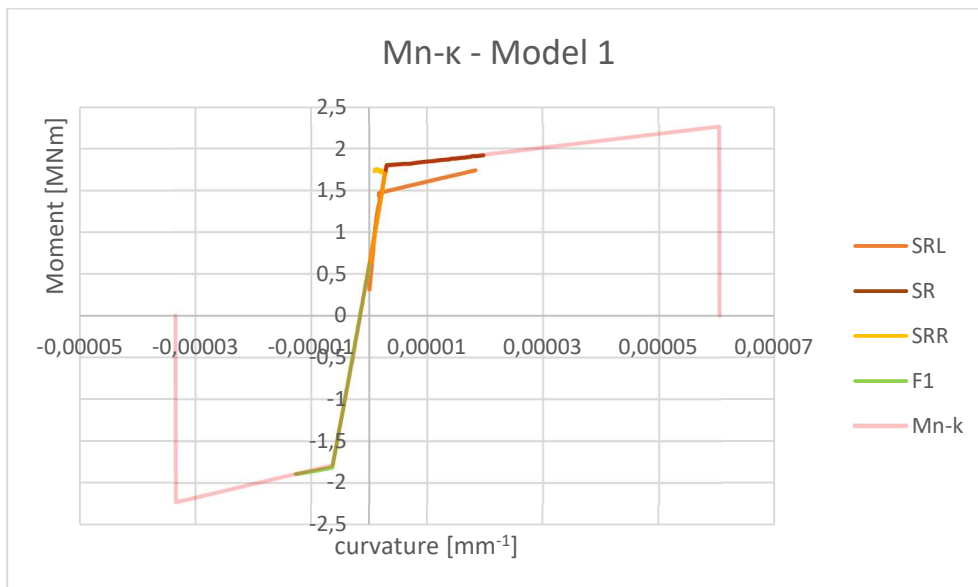


Figure 22, moment development, Model 1 (p2)

Points F2, SLL, SL, SR, SRR and F1 all behave as prescribed, following the  $M_n$ - $\kappa$  diagram. However, it is observed that the lines for SLR and SRL do not behave as prescribed. This is because these nodes are connected to an element with two different material properties, namely the combined beam (CB-c) and the cross beam (TB-c). This results in an incorrect averaged moment and displacement. Also, it can be observed that SL goes further than the  $M_n$ - $\kappa$  diagram, this is due to the input  $M_n$ - $\kappa$  diagram for Models 1 & 2 being an adjusted diagram that goes beyond the  $M_u^-$  &  $M_u^+$ . In the Table here below, you can see in which load step each point passes a certain curvature, and moments respectively.

Table 9, points of interest curvature development – Model 1

	$K_{cr}^+$	$K_y^+$	$K_u^+$		$K_{cr}^-$	$K_y^-$	$K_u^-$
<b>SLL</b>	4	47	-	<b>F2</b>	-	-	-
<b>SL</b>	4	42	58	<b>F1</b>	3	57	
<b>SLR</b>	3	42	-				
<b>SRL</b>	3	40	-				
<b>SR</b>	3	32	-				
<b>SRR</b>	3	-	-				

In the figures below, the moment distribution at load step 3, 32 (phase – LS 29) & 58 (phase – LS 55). Each figure shows the curvature distribution in ‘auto-scale’ and with ‘specific value’, the ‘specific values’ will be within the following ranges:  $[K_{cr}^-, K_{cr}^+]$ ,  $[K_y^-, K_y^+]$  &  $[K_u^-, K_u^+]$  &  $[M_{cr}^-, M_{cr}^+]$ ,  $[M_y^-, M_y^+]$  &  $[M_u^-, M_u^+]$ . Please note, Appendix IIIc and Appendix III d, show the development of the curvature ( $\kappa_z$ ) and moments ( $M_z$ ), a figure for every five load steps.

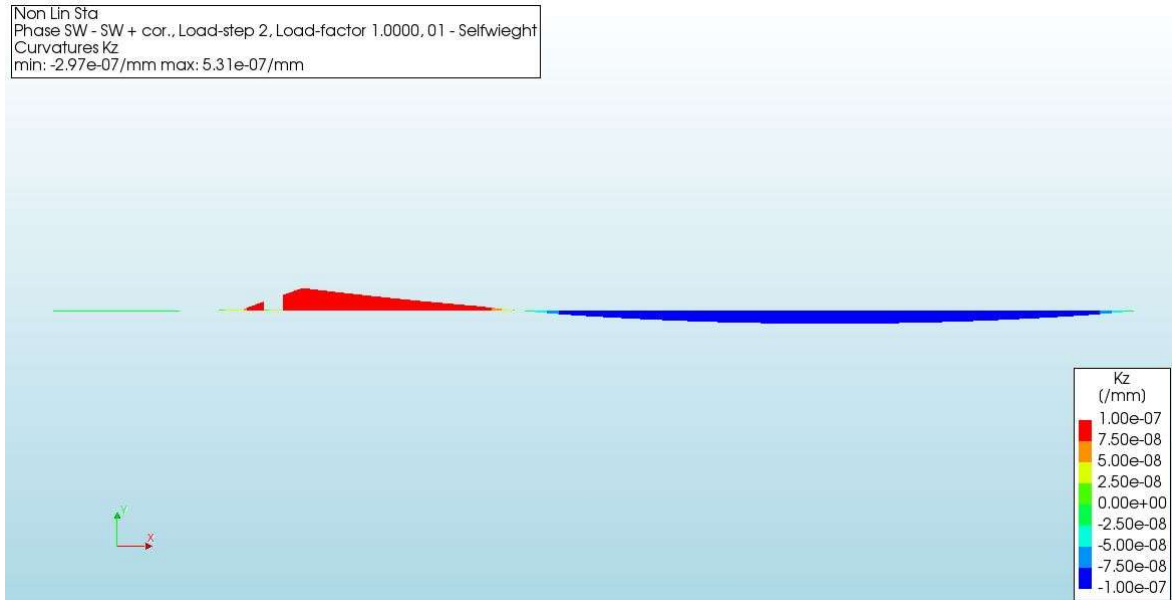


Figure 23, curvature ( $k_z$ ) at load step 3, Model 1

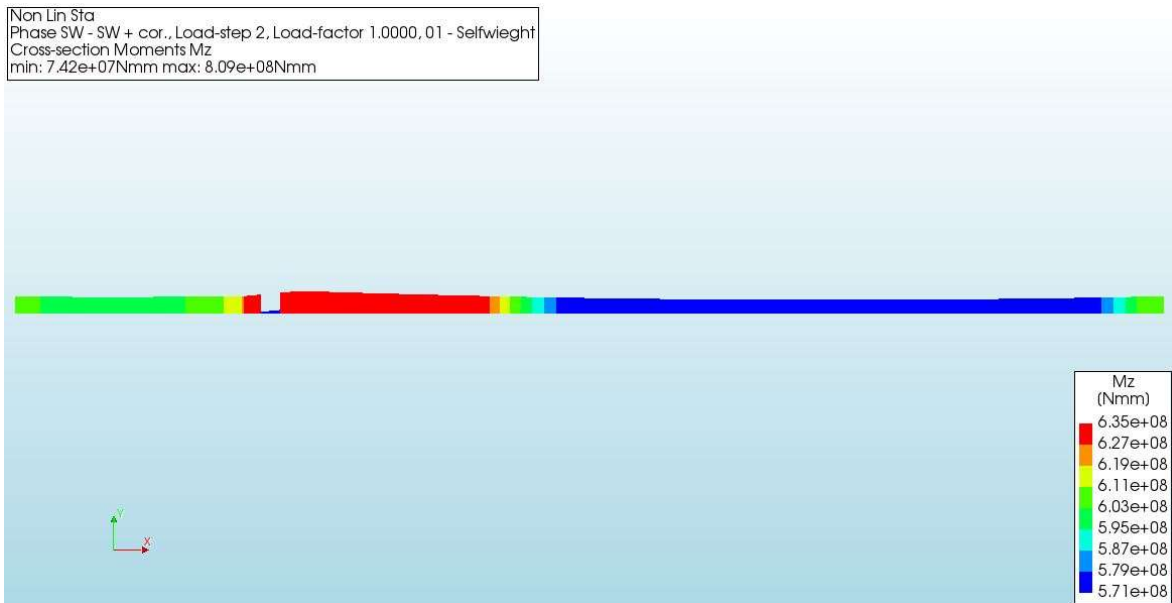


Figure 24, moment ( $M_z$ ) at load step 3, Model 1

Non Lin Sta  
 Phase - AP - Applied Load, Load-step 29, Load-factor 0.28000, 03 - Applied Load  
 Curvatures Kz  
 min: -3.06e-06/mm max: 3.00e-06/mm

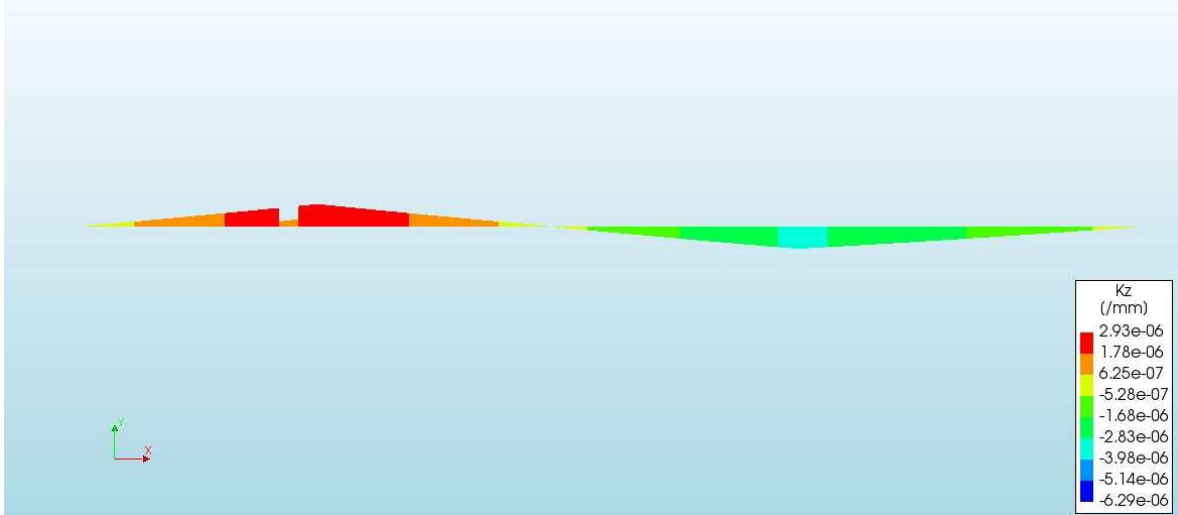


Figure 25, curvature (kz) at load step 32 (29), Model 1

Non Lin Sta  
 Phase - AP - Applied Load, Load-step 29, Load-factor 0.28000, 03 - Applied Load  
 Cross-section Moments Mz  
 min: -5.57e+08Nmm max: 1.80e+09Nmm

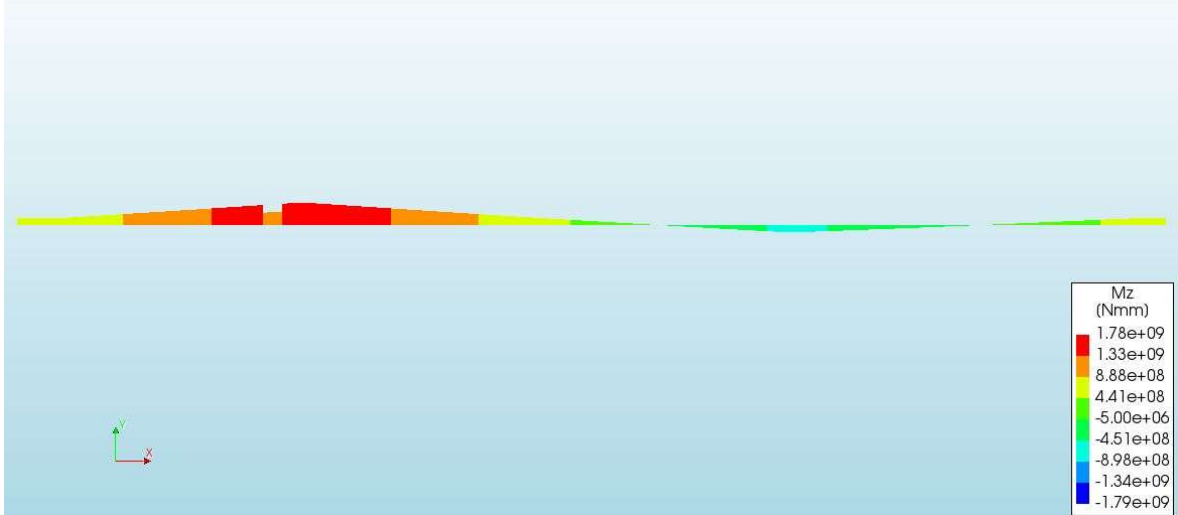


Figure 26, moment (Mz) at load step 32 (29), Model 1

Non Lin Sta  
 Phase - AP - Applied Load, Load-step 54, Load-factor 0.53000, 03 - Applied Load  
 Curvatures Kz  
 min: -6.44e-06/mm max: 5.78e-05/mm



Figure 27, curvature (kz) at load step 58 (55), Model 1

Non Lin Sta  
 Phase - AP - Applied Load, Load-step 55, Load-factor 0.54000, 03 - Applied Load  
 Cross-section Moments Mz  
 min: -1.89e+09Nmm max: 2.27e+09Nmm

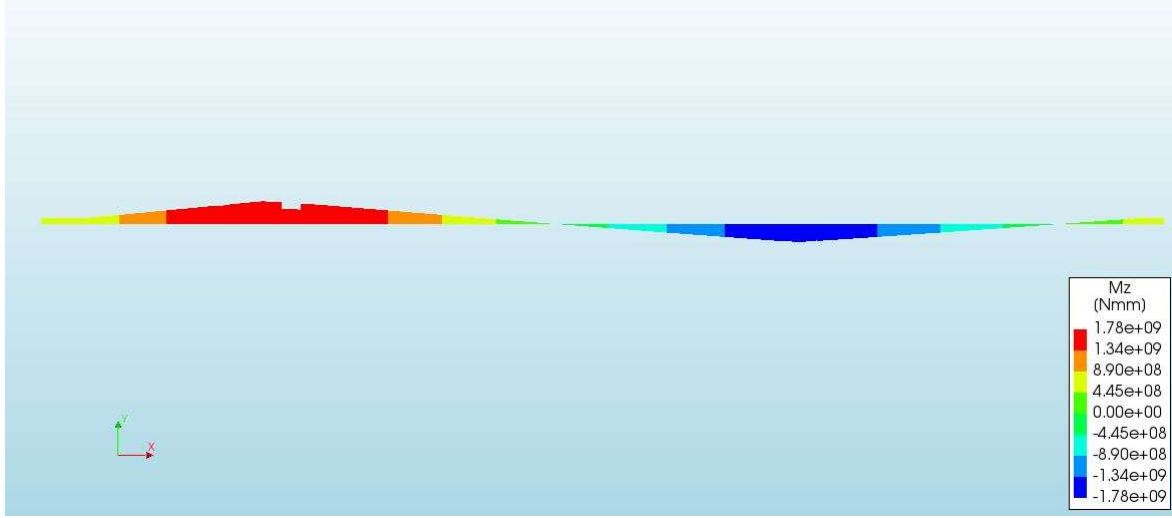


Figure 28, moment (Mz) at load step 58 (55), Model1

Examining the moment development at the six support points (Figure 21, Figure 22 & Table 9), it can be observed that SR is the first to reach the  $M_y^+$  at step 32. Each point, except SRR, reaches this point in subsequent steps. However, it is SL that reaches  $M_u^+$  first, indicating a redistribution of force to SL once SR reaches its yield point. In the next step, SL goes beyond the ultimate moment, resulting in the model's failure. Around the support is also where the largest (absolute) moments are developed. Additionally, the beam elements never go beyond the  $M_y^-$ , with the F1 point having the highest (negative) moment. In Appendix IIIe, an overview of which parts of Model 1 are in which phase of the  $M_n$ - $\kappa$  diagram can be found.

Further examination of the figures, tables and Appendix III – Additional information Chapter 3, after the initial loads are applied and the remaining loads (F1 & F2) of the model are applied. It can be observed that the curvature and moment over most of the right beam region do not change in orientation; however, there is a region that does change, best seen in the Appendix IIIe.

### Chapter 3.3.2 – FEM Analysis, Model 2

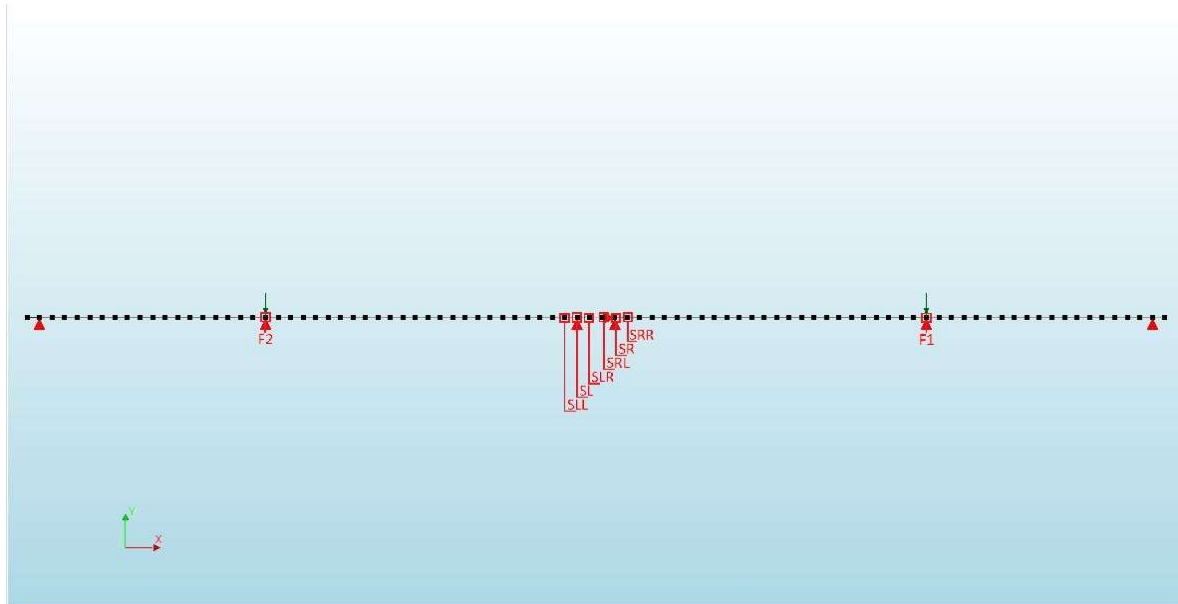


Figure 29, Model 2 with points (nodes) of interest

<b>F2</b>	location of F2	<b>SRL</b>	Right Support, left
<b>SLL</b>	Left Support, left	<b>SR</b>	Right Support
<b>SL</b>	Left Support, left	<b>SRR</b>	Right Support, right
<b>SLR</b>	Left Support, right	<b>F1</b>	location of F1

An overview of 8 points of interest in Model 2 can be seen in the Figure and Table above. For each point, the moment and curvature development were calculated and taken from Diana. The resulting  $M_n$ - $\kappa$  diagram for each point can be seen in the figures below. Note the calculated  $M_n$ - $\kappa$  diagram in the background of the figure, referred to as TB-c. It's important to note that Diana calculates curvature and moment on the left and right sides of each node. Therefore, the values represented in the figures are averaged values over the two sides.

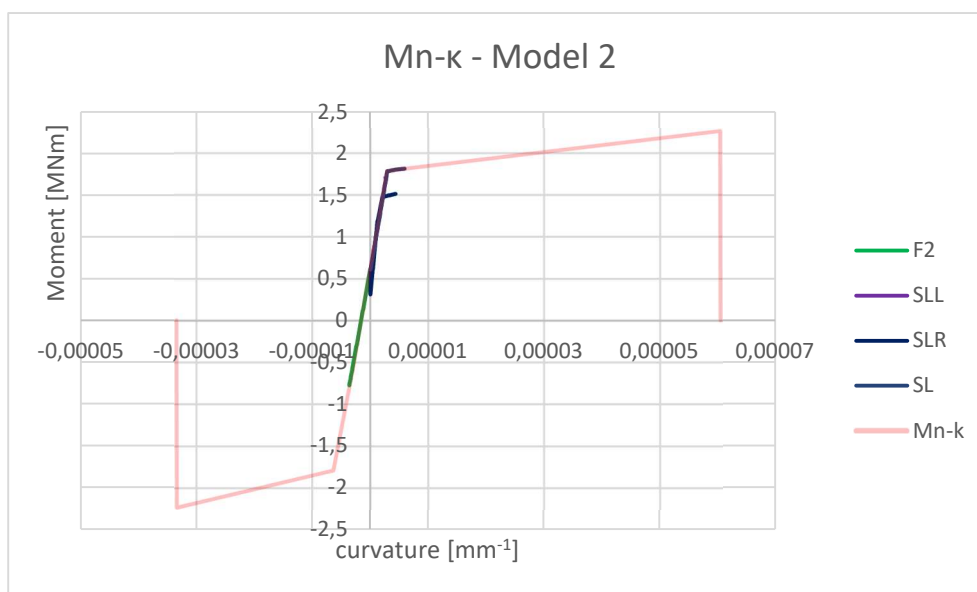


Figure 30, moment development, Model 2 (p1)

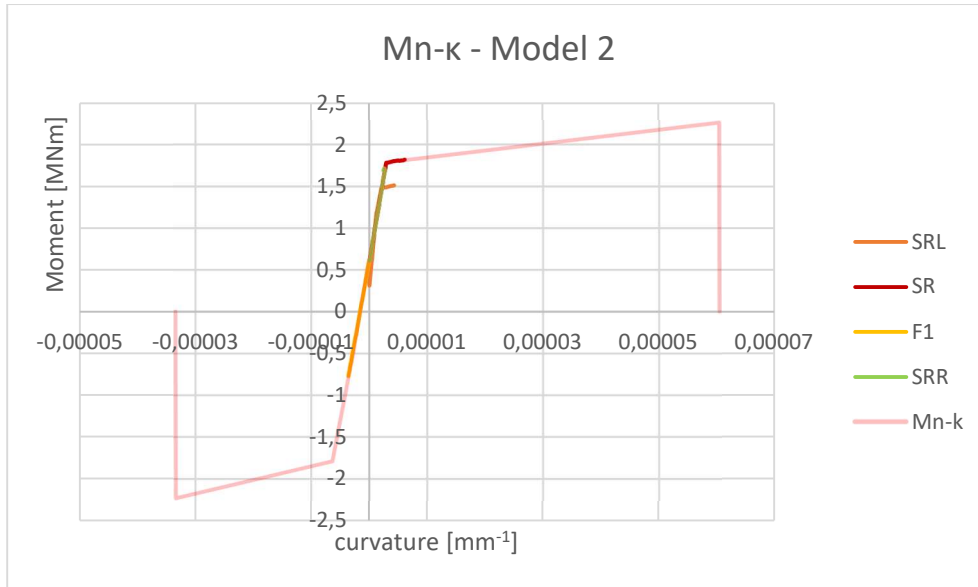


Figure 31, moment development, Model 2 (p2)

This time, all points behave as prescribed and follow the  $M_n$ - $\kappa$  diagram; however, they do not travel far on the diagram. It can also be observed that the lines for SLR and SRL do not exactly follow the  $M_n$ - $\kappa$  diagram, for the same reason as explained in Chapter 3.3.1 – FEM Analysis, Model 1. In the Table here below, an overview of the points of interest at which load step each point passes a certain curvature and moment respectively.

Table 10, points of interest curvature development – Model 2

	$\kappa_{cr}^+$	$\kappa_y^+$	$\kappa_u^+$		$\kappa_{cr}^-$	$\kappa_y^-$	$\kappa_u^-$
<b>SLL</b>	3	-	-	<b>F2</b>	-	-	-
<b>SL</b>	3	51	-	<b>F1</b>	3	-	-
<b>SLR</b>	3	-	-				
<b>SRL</b>	3	-	-				
<b>SR</b>	3	51	-				
<b>SRR</b>	3	-	-				

In the figures below, the moment distribution at load steps 3 & 51 (phase – LS 47) Each figure shows the curvature distribution in ‘auto-scale’ and with ‘specific value’, the ‘specific values’ will be within the following ranges:  $[\kappa_{cr}^-, \kappa_{cr}^+]$ ,  $[\kappa_y^-, \kappa_y^+]$ ,  $[M_{cr}^-, M_{cr}^+]$  &  $[M_y^-, M_y^+]$ . Please note Appendix IIIf and Appendix IIIg, show the development of the curvature ( $\kappa_z$ ) and moments ( $M_z$ ), a figure for every five load steps.

Non Lin Sta  
Phase - AP - ST II, Start-step 1, Load-factor 1.0000  
Curvatures Kz  
min: -3.10e-07/mm max: 5.44e-07/mm

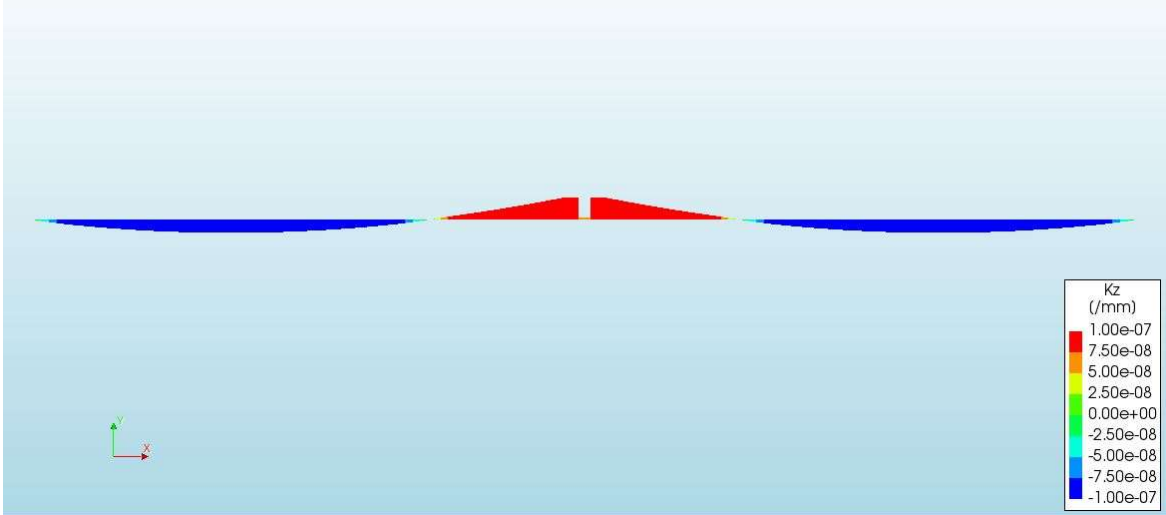


Figure 32, curvature (kz) at load step 3, Model 2

Non Lin Sta  
Phase - AP - ST II, Start-step 1, Load-factor 1.0000  
Cross-section Moments Mz  
min: 2.05e+08Nmm max: 8.15e+08Nmm

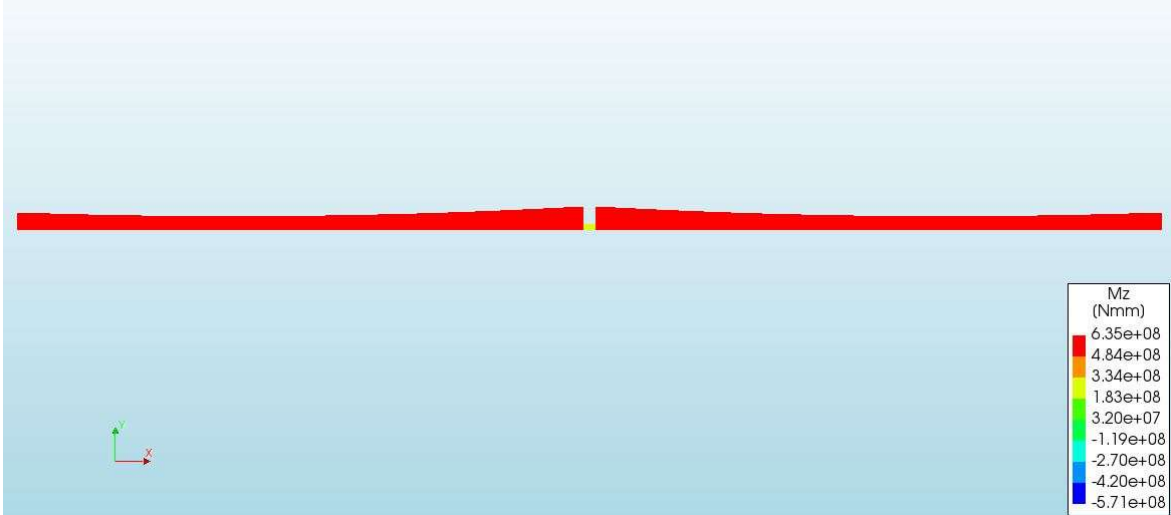


Figure 33, moment (Mz) at load step 3, Model 2

Non Lin Sta  
 Phase - AP - Applied Load, Load-step 47, Load-factor 0.46000, 03 - Applied Load  
 Curvatures Kz  
 min: -2.98e-06/mm max: 2.90e-06/mm

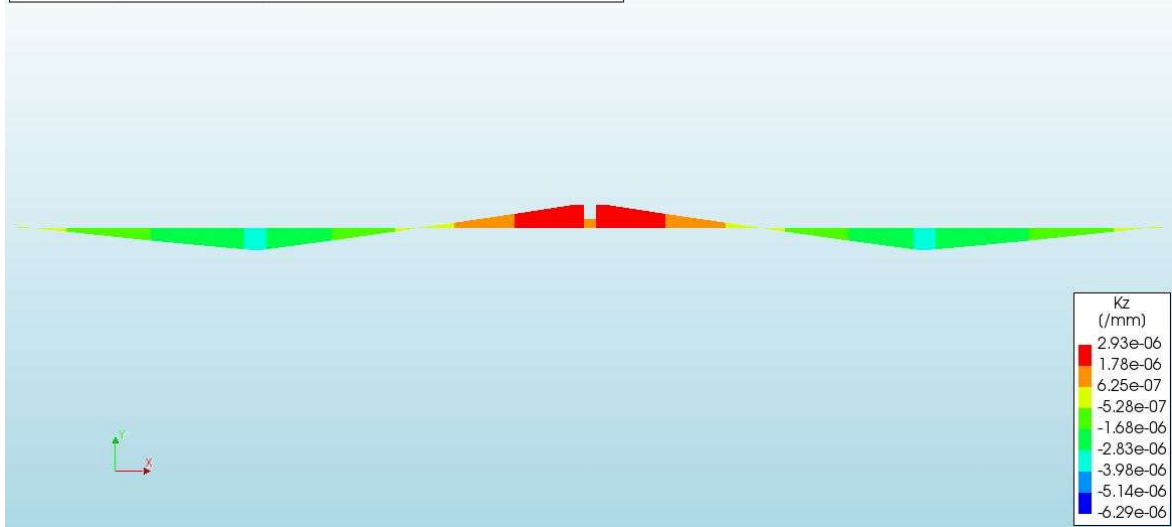


Figure 34, curvature (kz) at load step 51 (47), Model 2

Non Lin Sta  
 Phase - AP - Applied Load, Load-step 47, Load-factor 0.46000, 03 - Applied Load  
 Cross-section Moments Mz  
 min: -5.28e+08Nmm max: 1.77e+09Nmm

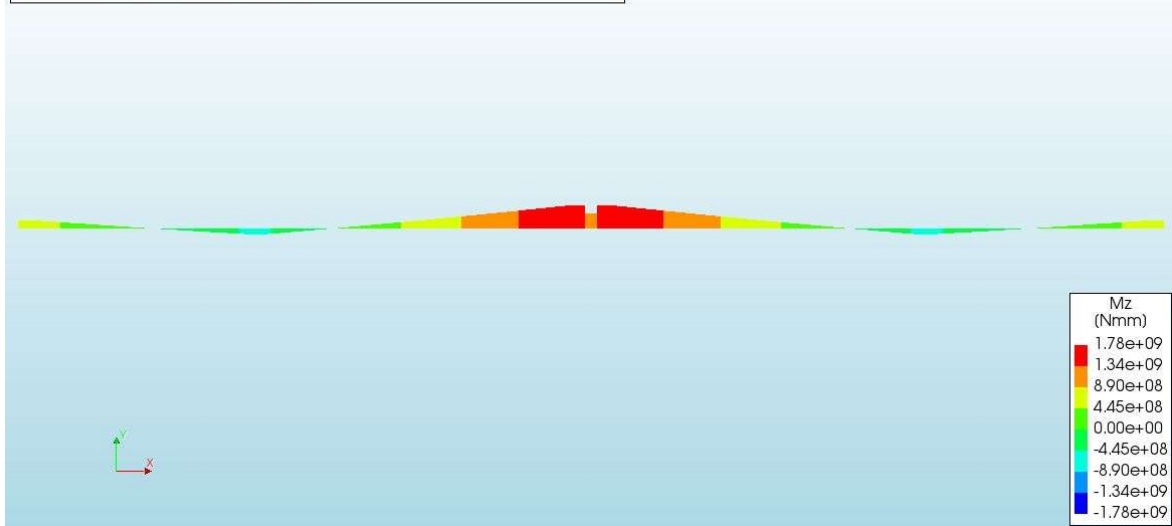


Figure 35, moment (Mz) at load step 51 (47), Model 2

Examining the moment development at the six support points (Figure 30, Figure 31 & Table 10), it can be observed that for Model 2, both the curvature and moment in the beams develop symmetrically. No single point takes the lead at any point during loading, this is to be expected due to the symmetry of the model itself. Again, the largest moment and curvature develop around the cross beam, similar to Model 1.

Further examination of the figures, tables and Appendix III – Additional information Chapter 3, after the initial loads are applied and the displacement-controlled load is applied, the curvature and moment over both beams do change in direction. Again, there is a region that goes from a positive moment to a negative moment, as seen in the curvature figures Appendix IIIf.

### Chapter 3.3.3 – FEM Analysis, Model 3

The initial load steps of Models 1 & 3 will be examined in this chapter. In the figure here below the results of the nonlinear analysis of Models 1 & 3 can be seen, each figure showing the moment ( $M_z$ ) of each model at the end of a phase.

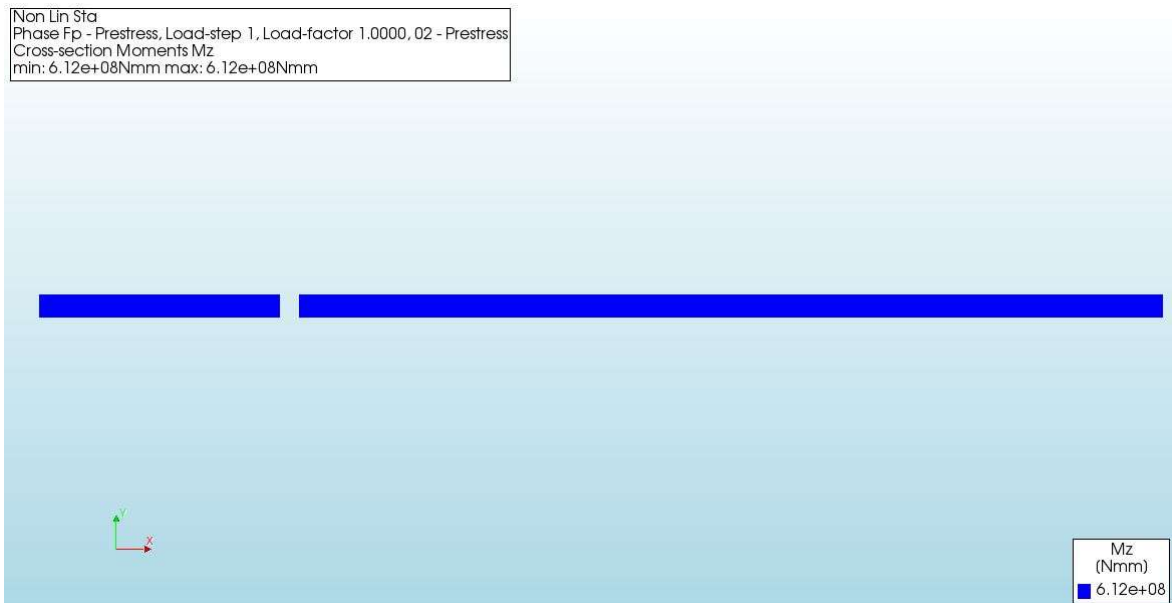


Figure 36, Model 1 phase 1

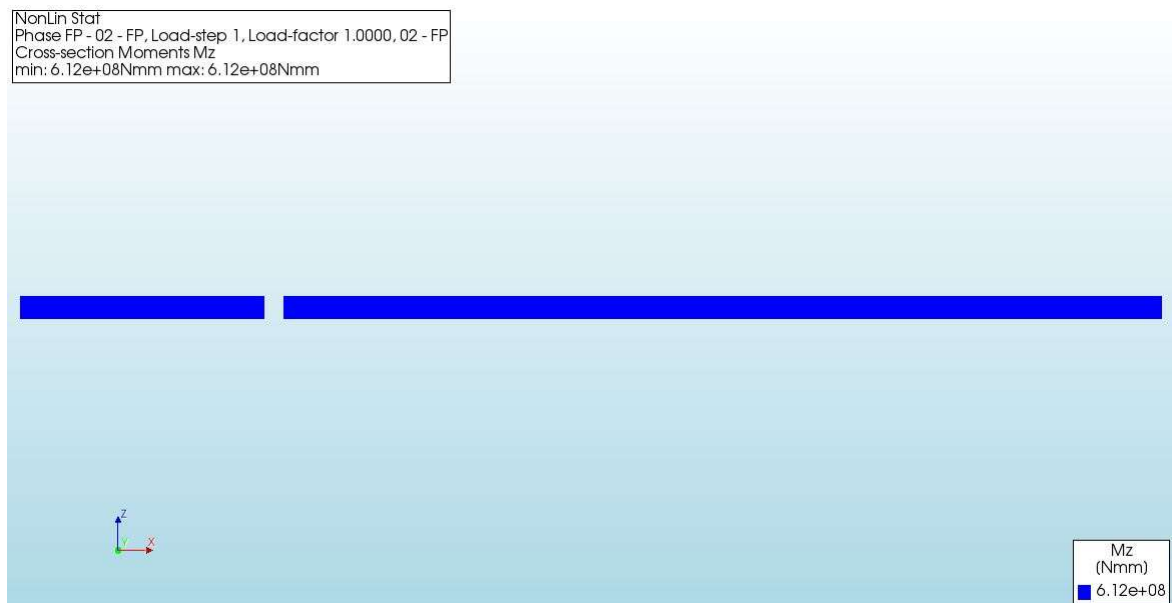


Figure 37, Model 3 phase 1

Non Lin Sta  
Phase SW - ST I, Start-step 1, Load-factor 1.0000  
Cross-section Moments Mz  
min: 1.20e+07Nmm max: 6.14e+08Nmm



Figure 38, Model 1 phase 2

NonLin Stat  
Phase - SW - ST II, Start-step 1, Load-factor 1.0000  
Cross-section Moments Mz  
min: 1.20e+07Nmm max: 6.14e+08Nmm



Figure 39, Model 3 phase 2

Non Lin Stat  
Phase - AP - ST II, Start-step 1, Load-factor 1.0000  
Cross-section Moments Mz  
min: 1.08e+08Nmm max: 8.17e+08Nmm

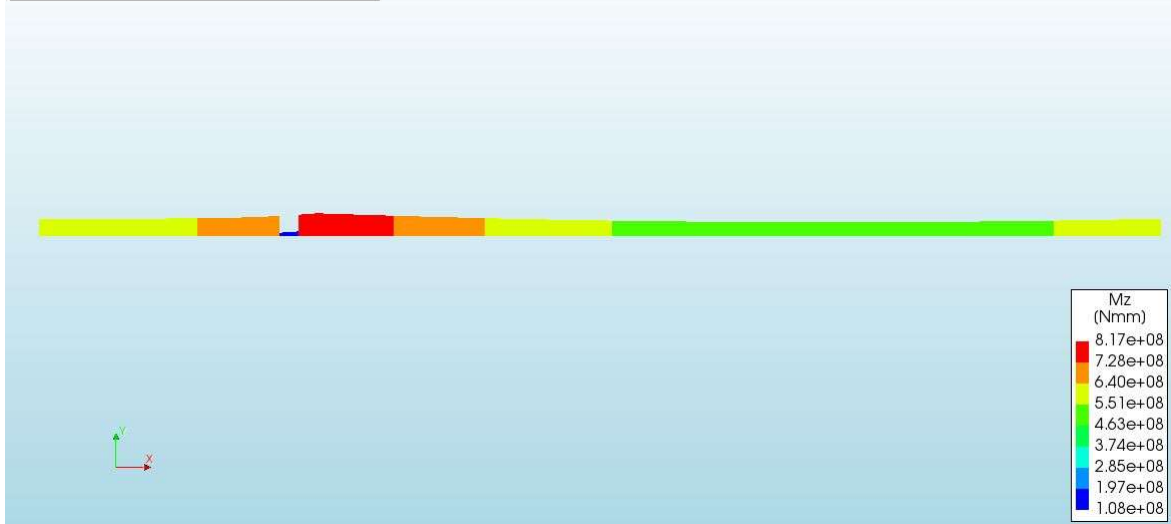


Figure 40, Model 1 phase 3

NonLin Stat  
Phase - AP - ST I, Start-step 1, Load-factor 1.0000  
Cross-section Moments Mz  
min: 1.08e+08Nmm max: 8.17e+08Nmm

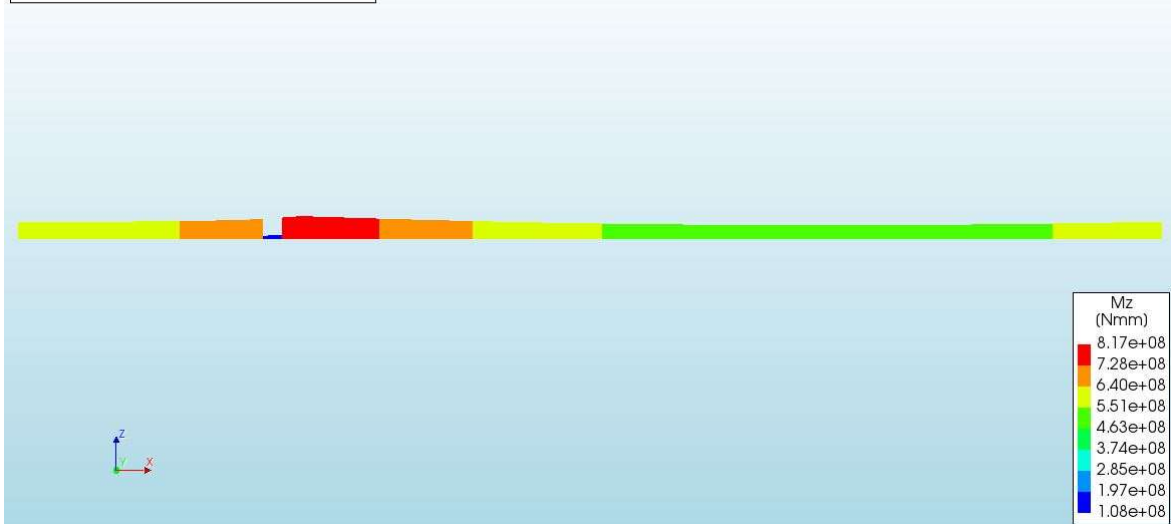


Figure 41, Model 3 phase 3

In all three sets of figures, it can be observed that the graphs are alike. The moments are the same, in both direction and scale. It can be assumed that the translation into the 3D modelling space was successfully done.

## Chapter 4 – Case Study 2

---

Case Study 2 involves constructing a full bridge deck model in a 3D environment and subjecting it to a traffic load. Two models will be created, both utilizing the same cross-sections for their elements, with the same dimensions, and material properties and lastly, the same traffic load will be applied to both models. The only difference between the models will be in their respective beam lengths. The traffic load applied will correspond to Load Model 1, specified in the NEN and RBK standards.

### *Chapter 4.1 – Case Study, Description*

The objective of this case will be to analyse the development of the moment and curvature changes over the length of the individual beams when subjected to the traffic load. The Models will be evaluated for their ability to withstand the applied traffic load, and the development of moment and curvature over the length of the beam will be scrutinized.

A key aspect of this case study involves determining the appropriate traffic load for the models, utilizing the ‘Nederlandse Normen’ (NEN) and the ‘Richtlijnen Beoordeling Kunstwerken’ (RBK) standards. The Service Limit State (SLS) and Ultimate Limit State (ULS) criteria will be established and applied to the models.

Contrary to Case Study 1, Case Study 2 will focus on analysing the structure integrity of the FEM models and assessing their ability to withstand the SLS and ULS. The case study will utilise characteristic values, as seen in Chapter 1.3 – Material properties of the Test Beam.

### *Chapter 4.2 – FEM Models*

Two 3D models, Models 4 & 5, will be developed. These models will comprise three main element sets: the combined beams, the support element, and the bridge deck. The combined beam and support elements will be modelled using the same element and material property types as seen for Model 3. Model 3 will be used as the starting point for the development of Models 4 & 5, they will share the element types, phasing, and other properties. In the Figure 42, FEM Model 4 can be seen and Figure 43, FEM Model 5 can be seen.

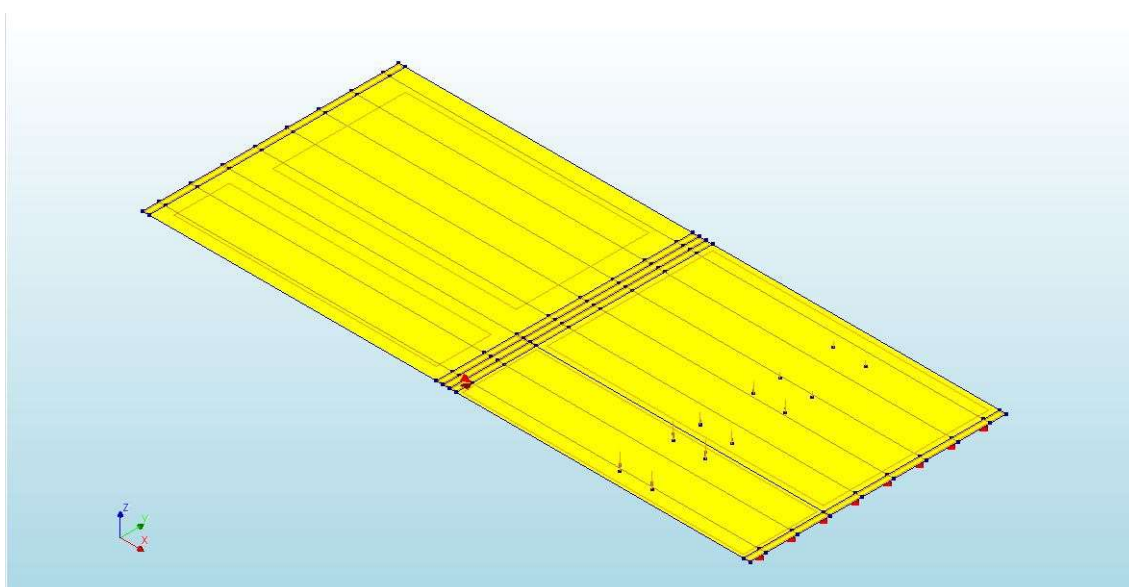


Figure 42, FEM Model 4

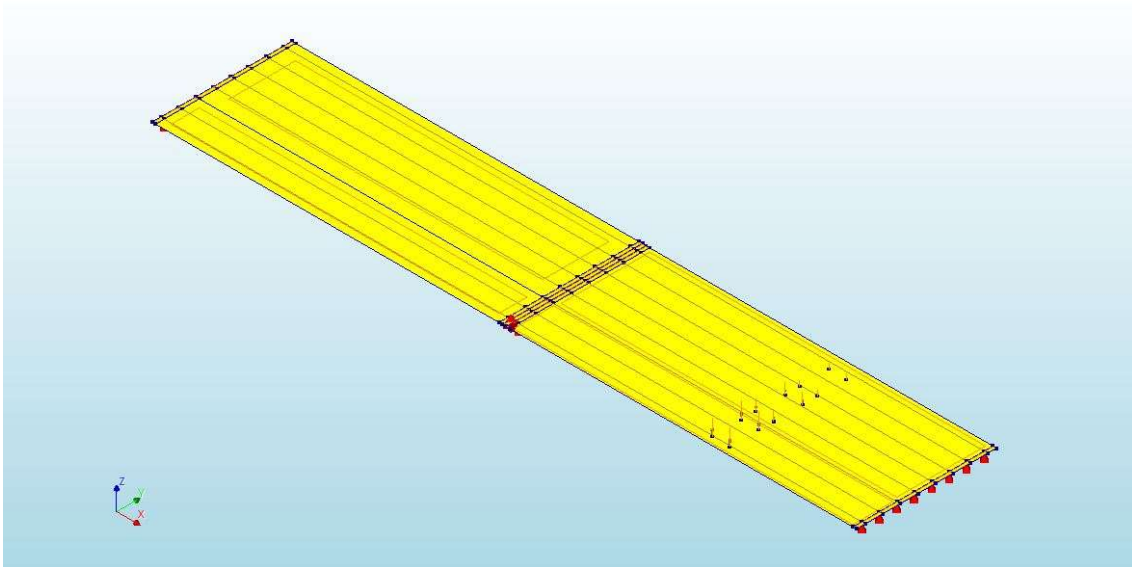


Figure 43, FEM Model 5

#### Chapter 4.2.1 – FEM Models, Description

The combined beam and cross beam elements will be modelled using a “Class-I Beams 3D”. Whereas the bridge deck elements will be modelled using “Flatt Shell” elements. The eight combined beams will be interconnected by adding a road deck element, represented by elements BDL & BDR. Although adding a road deck element increases the overall strength of the model, it is necessary to accurately model the transverse load distribution. A cracked concrete stiffness will be used for the deck, with the stiffness as  $E_{cm,dl}/3$ . The left deck will be connected to the right deck by the middle support element (M-Sup), consistent with the other models. The traffic load will be applied as described here below.

Models 4 will have a beam length like that of the Test beam and Model 1. Whereas Model 5 will have a beam length of 23450 [mm], this is the maximum length allowed if we use the ratio:  $L/h_b \approx 22 \rightarrow$  with  $h_b = 1070$  [mm] we get a  $L = 23540$  [mm]. For both models, the width will be determined by the traffic load, Load Model 1. The minimum width needed to apply a traffic load, from Load Model 1, is 9000 mm. However, our beams have a width of 1200 mm. Therefore, we need  $n_{beams} = 9000/1200 = 7.5 \rightarrow 8, W = 8 * 1200 = 9600$ [mm].

Models 4 & 5 will again introduce phases to the analysis to replicate the different construction phases of the beam and bridge construction. Models 4 & 5 will first have an initial phase with only the beams; they will be loaded by the prestress forces (01 -0- Prestress) and in the same phase by their self-weight and the correction load (02 -G- SW Beams). In phase two, the beams will connect, secondly connecting the decks to the beams on the left and right, and lastly, the mid-support (M-SUP.) to connect the left with the right side. In this phase, the self-weight of the mid-support element will be applied to the models (03 -G-SW SUP), and the permanent loads (04-P-Perm.). And lastly, the three sets of traffic loads, are as follows: 04 -P- Perm. Load, 05 -Qki- TL q1, 06 -Qki- TL q2 & 07 -Qki- TL F.

The above-mentioned loads describe Load Model 1, a traffic load scenario from NEN and RBK. In short, this traffic load scenario consists of a uniformly distributed force (Load 05 -Qki- TL q1 & 06 -Qki- TL q2) and axle concentrated loads (07 -Qki- TL F). A detailed explanation and calculation of the traffic load can be found in Appendix IVa.

#### Chapter 4.2.2 – FEM Models, Analysis

Models 4 & 5 will undergo a total of four analyses: a structural linear static analysis and three nonlinear static analyses. All three nonlinear analyses will use the same loads and phases. However, each analysis will differ in either safety factor, the extent of the load steps, or both. This analysis aims to examine how the bridge models react to the traffic load. By introducing 'Combinations' in the load case, Diana allows an easy method to combine Load Cases into one step and multiply them by their

appropriate safety factor, which is detailed in Chapter I. These load combinations will be used to recreate the two distinct load scenarios, namely the standard traffic load and the ULS traffic load.

#### Chapter 4.2.4 – FEM Models, Output

Outputs for Models 4 and 5 will be the displacement, curvature, and moments. All of which will be examined to determine stiffness development.

In Appendix IVb, an overview of the properties of the models can be found, including Diana model characteristics, general dimensions of the beams, material and cross-sectional properties, support types, the applied load values, and mesh properties.

### Chapter 4.3 – FEM Analysis

#### Chapter 4.3.1 – FEM Analysis, Model 4

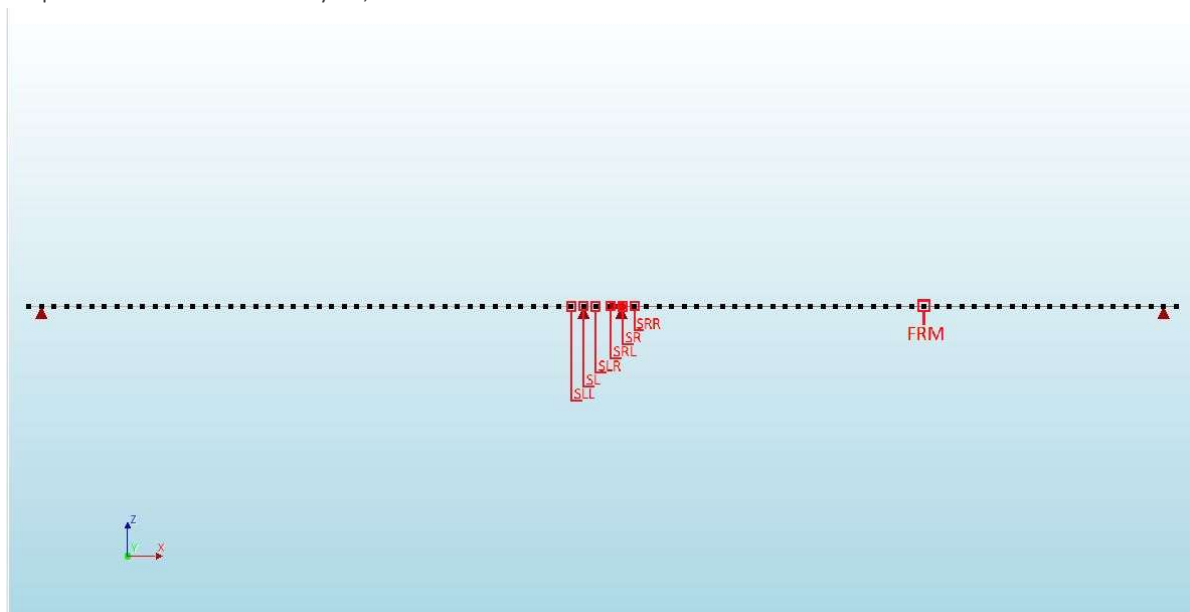


Figure 44, Model 4 with points (nodes) of interest

<b>SLL</b>	Left Support, left		<b>SR</b>	Right Support
<b>SL</b>	Left Support, left		<b>SRR</b>	Right Support, right
<b>SLR</b>	Left Support, right		<b>FRM</b>	the location between the two F1 points
<b>SRL</b>	Right Support, left			

An overview of 8 points of interest in Model 4 can be seen in the figure here above. These points are located around the cross beam section and at the centre of the traffic load, the right bottom beam will be examined. For each point, the moment and curvature development were calculated and taken from Diana. The resulting  $M_n-k$  diagram of each point can be seen in the figure below. Figure 45 and Figure 46 show the development till load step 100 (102) at which point the ULS is reached, whereas Figure 47 and Figure 48 show the development until failure. Note the calculated  $M_n-k$  diagram in the background of the figure, referred to as CB-m. It's important to note that Diana calculates curvature and moment on the left and right sides of each node. Therefore, the values represented in the figures are averaged values over the two sides. Also, note that all the results presented in this chapter are from the ULS (till failure) analyses.

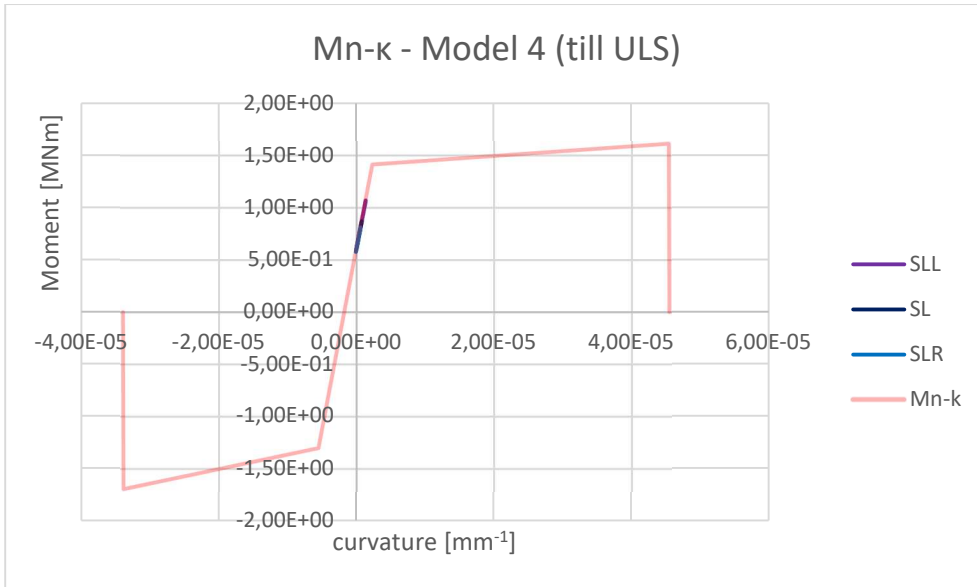


Figure 45, moment development, Model 4 till ULS (Load Step 100 (102)) (p1)

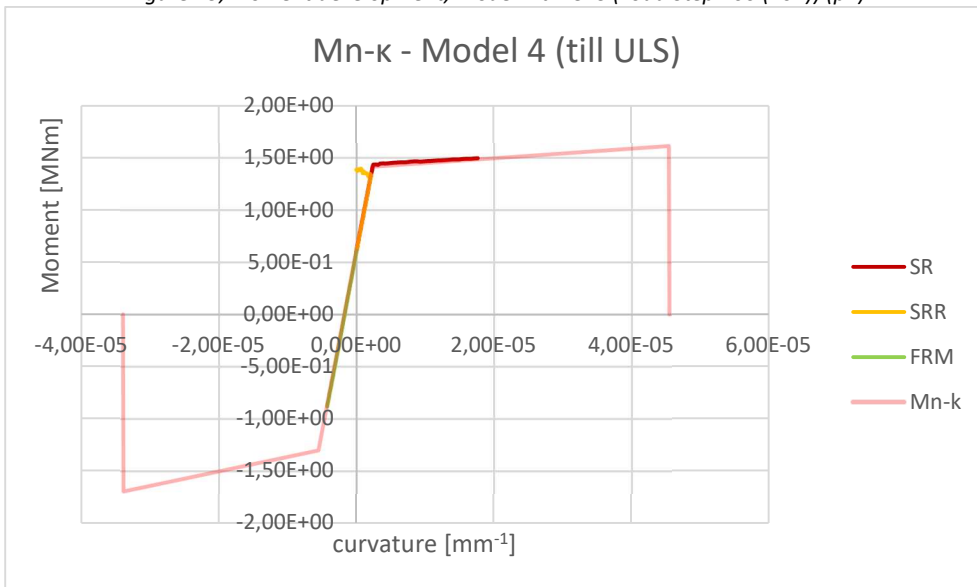


Figure 46, moment development, Model 4 till ULS (Load Step 100 (102)) (p2)

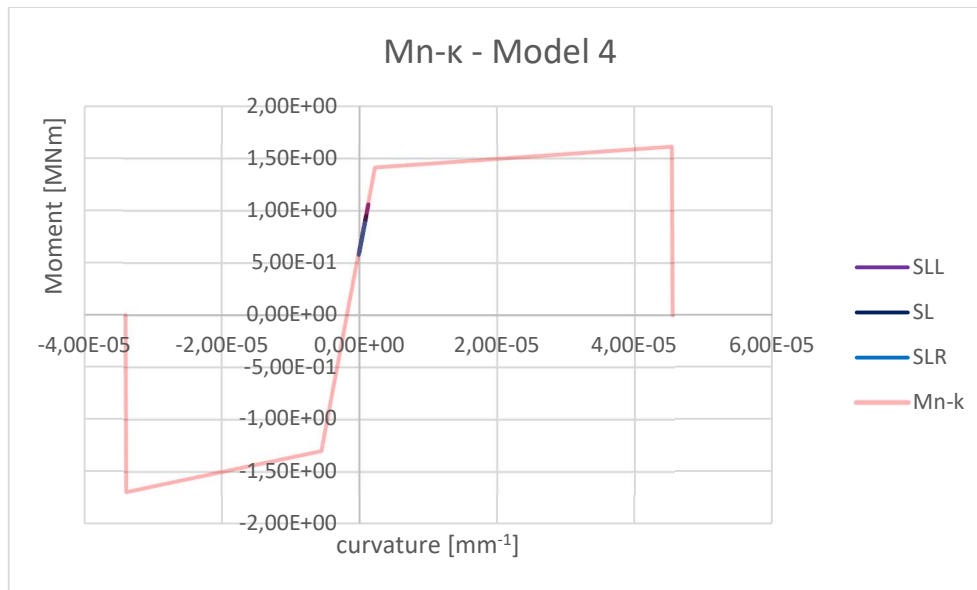


Figure 47, moment development, Model 4 (p1)

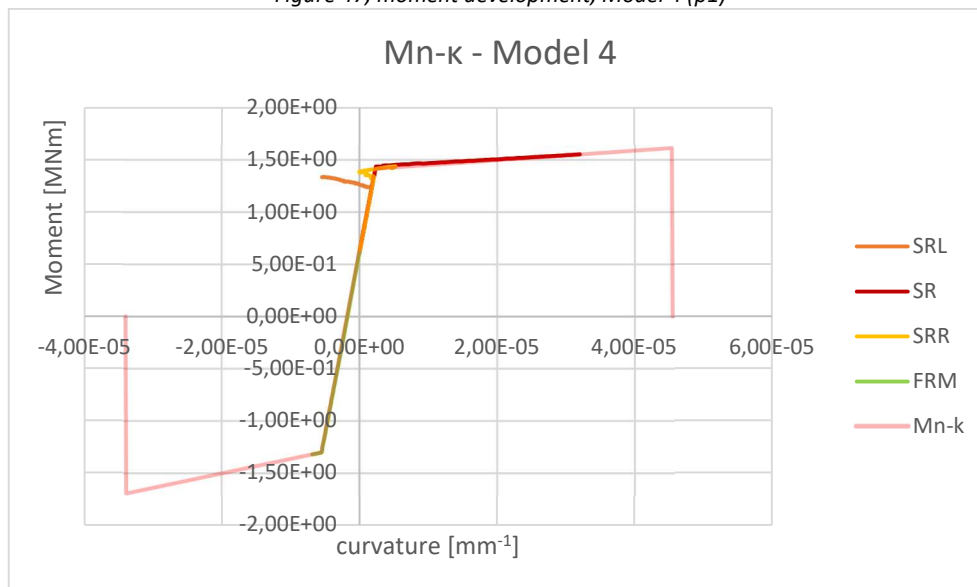


Figure 48, moment development, Model 4 (p2)

Points SLL, SL, SLR, and SR all behave as prescribed and follow the  $M_n$ - $\kappa$  diagram. However, the lines for SRL and SRR deviate from the  $M_n$ - $\kappa$  diagram. Upon closer examination, it can be observed that SRL deviates at load step 80, where the curvature decreases, turning into a negative curvature, while the moments continue to increase. Point SRR deviates at step 70 and returns at step 97. In the Table below, an overview of the points of interest and their curvature development can be seen.

Table 11, points of interest curvature development – Model 4

	$K_{cr}^-$	$K_{cr}^+$	$K_y^+$	$K_u^+$		$K_{cr}^-$	$K_y^-$	$K_u^-$
<b>SLL</b>	2	3	-	-	<b>FRM</b>	2	133	-
<b>SL</b>	2	3	-	-				
<b>SLR</b>	2	12	-	-				
<b>SRL</b>	2 & 94	3	-	-				
<b>SR</b>	2	3	67	-				
<b>SRR</b>	2 & 96	6 & 97	119	-				

When load step 102 is reached, where the ULS is met, all points have passed their cracking curvature. However, point SR has passed its yielding curvature.

In the figures below, the moment distribution at load steps 2, 67 (phase 2 - LS 65), 104 (phase 2 - LS 102), 133 (phase 2 - LS 129) & the final step 139 (phase 2 - LS 137) can be observed. Each figure shows the curvature distribution with 'auto-scale' and 'specific value', where the 'specific values' fall within the following ranges:  $[K_{cr}^-, K_{cr}^+]$ ,  $[K_Y^-, K_Y^+]$  &  $[K_U^-, K_U^+]$  &  $[M_{cr}^-, M_{cr}^+]$ ,  $[M_Y^-, M_Y^+]$  &  $[M_U^-, M_U^+]$ . Please note Appendix IVc and Appendix IVd which illustrates the development of curvature ( $\kappa_z$ ) and moments ( $M_z$ ), providing a figure for every 10 load steps.

Non Lin Sta ULS (till failure)  
 Set state - ST 1, Start-step 1, Load-factor 1.0000  
 Curvatures Kz  
 min: -8.70e-07/mm max: 7.19e-08/mm

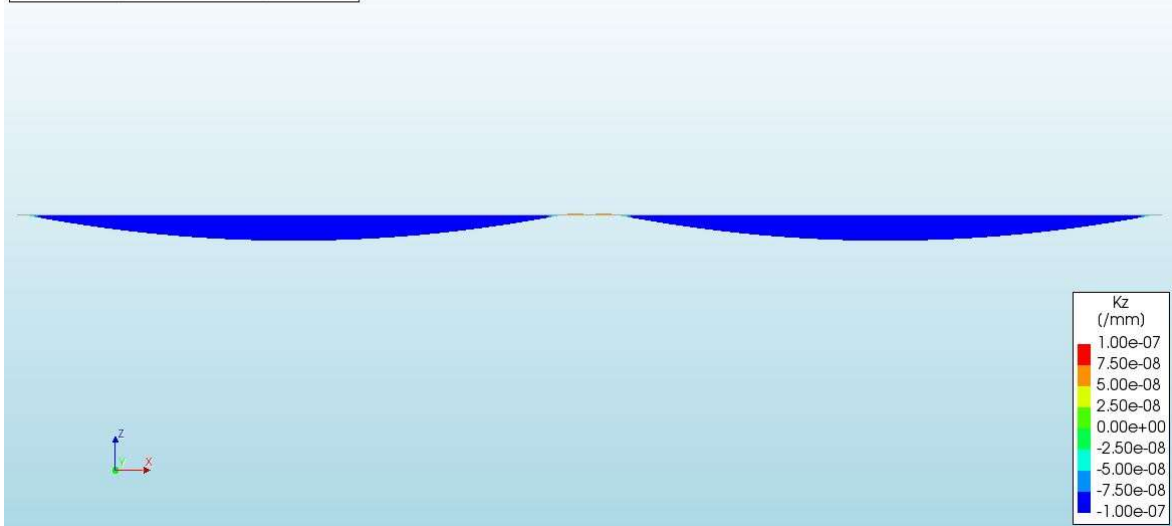


Figure 49, curvature ( $\kappa_z$ ) at load step 3, Model 4

Non Lin Sta ULS (till failure)  
 Set state - ST 1, Start-step 1, Load-factor 1.0000  
 Cross-section Moments Mz  
 min: 3.11e+08Nmm max: 6.38e+08Nmm

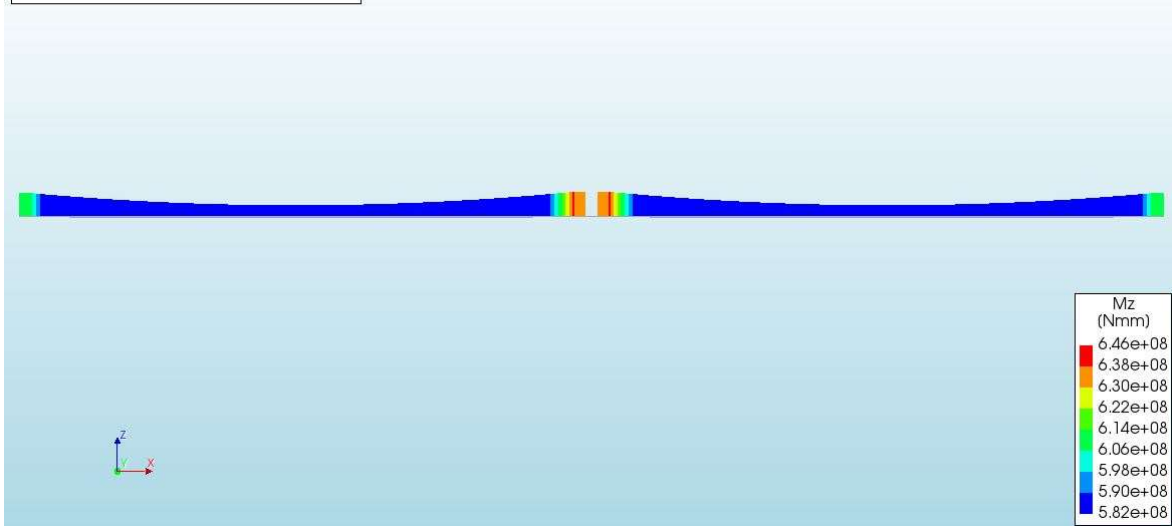


Figure 50, moment ( $M_z$ ) at load step 3, Model 4

Non Lin Sta ULS (Till Failure)  
 Set state - 04 - TL + Perm., Load-step 65, Load-factor 0.63000  
 Curvatures Kz  
 min: -2.90e-06/mm max: 2.33e-06/mm

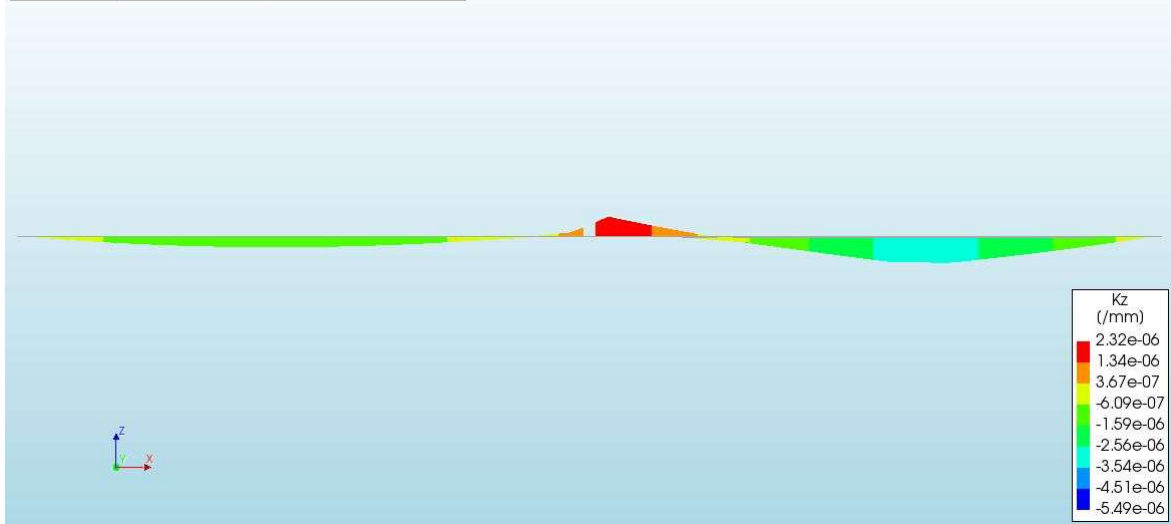


Figure 51, curvature (kz) at load step 67 (65), Model 4

Non Lin Sta ULS (Till Failure)  
 Set state - 04 - TL + Perm., Load-step 65, Load-factor 0.63000  
 Cross-section Moments Mz  
 min: -4.11e+08Nmm max: 1.41e+09Nmm

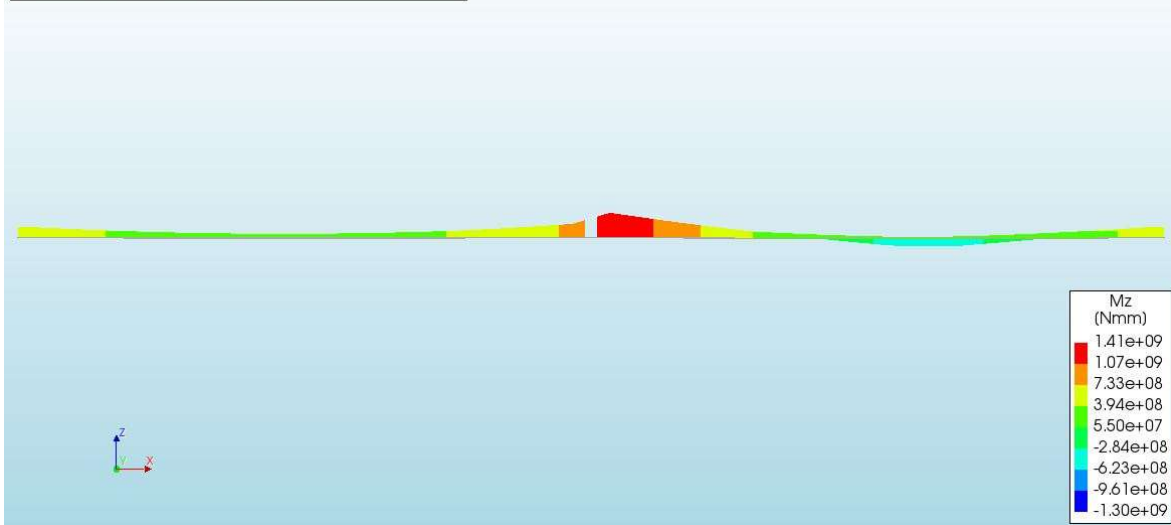


Figure 52, moment (Mz) at load step 67 (65), Model 4

Non Lin Sta ULS (Till Failure)  
 Set state - 04 - TL + Perm., Load-step 102, Load-factor 1.0000  
 Curvatures Kz  
 min: -4.35e-06/mm max: 2.22e-05/mm

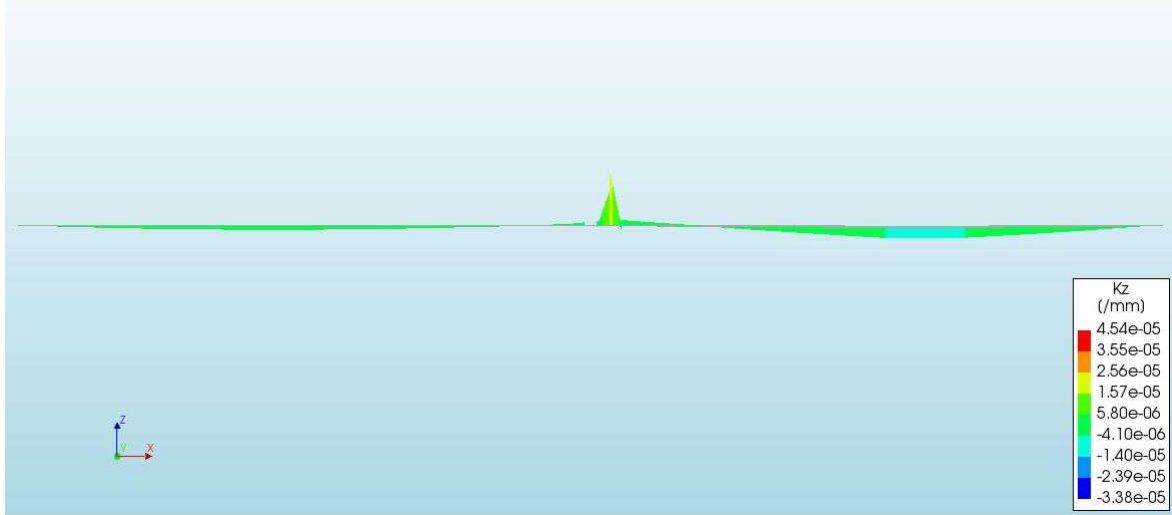


Figure 53, curvature (kz) at load step 104 (102), Model 4

Non Lin Sta ULS (Till Failure)  
 Set state - 04 - TL + Perm., Load-step 102, Load-factor 1.0000  
 Cross-section Moments Mz  
 min: -9.09e+08Nmm max: 1.50e+09Nmm

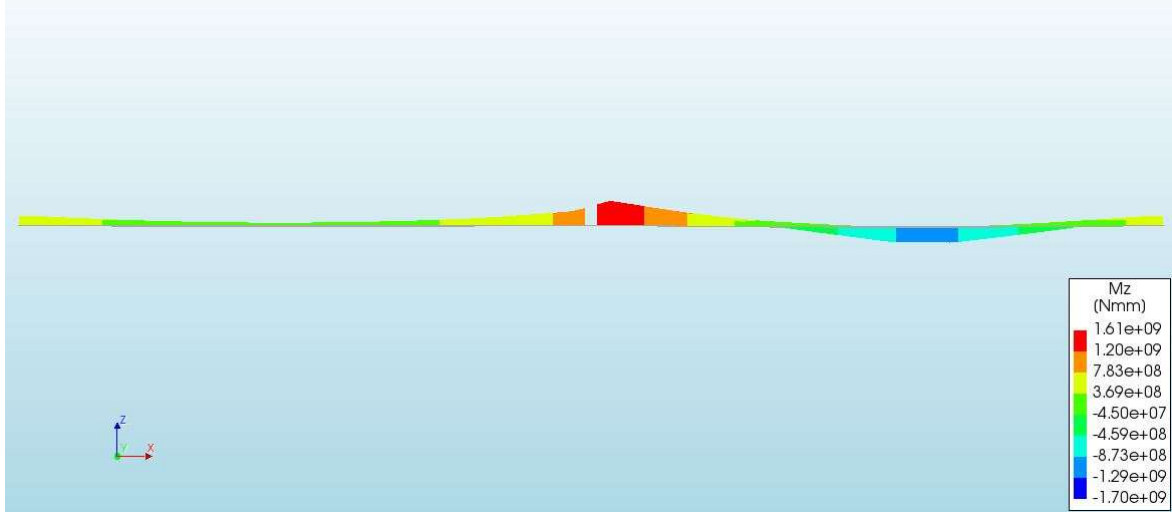


Figure 54, moment (Mz) at load step 104 (102), Model 4

Non Lin Sta ULS (Till Failure)  
 Set state - 04 - TL + Perm., Load-step 137, Load-factor 1.3500  
 Curvatures Kz  
 min: -7.78e-06/mm max: 3.31e-05/mm

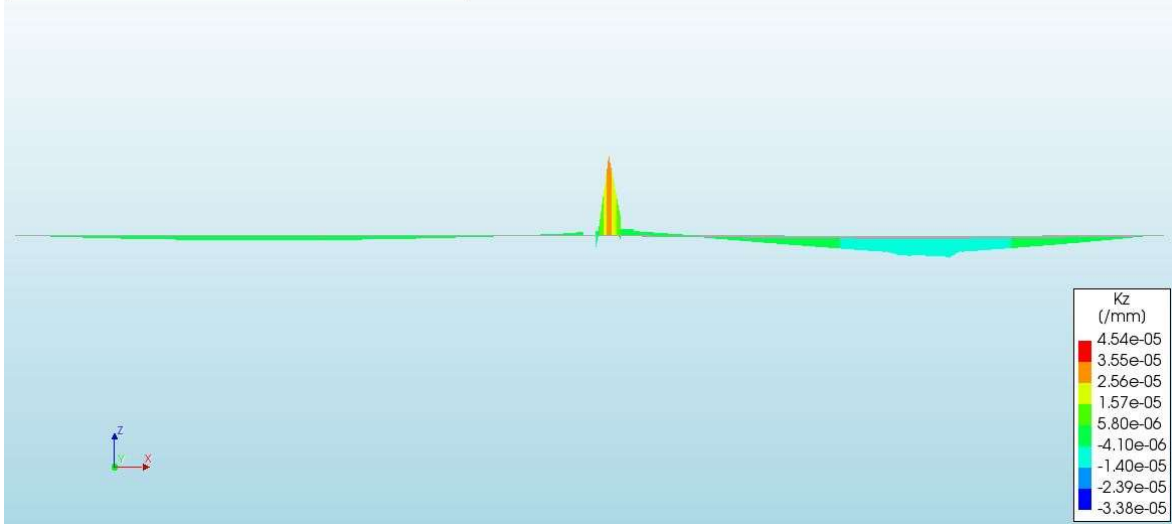


Figure 55, curvature (kz) at load step 133 (129), Model 4

Non Lin Sta ULS (Till Failure)  
 Set state - 04 - TL + Perm., Load-step 137, Load-factor 1.3500  
 Cross-section Moments Mz  
 min: -1.33e+09Nmm max: 1.55e+09Nmm

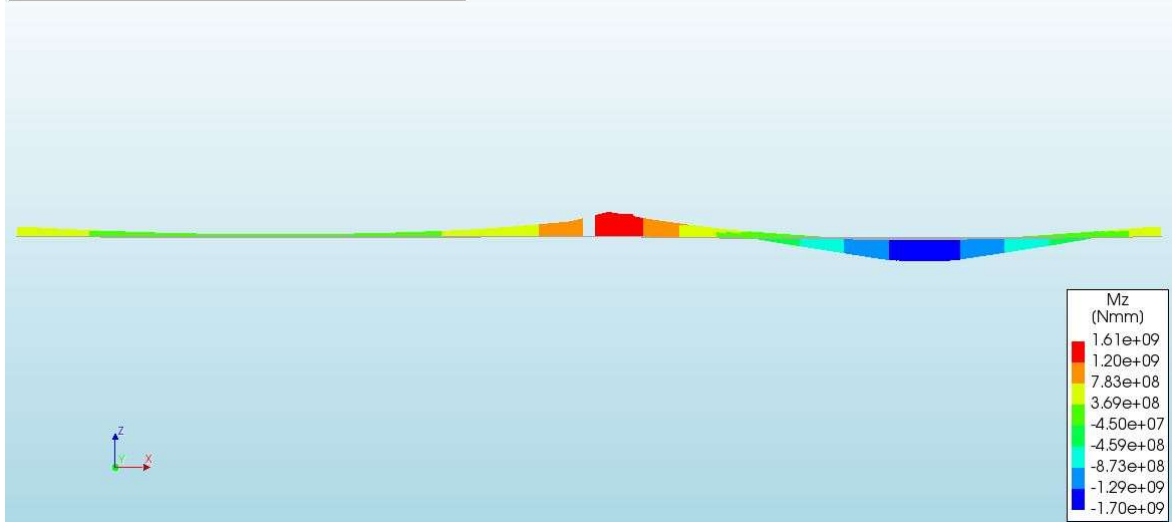


Figure 56, moment (Mz) at load step 133 (129), Model 4

Non Lin Sta ULS (Till Failure)  
 Set state - 04 - TL + Perm., Load-step 129, Load-factor 1.2700  
 Curvatures Kz  
 min: -5.49e-06/mm max: 3.07e-05/mm

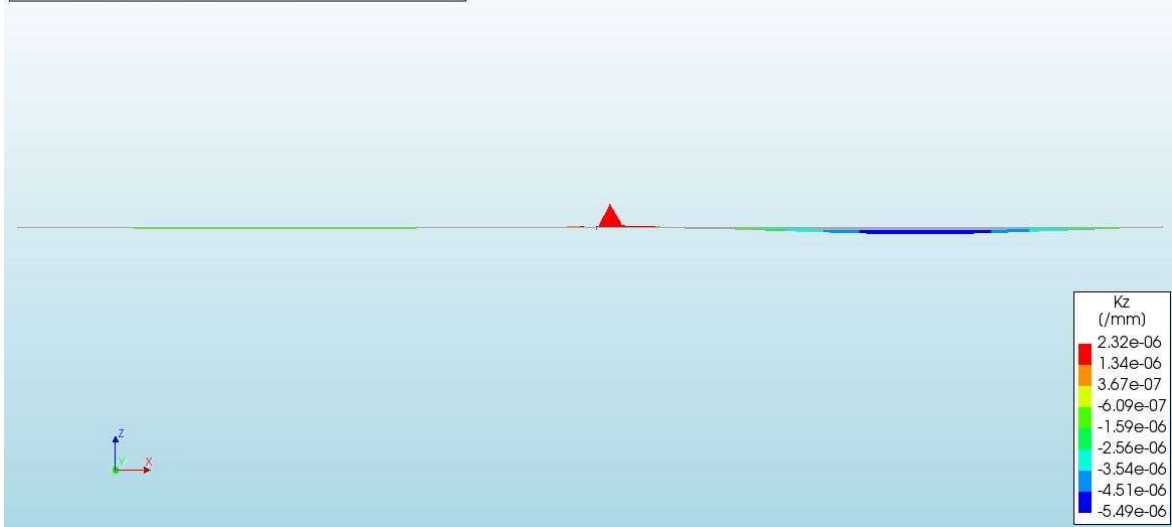


Figure 57, curvature (kz) at load step 139 (137), Model 4

Non Lin Sta ULS (Till Failure)  
 Set state - 04 - TL + Perm., Load-step 129, Load-factor 1.2700  
 Cross-section Moments Mz  
 min: -1.30e+09Nmm max: 1.54e+09Nmm

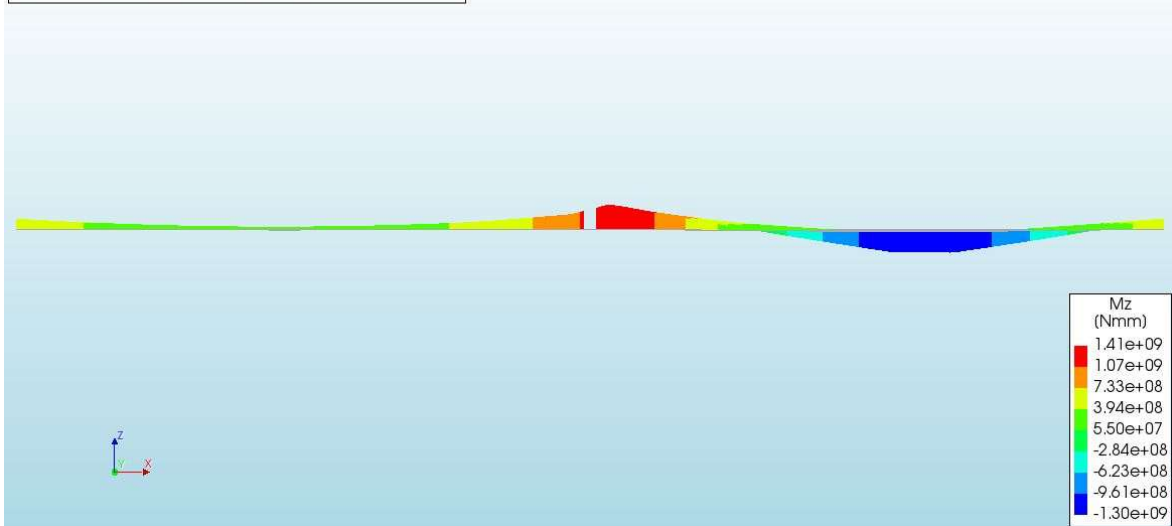


Figure 58m moment (Mz) at load step 139 (137), Model 4

It can be observed that the moments on the right side of the model produce higher values compared to the left side, with the bottom beam generating the highest, as expected. Further examination of the development of the moment at the six support points of interest (Figure 47, Figure 48 & Table 11), SR is the first to reach  $M_y^+$  at step 67. Point SRR also reaches  $M_y^+$  at step 97. Point FRM only reaches  $M_y^-$ , and further inspection of the model shows that the region around this point (FRM) also reaches this moment. Note that throughout the whole model, no node reaches  $M_u^-$  or  $M_u^+$ . With the highest negative moment at the point FRM and the highest positive moment at point SR.

Examining the figures in Appendix IVd, a region which changes its moment orientation can be observed. A region where the moments increase in value until load step 130. However, in the next figure for load step 140, this region has decreased, and in the final image, the region has once again increased. This phenomenon is not very pronounced in the curvature figures, as shown in Appendix IVe.

Chapter 4.3.2 – FEM Analysis, Model 5

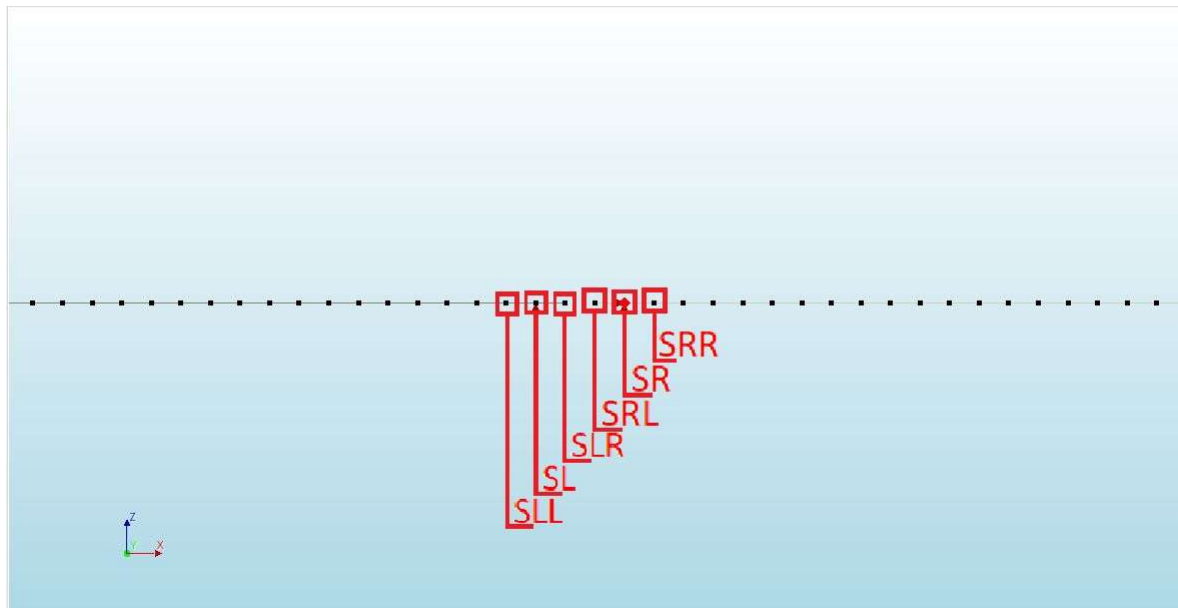


Figure 59, Model 5 with points (nodes) of interest

<b>SLL</b>	<b>Left Support, left</b>	<b>SR</b>	<b>Right Support</b>
<b>SL</b>	Left Support, left	SRR	Right Support, right
<b>SLR</b>	Left Support, right	FRM	the location between the two F1 points
<b>SRL</b>	Right Support, left		

An overview of 8 points of interest in Model 5 can be seen in the figure here above. These points are located around the cross beam section and at the centre of the traffic load, the right bottom beam will be examined. For each point, the moment and curvature development were calculated and taken from Diana. The resulting  $M_n$ - $\kappa$  diagram of each point can be seen in the figure below. Note the calculated  $M_n$ - $\kappa$  diagram in the background of the figure, referred to as CB-m. It's important to note that Diana calculates curvature and moment on the left and right sides of each node. Therefore, the values represented in the figures are averaged values over the two sides. Also, note that all the results presented in this chapter are from the ULS (till failure) analyses.

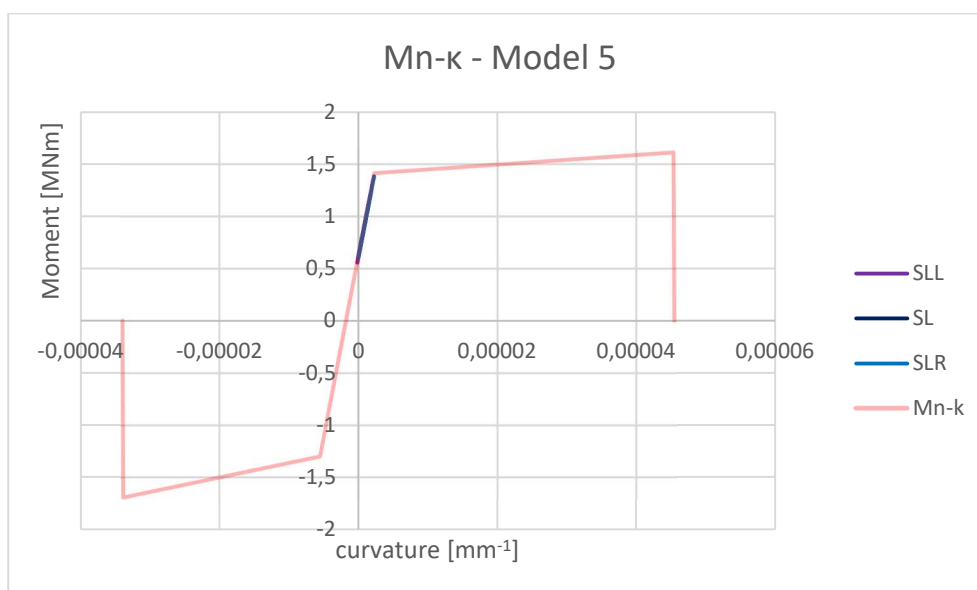


Figure 60, moment development, Model 5 (p1)

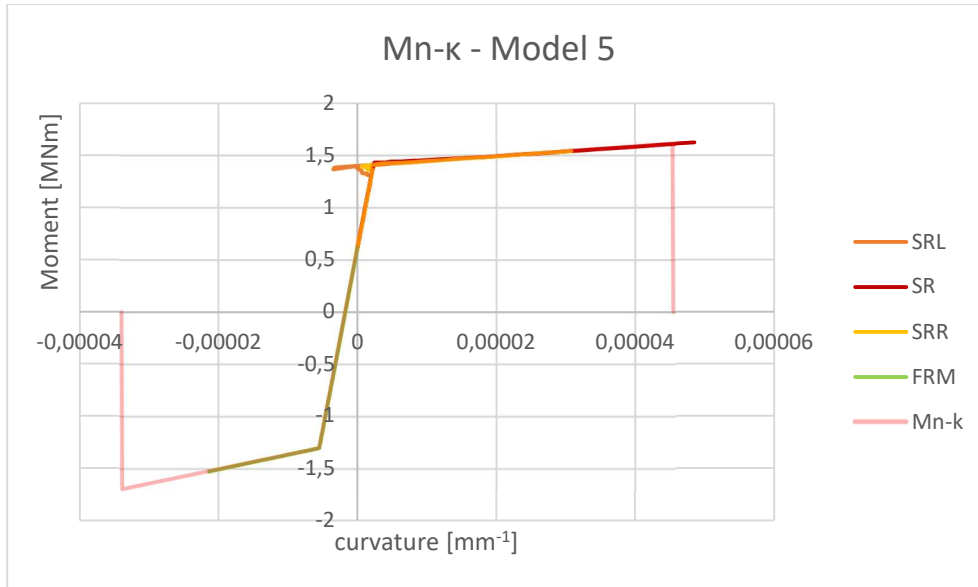


Figure 61, moment development, Model 5 (p2)

Points SLL, SL, SLR, and SR all adhere to the prescribed  $M_n$ - $\kappa$  diagram. However, the lines for SRL and SRR deviate from the  $M_n$ - $\kappa$  diagram. Upon closer examination, it is observed that SRL deviates at load step 28, and SRR deviates at step 31. SRL returns to the diagram at step 39, and SRR returns at step 34. In the Table below, an overview of the points of interest and their curvature development can be seen.

Table 12, points of interest curvature development – Model 5

	$\kappa_{cr}^-$	$\kappa_{cr}^+$	$\kappa_y^+$	$\kappa_u^+$		$\kappa_{cr}^-$	$\kappa_y^-$	$\kappa_u^-$
<b>SLL</b>	2	3	-	-	<b>FRM</b>	2	33	-
<b>SL</b>	2	3	-	-				
<b>SLR</b>	2	3	-	-				
<b>SRL</b>	2 & 39	3 & 45	47	-				
<b>SR</b>	2	3	27	51				
<b>SRR</b>	2	3	37	-				

Additionally, in the figures below, the moment distribution at load step 3, 27 (phase 2 - LS 25), 33 (phase 2 - LS 31) & 51 (phase 2 - LS 49) can be observed. Each figure displays the curvature distribution in 'auto-scale' and with 'specific value'. The 'specific values' will be within the following ranges:  $[\kappa_{cr}^-, \kappa_{cr}^+]$ ,  $[\kappa_y^-, \kappa_y^+]$  &  $[\kappa_u^-, \kappa_u^+]$  &  $[M_{cr}^-, M_{cr}^+]$ ,  $[M_y^-, M_y^+]$  &  $[M_u^-, M_u^+]$ . Please note that Appendix IVf and Appendix IVg show the development of curvature ( $\kappa_z$ ) and moments ( $M_z$ ), with a figure for every 10 load steps.

Non Lin Sta ULS  
Load State - AL - ST II, Start-step 1, Load-factor 1.0000  
Curvatures Kz  
min: -4.09e-06/mm max: 4.30e-07/mm

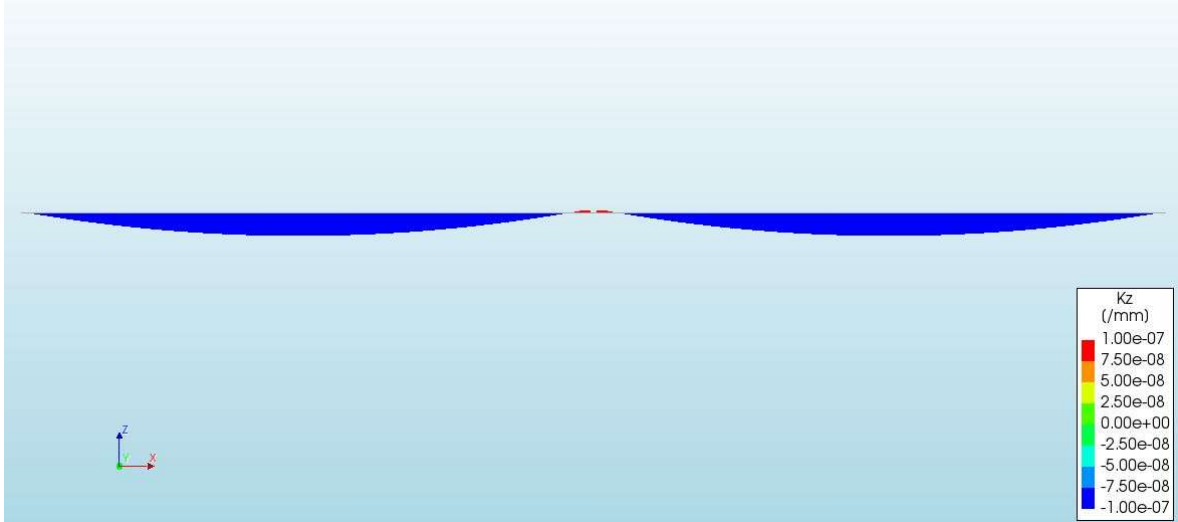


Figure 62, curvature (kz) at load step 3, Model 5

Non Lin Sta ULS  
Load State - AL - ST II, Start-step 1, Load-factor 1.0000  
Cross-section Moments Mz  
min: -8.12e+08Nmm max: 7.61e+08Nmm

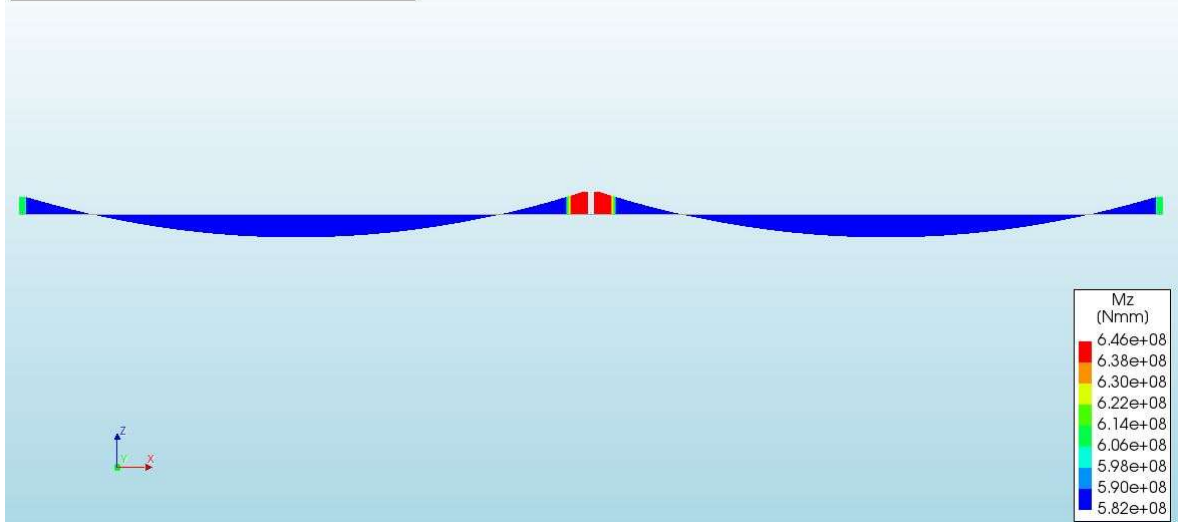


Figure 63, moment (Mz) at load step 3, Model 5

Non Lin Sta ULS  
 Phase 2, Load-step 25, Load-factor 0.23000  
 Curvatures Kz  
 min: -5.15e-06/mm max: 2.36e-06/mm

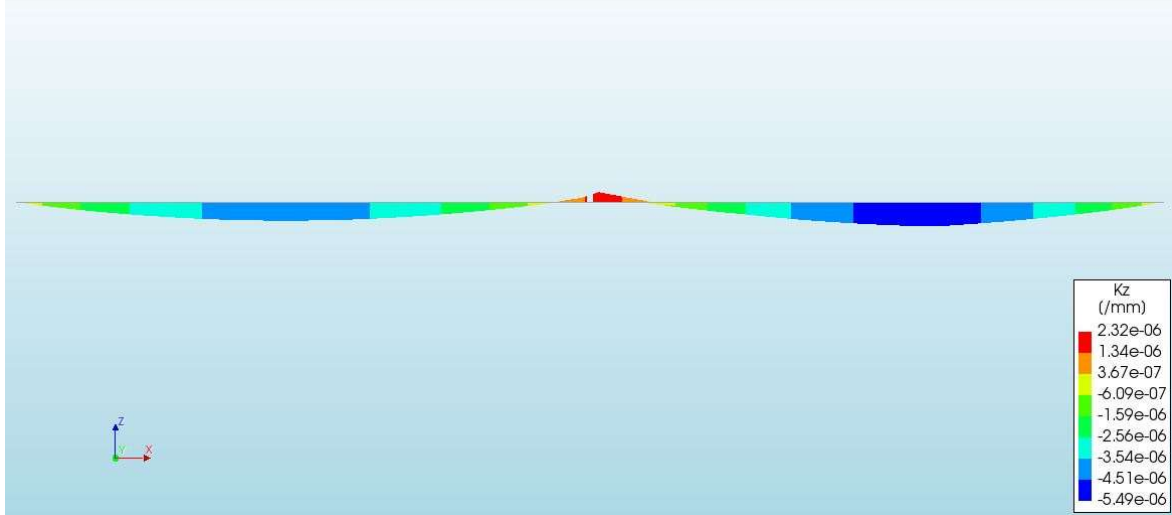


Figure 64, curvature (kz) at load step 27 (25)

Non Lin Sta ULS  
 Phase 2, Load-step 25, Load-factor 0.23000  
 Cross-section Moments Mz  
 min: -1.18e+09Nmm max: 1.42e+09Nmm

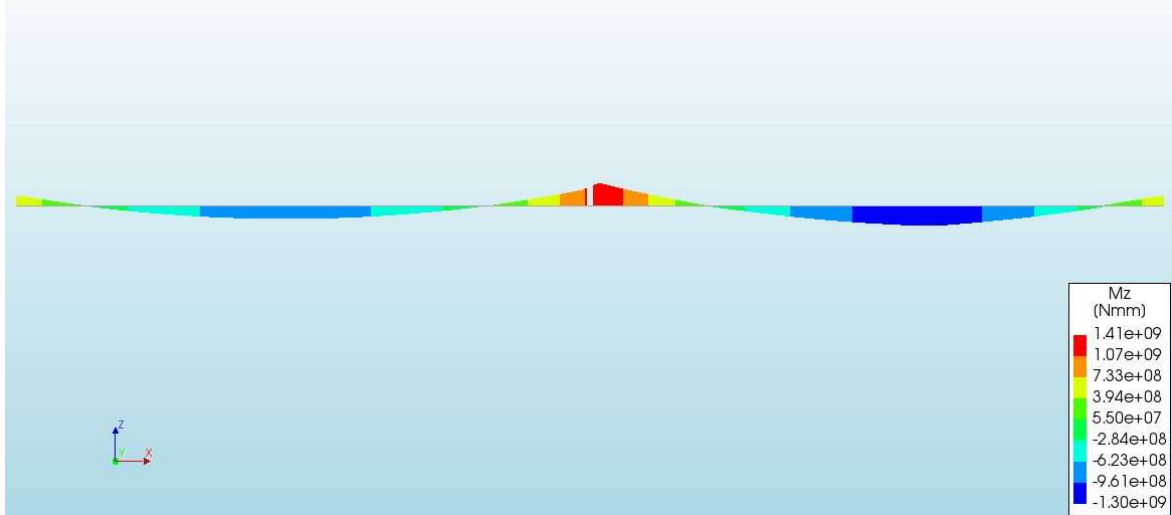


Figure 65, moment (Mz) at load step 27 (25), Model 5

Non Lin Sta ULS  
Phase 2, Load-step 31, Load-factor 0.29000  
Curvatures Kz  
min: -6.49e-06/mm max: 1.26e-05/mm

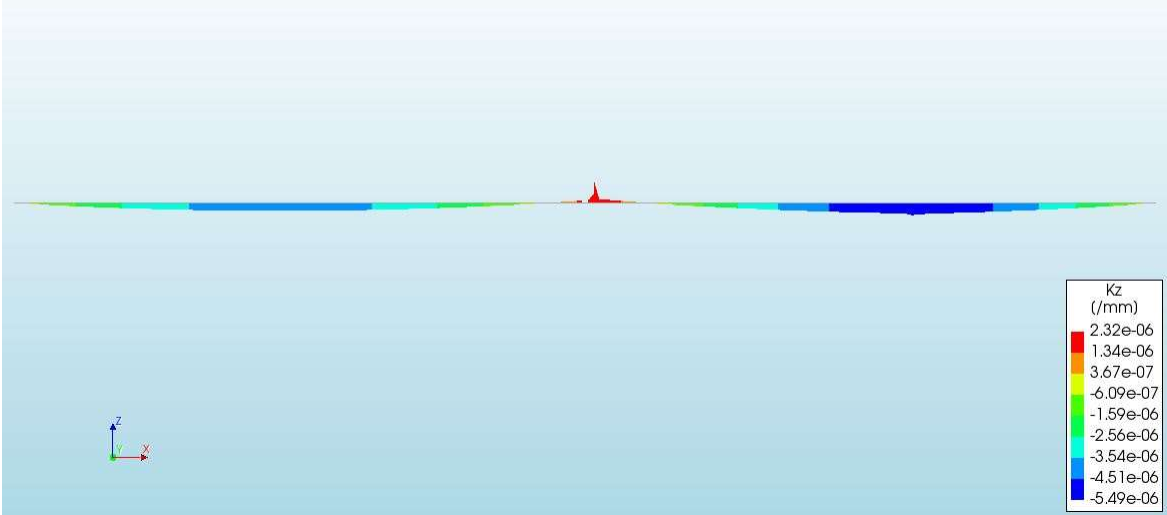


Figure 66, curvature (kz) at load step 33 (31), Model 5

Non Lin Sta ULS  
Phase 2, Load-step 31, Load-factor 0.29000  
Cross-section Moments Mz  
min: -1.31e+09Nmm max: 1.46e+09Nmm

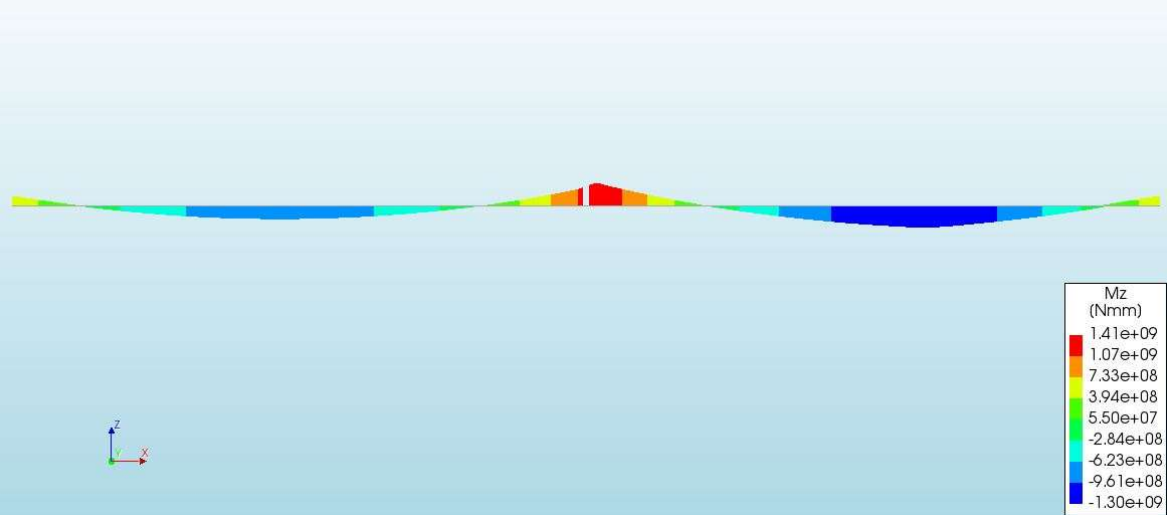


Figure 67, moment (Mz) at load step 33 (31), Model 5

Non Lin Sta ULS  
 Phase 2, Load-step 49, Load-factor 0.47000  
 Curvatures Kz  
 min: -2.12e-05/mm max: 4.65e-05/mm

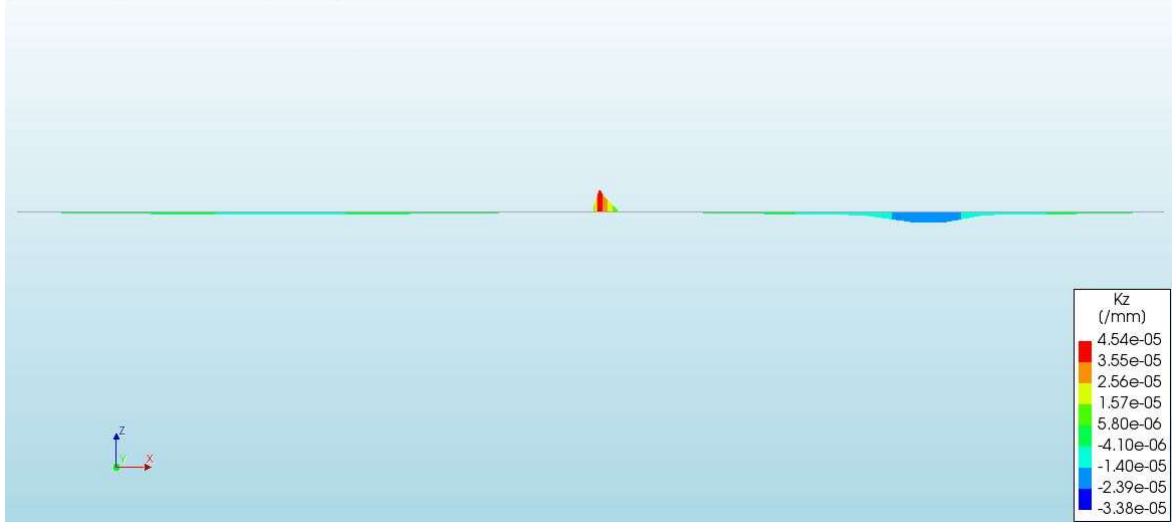


Figure 68, curvature (kz) at load step 51 (49), Model 5

Non Lin Sta ULS  
 Phase 2, Load-step 49, Load-factor 0.47000  
 Cross-section Moments Mz  
 min: -1.52e+09Nmm max: 1.62e+09Nmm

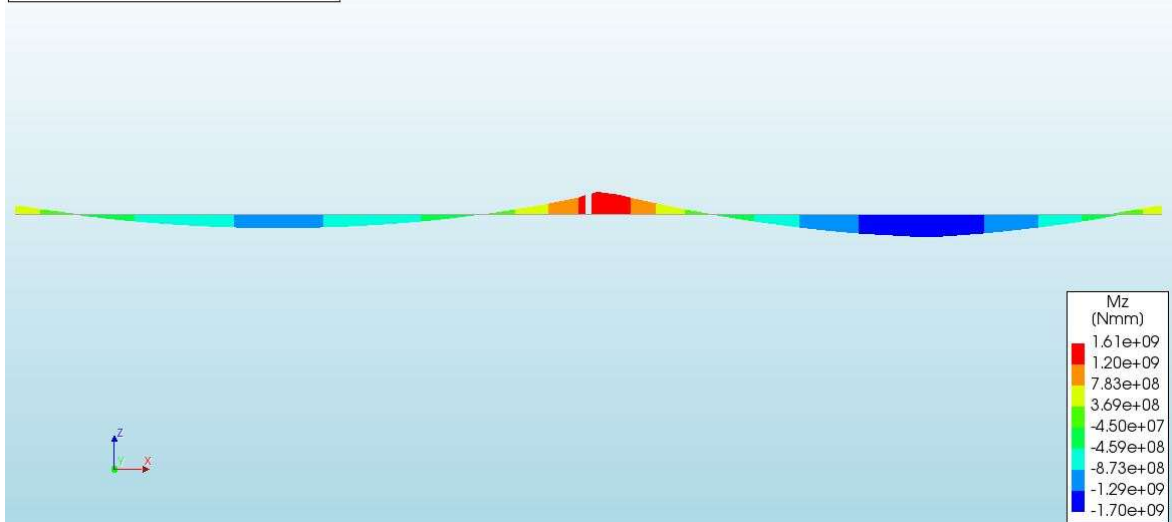


Figure 69, moment (Mz) at load step 51 (49), Model 5

Firstly, it can be observed that moments on the right side of the model produce higher values compared to the left side, with the bottom beam generating the highest, as expected. Further examination, of the development of the moment at the six support points (Figure 60, Figure 61 & Table 12), it can be determined that SR is the first to reach  $M_y^+$  at step 27. Each point around the right support reaches  $M_y^+$  at some point, with the point around the left support never reaching  $M_y^+$ , and ultimately, point SR reaches  $M_u^+$ . In the next step, the model fails. With further examination, the beam elements never reach  $M_u^-$ , with the highest (negative) Moment occurring at point FRM, surpassing  $M_y^-$ . Again, the highest moments are produced at points SR with the highest positive moment and FRM with the highest negative moment. Examining the figures Appendix IVg, the phenomenon of changing moment orientation can again be observed. However, this time the model fails prematurely before anything unique or interesting happens.

## Discussion

### Moment-curvature Diagrams

When examining the four moment-curvature diagrams in Chapter 2.3 – Moment-Curvature Diagrams, Figure 11, Figure 12, Figure 13 & Figure 14, some intriguing differences can be observed—some of which might be expected, while others require further analysis. First off, let's consider the difference in the number of points for the combined beam diagram compared to the cross beam diagram. The additional  $M_y^-$  point was added due to a change in slope before and after the point. However, this point was later abandoned, as Diana works best with as few points as possible.

Each diagram seems to have its curvature range, which is expected as each diagram originates from a cross-section that uses a different combination of cross-sectional dimensions, elements, and materials. However, it is worth noting that the diagrams of the combined beams (Figure 12) utilizing characteristic values to show clear endpoints. After reaching the moments around the  $M_u^-$  or  $M_u^+$  point, the graph descends or ascends towards the x-axis. In contrast, the combined beam with tested values (Figure 13) only dips after the  $M_u^-$  point but appears to continue after the  $M_u^+$  point is reached. This underscores the importance of calculating the unique moment points and not solely relying on the diagram generated by the Python script.

Another aspect to note is that, for the two combined beam diagrams, the cracking moments occur at arbitrary curvatures. When searching for these points, it became apparent that the Python script could not find them. Either the strain at a given curvature was too large or too small, or the script could not find it regardless of input values. Ultimately, a curvature and moment were selected at which the strain value was larger than the strain conditions. In the table below, the curvature, strains and moments behaviour around the cracking moment can be seen.

Table 13, cracking curvature CB-c

$\kappa$ [mm <sup>-1</sup> ]	$\epsilon$ [%o]	$M_n$ [Nmm]	$\kappa$ [mm <sup>-1</sup> ]	$\epsilon$ [%o]	$M_n$ [Nmm]
-1.00e-08	0.065	541e+06	1.00e-08	0.066	611e+06
-2.00e-08	Not Found		2.00e-08	Not Found	
-9.00e-08	Not Found		9.00e-08	Not Found	
-10.00e-08	0.998	570e+06	10.40e-08	1.015	635e+06

Table 14, cracking curvature CB-m

$\kappa$ [mm <sup>-1</sup> ]	$\epsilon$ [%o]	$M_n$ [Nmm]	$\kappa$ [mm <sup>-1</sup> ]	$\epsilon$ [%o]	
-1.00e-08	0.098	546e+06	1.00e-08	0.099	590e+06
-2.00e-08	Not Found		2.00e-08	Not Found	
-9.00e-08	Not Found		9.00e-08	Not Found	
-10.00e-08	1.010	582e+06	10.00e-08	1.012	646e+06

This in turn leads to the next issue: the difference in bending stiffness (EI) across the entire moment-curvature diagram is not as expected. When examining the  $M_n$ - $\kappa$  diagram of the combined beam and cross beam, with characteristic values as seen in Figure 12 and Figure 14. And the table below, shows the bending stiffness between the different unique moments.

Table 15, bending stiffness of the CB-c and TB-c

	Combined Beam (CB-c)			Cross Beam (TB-c)		
	$\kappa$ [mm <sup>-1</sup> ]	$M_n$ [Nmm]	EI [Nmm <sup>2</sup> ]	$\kappa$ [mm <sup>-1</sup> ]	$M_n$ [Nmm]	EI [Nmm <sup>2</sup> ]
$M_u^-$	-3,38E-05	-1,70E+09	1,38E+13	-8,42E-05	-1,03E+09	2,49E+12
$M_y^-$	-5,49E-06	-1,30E+09	3,50E+14	-2,79E-06	-8,32E+08	-4,07E+12
$M_{cr}^-$	-1,07E-07	5,82E+08	2,24E+14	-2,44E-07	-8,42E+08	3,45E+15
$M_0$	0	6,06E+08	3,74E+14	0	0	3,50E+15
$M_{cr}^+$	1,07E-07	6,46E+08	3,45E+14	2,48E-07	8,68E+08	3,16E+14
$M_y^+$	2,32E-06	1,41E+09	4,64E+12	3,22E-06	1,81E+09	7,91E+12
$M_u^+$	4,54E-05	1,61E+09		5,93E-05	2,25E+09	

When observing the stiffnesses for the combined beam between  $M_0$  and both cracking moments ( $M_{cr}^-$  &  $M_{cr}^+$ ) are unusual, as seen in Table 15. A larger stiffnesses between  $M_{cr}^-$  and  $M_0$  or  $M_0$  and  $M_{cr}^+$  can be observed, compared to the stiffnesses between  $M_y^-$  and  $M_{cr}^-$  or  $M_{cr}^+$  and  $M_y^+$ . In contrast, the stiffnesses of the cross beam do show reasonable stiffness between the moment regions, other than between  $M_y^-$  and  $M_{cr}^-$ .

Additionally, for both cross beam diagrams, the negative cracking moment ( $M_{cr}^-$ ) is larger than the two negative moments, the yielding ( $M_y^-$ ) and ultimate ( $M_u^-$ ) moments. Normally, this should be a concerning fact, as the moment capacity of an element should always be determined based on the ultimate moment capacity and not on the cracking moment. However, this discrepancy only occurs in the negative curvature region. The cross beam was never designed to bear a negative moment. Further examination into whether this will also be the case for all the Diana models must be done, and if so, it might not be a cause of concern.

### Case Study 1

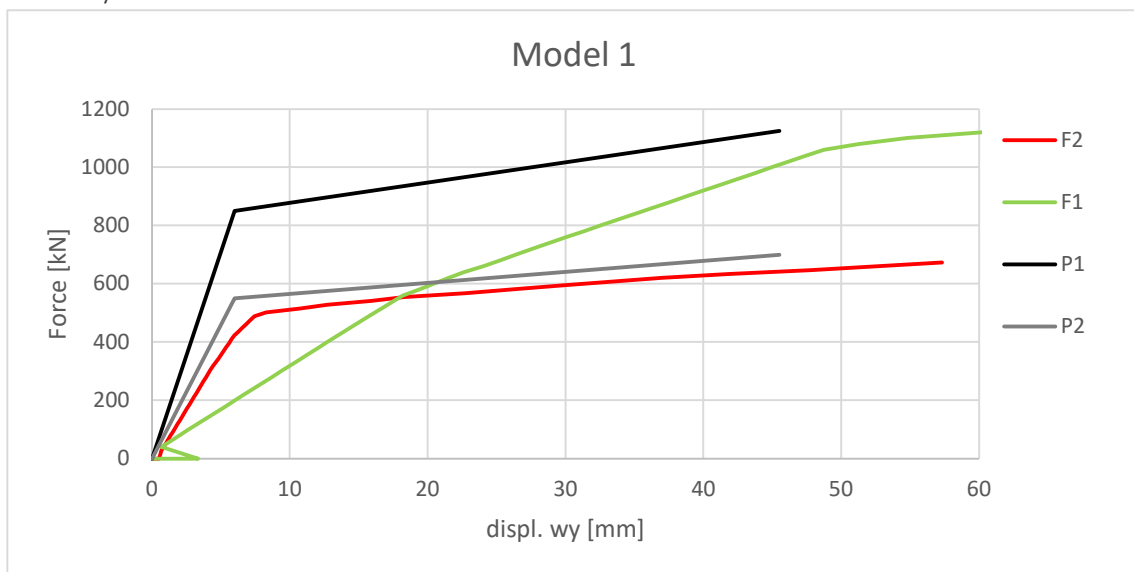


Figure 70, force-to-displacement graph Model 1

In the above Figure, the displacement-to-force diagram (F-w diagram) for Model 1 can be observed. Depicting the increase in force and displacement of points F1 & F2 from Model 1 in comparison to the results from the Report. The results from the Report were simplified into the two lines shown in the figure, P1 & P2. While F2 shows a very similar development compared to the Report P2, it doesn't reach the same maximum force. Conversely, the development of F1 doesn't align with the Report at all, although it comes close to the maximum force in the Report but at a significantly larger displacement.

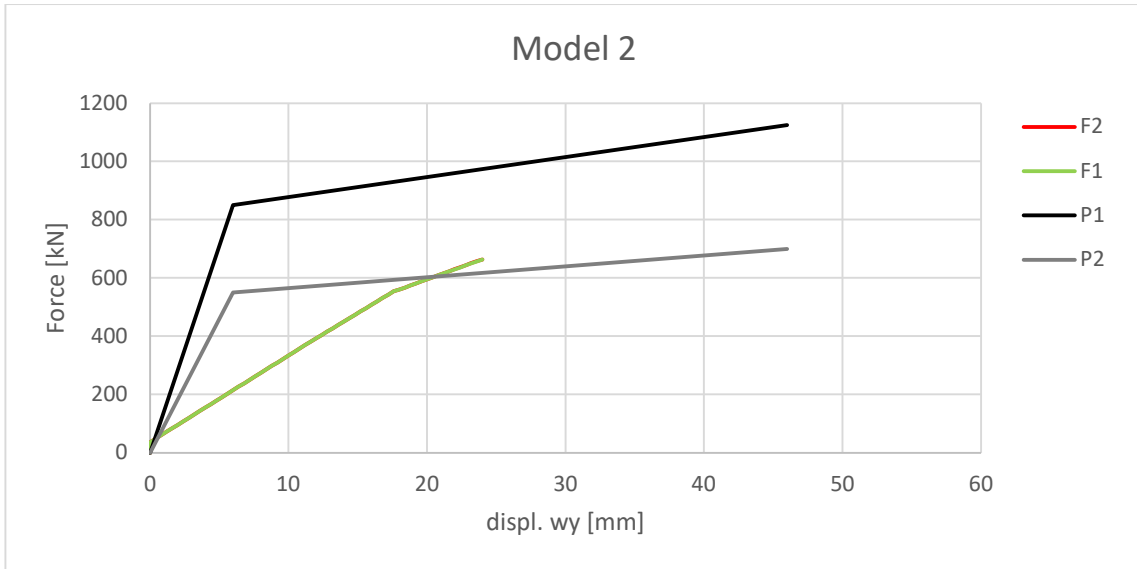


Figure 71, force-to-displacement graph Model 2

In the above Figure, the displacement-to-force diagram for Model 2 can be observed. Portraying F1 & F2 compared to the results from the Report. Note that this time, the lines for F1 & F2 overlap due to the symmetry of Model 2. Once again, the force-to-displacement does not align with the graph from the Report. Moreover, the maximum values of the Report are not reached, neither for force nor displacement.

Upon closer inspection of both figures, a clear change in slope in both graphs can be observed. Particularly in Figure 70 (Model 1), three different slopes in the line for Load F1 are noted. However, these changes in slopes do not correspond to points F1 or F2 surpassing a unique moment point, and therefore no change in stiffness as seen in its moment-curvature diagram. If vertical lines were to be added, representing the load step at which Load F1 surpasses a unique moment point. The Figure 72 is made, with the load steps as seen in Table 9. It can now be observed that there is a correlation between Point SL and F1; when SL reaches a certain unique moment point the graph for F1 changes slope.

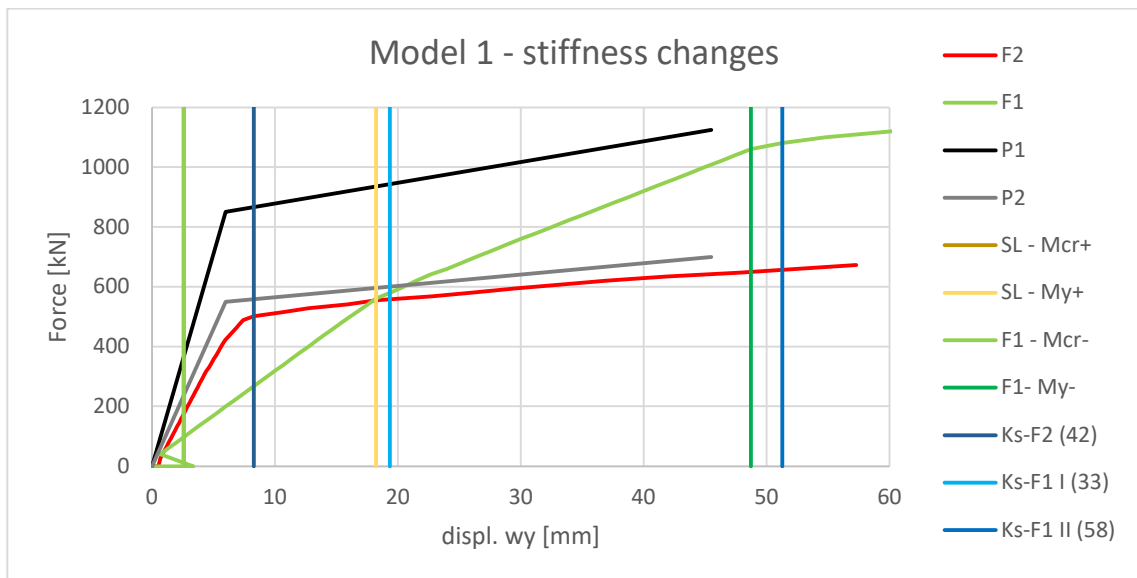


Figure 72, force-to-displacement graph Model 1 with stiffness changes (Ks)

Another interesting observation is at load step 33; the region to the right of the intermediate support changes in curvature orientation, as seen in Appendix IIIe. This region shifts from a positive cracking curvature to a negative one, with the negative curvature moving closer to the intermediate support. This lines up with behaviour in Figure 72, that there is a change in stiffness in the F1 graph at load step 33.

#### Case Study 2

Model 4 can reach a load factor of 1.00 for the ULS test and can continue an additional 37 steps until it fails at load step 139 or 1.37 times the Permanent Loads. With no points in the model surpassing either of the two ultimate moments, it can therefore be said that this model can handle the ULS traffic Load. Examining the Figure 45 and Figure 46 again, we see that only point SR has entered the final part of its respective  $M_n-k$  diagram.

However, the points at the intermediate support show a peculiar behaviour. Examining Table 11 Appendix IVe, it can be observed that for point SRL, there's an increase in curvature until load step 77 before returning and ultimately changing in orientation at load step 94. This could be critical for the FEM model as well as for an actual bridge, as the cross beam section cannot handle high negative moments.

Model 5 does not reach a load factor 1.00 for the ULS test; it fails at 0.49 of the Permanent Loads. This, however, is not indicative, as the combined beam cross-section was never designed for a bridge of this length. Further analyses must be done on a longer bridge's design before any definitive conclusions can be made.

For both models 4 & 5, a change in the orientation of the curvature can be observed, Appendix IVd and Appendix IVg show how the curvature of the beam around the intermediate support changes. The region which starts with a positive curvature decreases in length as the traffic load increases. This is particularly evident in the case of Model 4, as Model 4 has a greater number of load steps compared to Model 5.

## Conclusion

---

### Research Question and Sub-Questions

#### Sub-Questions:

- I. How closely does the structural behaviour of beam S10H1A, as depicted by the  $M_n$ - $\kappa$  diagram, align with the outcomes obtained from actual testing?
  - Load F1 from FEM Model 1 ultimately reached the same load as load P1 from the Report but at a significantly larger deformation. The stiffness of load F1 in the first part of the analysis was noticeably less than that of the Report. However, Load F2 from FEM model 1 had a result similar to those of the Report.
  - Changing the model's load control to a displacement control did not improve the overall performance of the models. FEM model 2 never reached the same load or displacement compared to the Report.
  - Due to multiple simplifications and choices made, especially when it comes to the choices surrounding the cracking curvature, the results of our model show clear differences when compared to the Report.
- II. How does the structural integrity of a bridge model, as depicted by the  $M_n$ - $\kappa$  diagram, hold up when subjected to traffic loads?
  - FEM Model 4 not only withstood the traffic load and its ULS version but also surpassed it and ran an additional 37 (out of 100) steps.
  - FEM Model 5, however, was not able to withstand the traffic load, either the base or ULS version; it only withstood 49 out of 100 steps of the traffic load.
- III. Are there specific areas within the bridge model exhibiting significant alterations in curvature and moment development during the application of traffic loads?
  - Throughout all FEM models, regions were identified that either changed or deviated from their respective  $M_n$ - $\kappa$  diagrams, areas to note:
    - i. In all models, near the intermediate support and at the side of the largest applied load, it could be observed that the curvature changed in orientation as their load increased.
    - ii. In all models, at their unique points SLR and SRL a behaviour concurrent with their two distinct  $M_n$ - $\kappa$  diagrams for one node was identified, leading to results that averaged out and did not overlap with either diagram.
  - FEM model 4's point SRL displayed behaviour unlike any of its counterparts. As the traffic load increased, the positive moment increased at the intermediate support, as expected. However, point SRL started to decrease and ultimately changed its curvature orientation, entering the negative region of its respective  $M_n$ - $\kappa$  diagram.
  - All 5 FEM models followed their respective  $M_n$ - $\kappa$  diagrams when the loads were applied. However, this was only the case after adjusting the model using the Diana Analysis command 'line search' at the equilibrium iterations option menu.
  - It must be noted that; the cracking moments in  $M_n$ - $\kappa$  diagrams for the combined beam, were simplified such that they do not account for a proper cracking moment. Resulting in an unclear change in stiffness between the uncracked and cracked regions of their respective  $M_n$ - $\kappa$  diagrams.

- IV. Can the FEM models accurately identify and replicate the occurrence of cracking regions based on changes in curvature and moment regions during simulations?
- The models followed their respected  $Mn-\kappa$  diagrams, which can be used to inspect and identify in which region of their diagram any point is.
  - However, the Python code was not able to find and, therefore, calculate the correct cracking moments for the combined beams, leading to limitations with the FEM models.
  - It must be noted that; the cracking moments in  $Mn-\kappa$  diagrams for the combined beam, were simplified such that they do not account for a proper cracking moment. Resulting in an unclear change in stiffness between the uncracked and cracked regions of their respective  $Mn-\kappa$  diagrams.

#### Main Question

How does the stiffness degradation affect the structural behaviour of a continuous prestressed girder beam around the intermediate supports?

- All models ultimately failed when one or more nodes entered the final stages of their respected  $Mn-\kappa$  diagrams.
- Models 1 (&2) showed how a change in the moment region and subsequent change in bending stiffness could affect the slope of the load-to-displacement graph.
- Model 4 showed that the curvature of an element or node, around the intermediate support might change rapidly, leading to a possible failure within the model.
- Appendix III d & Appendix III e, along with Appendix IV d & Appendix IV e models 1 & 4, showed how the change in the moment region around the intermediate support altered the distribution of loads over the whole model, leading to some nodes rapidly increasing in curvature and moment.

#### Recommendations & subsequent research

One of the prominent errors in the moment-curvature diagrams, of the combined beam, is in the calculation for the cracking moments. These were derived and calculated to be within the vicinity of their strain condition, but not within a reasonable margin. Improving on the cracking moment calculation or search process is imperative for subsequent research on this topic or method.

Additionally, for the moment-curvature diagram calculations, various simplifications were made. Over time, these cumulative simplifications can significantly influence the results. In subsequent research, a more complex cross-section could be used to calculate a more accurate moment-curvature diagram. With emphasis on the individual materials and their respective properties.

Upon reflection on the FEM models, several aspects can be refined, particularly when making mesh choices. While choosing the mesh/element size, this thesis adhered to the recommendations and standards described in the Guideline for Nonlinear Finite Elements (Hendriks & Roosen, 2020). This approach resulted in some issues at the intermediate support and its nodes, as the properties of these nodes were a combination of the cross beam and combined beam  $Mn-\kappa$  diagrams. Resulting in this region having elements with unique and deviating behaviour.

And lastly, a combination of the two aforementioned points should be considered. The cross beam section needs to be investigated in more detail, with its cross-section and properties expressed with greater complexity when calculating its moment-curvature diagram. In this report, the region where the combined beam transitions to the cross beam were not modelled accurately; it was treated as a sudden change in both the element and cross-section.

## References

---

- Beguin, J., van der Wilt, K., & Fennis, S. (2021). *Richtlijnen Ontwerp Kunstwerken*.
- Beton, H. (2021). HRP-ligger / HIP-ligger. Haitsma.
- Calavera, J. (2004). *Precast Bridges*.
- Dr. Denise, C. S., & ir. Wijtze, P. K. (2015). *Project: Reduced models in DIANA - A fast method for preliminary assessment of concrete*.
- Experiment on precast continuous girders. (2023).
- Hendriks, M. A., & Roosen, M. A. (2020). *Guidelines for Nonlinear Finite Element*.
- (sd). *NEN-EN 1991-2: Eurocode 1: Actions on structures - Part 2: Traffic loads on bridges*.
- (2019). *NEN-EN 1991-2+C1/NB: Eurocode 1: Actions on structures – Part 2: Traffic loads on bridges*.
- (2011). *NEN-EN 1992-1-1+C2/NB: Eurocode 2: Design of concrete structures – Part 1-1: General rules and rules for buildings*.
- (2011). *NEN-EN 1992-1-1+C2; Eurocode 2: Design of concrete structures – Part 1-1: General rules and rules for buildings*.
- Prof.dr.ir.Dr.-Ing.h.c. Walraven, J., & dr.ir.drs. Braam, C. (2019). *Lectures CIE3150/4160 - Prestressed concrete*.
- SATO, T., SHIMADA, I., & KOBAYASHI, H. (2002). *A Simple Numerical Method for Biaxial Bending Moment-Curvature Relations of Reinforced Concrete Column Sections*.
- Sliedrecht, H., Smith, S., & Roosen, M. (sd). *Modellering stijfheden in langsrichting van* .  
Rijkswaterstaat.

## Appendix

### Appendix I – Additional information Chapter 1

#### Appendix Ia

##### Dimensions of the combined beam & Cross Beam

Longitudinal dimensions			
Element	Length [mm]	Point	Distance* [mm]
Left Beam	3500	Left Force	630
Cross Beam	1250	Left Support	3250
Right Beam	11250	Middle Support	3750
		Right Force	9940
		Right Support	14500

Distance\*, denotes the distance from left to right.

Cross-sectional dimensions			
	Height [mm]	Element	Height* [mm]
Top layer	160	RS top 2	1025
Connection	10	RS top 1	951
Inv. T-Beam	900	Prestress**	85
		RS bottom	60

Height\*, denotes the distance to the bottom.

Prestress\*\*, denotes the distance for a combined single point for all prestress tendons.

#### Appendix Ib

##### Parameters of the combined beam & Cross Beam

	Value	Unit	Description	Equation/Notes
$H_T$	900	mm	Height HRP-900	
$H_{con}$	10	mm	Height connection	
$H_{dl}$	160	mm	Height top layer	
$H$	1070	mm	Height combined beam	Also, Height cross beam/support block
$B_T$	1180	mm	Width bottom flange	
$B_{T,w}$	300	mm	Width web	
$B_{con}$	270	mm	Width connection	
$B_{dl}$	1200	mm	Width top layer	Also, Width cross beam/support block
$A_T$	435000	mm <sup>2</sup>	Area HRP-900	
$A_{con}$	2700	mm <sup>2</sup>	Area connection	
$A_{dl}$	192000	mm <sup>2</sup>	Area top layer	
$A$	629700	mm <sup>2</sup>	Total area of the combined beam	$A = A_T + A_{con} + A_{dl}$
$A_{CB}$	1284000	mm <sup>2</sup>	Total area of the cross beam	$A_{CB} = H * B_{dl}$
$V_T$	316	mm	Centroid from the bottom	
$V$	524.04	mm	Centroid from the bottom, combined beam	$V = \frac{A_T H_T/2 + A_{con} (H_{con}/2 + H_T) + A_{dl} (H_{dl}/2 + H_T)}{A}$
$I_T$	30.90e9	mm <sup>4</sup>	Moment of inertia, HRP-900	

$W_{T,b0}$	5.29e7	mm <sup>3</sup>	Section modulus at initial stress state	$W_{T,b0} = \frac{I_p}{(H_T - V_T)}$
$W_{T,t0}$	9.78e7	mm <sup>3</sup>	Section modulus at initial stress state	$W_{T,t0} = \frac{I_p}{V_T}$
$\rho_T$	2299	kg/m <sup>3</sup>	Density	
$\rho$	2333	kg/m <sup>3</sup>	Density, combined beam	

## Appendix Ic

### Initial Loads on Test Beam

#### *Initial Loads -Self-weight*

The report gives us a combined weight of 2333 [kg/m<sup>3</sup>], which will be used as the self-weight value for all the models. An important aspect to keep in mind is that this weight corresponds to the actual combined beam and its shape as seen in Figure 2, cross-section A-A [5].

In Chapters 3 & 4, when FEM models are made, a simplified version of the cross-section of the combined was used. A correcting force was applied to the models to correct for this adjustment.

#### *Initial Loads -Prestressing Loads*

An important aspect of inverted T-beams is the presence of prestressed tendons. These tendons apply force and moment to the beam. In this case, the beam has 22 tendons over the full span, as seen in Figure 3, cross-section B-B. Each tendon, in turn, is prestressed to an initial load of 79.0 [kN]. A reduction of 20% over time and a single point upon which the load is applied to the beam (Appendix Ia) will be assumed. In the tables below, all information of interest about tendons can be found.

Table 16, overview prestress parameters I

	Value	Unit	Description
$F_{p,1}$	79	kN	Initial load of one tendon, at t=0
$n_p$	22	-	Number of tendons
$A_{p,1}$	100	mm <sup>2</sup>	Area of one tendon
$A_p$	2200	mm <sup>2</sup>	Total tendon
$F_{p,0}$	1738,00	kN	Initial load of all tendons, at t=0
$F_{p,\infty}$	1390,40	kN	Load of all tendons, at t= $\infty$

Table 17, overview prestress parameters II

	Value	Unit	Description
$h_{ep,1}$	60	mm	Distance to the bottom of the beam
$n_{p,1}$	14	-	Number of tendons on this row
$h_{ep,2}$	110	mm	Distance to the bottom of the beam
$n_{p,2}$	6	-	Number of tendons on this row
$h_{ep,3}$	185	mm	Distance to the bottom of the beam
$n_{p,3}$	2	-	Number of tendons on this row
$h_{p,t}$	85	mm	$h_{p,t} = \frac{h_{ep,1}n_{p,1} + h_{ep,2}n_{p,2} + h_{ep,3}n_{p,3}}{n_p}$
$M_{p,\infty}$	605,03	kNm	Moment on the beam, at t= $\infty$ with $M_{p,\infty} = F_{p,\infty} * (V_s - h_{p,t})$

## Appendix Id

### Construction Phases, and Initial Stress Calculation

The combined beam is constructed in several phases. First, the prefabricated inverted T-beam girder is made, and its prestress load is applied during fabrication. It is then brought to the construction site, where the top layer is poured in-situ, and lastly, any additional layer are added after this phase, e.g., the road deck. These multiple phases produce a difference in initial stresses over the height of the beam, as the inverted T-Beam is already under compressive stress due to the prestress before the top layer is poured and hardened. This difference in initial stress must be considered during the subsequent calculation. This will be done in the following steps:

- the initial stress in the inverted T-beam will be calculated.
- these stresses will be converted to strains.
- the strains will be extrapolated to the top layer.
- these strains will be introduced to the stress-strain relationships of a materials in the top layer.

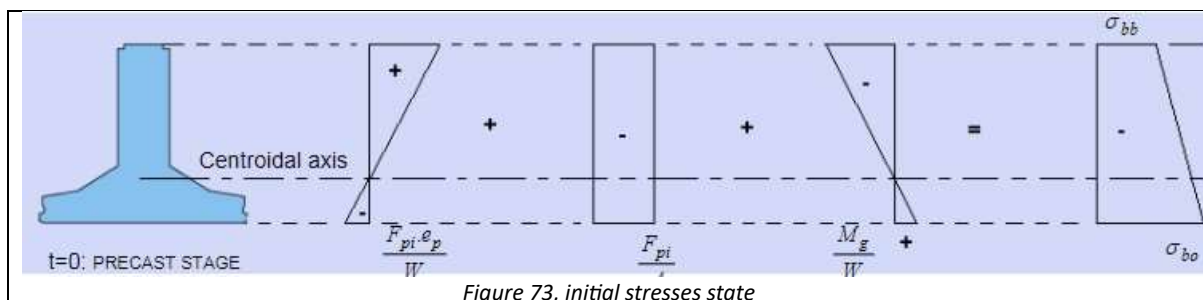


Figure 73, initial stresses state

Using the figure here above as a guide, the initial stress in the inverted T-beam can be calculated, all values used can be found in previous.  $M_g$  is the moment produced by the self-weight of the inverted T-beam; it can be divided as:  $M_g = 1/8 q_{sw,T} L_T^2 = 232414644.73 [Nmm]$ , with  $q_{sw,T} = A_T \rho_T g = 14.69 [N/mm]$ . And this leads us to the initial stress:

Table 18, initial stresses

	Stress [N/mm <sup>2</sup> ]	
Bottom T-beam ( $\sigma_{T,bo}$ )	-5.72	$\sigma_{T,bo} = -\frac{F_{pi}e_p}{W_{b0}} - \frac{F_{pi}}{A_b} - \frac{M_g}{W_{b0}}$
Top T-beam ( $\sigma_{T,to}$ )	-0.80	$\sigma_{T,to} = +\frac{F_{pi}e_p}{W_{t0}} - \frac{F_{pi}}{A_b} + \frac{M_g}{W_{t0}}$

With the initial stresses, the strain over the height of the combined beam can be calculated, note that for the tested values and characteristic values. The initial strains will differ as the E-modulus vary for the two sets of values. First, the strains at the top and bottom will be calculated, using  $\varepsilon_{T,to} = \frac{\sigma_{T,to}}{E_{cm,T}}$  &  $\varepsilon_{T,bo} = \frac{\sigma_{T,bo}}{E_{cm,T}}$  these values can be determined, then extrapolate to the height of the elements in the top layer.

Table 19, overview initial strains

Element	Height [mm]	Tested Value	Char. Values
		Strain [‰]	Strain [‰]
T-beam, bottom	0	-15.76e-2	-25.03e-2
T-beam, top	900	-2.20e-2	-3.50e-2
Top layer, bottom	910	-2.05e-2	-3.26e-2
RS-t1	951	-1.44e-2	-2.28e-2
RS-t2	1025	-0.32e-2	-0.51e-2
Top layer, top	1070	0.36e-2	0.57e-2
Top layer, avg.	990	-0.85e-2	-1.35e-2

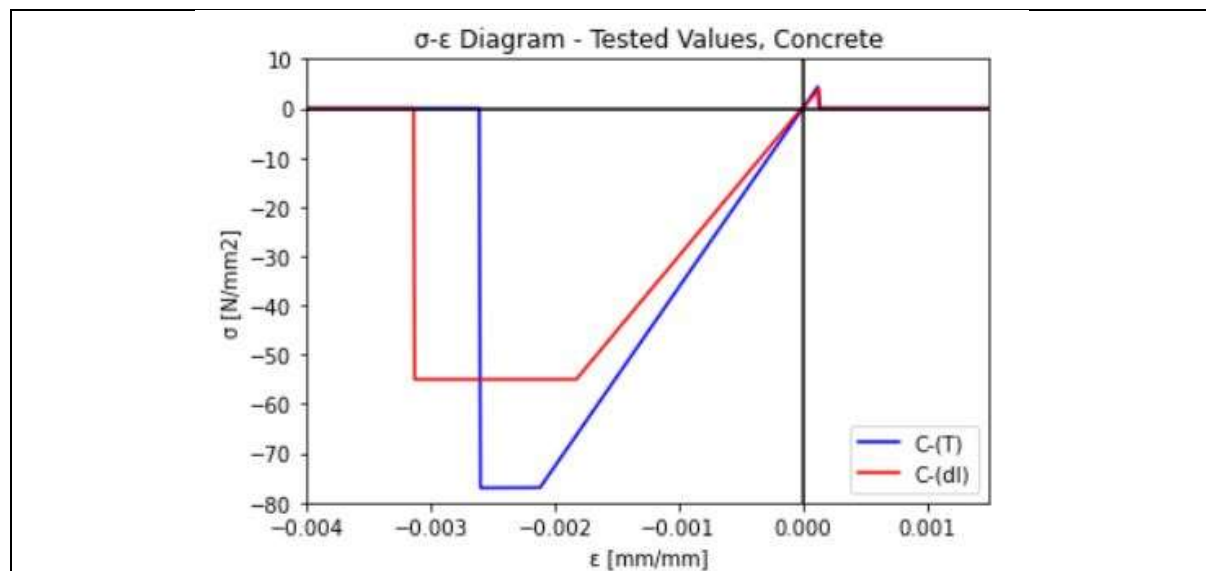
## Appendix Ie

### Material Properties, S10H1A

The values shown are for the two concrete materials, 3 reinforcement steels and prestress tendon. The values and the method used to calculate or determine the values can be seen in the tables here below. Note the denoting: T for the inverted T-beam girder, dl for the top layer,  $t_2$  for the top flange Longitudinal reinforcement number 2,  $t_1$  for the top flange Longitudinal reinforcement number 1, b for the bottom flange Longitudinal reinforcement, and P for the prestressing steel.

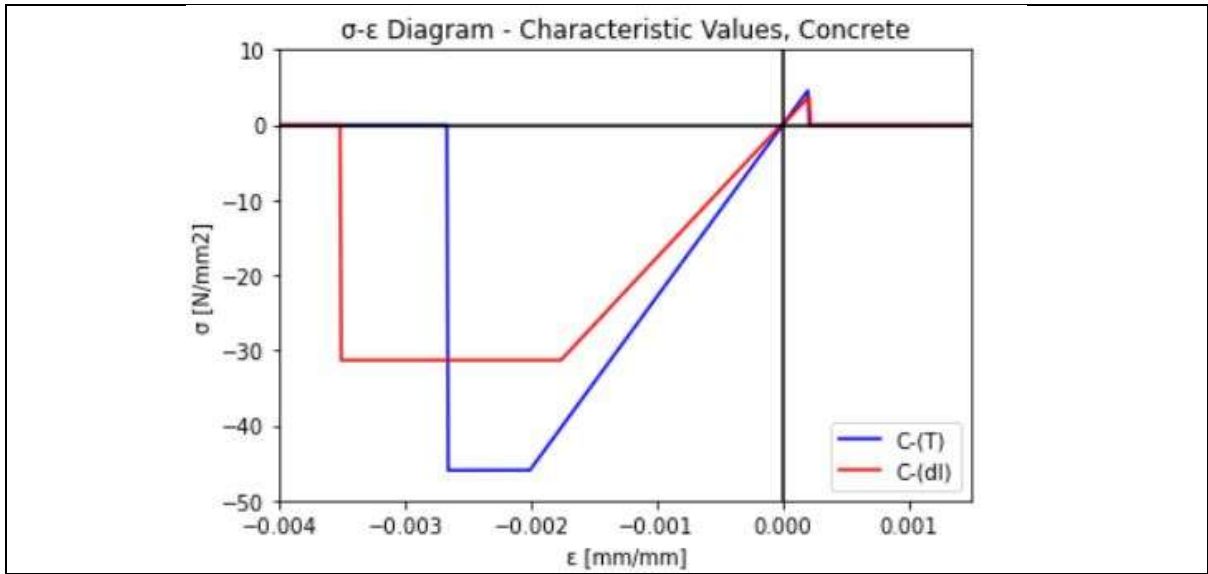
#### Tested Values, Concrete

	C <sub>tv</sub> -(T)	C <sub>tv</sub> -(dl)	Unit	Method
$f_m$	77	55	N/mm <sup>2</sup>	Report
$f_{ctm}$	4.58	3.97	N/mm <sup>2</sup>	Tabel 3.1 (NEN-1992-1-1) & RTD 2.3.1, using $f_m$
$E_{cm}$	40585.41	36688.63	N/mm <sup>2</sup>	Tabel 3.1 (NEN-1992-1-1) & RTD 2.3.1, using $f_m$
$\epsilon_{3k}$	2.12	1.82	-	Tabel 3.1 (NEN-1992-1-1) & RTD 2.3.1, using $f_m$
$\epsilon_{3uk}$	2.61	3.13	-	Tabel 3.1 (NEN-1992-1-1) & RTD 2.3.1, using $f_m$
$\epsilon_{ctm}$	0.13	0.13	-	$\epsilon_{ctm} = \frac{\epsilon_{3k}}{f_{cd}} * f_{ctm}$



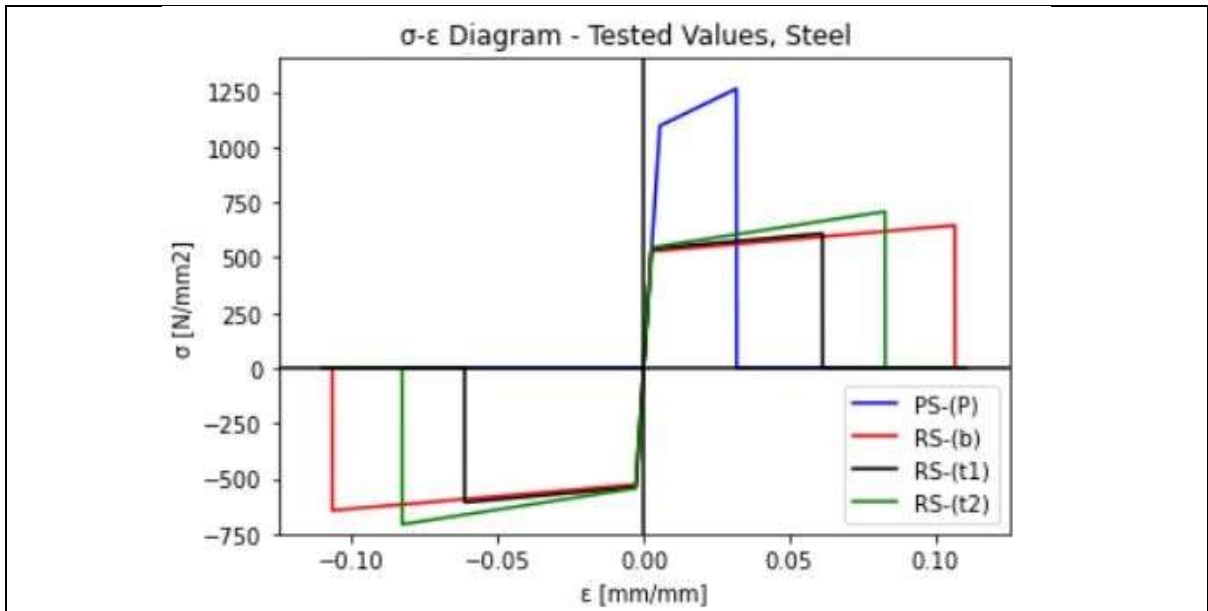
#### Characteristic Values, Concrete

	C <sub>cv</sub> -(T)	C <sub>cv</sub> -(dl)	Unit	Method
$f_m$	77	55	N/mm <sup>2</sup>	Report
$f_{ck}$	69	47	N/mm <sup>2</sup>	Tabel 3.1 (NEN-1992-1-1) & RTD 2.3.1
$f_{cd}$	46	31.33	N/mm <sup>2</sup>	$f_{cd} = \frac{f_{ck}}{\gamma_c}$ , with $\gamma_c = 1.5$
$f_{ctm}$	4.59	3.91	N/mm <sup>2</sup>	Tabel 3.1 (NEN-1992-1-1) & RTD 2.3.1
$E_{cm}$	40585.41	36688.63	N/mm <sup>2</sup>	Tabel 3.1 (NEN-1992-1-1) & RTD 2.3.1
$\epsilon_{3k}$	2.01	1.75	‰	Tabel 3.1 (NEN-1992-1-1) & RTD 2.3.1
$\epsilon_{3uk}$	2.66	3.50	‰	Tabel 3.1 (NEN-1992-1-1) & RTD 2.3.1
$\epsilon_{ctm}$	0.20	0.22	‰	$\epsilon_{ctm} = \frac{\epsilon_{3k}}{f_{cd}} * f_{ctm}$



Tested Values, Reinforcement Steel and Prestressing Steel

	RS-(t2)	RS-(t1)	RS-(b)	PS-(P)	Unit	Method
$f_{ym}$	539	536	524	1619	N/mm <sup>2</sup>	Report & RTD 2.3.2
$f_{um}$	702	605	642	1865	N/mm <sup>2</sup>	Report & RTD 2.3.2
$E_{ym}$	19800	203000	213000	195000	N/mm <sup>2</sup>	Report & RTD 2.3.2
$\epsilon_y$	2.46	2.64	2.72	7.88	‰	$\epsilon_y = \frac{f_y}{E_y}$
$\epsilon_u$	82.60	61.20	106.50	35.00	‰	Report & RTD 2.3.2

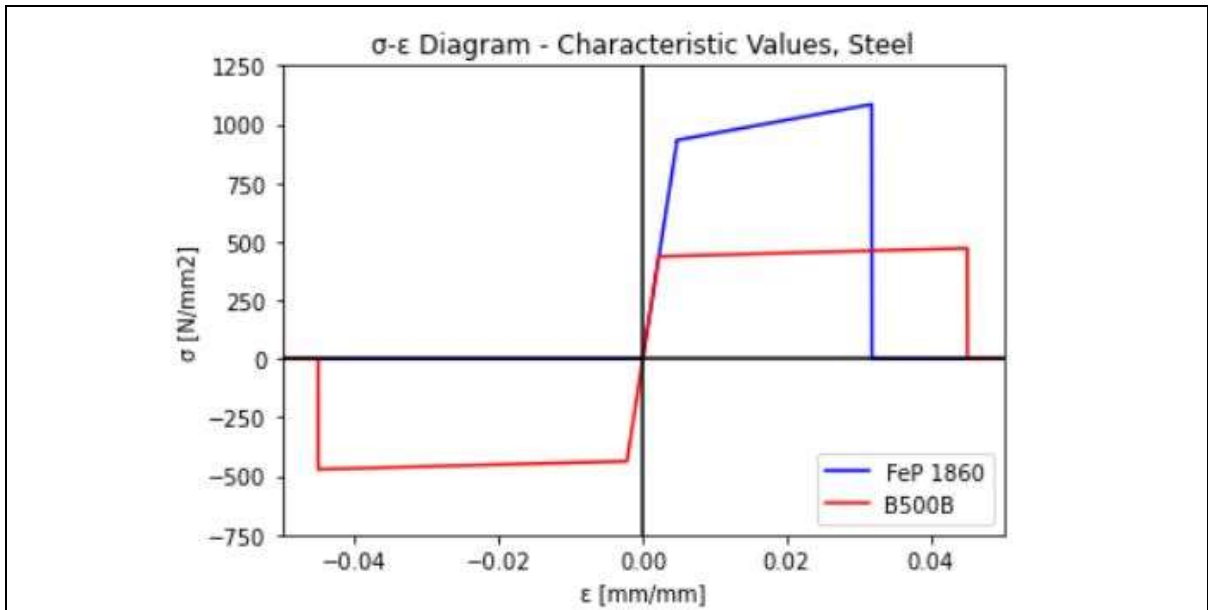


Characteristic Values, Reinforcement Steel and Prestressing Steel

	B500B	Unit	Method
$f_y$	500.00	N/mm <sup>2</sup>	NEN-1992-1-1 3.2.7 & RTD 2.3.2.1
$f_{yd}$	434.78	N/mm <sup>2</sup>	$f_{yd} = \frac{f_y}{\gamma_s}$ , with $\gamma_s = 1.15$
$f_u$	540	N/mm <sup>2</sup>	NEN-1992-1-1 3.2.7 & RTD 2.3.2.1

$f_{ud}$	469.57	N/mm <sup>2</sup>	$f_{ud} = \frac{f_u}{\gamma_s}, \text{ with } \gamma_s = 1.15$
$E_y$	200000	N/mm <sup>2</sup>	NEN-1992-1-1 3.2.7 & RTD 2.3.2.1
$\epsilon_{yd}$	2.17	‰	$\epsilon_y = \frac{f_y}{E_y}$
$\epsilon_{ud}$	45.00	‰	NEN-1992-1-1 3.2.7 & RTD 2.3.2.1

	FeP 1860	Unit	Method
$f_{pk}$	1860	N/mm <sup>2</sup>	NEN-1992-1-1 3.3.6 & RTD 2.3.2.2
$f_{pd}$	1690.91	N/mm <sup>2</sup>	$f_{pd} = \frac{f_{pk}}{\gamma_{s,p}}, \text{ with } \gamma_{s,p} = 1.1$
$f_{p0.1k}$	1691	N/mm <sup>2</sup>	NEN-1992-1-1 3.3.6 & RTD 2.3.2.2
$f_{p0.1d}$	1537.27	N/mm <sup>2</sup>	$f_{p0.1d} = \frac{f_{p0.1k}}{\gamma_{s,p}}, \text{ with } \gamma_{s,p} = 1.1$
$E_{yp}$	195000	N/mm <sup>2</sup>	NEN-1992-1-1 3.3.6 & RTD 2.3.2.2
$\epsilon_{ypd}$	7.88	‰	$\epsilon_{ypd} = \frac{f_{p0.1d}}{E_{yp}}$
$\epsilon_{upd}$	35.00	‰	NEN-1992-1-1 3.3.6 & RTD 2.3.2.2



## Appendix II – Additional information Chapter 2

### Appendix IIa

#### Detailed explanation on PM array

The first parameter in the PM will be an array with the relative height, named array H. By defining a 0-axis in the beam, a fictional horizontal line will be placed in the middle of the beam, at 535 [mm] from the bottom. Array H will calculate the distance from the 0-axis to the layer, with values below the 0-axis being negative, and all values above being positive. This array will help us to get the correct distance and integer when we will look at the stresses and strains (positive for tensile and negative for compression).

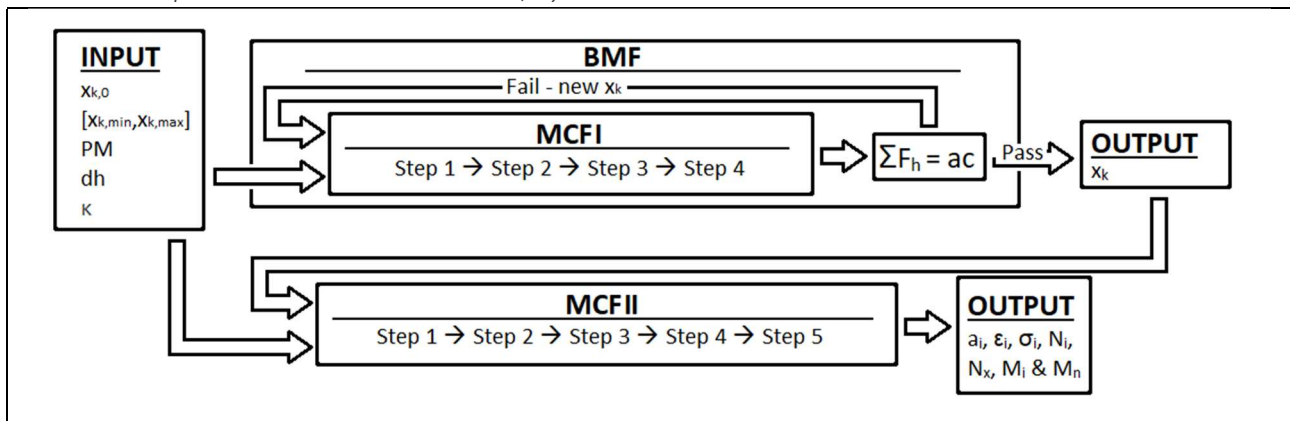
The 2<sup>nd</sup> parameter will be the cross-sectional width at a given height. A function will be created to account for varying width over the height of the combined beam. This function gives us the width at the a given height; note that the function takes the height as given by array H.

The remaining parameters, 3 up till 7, are all material properties. The 3<sup>rd</sup> parameter is an array of concrete properties, these values are needed to calculate the stress at a given strain. The PM will distinguish between the two concrete types at the appropriate height. Parameters 4, 5 and 6 are linked to the steel reinforcements and prestressing steel; at the heights of the steels parameters 4 will have the total area of the respected reinforcement steel or prestress tendons. Whereas parameter 5 will have an array of the corresponding steels material properties, and parameter 6 for the prestressing tendon. Lastly, parameter 7 gives us an additional centre prestressing force to calculate the compressive zone, as seen in Figure 7, Chapter I.

Things to note not every layer will need a value for the reinforcement steel or prestress, not all layers have reinforcement steel e.g., Therefore, I will add a null parameter array for the layers which only have concrete.

### Appendix IIb

#### Detailed explanation on Final Calculation, Python Code



A more detail explanation on the calculation done within the MCF, using the textbook as reference. This function will take the PM array, slice height (dh), accuracy condition (ac), curvature range ( $\kappa$ ) and an initial compressive height ( $x_k$ ) as input.

Step 1, determining the value  $a_i$  for each layer. This  $a_i$  is the distance for a layer to  $x_k$ , this can determine with the equation:  $a_i = H_i - x_k - dh/2$ , the give height ( $H_i$ ) of each layer is provide by parameter 1 from the PM array, and  $x_k$  and  $dh$  are initial input values.

Step 2, determining the strains ( $\epsilon_i$ ) for each layer. In Figure 9 we see how a curvature in a beam gives us a strain gradient over the height of the beam, with  $a_i$  calculated following the equation:  $\epsilon_i = a_i * \kappa$ ,  $\kappa$  is provided as an input value.

Step 3, determining the stresses ( $\sigma_i$ ) for each layer. The calculated strains are than put into the stress-strain functions; the PM array provides the corresponding material property array needed to run the

stress-strain functions. As mentioned in Chapter 2.2.1 – Cross-sectional Parameter Matrix., the PM array will provide the correct parameter arrays for each layer. For example, the layer at height  $h_p$  (prestressing height) will have parameter array for concrete, for the prestressing steel and a null parameter array for the reinforcement steel.

To conclude, this gives us the following equation:  $\sigma_{t,i} = \sigma_{c,i} + \sigma_{s,i} + \sigma_{SP,i}$ , with  $\sigma_{c,i} = sig_c(\varepsilon_i)$ ,  $\sigma_{s,i} = sig_s(\varepsilon_i)$  &  $\sigma_{SP,i} = sig_{SP}(\varepsilon_i) + P_{m,\infty}$ . Also note the  $P_{m,\infty}$ , we see in Figure 9 that we need to balance the internal with the external forces as shown in chapter 7.2.

Step 4, determine the normal force ( $N_x$ ) at the given  $\kappa$ . With the stresses now known, the normal force produced for each layer can be calculated, with the following equation:  $N_i = \sigma_i * dh * W$ , with  $W$  as the width of that layer and provide by the PM array. However, the stresses were calculated per material over the height, still must now extend to the normal forces. This leads to the adjusted equation to:  $N_i = \sigma_{c,i} * dh * W + \sigma_{s,i} * A_s + \sigma_{SP,i} * A_{SP}$ , with  $A_s$  and  $A_{SP}$  provided by the PM. Lastly, the sum of all the normal forces per layer are taken to calculate the normal force ( $N_x$ ), written in equation form:  $N_x = \sum N_i$ . Note that this is also the sum of the horizontal forces ( $\sum F_h$ ).

Step 5, determining the moment ( $M_n$ ). The code is written such that  $N_i$  and  $a_i$  are array of equal length, representing the layer number. Multiplying  $N_i$  and  $a_i$  will gives all the moments produced, per layer, written in equation form:  $M_i = N_i * a_i$ . Again, taking the sum of the produced moments to get the total moment at a curvature:  $M_n = \sum M_i$ .

## Appendix IIc

### Verifying the Python Script

#### Mayor Errors

A quick explanation on how I created and verified my code. I initially started with a simple square cross section with no rebar, and examined and verified my results. I then gradually adjusted the code until I reached the complex and nonhomogeneous cross section of the combined beam. In this part of the report, I will use the calculation and graphs from the cross beam section and combined beam, both with characteristic material values, when describing some of the errors. With the initial curvature range of  $[-5.0e-05;6.5e-05]$ , with steps of  $5.0e-07$ . As I increased the complexity of the cross-section two mayor errors emerged, namely: no  $x_k$  value could be found around  $\kappa=0$  and strange value for  $x_k$  for  $\kappa < -3.00e-05$  (this  $\kappa$  varied over the four cross-sections).

Throughout the entire process I used several methods to check if my code works as prescribed according to the norms or theories, I based them on. The primary method I used to check and examine the behaviour of the MCF and BMF, was a brute force calculation where all possible  $x_k$ , with a range four times the height of the cross-section, were calculated. This calculation provides an overview of the  $\sum F_h$  for any  $x_k$  at any  $\kappa$ . This calculation results in a  $\sum F_h$ - $x_k$  graph, which allows me to identify where the condition  $\sum F_h = 0$  is met, as this is the point where the graph intersect the x-axis.

Using this brute force approach, I examined the two regions where we could not find a  $x_k$  which met the condition. The first region around  $\kappa=0$ , using the brute force script with a  $\kappa$  range of  $[-1.00e-07; 1.00e-07]$ , with 5 steps. Two interesting things emerged: for  $\kappa$ 's around 0, the  $x_k$  would not be within the cross-section of the beam, and for the  $\kappa=0$ , there is no part of the  $\sum F_h$ - $x_k$  graph that intersects with the x-axis, thus no point meets the condition.

In the figures below, I added the  $\sum F_h$ - $x_k$  graphs for  $\kappa=-0.50e-08$  &  $\kappa=0$ . Note the red vertical lines are the top and bottom edge of the combined beam and the y-axis is the middle of the beam.

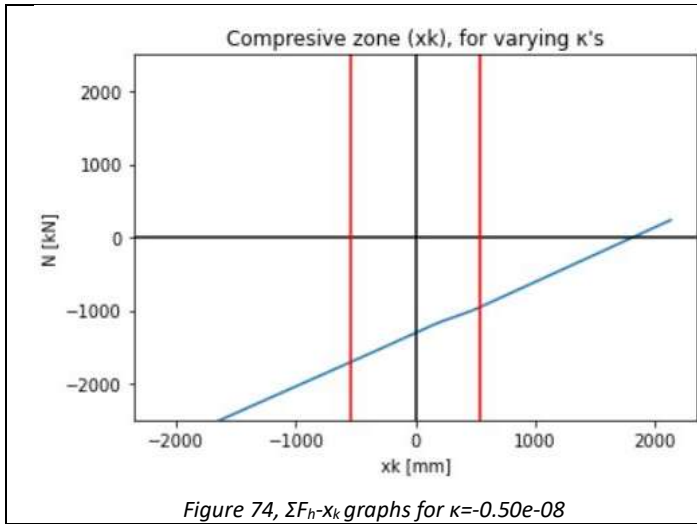


Figure 74,  $\Sigma F_h-x_k$  graphs for  $\kappa=-0.50e-08$

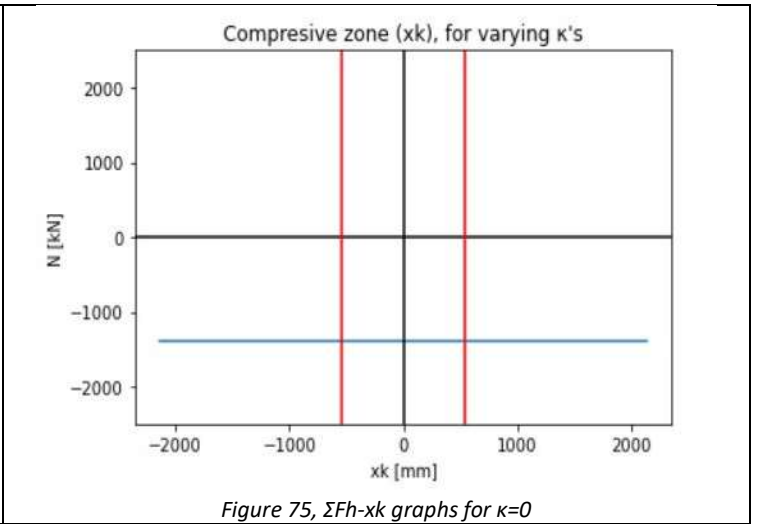


Figure 75,  $\Sigma F_h-x_k$  graphs for  $\kappa=0$

For the second region,  $\kappa < -3.00e-05$  we see a different mistake occurring: namely, we get two or more intersections with the x-axis, and therefore two or more  $x_k$  values that meet the condition. Using the brute force script, I examined the region  $[-3.50e-05; -3.00e-05]$ , with five steps. In Figure 76, Figure 77, Figure 78 & Figure 79, you can see the  $\Sigma F_h-x_k$  graphs for  $\kappa=-3.5e-05$ ,  $\kappa=-3.4e-05$ ,  $\kappa=-3.3e-05$  &  $\kappa=-3.2e-05$ . Note the orange lines are at  $\pm 250$  [mm] from the middle of the combined beam the red vertical lines are the top and bottom edge of the combined beam, and the y-axis is the middle of the beam.

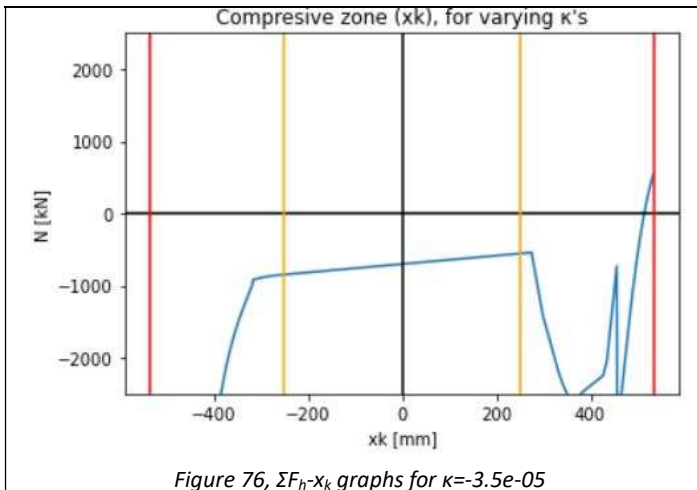


Figure 76,  $\Sigma F_h-x_k$  graphs for  $\kappa=-3.5e-05$

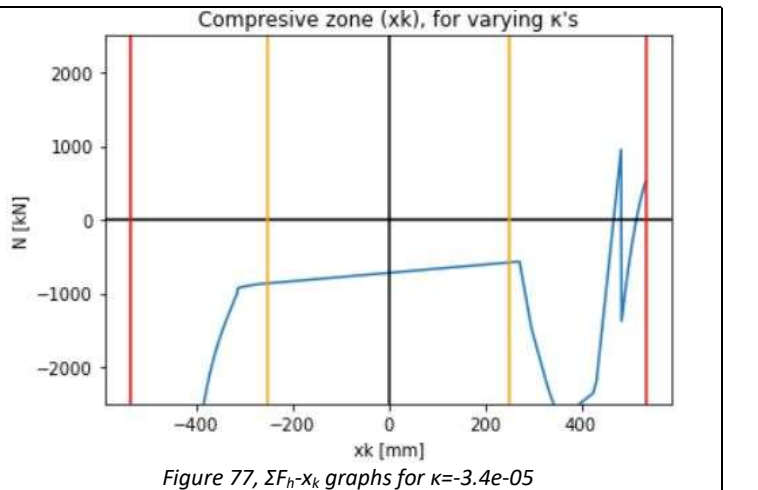


Figure 77,  $\Sigma F_h-x_k$  graphs for  $\kappa=-3.4e-05$

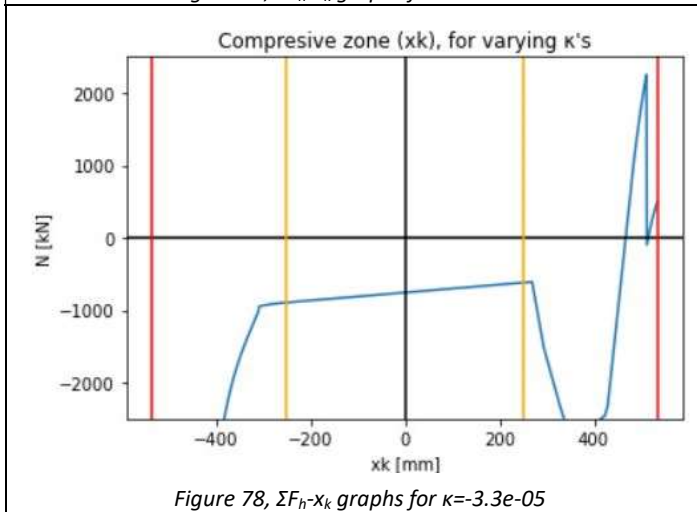


Figure 78,  $\Sigma F_h-x_k$  graphs for  $\kappa=-3.3e-05$

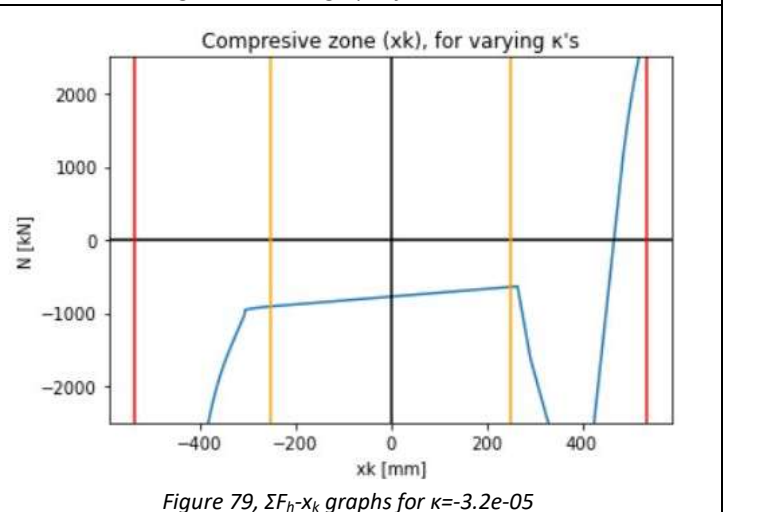


Figure 79,  $\Sigma F_h-x_k$  graphs for  $\kappa=-3.2e-05$

For both cases we will need to adjust the input: initial  $x_k$  when we run the BMF. This changes the range within which the BMF searches for the actual  $x_k$ . For  $\kappa=0$  we need a more direct solution we will simply make the  $x_k=0$  (from the middle of the beam) at  $\kappa=0$ .

Both these changes lead us to a somewhat tedious piece of script to find all the  $x_k$  within the  $\kappa$  range  $[-5.0e-05;6.5e-05]$ , as seen in Figure 81. These errors only occurred with the more complex cross-sections of the combined beam and not for the cross beam cross-section, as seen in the same piece of code for the cross beam section in Figure 80.

```
#Main calculation
#BMF
for i in range(len(kappa)):
    #print('I',i,kappa[i])
    x_k[i] = bi_x(-0.5*h0,0.5*h0,ac,HM,dh,kappa[i])

for i in range(kl):
    a[i],eps[i],sig[i],N[i],M[i],N_k[i],M_k[i] = NnM(HM,dh,x_k[i],kappa[i])
```

Figure 80, main calculation - cross beam

```
#Main calculation
#BMF
for i in range(len(kappa1)):
    if i <= ic2:
        #print('I',i,kappa[i])
        x_k[i] = bi_x(-0.5*h0,0.5*h0,ac,HM,dh,kappa1[i])
    if ic2 < i <= ih-4:
        #print('II',i,kappa[i])
        x_k[i] = bi_x(-0.5*h0,0.5*h0,ac,HM,dh,kappa1[i])
    if ih-4 < i < ih:
        #print('III',i,kappa[i])
        x_k[i] = bi_x(-2*h0,2*h0,ac,HM,dh,kappa1[i])
    if i == ih:
        #print('IV',i,kappa[i])
        x_k[i] = -(h0/2-zw)
    if ih < i <= ih+3:
        #print('V',i,kappa[i])
        x_k[i] = bi_x(-2*h0,2*h0,ac,HM,dh,kappa1[i])
    if ih+3 < i <= ik-1:
        #print('VI',i,kappa[i])
        x_k[i] = bi_x(-h0/2,h0/2,ac,HM,dh,kappa1[i])

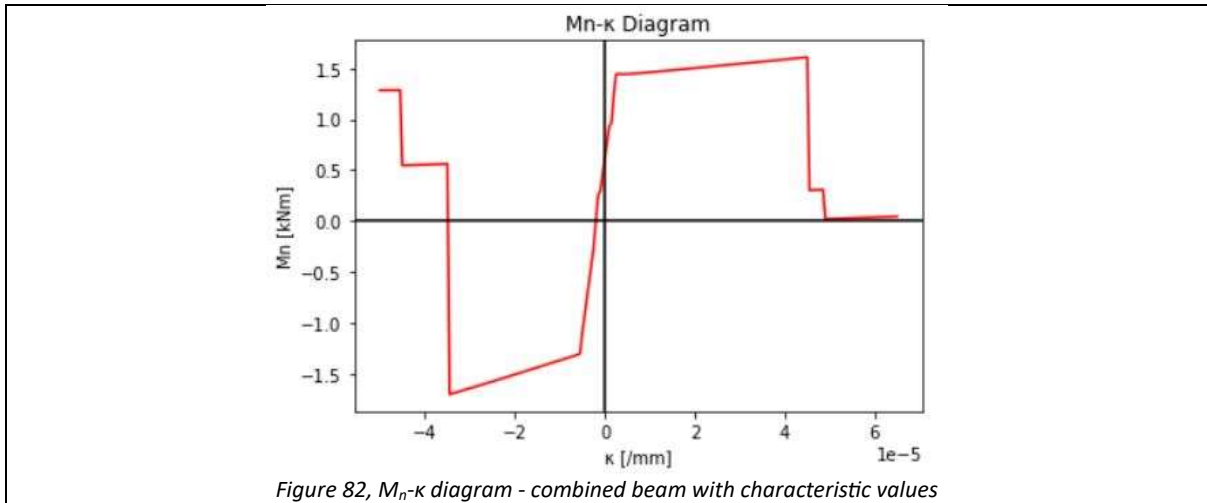
for i in range(len(kappa2)):
    #print('VII',ik+i,i,kappa[ik+i])
    x_k[ik+i] = bi_x(-0.5*h0,0.5*h0,ac,HM,dh,kappa2[i])

for i in range(kl):
    a[i],eps[i],sig[i],N[i],M[i],N_k[i],M_k[i] = NnM(HM,dh,x_k[i],kappa[i])
```

Figure 81, main calculation - combined beam

### Physical Behaviour

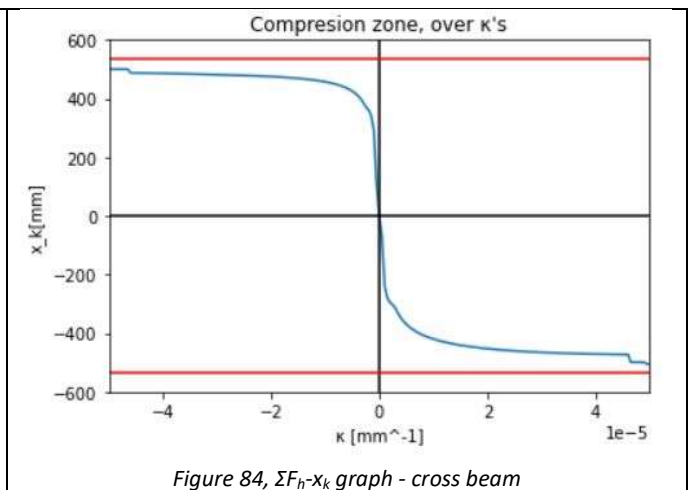
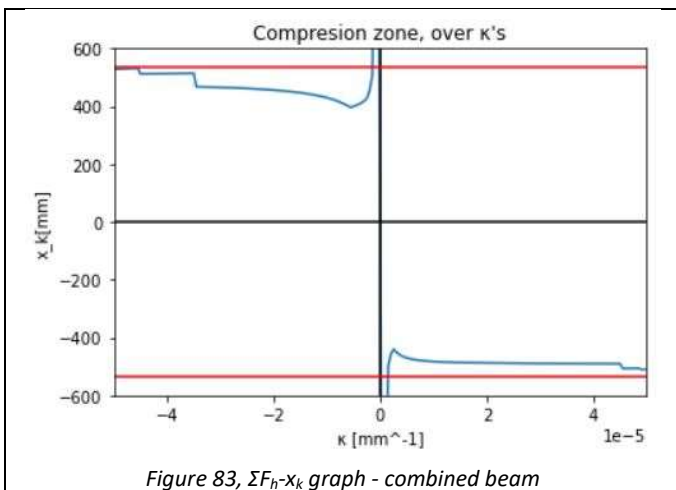
The Python script attempts to model actual behaviour; it is not bound by any physical limitations or rules. This flexibility is a strength, but it also poses a potential drawback. Therefore, we must check whether the model still behaves as prescribed and remains consistent with the laws of physics. In the figure below, you can observe the  $M_n$ - $\kappa$  diagram of the combined beam with characteristic values.



A simple check involves examining the moment values produced for different curvature values, essentially investigating which parts of the  $M_n$ - $\kappa$  diagram yield negative and positive integers. The assumption is that a positive curvature ( $\kappa$ ) will result in a positive moment ( $M_n$ ). If the diagram does not exhibit this expected trend, corrective measures must be applied to the script. This underscores the significance of the initial Height integer, parameter 1 from the PM, as it exerts a continuous influence on the calculation. As depicted in Figure 82, we indeed observe the production of positive moments with positive curvatures and vice versa.

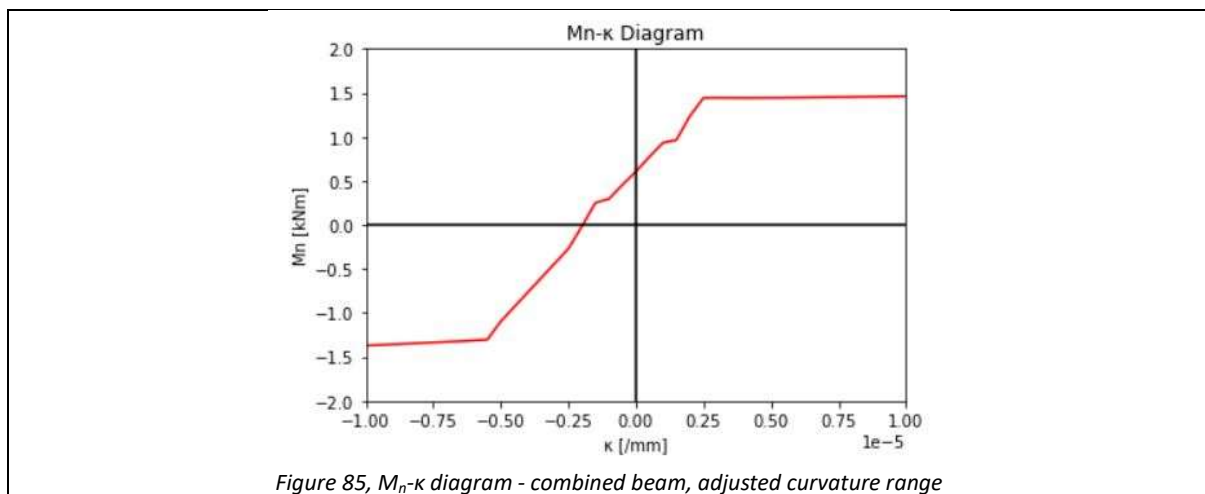
The second check involves examining the moment ( $M_n$ ) at  $\kappa=0$ . If the beam is straight and has no curvature, the moment at this point should only be produced by external forces. In the case of the combined beam, the only external forces are the prestress tendons, which apply a force on the beam, resulting in a moment equal to 605.0 [kNm]. As discussed in the previous chapter, I detailed how the script encountered difficulty finding an  $x_k$  for  $\kappa = 0$ , as depicted in Figure 75. Consequently, I made a simple fix to the script by assigning a fixed value to  $x_k$  at  $\kappa = 0$ , setting it to -14.85 [mm] from the centre horizontal line. Conversely, for the cross beam, which has no external forces applied to it, the script successfully found the  $x_k$  to be 0 [mm] at  $\kappa = 0$ , as expected.

Another check we can perform is to examine the progression of the  $x_k$  value over different  $\kappa$ 's. We would expect a graph with a smooth transition from one value to the next, with the progression of the  $x_k$  being in the top part of the beam for negative  $\kappa$ 's and in the bottom for positive  $\kappa$ 's. In the figures below, you can observe the compression zone's progression of the combined beam and cross beam with characteristic values. Note that the red horizontal lines represent the top and bottom edges of the beam.

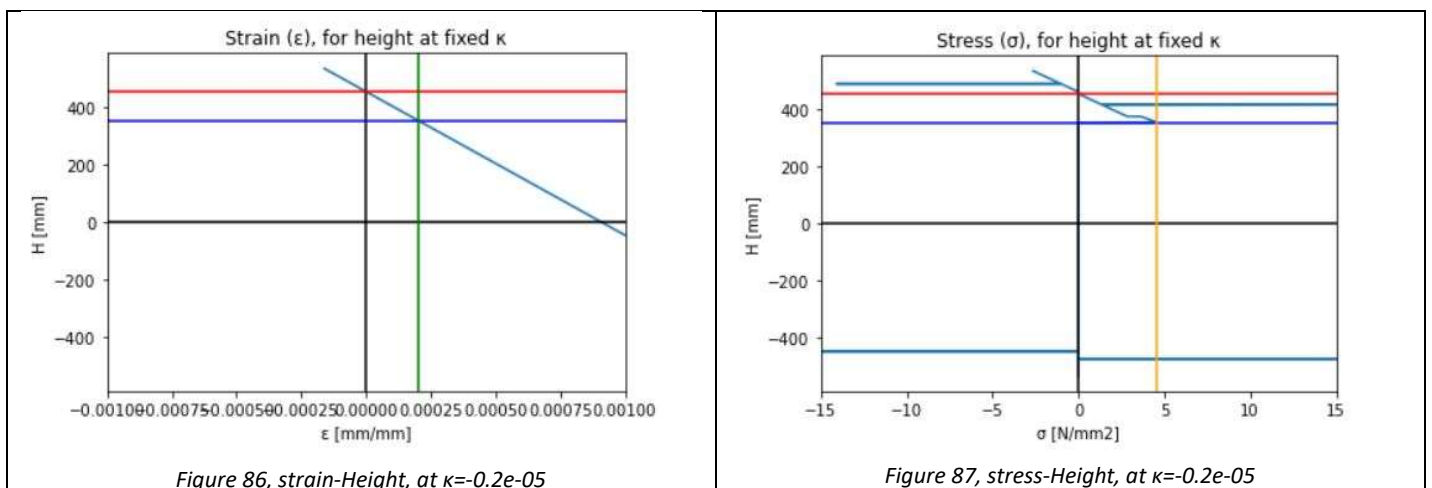


We observe a smooth progression in both cases, indicating that we are obtaining the reasonable values. However, an error becomes apparent around  $\kappa=0$  for the combined beam element, resulting in an  $x_k$  value outside of the beam. Additionally, there are noticeable jumps at the end of the lines in both graphs, suggesting that the results at those  $\kappa$ 's should be further examined. In Figure 82 & Figure 83,m we notice jumps in moments where the compression zone also jumps, and it becomes evident that these two jumps are related to each other.

The last simple check involves examining whether there are multiple slopes in the graph, corresponding to different moment regions such as uncracked concrete, cracked concrete, and steel yielding. These regions should be reflected in the graph. Upon closer examination of the figure below, which is a zoomed-in  $M_n-\kappa$  diagram of the combined beam with characteristic values, we do observe different slopes, which is a positive indication. However, a more detailed examination of the exact moment at which each region begins, and ends is warranted.



A more comprehensive examination that we can perform on the script involves assessing the strains and stresses at each curvature. Since the materials have different values for parameters such as the ultimate tensile or compressive strength, it is crucial to ensure that these limits are not exceeded.



In Figure 86 & Figure 87, the strain and stress distribution over the height of the beam at  $\kappa=-0.2e-05$  is depicted. The green line represents the maximum tensile strain ( $\epsilon_{ctm,T}$ ), the orange line indicates the maximum tensile strength ( $f_{ctm,T}$ ) allowed in the inverted T-beam, the blue line represents the height at which the maximum tensile strain and strength occur, and the red line signifies the height of the compression zone. Clearly, the maximum tensile strength is not surpassed.

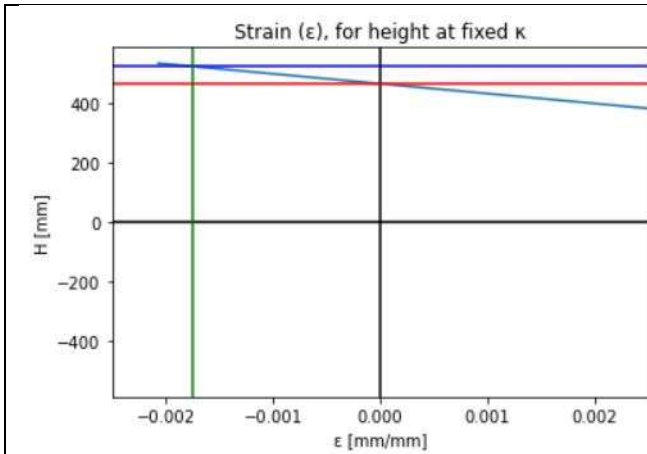


Figure 88, strain-Height, at  $\kappa=-3.0e-05$

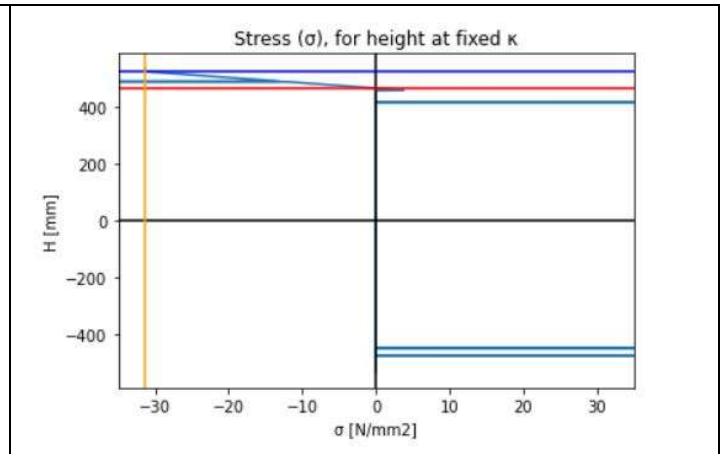


Figure 89, stress-Height, at  $\kappa=-3.0e-05$

In Figure 88 & Figure 89, the strain and stress distribution over the height of the beam at  $\kappa=-3.0e-5$  is shown. The green line marks the end of the elastic region ( $\epsilon_{3k,dl}$ ), the orange line represents the maximum compressive strength ( $f_{cd,dl}$ ) allowed in the top layer, the blue line corresponds to the height at which the maximum tensile strain and strength occur, and the red line indicates the height of the compression zone. Again, it is evident that the maximum compressive strength is not surpassed. There are additional cases and physical phenomena that the input parameters produce, which should be examined. Some of these include the ultimate tensile and compressive strength of the reinforcement steels, changes in stiffness in the reinforcement steels, and the progression of the prestress force. For each Mn- $\kappa$  diagram, I carefully examined whether these cases behaved correctly.

Appendix III – Additional information Chapter 3

Appendix IIIa

FEM properties Model 1&2

Initial Settings

	Model 1	Model 2	Units
Analysis	Structural	Structural	
Dimensions	Two dimensional	Two dimensional	
Model Size	100	100	m
Mesher type	Hexa/Quad	Hexa/Quad	
Mesh order	Linear	Linear	

Geometry

	Model 1	Model 2		
Element	Length	Length	Units	Material
BL1	-	250	mm	Concrete - TB
BL2	630	4520	mm	Concrete - TB
BL3	2620	6230	mm	Concrete - TB
BL4	250	250	mm	Concrete - TB
M-Sup.	250	250	mm	Concrete - CB
BR1	250	250	mm	Concrete - TB
BR2	6230	6230	mm	Concrete - TB
BR3	4520	4520	mm	Concrete - TB
BR4	250	250	mm	Concrete - TB

Materials

Element Class	Class-I Beams 2D	Class-I Beams 2D
Materials	Concrete – TB	Concert - CB
Geometry	T-Beam + DL	SUP

Materials – Properties I

	Concrete - TB	Units
Class	Concrete and masonry	-
Material model	Total strain-based crack model	-
Young's Modulus	40585.4	N/mm <sup>2</sup>
Poison's ratio	0.2	-
Mass density	2.333e-09	T/mm <sup>3</sup>
Gen. stress-strain relation	Elongation strain - Force	Curve – M <sub>n</sub> -κ Diagram
	Dummy stress-strain relation	M <sub>n</sub> -κ Diagram, TB-c

Materials – Properties II

	Concrete - CB	Units
Class	Concrete and masonry	
Material model	Total strain-based crack model	
Young's Modulus	36688.6	N/mm <sup>2</sup>
Poison's ratio	0.2	-
Mass density	2.333e-09	T/mm <sup>3</sup>
Gen. stress-strain relation	Elongation strain - Force	Curve – M <sub>n</sub> -κ Diagram
	Dummy stress-strain relation	M <sub>n</sub> -κ Diagram, CB-c

### Element Geometries

	T-Beam + DL	CB	Units
Shape	I-shape	Rectangular	-
Height (h)	1070	1070	mm
Width of top flange (b1)	983	-	mm
Width of bottom flange (b2)	1180	1200	mm
Thickness of top flange (t1)	160	-	mm
Thickness of bottom flange (t2)	221.83	-	mm
Thickness of web (t3)	300	-	mm

### Mesh - Properties

	Model 1&2	Units
Target Type	Shape	-
Seeding method	Element size	-
Desired size	250	mm

Note: the mesh size was determined using the RTD, Chapter 2.5.5.

### Supports

	Model 1	Model 2
Initial Supports		
Left beam Left Sup.	Fixed vertical	Fixed vertical
Left beam Right Sup.	Fixed horizontal &vertical	Fixed horizontal &vertical
Right beam Left Sup.	Fixed vertical	Fixed vertical
Right beam Right Sup.	Fixed horizontal &vertical	Fixed horizontal &vertical
Combined Supports		
Left beam Left Sup.	-	Fixed vertical
Left beam Right Sup.	Fixed vertical	Fixed vertical
Right beam Left Sup.	Fixed horizontal &vertical	Fixed horizontal &vertical
Right beam Right Sup.	Fixed vertical	Fixed vertical
Displacement Supports		
Sup. Displ. I	-	Fixed vertical
Sup. Displ. II	-	Fixed vertical

### Loads – Load Cases

Load Cases	Load	Model 1	Units	Model 2	Units	Axis
01 - Prestress	$F_{p,L}$	1.39e+06	N	1.39e-06	N	x-axis
	$F_{p,R}$	-1.39e+06	N	-1.39e-06	N	x-axis
	$M_{p,L}$	6.08e+08	Nmm	6.08e+08	Nmm	My
	$M_{p,R}$	-6.08e+08	Nmm	-6.08e+08	Nmm	My
02 - Global Load	Deadweight	Dead weight	-	Dead weight	-	
	$q_{sw, cor.}$	-9.78e-02	N/mm	-9.78e-02	N/mm	
03 - Applied Load	F1	-2.00e+08	N	-40	mm	y-axis
	F2	-1.32e+08	N	-40	mm	y-axis

*Loads - Phases*

		Model 1	Model 2
Phase I	Elements	BL1, BL2, BI3, BR1, BR2, BR3 & BR4	BL1, BL2, BI3, BR1, BR2, BR3 & BR4
	Supports	Initial Supports	Initial Supports
	Loads	01 - Prestress	01 - Prestress
Phase II	Elements	BL1, BL2, BI3, BR1, BR2, BR3, BR4 & M-Sup.	BL1, BL2, BI3, BR1, BR2, BR3, BR4 & M-Sup.
	Supports	Combined Supports	Combined Supports
	Loads	02 - Global Load	02 - Global Load
Phase III	Elements	BL1, BL2, BI3, BR1, BR2, BR3, BR4 & M-Sup.	BL1, BL2, BI3, BR1, BR2, BR3, BR4 & M-Sup.
	Supports	Combined Supports	Combined Supports & Displacement Supports
	Loads	03 - Applied Load	03 - Applied Load

*Analysis – Non-linear Static Analysis*

	Load steps	Non-Linear effects	Equilibrium iterations
<b>Phase I – Prestress Forces</b>			
Prestress Forces	01 - Prestress	Physical nonlinear	Newton-Raphson
	Steps (1.00)		Modified (100 steps)
			Displ. & Force
			Line search - ON
<b>Phase II – Self-weight</b>			
Start step	Previous phase	Physical nonlinear	Newton-Raphson
	Steps (1.00)		Regular (10 steps)
			Displ. & Force
			Line search - ON
Self-weight	02 – Global Load	Physical nonlinear	Newton-Raphson
	Steps (1.00)		Modified (100 steps)
			Displ. & Force
			Line search - ON
<b>Phase III – Applied Load</b>			
Start step	Previous phase	Physical nonlinear	Newton-Raphson
	Steps (1.00)		Regular (10 steps)
			Displ. & Force
			Line search - ON
Applied	03 - Applied Load	Physical nonlinear	Newton-Raphson
	Steps (0.05(200))		Modified (1000 steps)
			Displ. & Force
			Line search - ON

*Outputs*

Model 1 & 2	DISPLACEMENT	TOTAL	TRANSLATION	GLOBAL
Model 2	FORCE	TOTAL	TRANSLATION	GLOBAL
Model 1 & 2	STRESS	TOTAL	MOMENT	LOCAL
Model 1 & 2	STRAIN	REACTION	MOMENT	LOCAL

Appendix IIIb

FEM properties Model 3

*Initial Settings*

	Model 3	Units
Analysis	Structural	
Dimensions	Three dimensional	
Model Size	100	m
Mesher type	Hexa/Quad	
Mesh order	Linear	

*Geometry*

Element	Length	Units	Element		Units	Material
BL1	250	mm	BR1	250	mm	Concrete - TB
BL2	4520	mm	BR2	6230	mm	Concrete - TB
BL3	6230	mm	BR3	4520	mm	Concrete - TB
BL4	250	mm	BR4	250	mm	Concrete - TB
M-Sup.	250	mm			mm	Concrete - CB

Materials

Element Class	Class-I Beams 3D	Class-I Beams 3D	Flat Shell
Materials	Concrete – TB	Concert - CB	Concrete Deck
Geometry	T-Beam + DL	SUP	Deck Thick.

*Materials – Properties I*

	Concrete – TB	Units
Class	Concrete and masonry	
Material model	Total strain-based crack model	
Young's Modulus	40585.4	N/mm <sup>2</sup>
Poison's ratio	0.2	-
Mass density	2.333e-09	T/mm <sup>3</sup>
Gen. stress-strain relation	Elongation strain - Force	Curve – M <sub>n</sub> -κ Diagram
	Dummy stress-strain relation	M <sub>n</sub> -κ Diagram, TB-m

*Materials – Properties II*

	Concrete - CB	Units
Class	Concrete and masonry	
Material model	Total strain-based crack model	
Young's Modulus	36688.6	N/mm <sup>2</sup>
Poison's ratio	0.2	-
Mass density	2.333e-09	T/mm <sup>3</sup>
Gen. stress-strain relation	Elongation strain - Force	Curve – M <sub>n</sub> -κ Diagram
	Dummy stress-strain relation	M <sub>n</sub> -κ Diagram, CB-m

Materials – Properties III

	Concrete – Concrete Deck	Units
Class	Concrete and masonry	
Material model	Linear elastic isotropic	
Young’s Modulus	12229.5	N/mm <sup>2</sup>
Poison’s ratio	0.2	-
Mass density	2.333e-09	T/mm <sup>3</sup>

Element Geometries

	T-Beam + DL	SUP	Deck	Units
Shape	I-shape	Rectangular	Thickness	
Height (h)	1070	1070	-	mm
Width of top flange (b1)	983	-	-	mm
Width of bottom flange (b2)	1180	1200	-	mm
Thickness of top flange (t1)	160	-	-	mm
Thickness of bottom flange (t2)	221.85	-	-	mm
Thickness of web (t3)	300	-	-	mm
Thickness	-	-	160	mm

Mesh

	Model 3	Units
Target Type	Shape	-
Seeding method	Element size	-
Desired size	250	mm

Note: the mesh size was determined using the RTD, Chapter 2.5.5.

Supports – Model 3

	Model 3
Initial Supports	
Left beam Left Sup.	Fixed z-axis
Left beam Right Sup.	Fixed x-axis, y-axis & z-axis
Right beam Left Sup.	Fixed x-axis, y-axis & z-axis
Right beam Right Sup.	Fixed z-axis
Combined Supports	
Left beam Left Sup.	Fixed z-axis
Left beam Right Sup.	Fixed z-axis
Right beam Left Sup.	Fixed x-axis, y-axis & z-axis
Right beam Right Sup.	Fixed z-axis
Displacement Supports	
Sup. Displ. I	Fixed z-axis
Sup. Displ. II	Fixed z-axis

Load Cases – Model 3

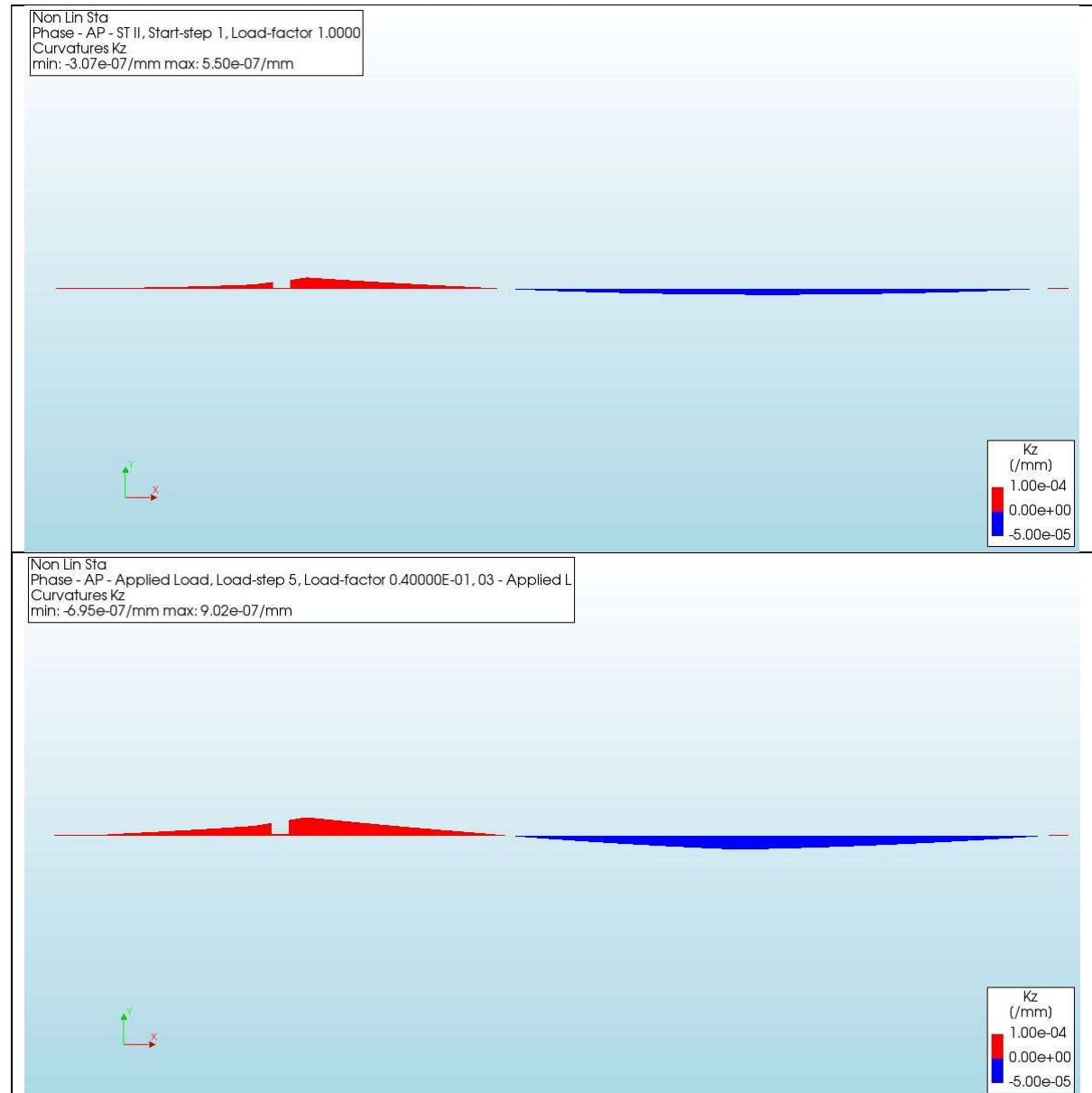
Load Cases	Load	Model 3	Units	axis
01 - Prestress	$F_{p,L}$	1.39e+06	N	x-axis
	$F_{p,R}$	-1.39e+06	N	x-axis
	$M_{p,L}$	6.08e+08	Nmm	$M_y$
	$M_{p,R}$	-6.08e+08	Nmm	$M_y$
02 - Global Load	Deadweight	Dead weight	-	
	$q_{sw, cor.}$	-9.78e-02	N/mm	
03 - Applied Load	F1	-40	mm	z-axis
	F2	-40	mm	z-axis

Output

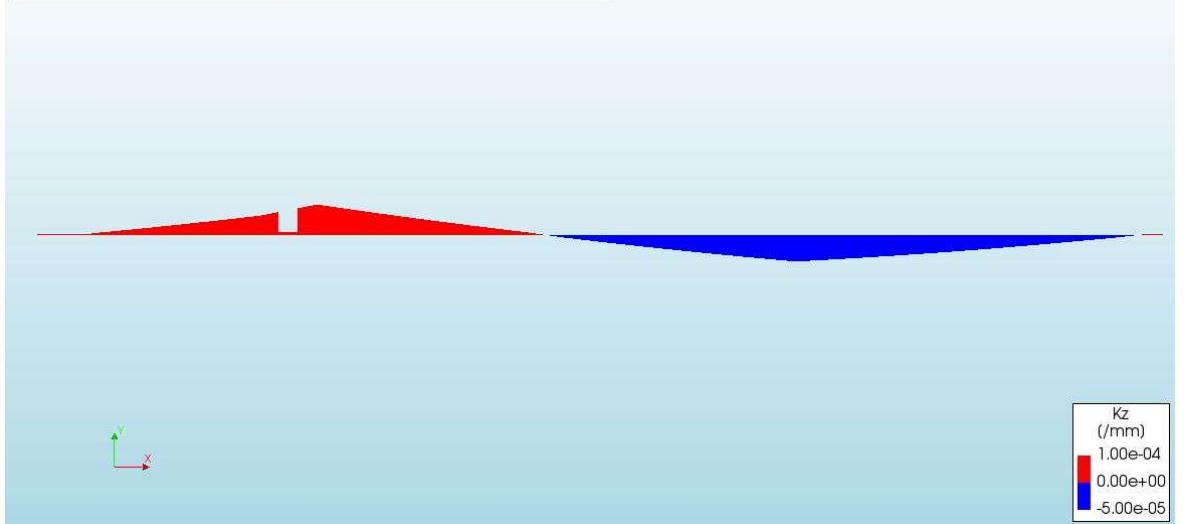
Model 3	DISPLACEMENT	TOTAL	TRANSLATION	GLOBAL
Model 3	FORCE	TOTAL	TRANSLATION	GLOBAL
Model 3	STRESS	TOTAL	MOMENT	LOCAL
Model 3	STRAIN	REACTION	MOMENT	LOCAL

# Appendix IIIc

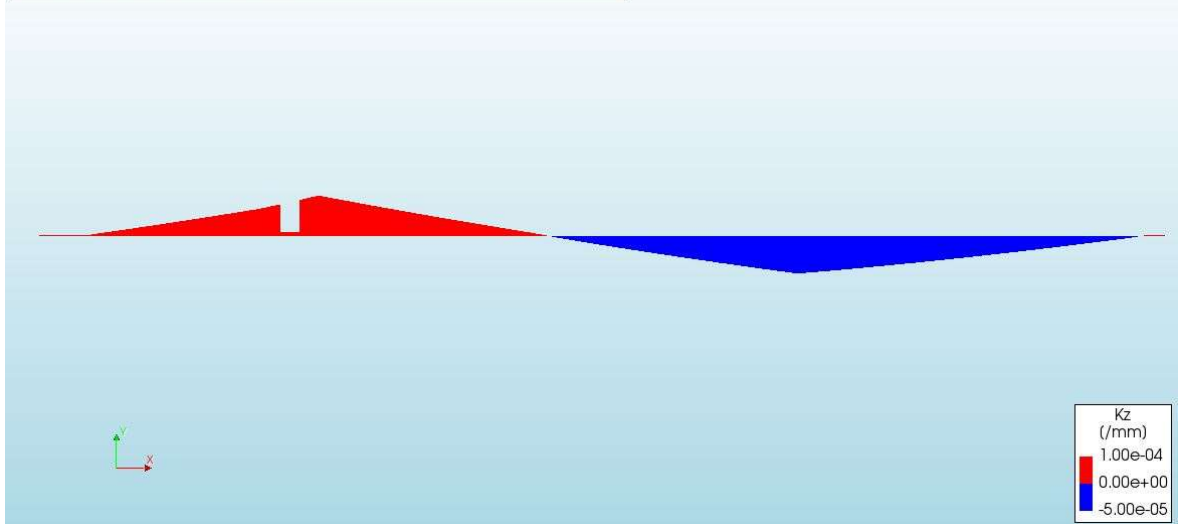
## Curvature ( $\kappa_z$ ) Model 1, every 5 load steps & final step



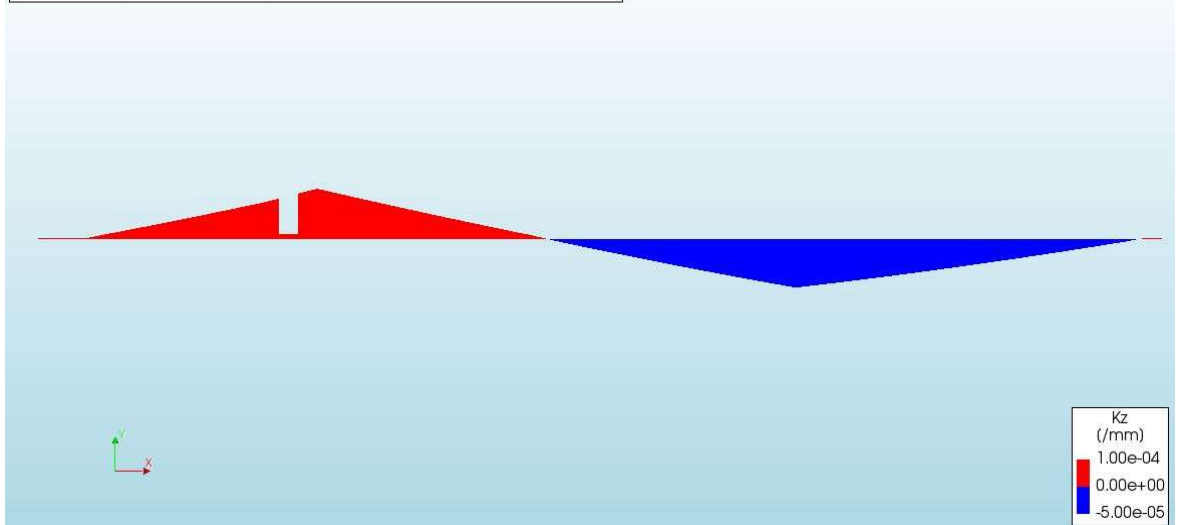
Non Lin Sta  
Phase - AP - Applied Load, Load-step 10, Load-factor 0.9000E-01, 03 - Applied  
Curvatures Kz  
min: -1.19e-06/mm max: 1.34e-06/mm



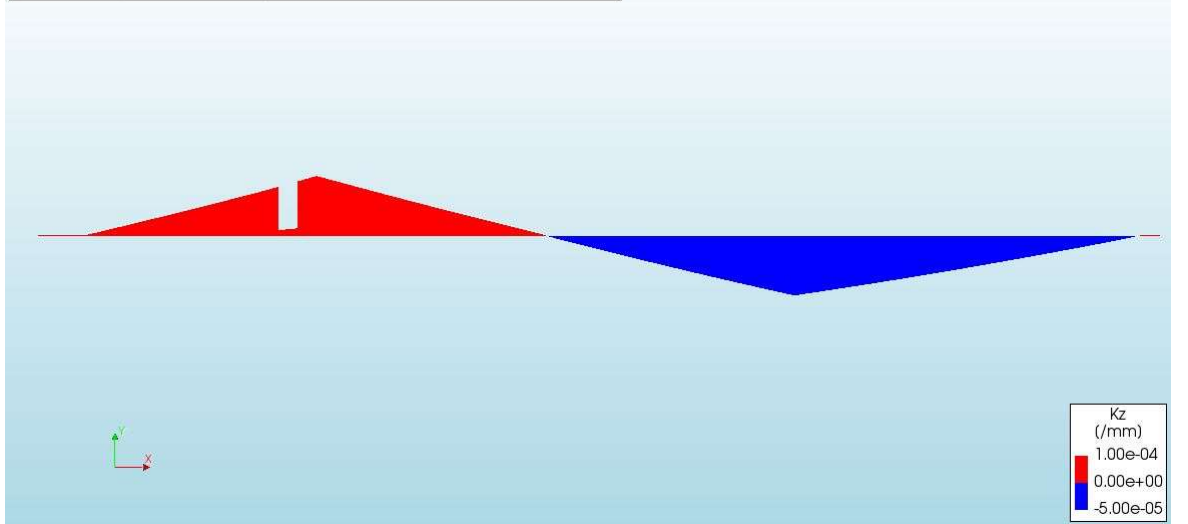
Non Lin Sta  
Phase - AP - Applied Load, Load-step 15, Load-factor 0.14000, 03 - Applied Load  
Curvatures Kz  
min: -1.68e-06/mm max: 1.78e-06/mm



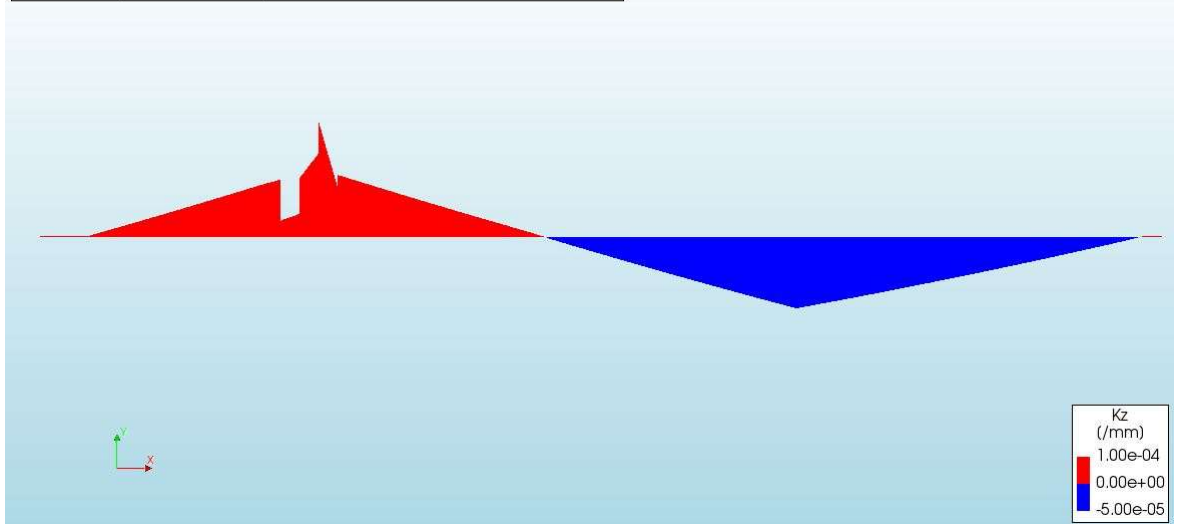
Non Lin Sta  
Phase - AP - Applied Load, Load-step 20, Load-factor 0.19000, 03 - Applied Load  
Curvatures Kz  
min: -2.17e-06/mm max: 2.22e-06/mm



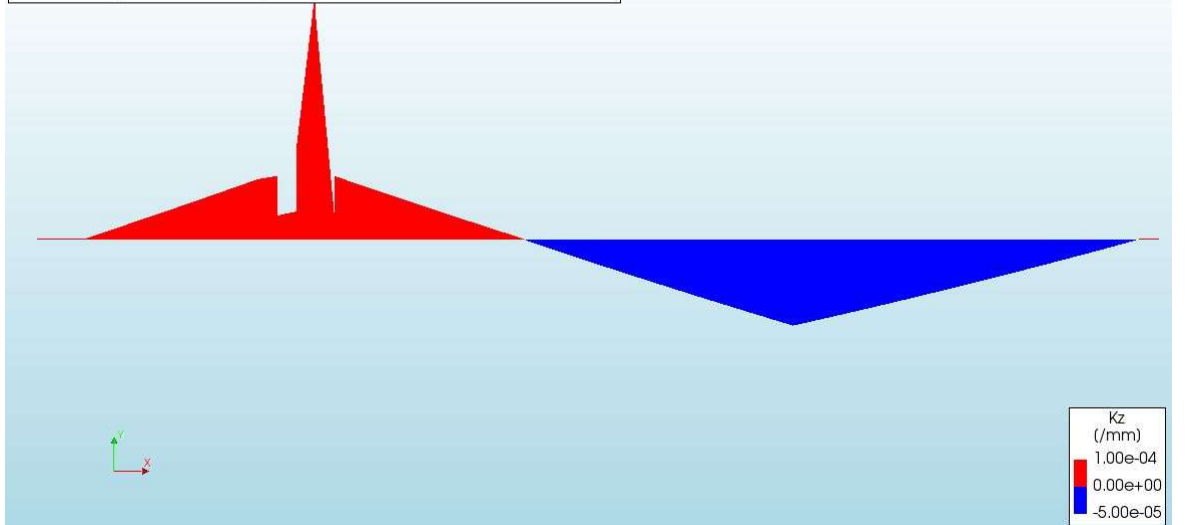
Non Lin Sta  
Phase - AP - Applied Load, Load-step 25, Load-factor 0.24000, 03 - Applied Load  
Curvatures Kz  
min: -2.66e-06/mm max: 2.66e-06/mm



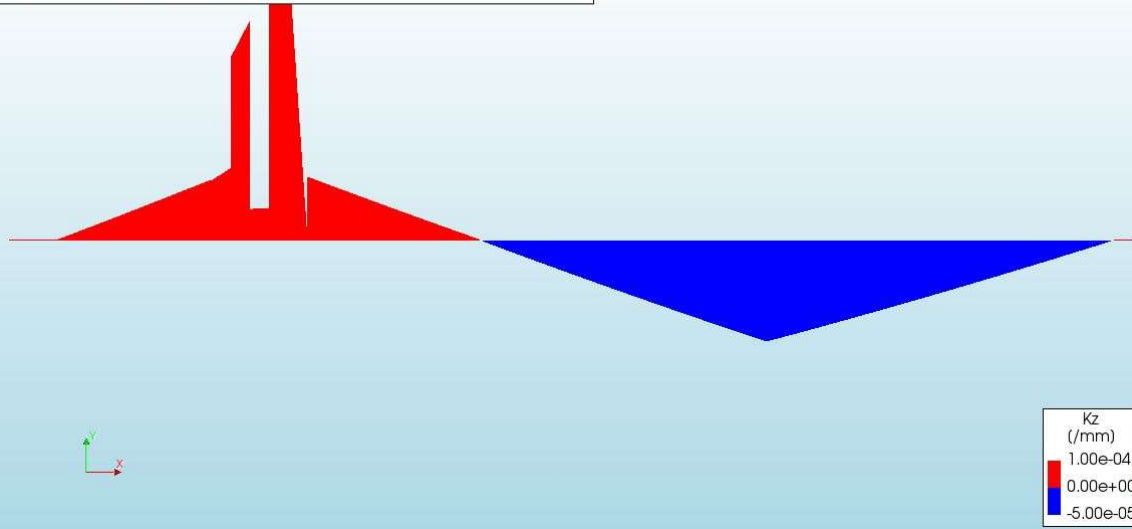
Non Lin Sta  
Phase - AP - Applied Load, Load-step 30, Load-factor 0.29000, 03 - Applied Load  
Curvatures Kz  
min: -3.19e-06/mm max: 5.15e-06/mm



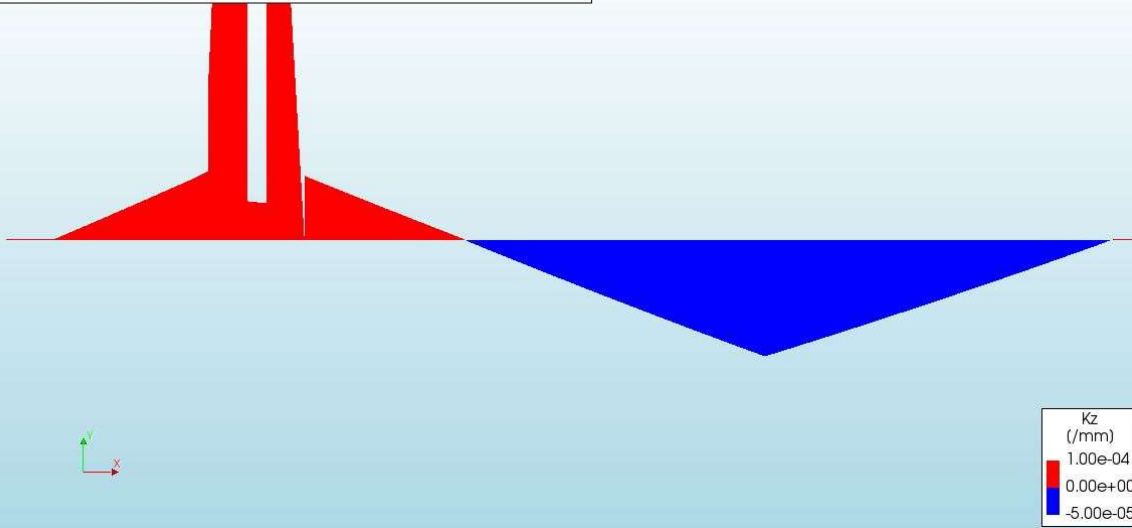
Non Lin Sta  
Phase - AP - Applied Load, Load-step 35, Load-factor 0.34000, 03 - Applied Load  
Curvatures Kz  
min: -3.84e-06/mm max: 1.11e-05/mm



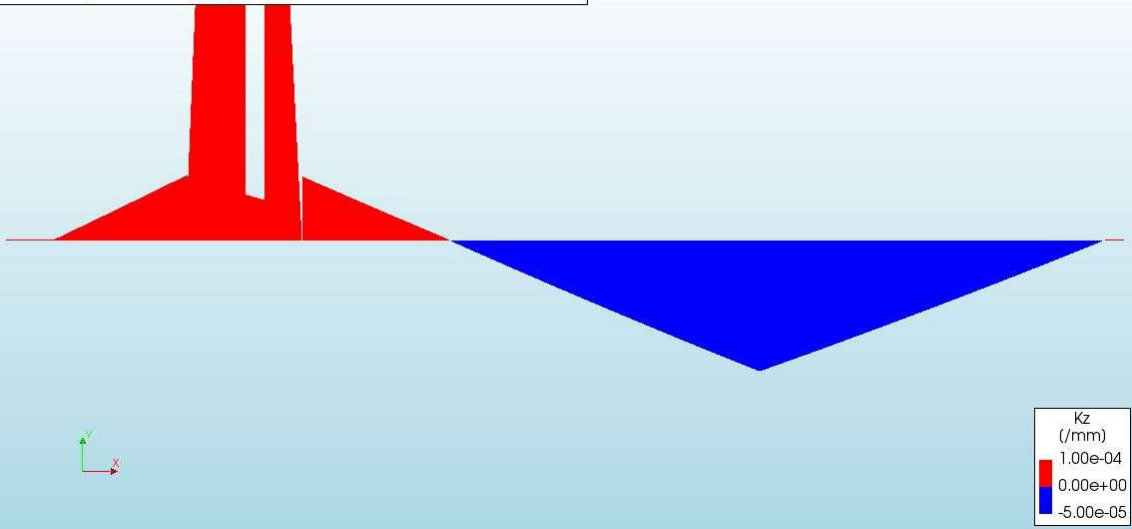
Non Lin Sta  
Phase - AP - Applied Load, Load-step 40, Load-factor 0.39000, 03 - Applied Load  
Curvatures Kz  
min: -4.50e-06/mm max: 1.35e-05/mm



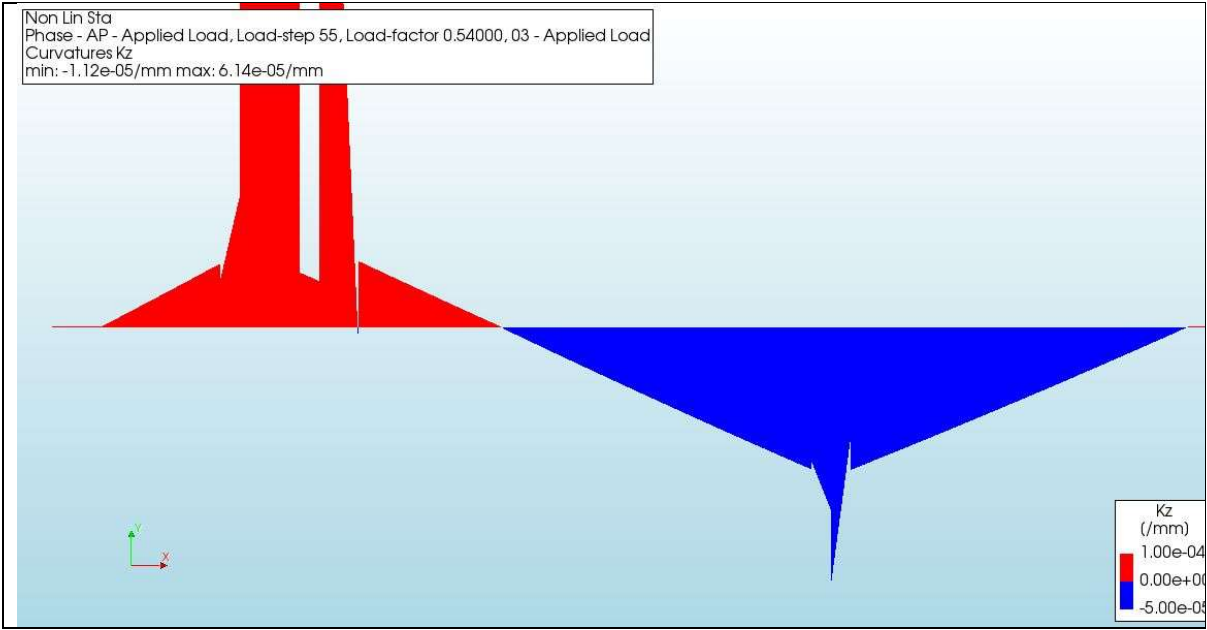
Non Lin Sta  
Phase - AP - Applied Load, Load-step 45, Load-factor 0.44000, 03 - Applied Load  
Curvatures Kz  
min: -5.17e-06/mm max: 2.59e-05/mm



Non Lin Sta  
Phase - AP - Applied Load, Load-step 50, Load-factor 0.49000, 03 - Applied Load  
Curvatures Kz  
min: -5.85e-06/mm max: 4.36e-05/mm

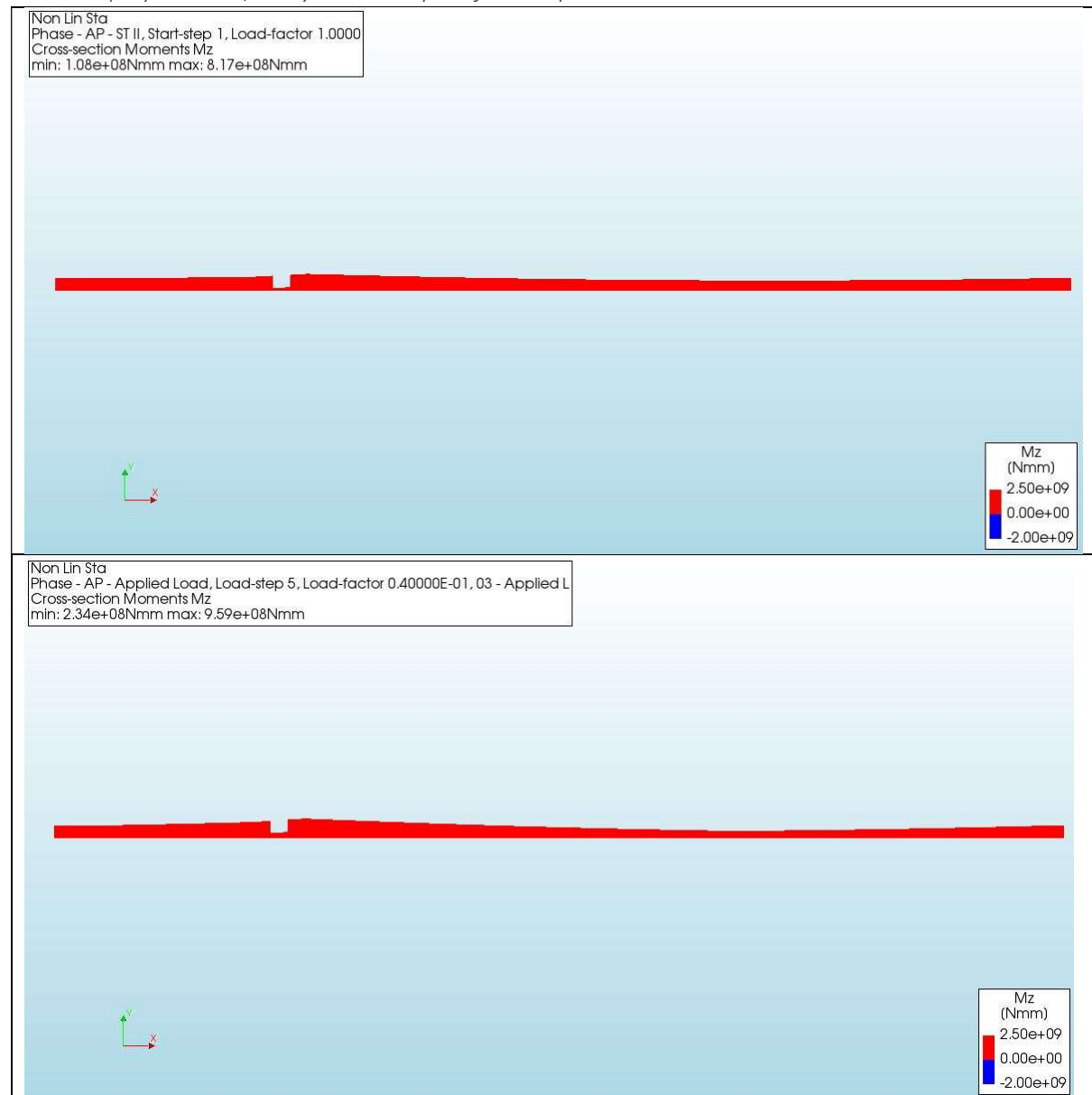


Non Lin Sta  
Phase - AP - Applied Load, Load-step 55, Load-factor 0.54000, 03 - Applied Load  
Curvatures Kz  
min: -1.12e-05/mm max: 6.14e-05/mm

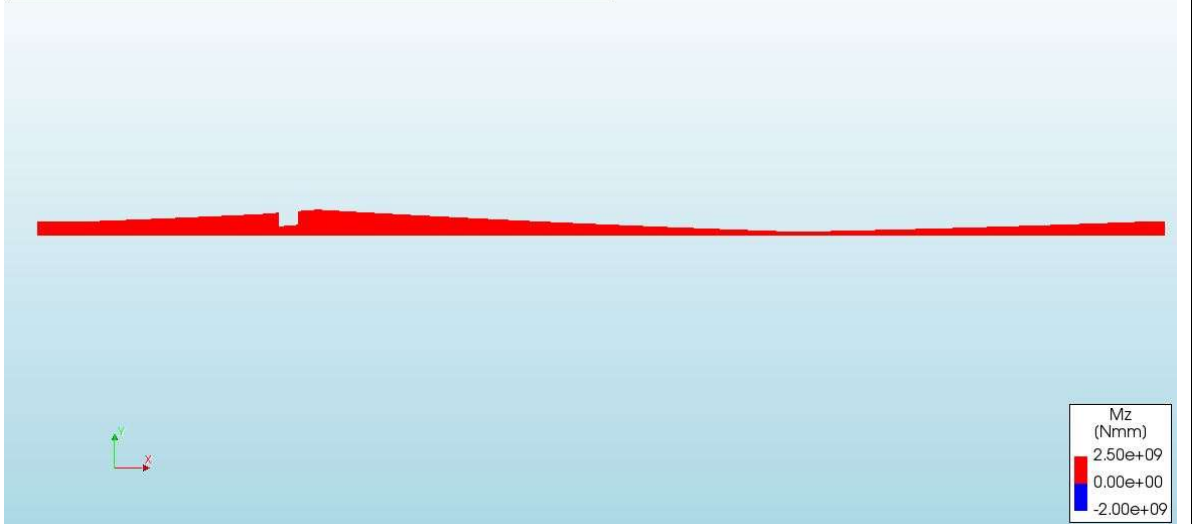


# Appendix III d

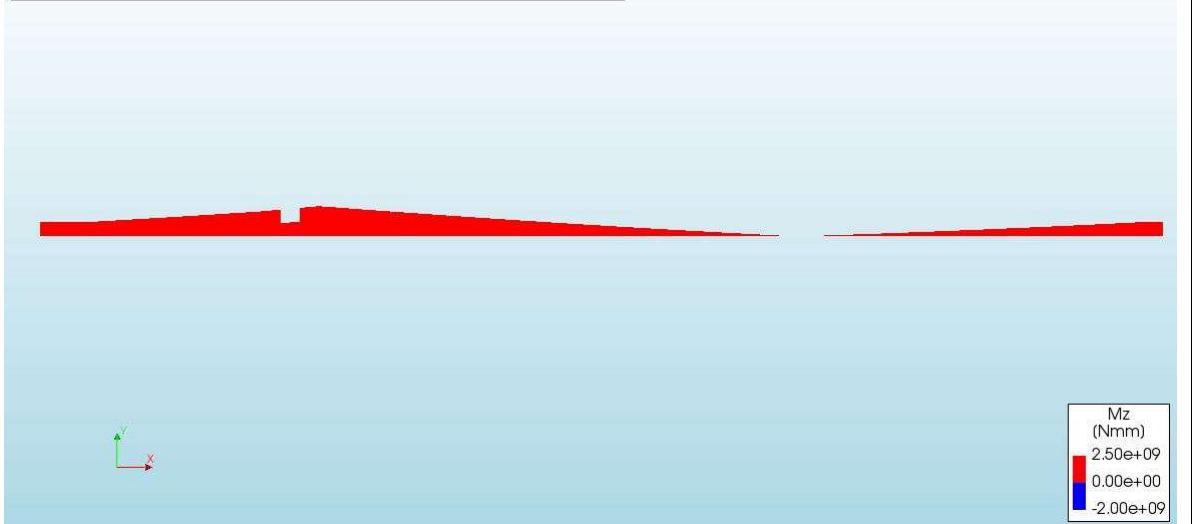
## Moment ( $M_z$ ) Model 1, every 5 load steps & final step



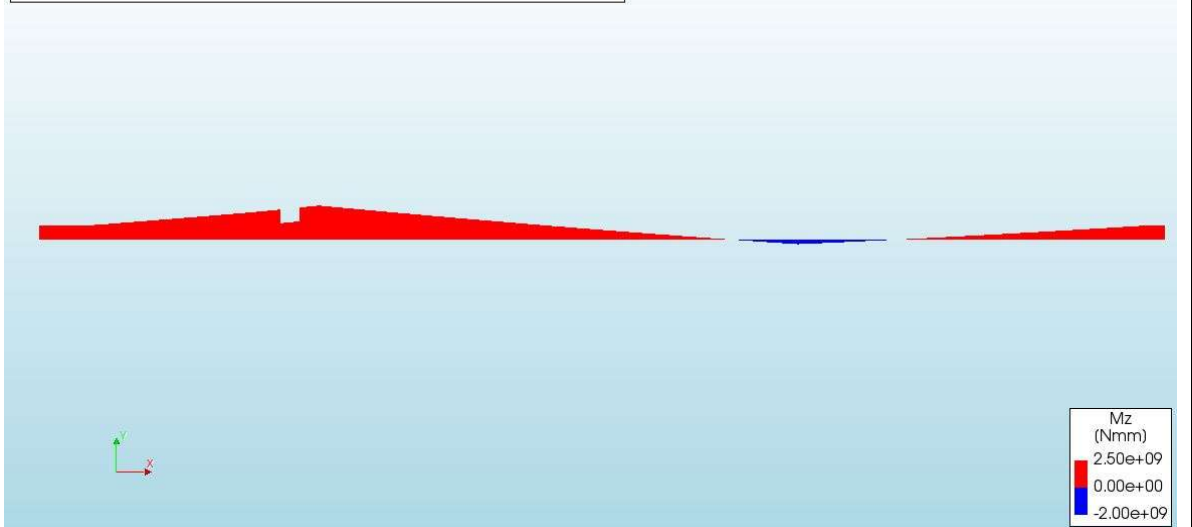
Non Lin Sta  
Phase - AP - Applied Load, Load-step 10, Load-factor 0.90000E-01, 03 - Applied  
Cross-section Moments Mz  
min: 1.56e+08Nmm max: 1.14e+09Nmm



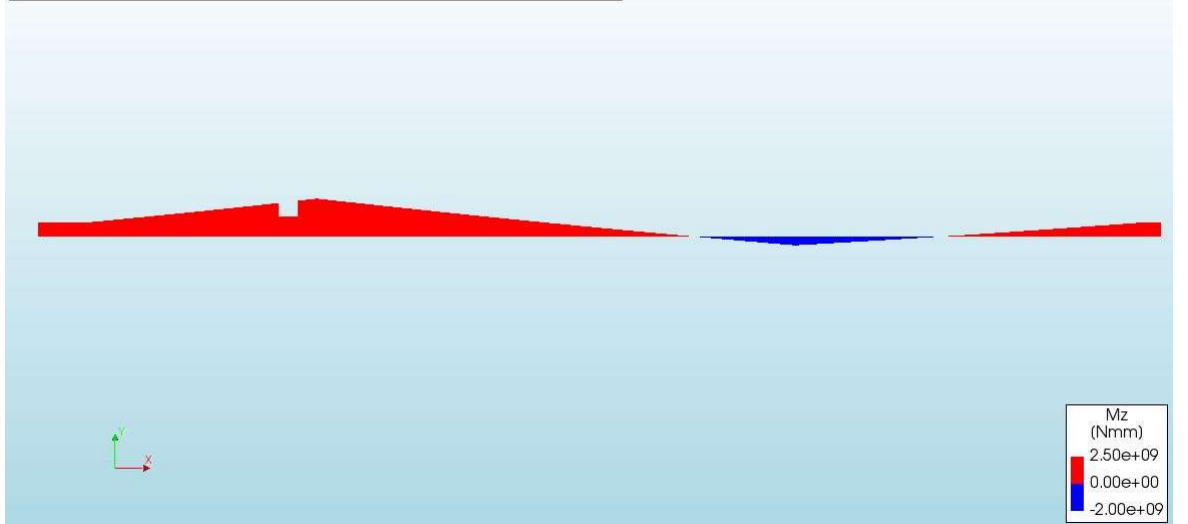
Non Lin Sta  
Phase - AP - Applied Load, Load-step 15, Load-factor 0.14000, 03 - Applied Load  
Cross-section Moments Mz  
min: -3.07e+07Nmm max: 1.32e+09Nmm



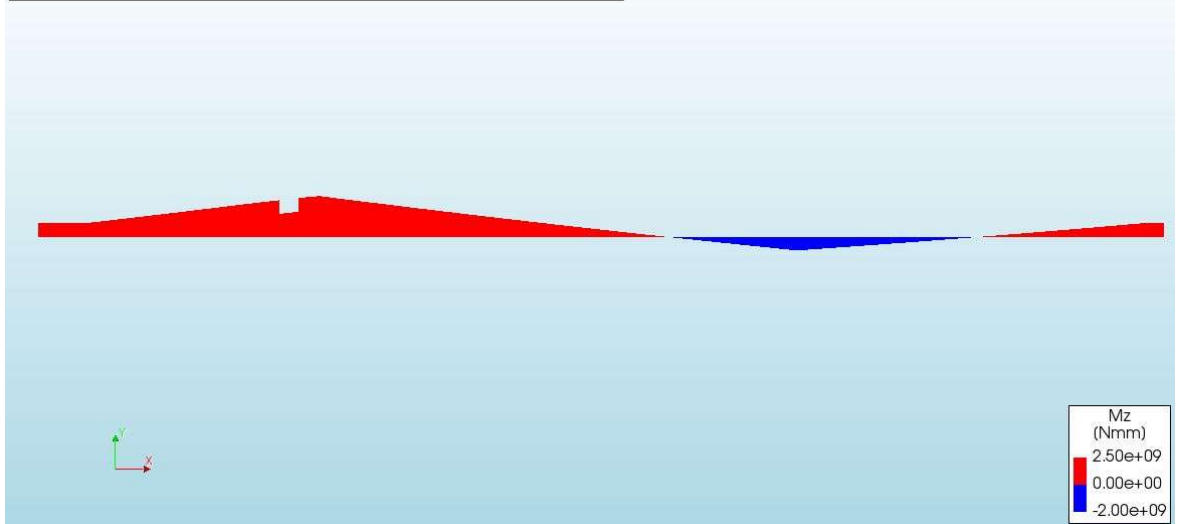
Non Lin Sta  
Phase - AP - Applied Load, Load-step 20, Load-factor 0.19000, 03 - Applied Load  
Cross-section Moments Mz  
min: -2.18e+08Nmm max: 1.49e+09Nmm



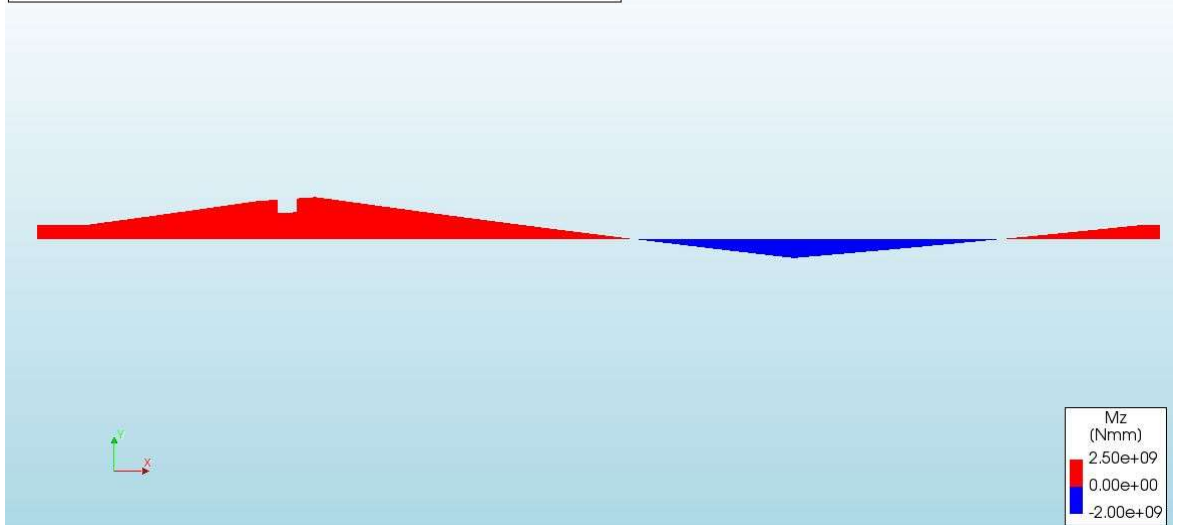
Non Lin Sta  
Phase - AP - Applied Load, Load-step 25, Load-factor 0.24000, 03 - Applied Load  
Cross-section Moments Mz  
min: -4.05e+08Nmm max: 1.67e+09Nmm



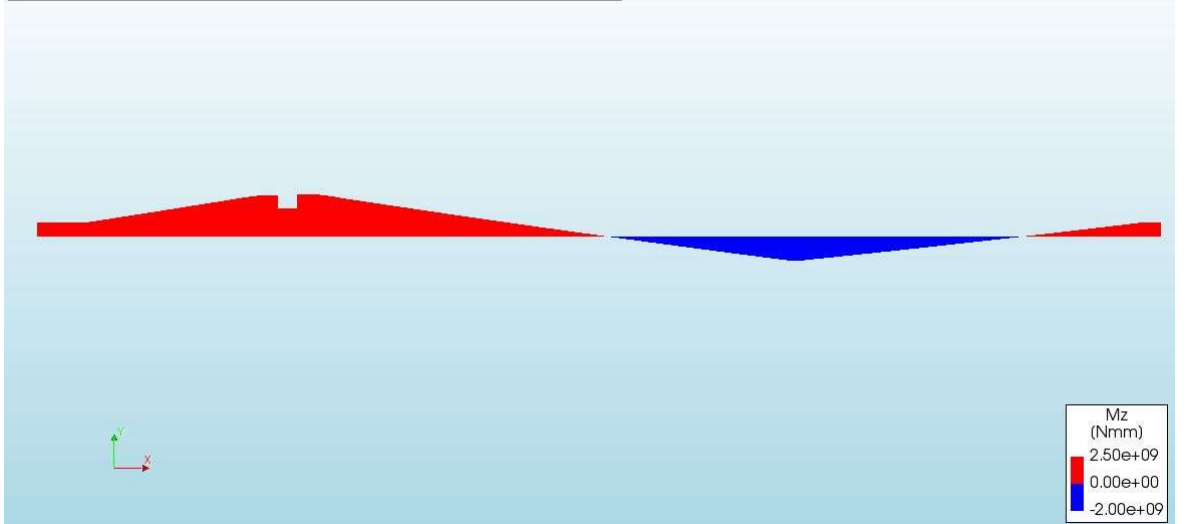
Non Lin Sta  
Phase - AP - Applied Load, Load-step 30, Load-factor 0.29000, 03 - Applied Load  
Cross-section Moments Mz  
min: -6.06e+08Nmm max: 1.81e+09Nmm



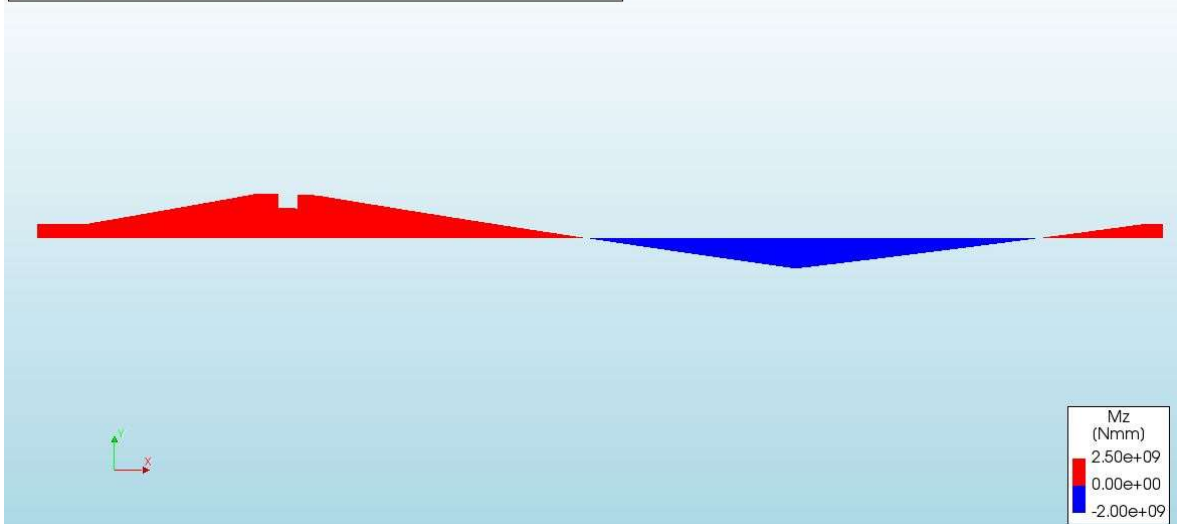
Non Lin Sta  
Phase - AP - Applied Load, Load-step 35, Load-factor 0.34000, 03 - Applied Load  
Cross-section Moments Mz  
min: -8.55e+08Nmm max: 1.85e+09Nmm



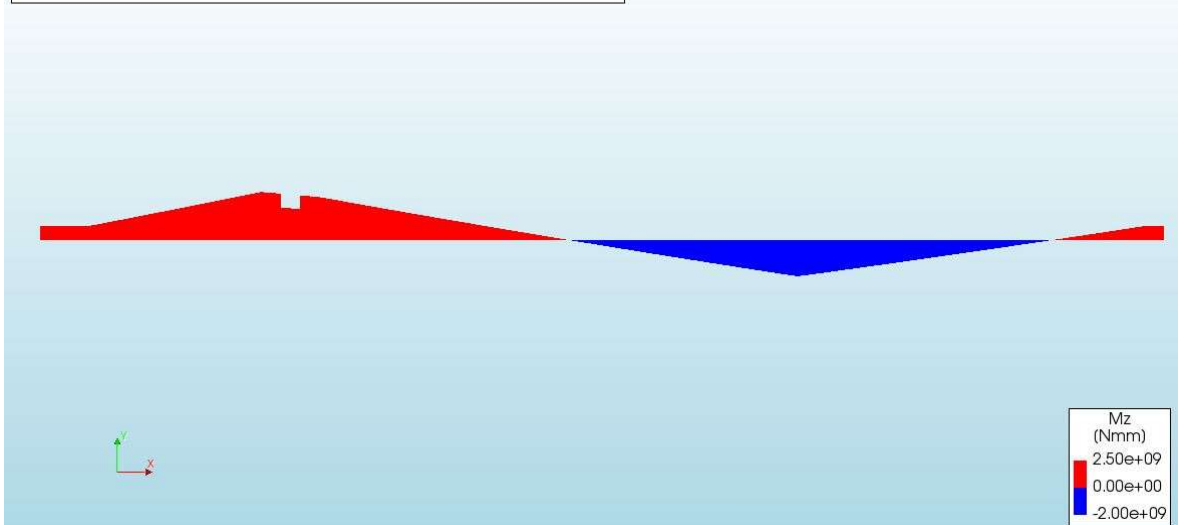
Non Lin Sta  
Phase - AP - Applied Load, Load-step 40, Load-factor 0.39000, 03 - Applied Load  
Cross-section Moments Mz  
min: -1.11e+09Nmm max: 1.87e+09Nmm



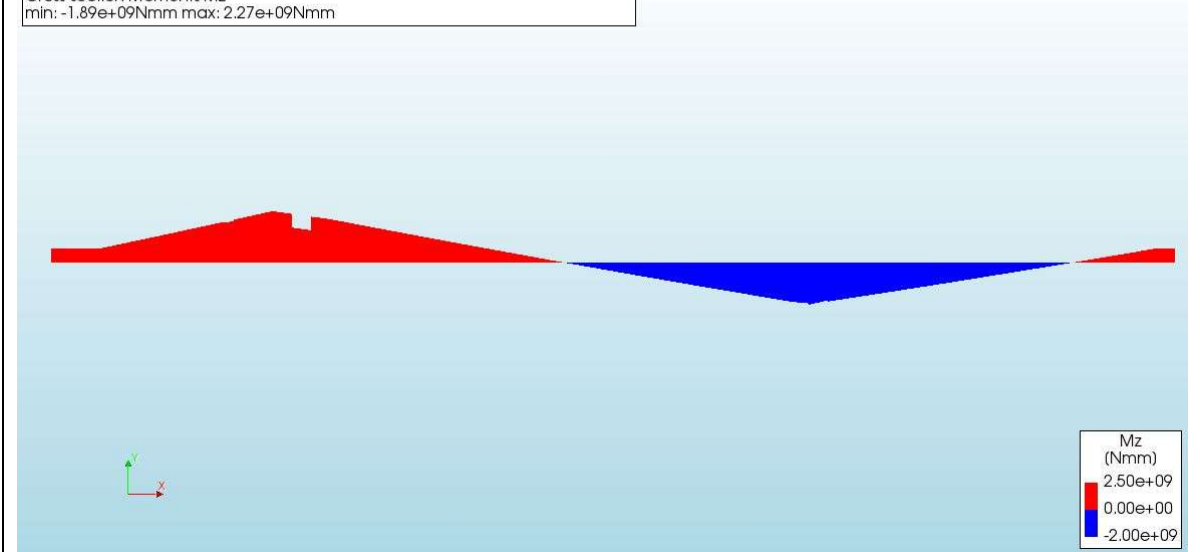
Non Lin Sta  
Phase - AP - Applied Load, Load-step 45, Load-factor 0.44000, 03 - Applied Load  
Cross-section Moments Mz  
min: -1.36e+09Nmm max: 1.97e+09Nmm



Non Lin Sta  
Phase - AP - Applied Load, Load-step 50, Load-factor 0.49000, 03 - Applied Load  
Cross-section Moments Mz  
min: -1.62e+09Nmm max: 2.12e+09Nmm



Non Lin Sta  
Phase - AP - Applied Load, Load-step 55, Load-factor 0.54000, 03 - Applied Load  
Cross-section Moments Mz  
min: -1.89e+09Nmm max: 2.27e+09Nmm



Appendix IIIe

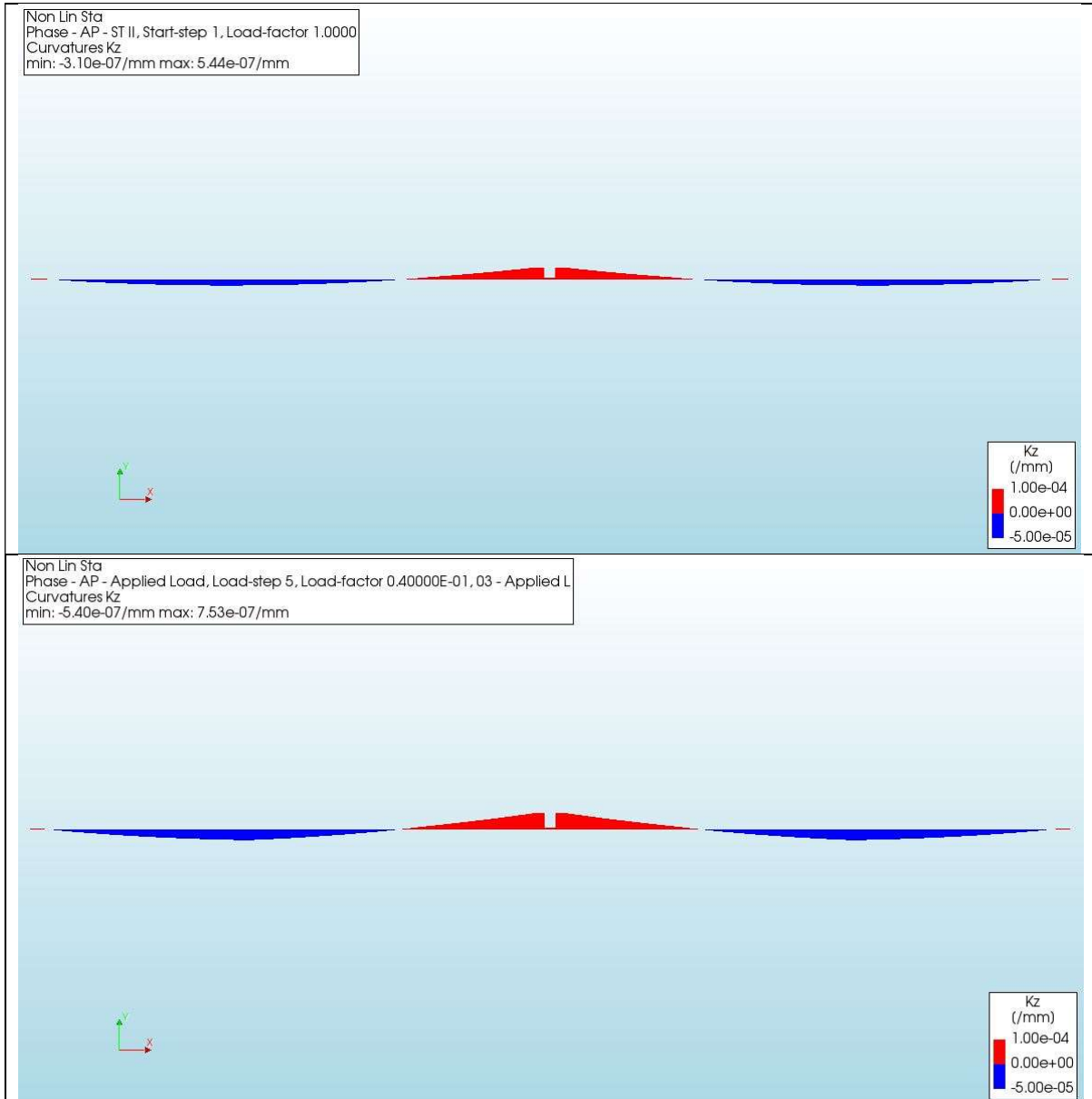
Curvature ( $\kappa_z$ ) development, Model 1

0	F2	SLL	SL	SLR	SRL	SR	SRR	F1
	0	0	0	0	0	0	0	0
2	0	0	0	0	0	0	0	0
3	0	0	0	1	1	1	1	-1
4	0	1	1	1	1	1	1	-1
5	0	1	1	1	1	1	1	-1
6	0	1	1	1	1	1	1	-1
7	0	1	1	1	1	1	1	-1
8	0	1	1	1	1	1	1	-1
9	0	1	1	1	1	1	1	-1
10	0	1	1	1	1	1	1	-1
11	0	1	1	1	1	1	1	-1
12	0	1	1	1	1	1	1	-1
13	0	1	1	1	1	1	1	-1
14	0	1	1	1	1	1	1	-1
15	0	1	1	1	1	1	1	-1
16	0	1	1	1	1	1	1	-1
17	0	1	1	1	1	1	1	-1
18	0	1	1	1	1	1	1	-1
19	0	1	1	1	1	1	1	-1
20	0	1	1	1	1	1	1	-1
21	0	1	1	1	1	1	1	-1
22	0	1	1	1	1	1	1	-1
23	0	1	1	1	1	1	1	-1
24	0	1	1	1	1	1	1	-1
25	0	1	1	1	1	1	1	-1
26	0	1	1	1	1	1	1	-1
27	0	1	1	1	1	1	1	-1
28	0	1	1	1	1	1	1	-1
29	0	1	1	1	1	1	1	-1
30	0	1	1	1	1	1	1	-1
31	0	1	1	1	1	1	1	-1
32	0	1	1	1	1	2	1	-1
33	0	1	1	1	1	2	1	-1
34	0	1	1	1	1	2	1	-1
35	0	1	1	1	1	2	1	-1
36	0	1	1	1	1	2	1	-1
37	0	1	1	1	1	2	1	-1
38	0	1	1	1	1	2	1	-1
39	0	1	1	1	2	2	1	-1
40	0	1	1	1	2	2	1	-1
41	0	1	1	1	2	2	1	-1
42	0	1	2	2	2	2	1	-1
43	0	1	2	2	2	2	1	-1
44	0	1	2	2	2	2	1	-1
45	0	1	2	2	2	2	1	-1
46	0	1	2	2	2	2	1	-1
47	0	2	2	2	2	2	1	-1
48	0	2	2	2	2	2	1	-1
49	0	2	2	2	2	2	1	-1
50	0	2	2	2	2	2	1	-1
51	0	2	2	2	2	2	1	-1
52	0	2	2	2	2	2	1	-1
53	0	2	2	2	2	2	1	-1
54	0	2	2	2	2	2	1	-1
55	0	2	2	2	2	2	1	-1
56	0	2	2	2	2	2	1	-1
57	0	2	2	2	2	2	1	-2
58	0	2	3	2	2	2	1	-2
59	0	2	3	2	2	2	1	-2

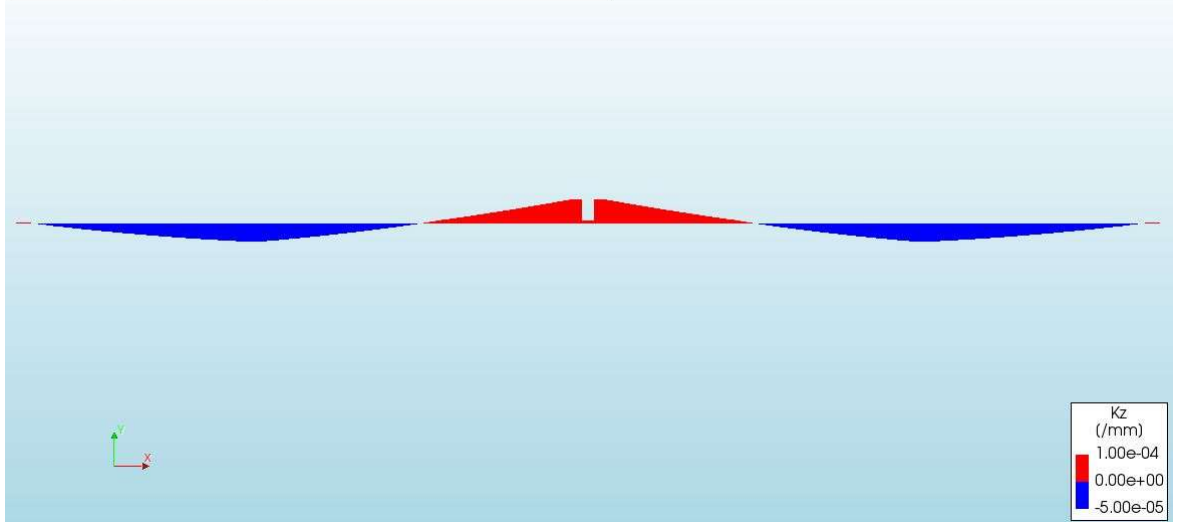
$\kappa_{U-}$	-3,33E-05	-3
$\kappa_{Y-}$	-6,29E-06	-2
$\kappa_{Cr-}$	-1,00E-07	-1
$\kappa_0$		0
$\kappa_{Cr+}$	1.00E-07	1
$\kappa_{Y+}$	2,93E-06	2
$\kappa_{U+}$	6,04E-05	3

# Appendix IIIf

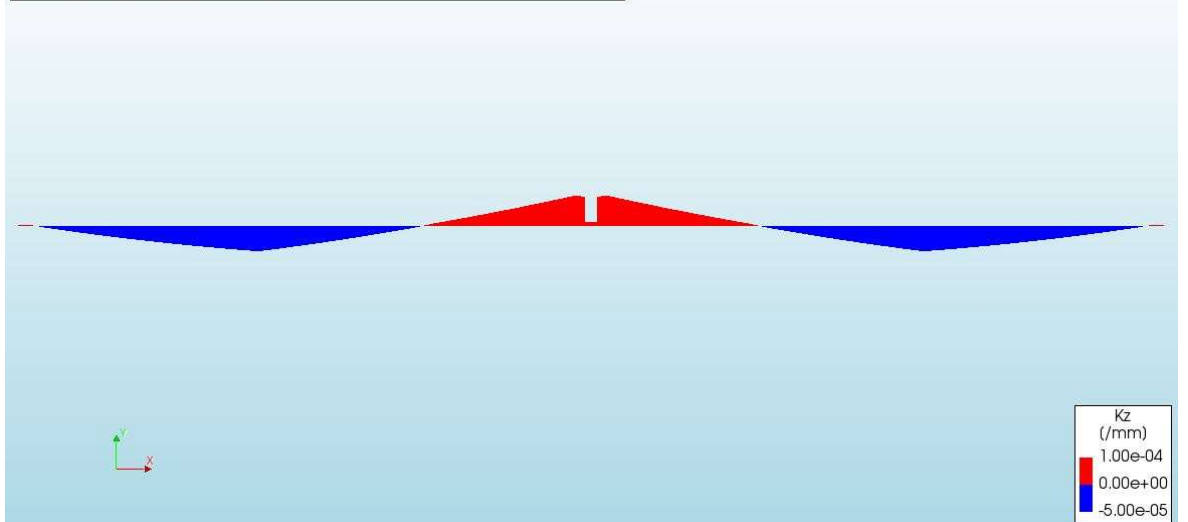
## Curvature ( $\kappa_z$ ) Model 2, every 5 load steps & final step



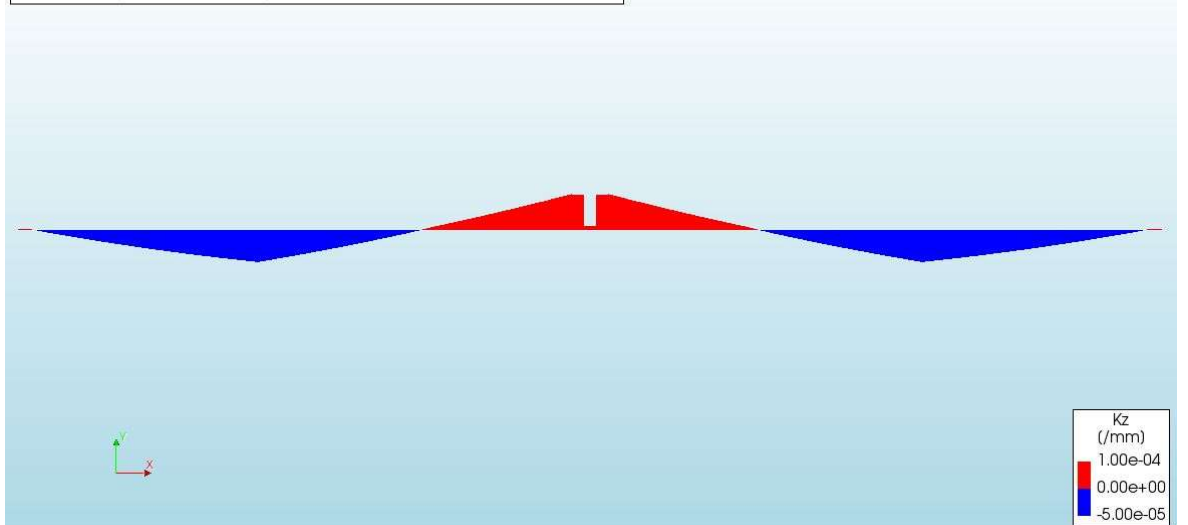
Non Lin Sta  
Phase - AP - Applied Load, Load-step 10, Load-factor 0.90000E-01, 03 - Applied  
Curvatures Kz  
min: -8.32e-07/mm max: 1.01e-06/mm



Non Lin Sta  
Phase - AP - Applied Load, Load-step 15, Load-factor 0.14000, 03 - Applied Load  
Curvatures Kz  
min: -1.12e-06/mm max: 1.27e-06/mm



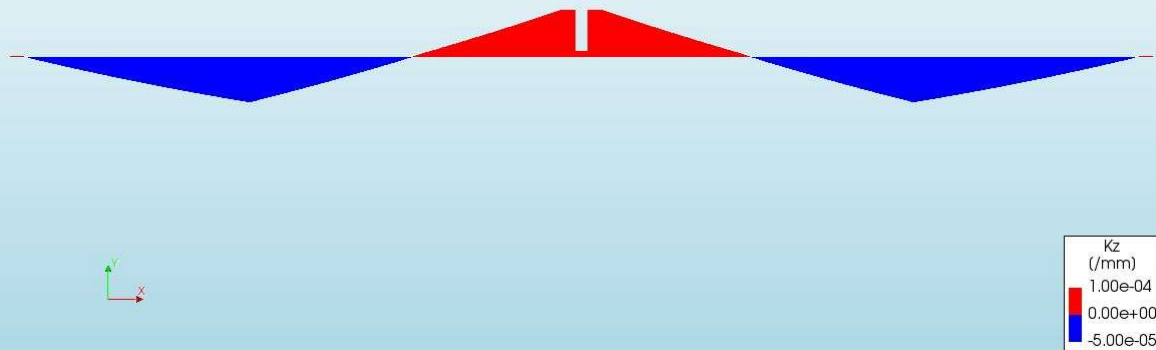
Non Lin Sta  
Phase - AP - Applied Load, Load-step 20, Load-factor 0.19000, 03 - Applied Load  
Curvatures Kz  
min: -1.42e-06/mm max: 1.54e-06/mm



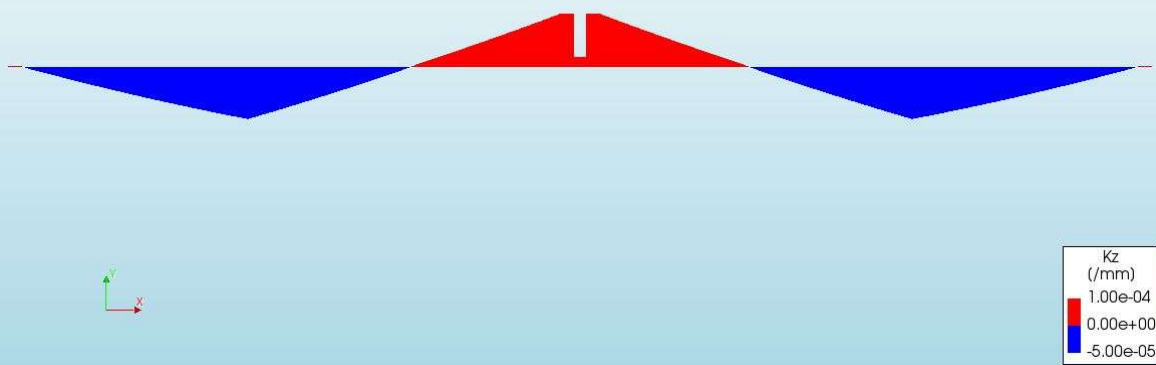
Non Lin Sta  
Phase - AP - Applied Load, Load-step 25, Load-factor 0.24000, 03 - Applied Load  
Curvatures Kz  
min: -1.71e-06/mm max: 1.80e-06/mm



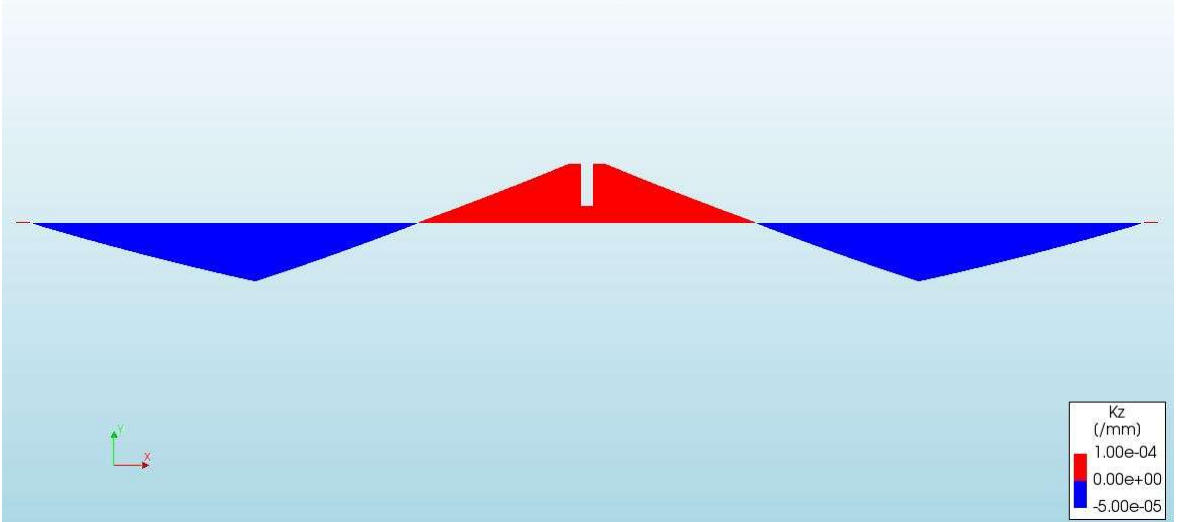
Non Lin Sta  
Phase - AP - Applied Load, Load-step 30, Load-factor 0.29000, 03 - Applied Load  
Curvatures Kz  
min: -2.00e-06/mm max: 2.06e-06/mm



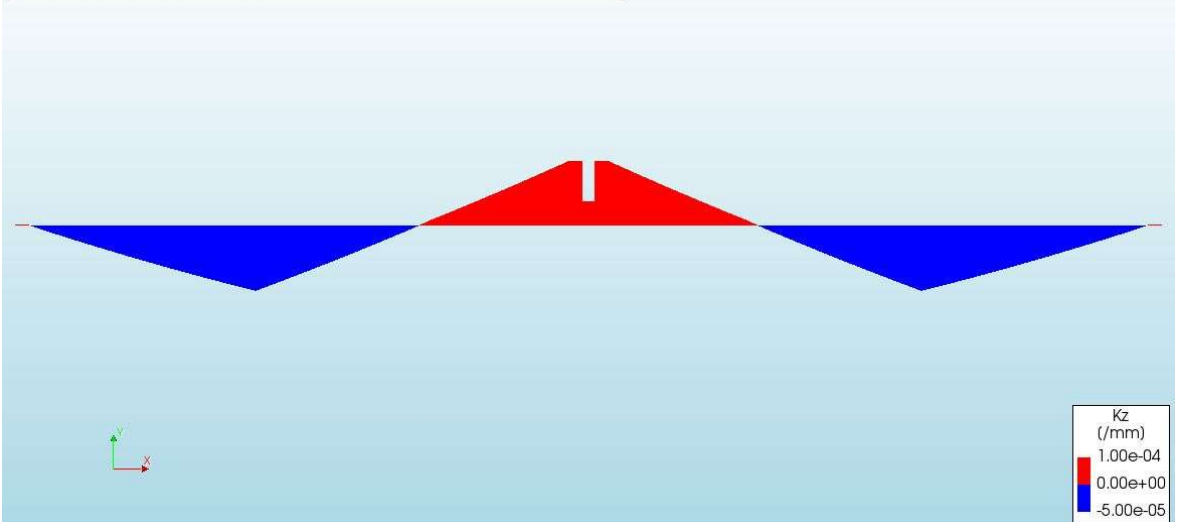
Non Lin Sta  
Phase - AP - Applied Load, Load-step 35, Load-factor 0.34000, 03 - Applied Load  
Curvatures Kz  
min: -2.29e-06/mm max: 2.31e-06/mm



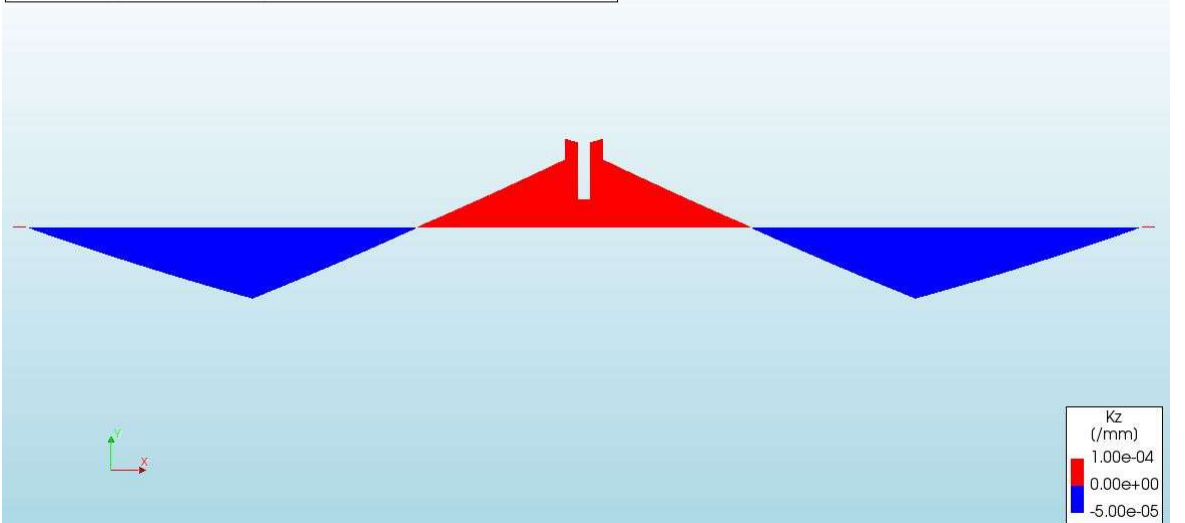
Non Lin Sta  
Phase - AP - Applied Load, Load-step 40, Load-factor 0.39000, 03 - Applied Load  
Curvatures Kz  
min: -2.58e-06/mm max: 2.55e-06/mm



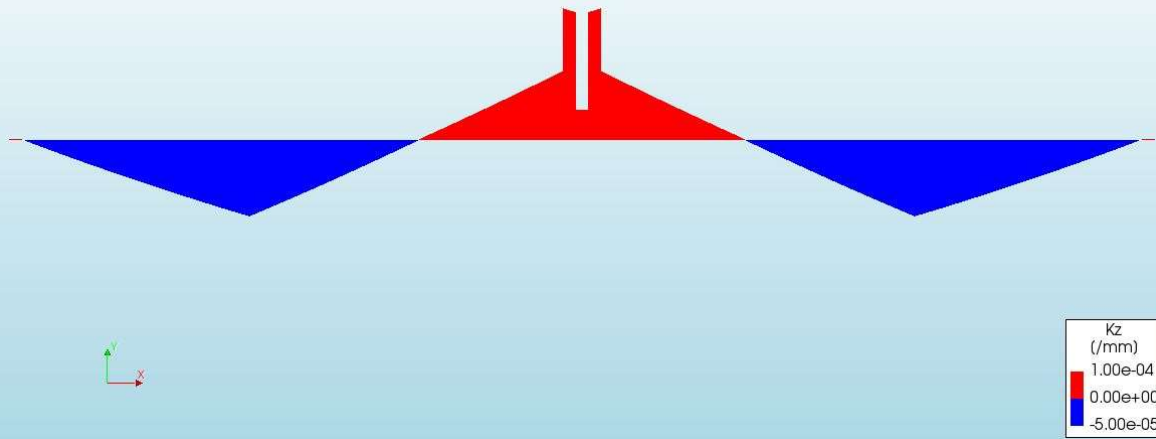
Non Lin Sta  
Phase - AP - Applied Load, Load-step 45, Load-factor 0.44000, 03 - Applied Load  
Curvatures Kz  
min: -2.87e-06/mm max: 2.80e-06/mm



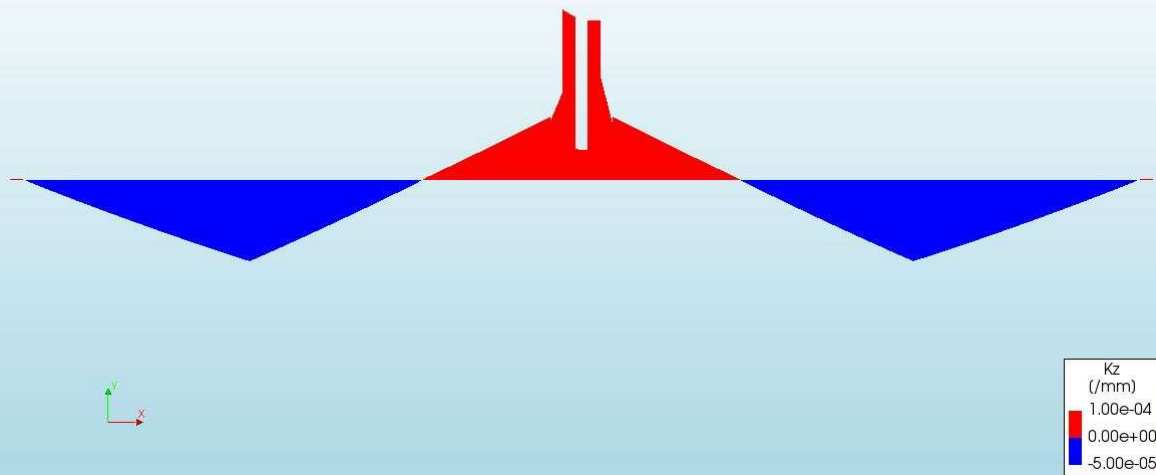
Non Lin Sta  
Phase - AP - Applied Load, Load-step 50, Load-factor 0.49000, 03 - Applied Load  
Curvatures Kz  
min: -3.12e-06/mm max: 3.85e-06/mm



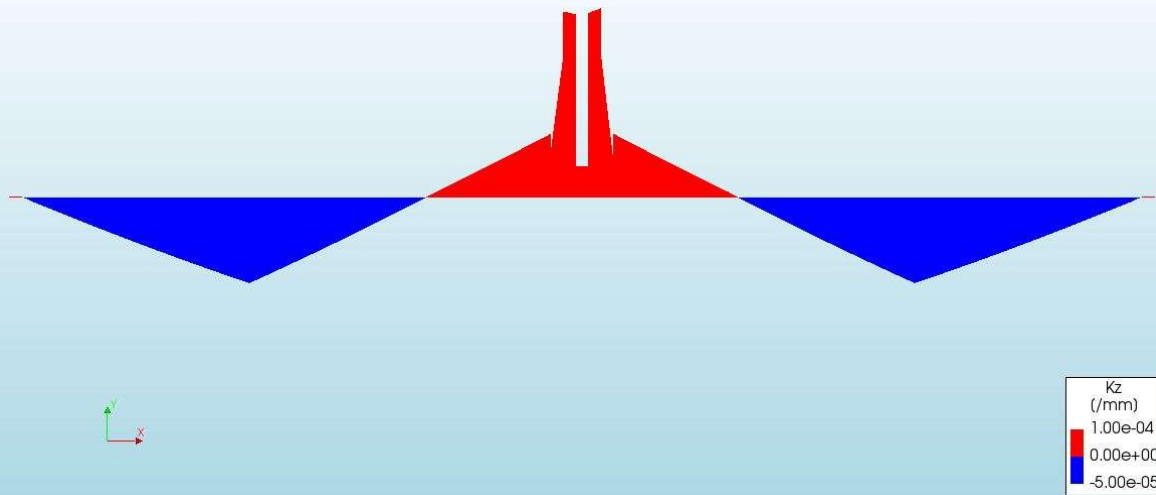
Non Lin Sta  
Phase - AP - Applied Load, Load-step 55, Load-factor 0.54000, 03 - Applied Load  
Curvatures Kz  
min: -3.35e-06/mm max: 5.71e-06/mm



Non Lin Sta  
Phase - AP - Applied Load, Load-step 60, Load-factor 0.59000, 03 - Applied Load  
Curvatures Kz  
min: -3.57e-06/mm max: 7.42e-06/mm

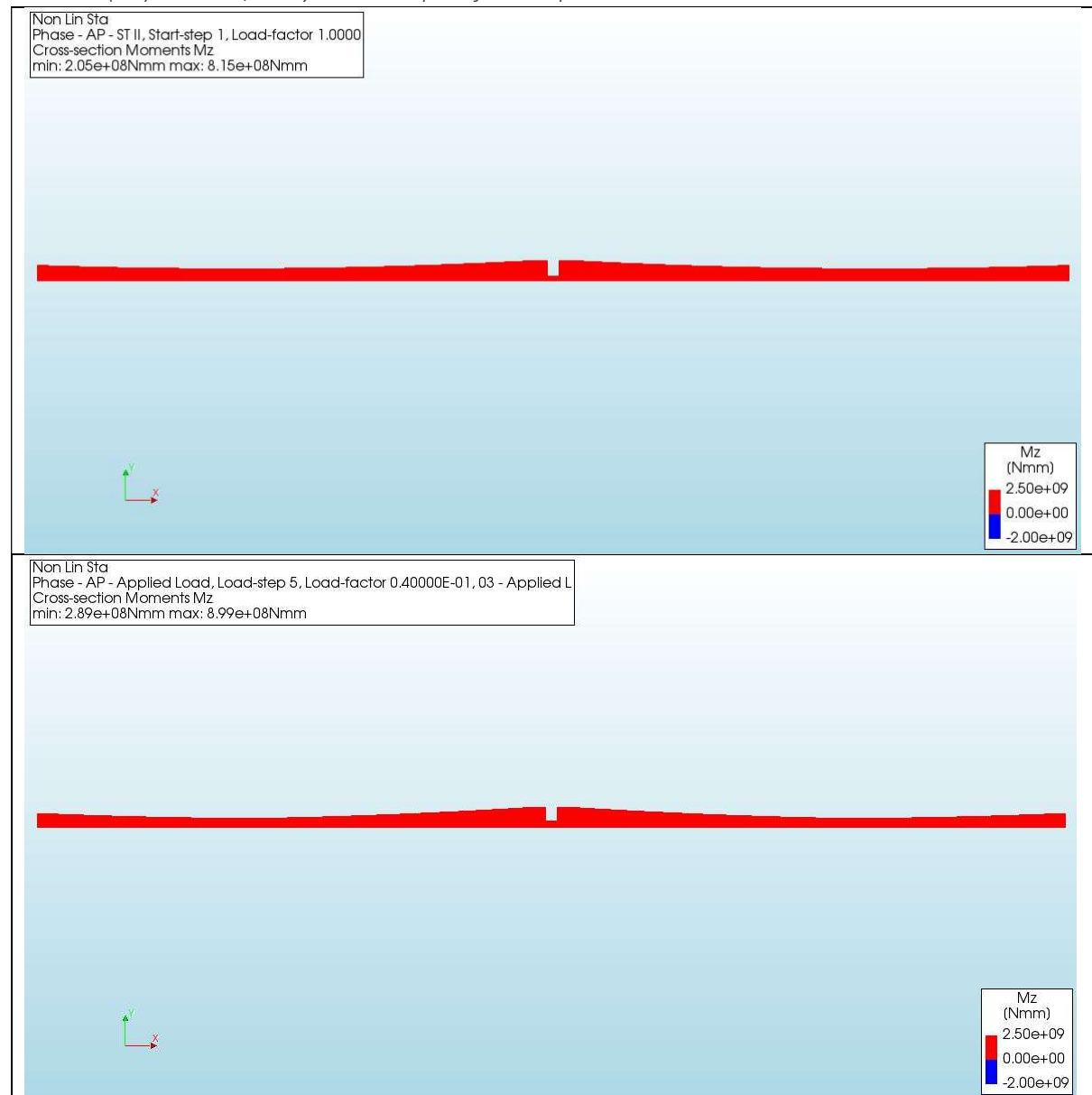


Non Lin Sta  
Phase - AP - Applied Load, Load-step 64, Load-factor 0.63000, 03 - Applied Load  
Curvatures Kz  
min: -3.75e-06/mm max: 8.21e-06/mm

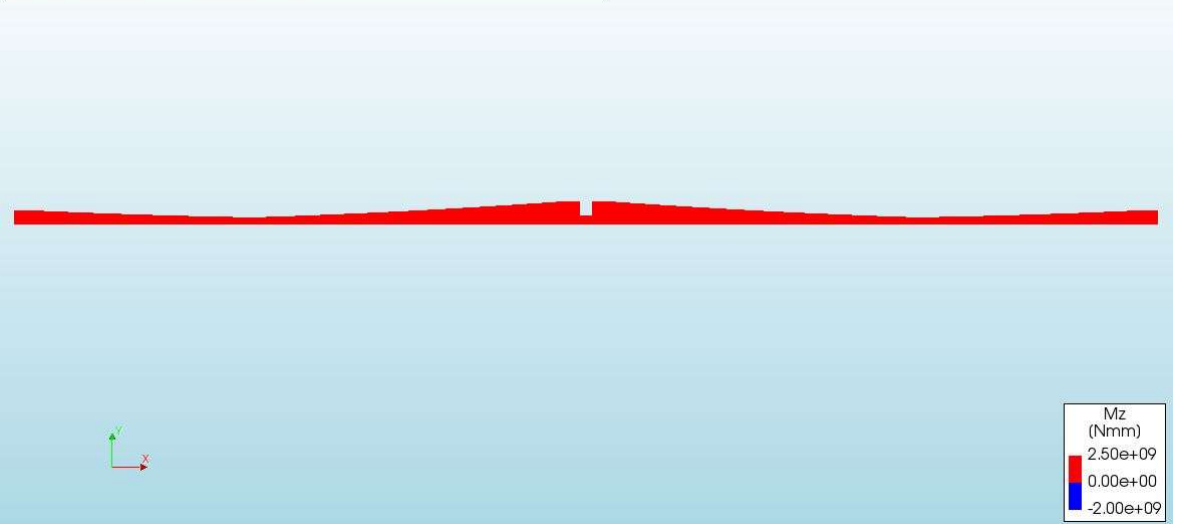


# Appendix IIIg

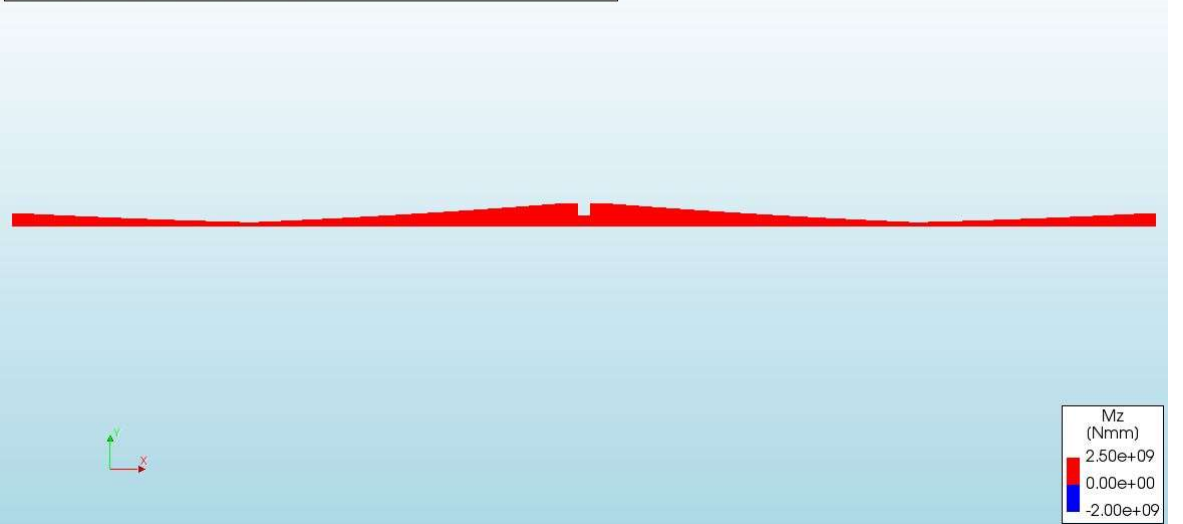
## Moment ( $M_z$ ) Model 2, every 5 load steps & final step



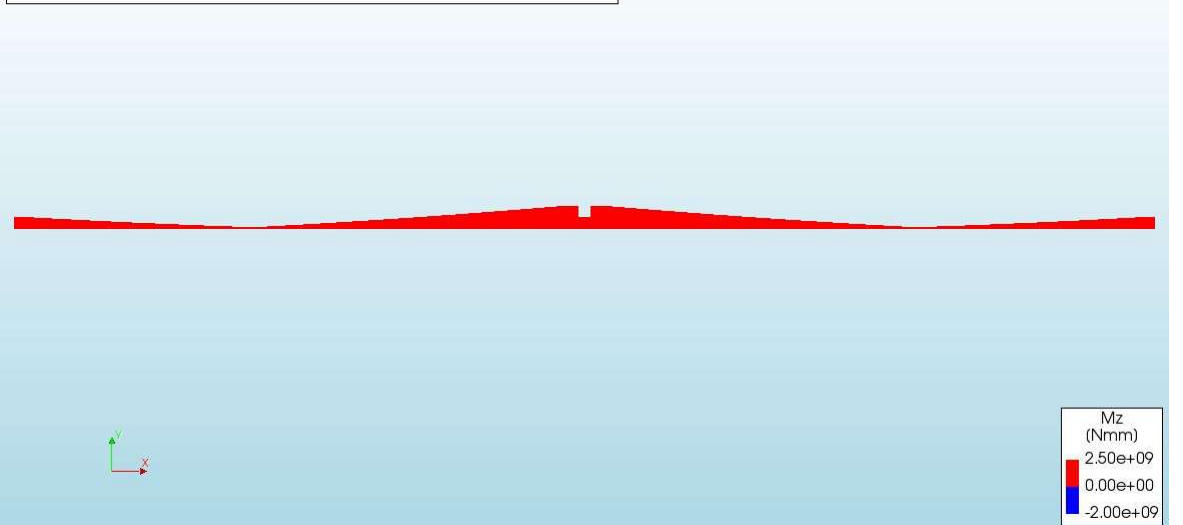
Non Lin Sta  
Phase - AP - Applied Load, Load-step 10, Load-factor 0.90000E-01, 03 - Applied  
Cross-section Moments Mz  
min: 2.91e+08Nmm max: 1.00e+09Nmm



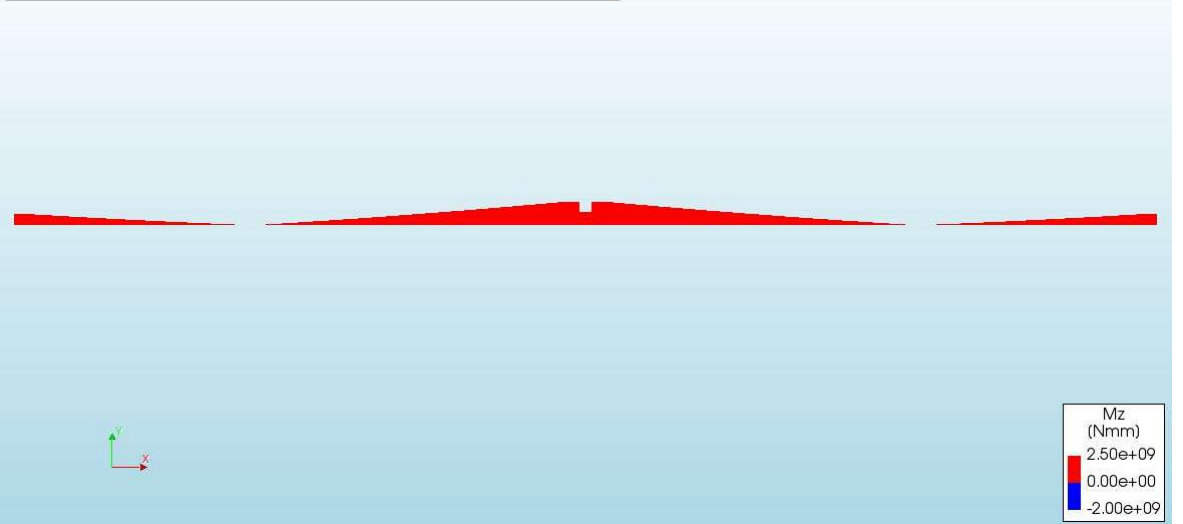
Non Lin Sta  
Phase - AP - Applied Load, Load-step 15, Load-factor 0.14000, 03 - Applied Load  
Cross-section Moments Mz  
min: 1.80e+08Nmm max: 1.11e+09Nmm



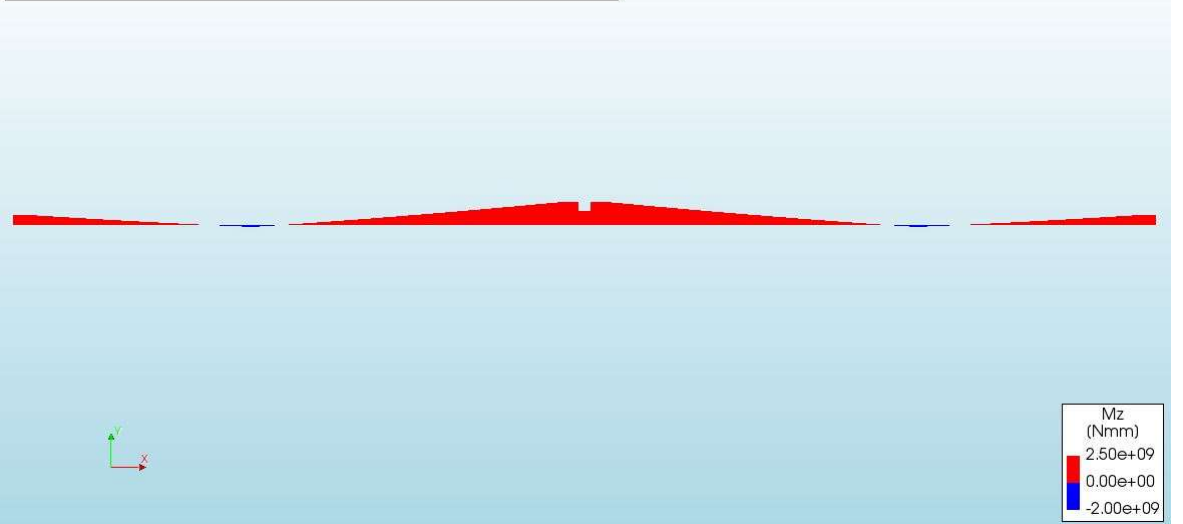
Non Lin Sta  
Phase - AP - Applied Load, Load-step 20, Load-factor 0.19000, 03 - Applied Load  
Cross-section Moments Mz  
min: 6.84e+07Nmm max: 1.22e+09Nmm



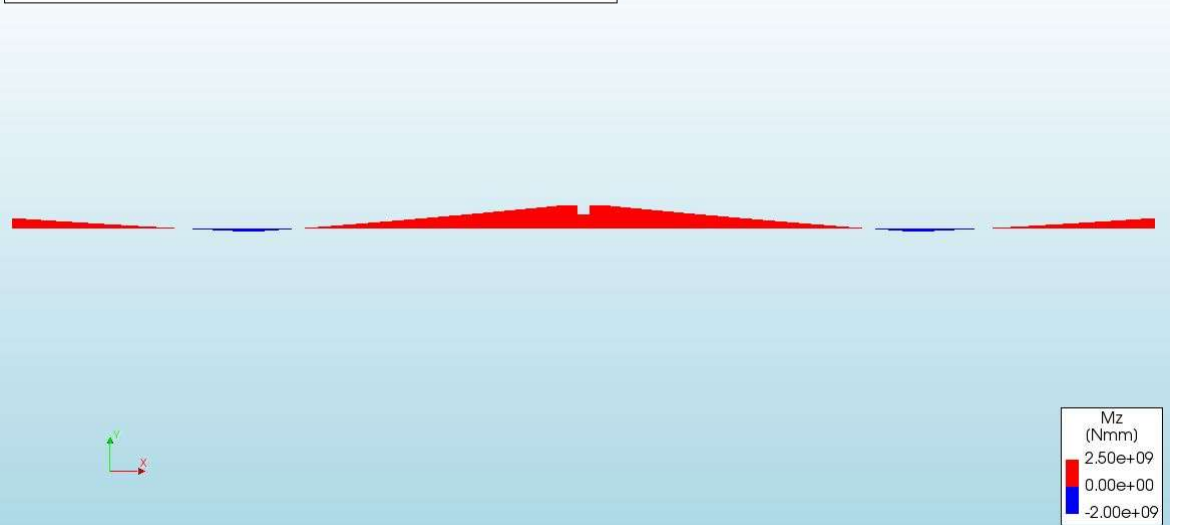
Non Lin Sta  
Phase - AP - Applied Load, Load-step 25, Load-factor 0.24000, 03 - Applied Load  
Cross-section Moments Mz  
min: -4.30e+07Nmm max: 1.32e+09Nmm



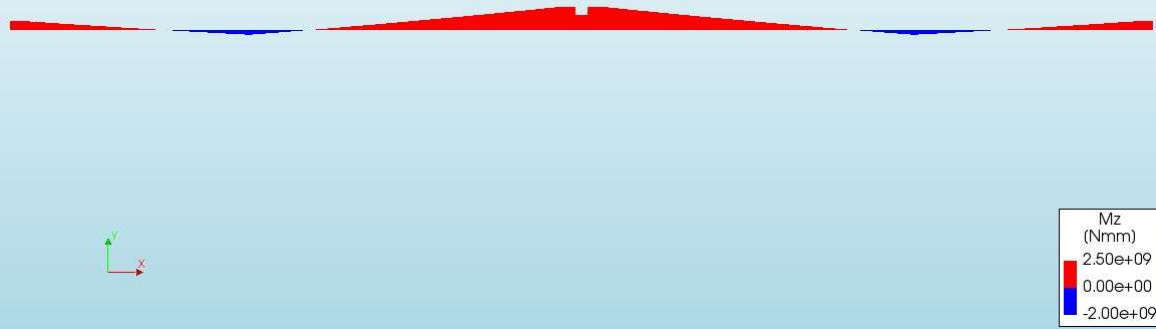
Non Lin Sta  
Phase - AP - Applied Load, Load-step 30, Load-factor 0.29000, 03 - Applied Load  
Cross-section Moments Mz  
min: -1.55e+08Nmm max: 1.43e+09Nmm



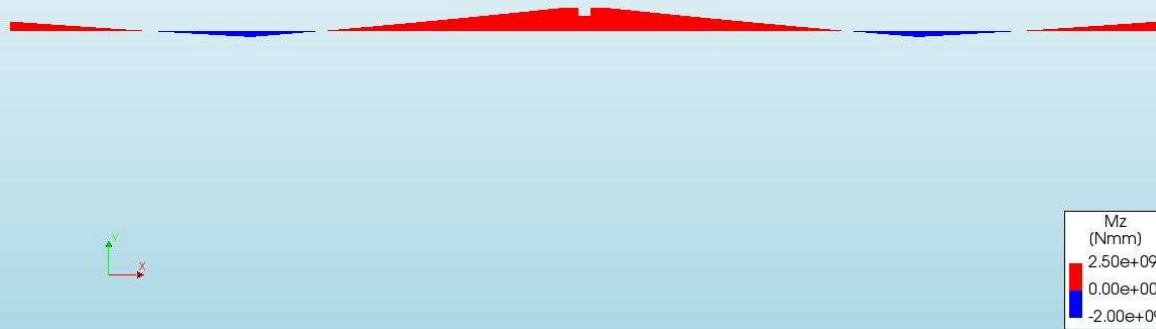
Non Lin Sta  
Phase - AP - Applied Load, Load-step 35, Load-factor 0.34000, 03 - Applied Load  
Cross-section Moments Mz  
min: -2.65e+08Nmm max: 1.53e+09Nmm



Non Lin Sta  
Phase - AP - Applied Load, Load-step 40, Load-factor 0.39000, 03 - Applied Load  
Cross-section Moments Mz  
min: -3.74e+08Nmm max: 1.63e+09Nmm



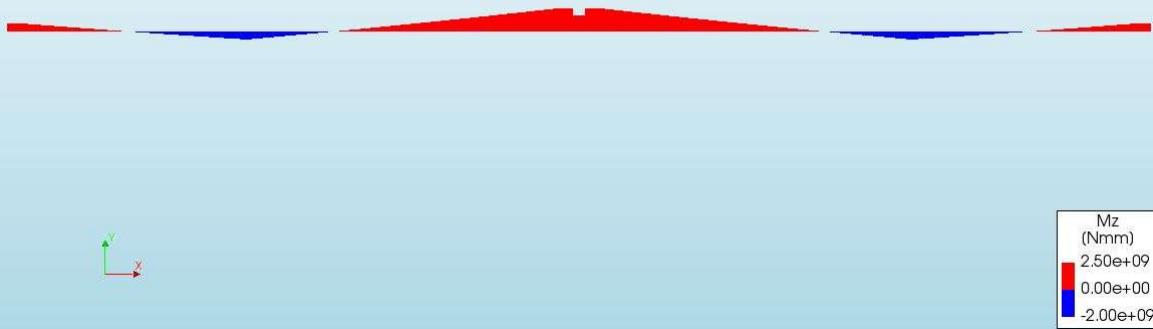
Non Lin Sta  
Phase - AP - Applied Load, Load-step 45, Load-factor 0.44000, 03 - Applied Load  
Cross-section Moments Mz  
min: -4.84e+08Nmm max: 1.73e+09Nmm



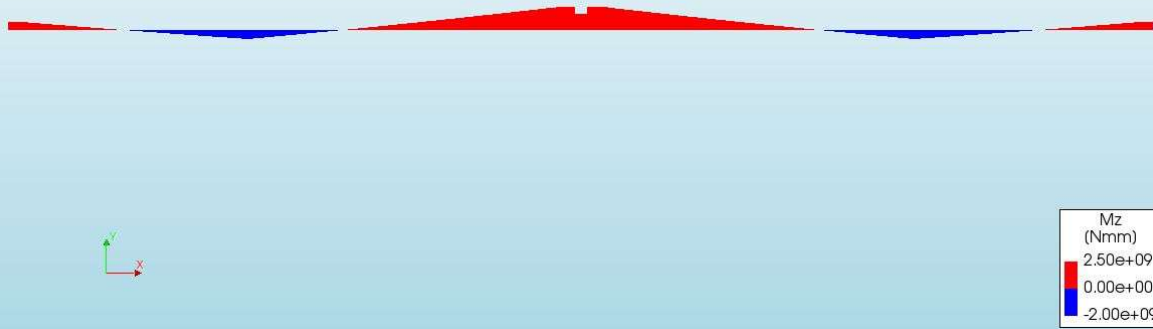
Non Lin Sta  
Phase - AP - Applied Load, Load-step 50, Load-factor 0.49000, 03 - Applied Load  
Cross-section Moments Mz  
min: -5.83e+08Nmm max: 1.79e+09Nmm



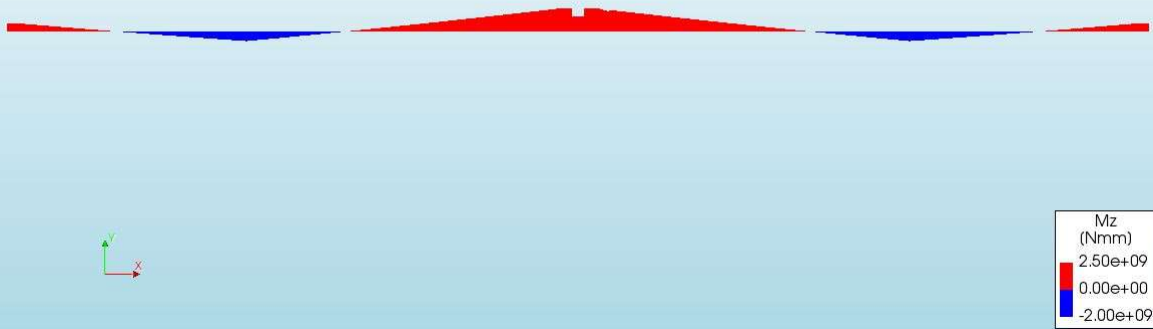
Non Lin Sta  
Phase - AP - Applied Load, Load-step 55, Load-factor 0.54000, 03 - Applied Load  
Cross-section Moments Mz  
min: -6.68e+08Nmm max: 1.80e+09Nmm



Non Lin Sta  
Phase - AP - Applied Load, Load-step 60, Load-factor 0.59000, 03 - Applied Load  
Cross-section Moments Mz  
min: -7.54e+08Nmm max: 1.82e+09Nmm



Non Lin Sta  
Phase - AP - Applied Load, Load-step 64, Load-factor 0.63000, 03 - Applied Load  
Cross-section Moments Mz  
min: -8.21e+08Nmm max: 1.86e+09Nmm



## Appendix IV – Additional information Chapter 4

### Appendix IVa

#### Traffic Load & Safety factors

##### Traffic Load

The inverted T-beams are primarily used as girder in concrete bridges, which, in turn, are primarily loaded by traffic. There are many different methods to test and describe traffic loads. In the Netherlands, the evaluating for traffic loads is governed by the 'Nederlandse Normen' (NEN) and the 'Richtlijnen Beoordeling Kunstwerken' (RBK). The NEN and RBK play a fundamental role in defining the traffic loads on structures and provide us with a template and norms to which the structure must be designed to withstand.

Chapter 4 from the NEN-EN 1991-2 will be used as a basis to draw up the load combination, NEN describes traffic loads as 'loads due to the road traffic, consisting of cars, lorries and special vehicles, give rise to vertical and horizontal, static and dynamic forces', Chapter 4.2.1 (1) from (NEN-EN 1991-2: Eurocode 1: Actions on structures - Part 2: Traffic loads on bridges). Moreover, NEN-EN 1990 and NEN-EN 1991-2+C1/NB and RBK 1.21 will be used for additional information. This report will ignore all horizontal forces and focus solely on the vertical forces.

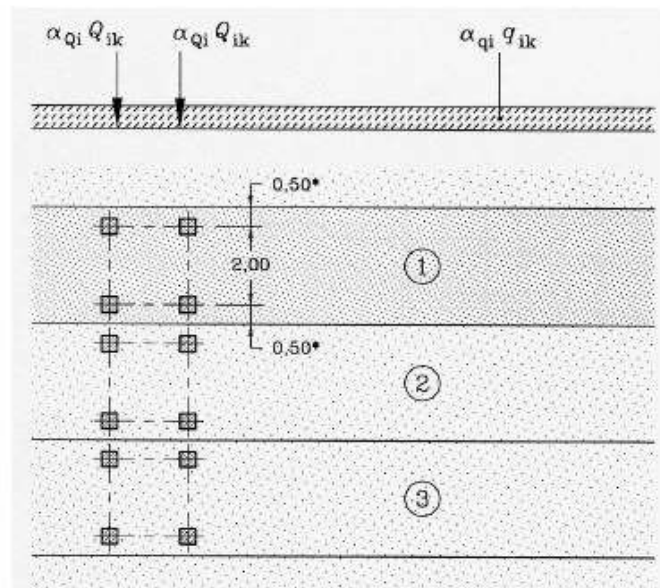
Ultimate Limit State (ULS) scenario will be de sole focus of this thesis. Using Load Model 1, the ULS was chosen as it describes the verification of a structure to be deemed safe for people and itself. The Load Model 1, ULS and my assumptions will ultimately describe the load values that will be applied to the FEM bridge model. In the figure here below the ULS is describe in factors and variable, safety factors (e.g.  $\gamma_G$  &  $\gamma_P$ ), frequency factors (e.g.  $\psi_{0,1}$ ), and Loads values (e.g.  $G_{k,j}$ ,  $Q_{k,i}$ ) can be seen.

$$\left\{ \begin{array}{l} \sum_{j \geq 1} \gamma_{G,j} G_{k,j} + \gamma_P P + \gamma_{Q,1} \psi_{0,1} Q_{k,1} + \sum_{i > 1} \gamma_{Q,i} \psi_{0,i} Q_{k,i} \end{array} \right. \quad (6.10a)$$
$$\left\{ \begin{array}{l} \sum_{j \geq 1} \xi_j \gamma_{G,j} G_{k,j} + \gamma_P P + \gamma_{Q,1} Q_{k,1} + \sum_{i > 1} \gamma_{Q,i} \psi_{0,i} Q_{k,i} \end{array} \right. \quad (6.10b)$$

Figure 90, ULS calculation formula

##### Load Model 1

The NEN provides options on how to best describe traffic effect as loads, one such option is the previously mentioned Load Model1. In Figure 91 'Figure 4.2a – Application of Load Model 1' from the NEN can be seen. Load Model 1 consists of a uniformly distributed force and axle concentrated loads. The values of these loads can best be seen in Figure 92, 'table 4.2 – Load Model 1: characteristic values'.



**Key**

- (1) Lane Nr. 1 :  $Q_{1k} = 300 \text{ kN}$  ;  $q_{1k} = 9 \text{ kN/m}^2$
- (2) Lane Nr. 2 :  $Q_{2k} = 200 \text{ kN}$  ;  $q_{2k} = 2,5 \text{ kN/m}^2$
- (3) Lane Nr. 3 :  $Q_{3k} = 100 \text{ kN}$  ;  $q_{3k} = 2,5 \text{ kN/m}^2$

\* For  $w_l = 3,00 \text{ m}$

**Figure 4.2a - Application of load Model 1**

Figure 91, Figure 4.2a - NEN 1991-2

**Table 4.2 - Load model 1 : characteristic values**

Location	Tandem system <i>TS</i>	<i>UDL</i> system
	Axle loads $Q_{ik}$ (kN)	$q_{ik}$ (or $q_{ik}$ ) (kN/m <sup>2</sup> )
Lane Number 1	300	9
Lane Number 2	200	2,5
Lane Number 3	100	2,5
Other lanes	0	2,5
Remaining area ( $q_{rk}$ )	0	2,5

Figure 92, Table 4.2 - NEN 1991-2

Load Model 1 describes a road width for a lane to be 3.00 [m], and the three axle concentrated loads to be distributed, one on each of the first three lanes. Therefore, the FEM bridge model will use a width of at least three lanes, thus 9.00 [m]. With Load Model 1, one must only need to define the adjustment factor and safety factors.

*General Assumptions and Other Factors*

The most extreme scenario possible will be examined in Case Study 2, and subsequently for the bridge models. This means selecting a road type, traffic type, and construction phase which provide this extreme scenario. This leads to following:

- A main road, which puts us in consequence class CC3 (NEN-EN 1990, B3.1)

- The highest frequency is given by lorry traffic, this leads to an adjustment factor  $\alpha_{Q1}=1.0$  &  $\alpha_{q1}=1.0$  (NEN-EN 1991-2+C1/nb, Table NB.1). However, with the addition to Table NB.1, the adjustment factors  $\alpha_{q1}=1.15$  &  $\alpha_{qi}=1.40$  (for  $i>1$ , or for all lanes other than lane 1) is given.
- The bridge will be in its operating phase; this, in conjunction with CC3, correction factor, and Table 2-2 (RBK1.21), gives the safety factor highlighted in Figure 93.

		Blijvend 6.10 a	Blijvend 6.10 a/b	Blijvend 6.10 b	Verkeer	Wind	Overig veranderlijk
	$\beta$ (CC3)	$\gamma_{Q1,sup}$	$\gamma_{G1,inf}$	$\xi\gamma_{Q1,sup}$	$\gamma_{Q,1}$	$\gamma_{Q,1}$	$\gamma_{Q,1}$
Nieuwbouwniveau	4,3	1,40	0,90	1,25	1,50	1,65	1,65
Verbouwniveau	3,6	1,30	0,90	1,15	1,30	1,60	1,50
Gebruiksniveau <sup>1</sup>	3,3	1,25	0,90	1,15	1,25	1,50	1,30
Afkeurniveau	3,1	1,25	0,90	1,10	1,25	1,50	1,30

**tabel 2-2: Partiële belastingfactoren voor verschillende veiligheidsniveaus**

Figure 93, Table 2-2, RBK

Table 20, overview safety factors

Load Type	Prestress (F <sub>p</sub> )	Self-weight (G)	Permanent (P)	Traffic Load (q <sub>1</sub> )	Traffic Load (q <sub>2</sub> & q <sub>3</sub> )	Traffic Load (Q <sub>1</sub> , Q <sub>2</sub> & Q <sub>3</sub> )
$\alpha$	1	1	1	1,15	1,4	1
$\psi*\gamma$	1	1,15	1,15	1,25	1,25	1,25
$\psi*\gamma*\alpha$	1	1,15	1,15	1,4375	1,75	1,25

To simplify the calculation for the top layer, an average value will be taken into account for the whole height of the top layer.

Appendix IVb

FEM properties Models 4&5

*Initial Settings*

	Model 4	Model 5	Units
Analysis	Structural	Structural	
Dimensions	Three dimensional	Three dimensional	
Model Size	100	100	m
Mesh type	Hexa/Quad	Hexa/Quad	
Mesh order	Linear	Linear	

*Geometry*

Element	length	Unit	Element	length	Unit	Material
BL1	11250	mm	BR1	23540	mm	Concrete - TB
BL2	11250	mm	BR2	23540	mm	Concrete - TB
BL3	11250	mm	BR3	23540	mm	Concrete - TB
BL4	11250	mm	BR4	23540	mm	Concrete - TB
BL5	11250	mm	BR5	23540	mm	Concrete - TB
BL6	11250	mm	BR6	23540	mm	Concrete - TB
BL7	11250	mm	BR7	23540	mm	Concrete - TB
BL8	11250	mm	BR8	23540	mm	Concrete - TB
Element	Length (M4)	Length (M5)	Width	Unit		Material
BDL	11250	23540	9600	mm		Concrete Deck
BDR	11250	23540	9600	mm		Concrete Deck
M-SUP.	250	-	-	mm		Concrete - CB

*Materials*

Element Class	Class-I Beams 3D	Class-I Beams 3D	Flat Shell
Materials	Concrete – TB	Concert - CB	Concrete Deck
Geometry	T-Beam + DL	SUP	Deck Thick.

*Materials – Properties I*

	Concrete – TB	Units
Class	Concrete and masonry	
Material model	Total strain-based crack model	
Young's Modulus	40585.4	N/mm <sup>2</sup>
Poisson's ratio	0.2	-
Mass density	2.333e-09	T/mm <sup>3</sup>
Gen. stress-strain relation	Elongation strain - Force	Curve – M <sub>n</sub> -κ Diagram
	Dummy stress-strain relation	M <sub>n</sub> -κ Diagram, TB-m

Materials – Properties II

	Concrete - CB	Units
Class	Concrete and masonry	
Material model	Total strain-based crack model	
Young's Modulus	36688.6	N/mm <sup>2</sup>
Poison's ratio	0.2	-
Mass density	2.333e-09	T/mm <sup>3</sup>
Gen. stress-strain relation	Elongation strain - Force	Curve – M <sub>n</sub> -κ Diagram
	Dummy stress-strain relation	M <sub>n</sub> -κ Diagram, CB-m

Materials – Properties III

	Concrete – Concrete Deck	Units
Class	Concrete and masonry	
Material model	Linear elastic isotropic	
Young's Modulus	12229.5	N/mm <sup>2</sup>
Poison's ratio	0.2	-
Mass density	2.333e-09	T/mm <sup>3</sup>

Element Geometries

	T-Beam + DL	SUP	Deck	Units
Shape	I-shape	Rectangular	Thickness	
Height (h)	1070	1070	-	mm
Width of top flange (b1)	983	-	-	mm
Width of bottom flange (b2)	1180	1200	-	mm
Thickness of top flange (t1)	160	-	-	mm
Thickness of bottom flange (t2)	221.85	-	-	mm
Thickness of web (t3)	300	-	-	mm
Thickness	-	-	160	mm

Mesh

	Model 4 & 5	Units
Target Type	Shape	-
Seeding method	Element size	-
Desired size	250	mm

Note: the mesh size was determined using the RTD, Chapter 2.5.5.

### Supports

	Model 4	Model 5
Initial Supports (Each Beams)		
beams Left Sup.	Fixed z-axis	Fixed z-axis
beams Right Sup.	Fixed x-axis, y-axis & z-axis	Fixed x-axis, y-axis & z-axis
Combined Supports (Each Beam)		
Beams Left Sup.	Fixed z-axis	Fixed z-axis
Beams Right Sup.	Fixed z-axis	Fixed z-axis
Combined Supports (Right First beam, additional)		
Left Support	Fixed x-axis & y-axis	Fixed x-axis & y-axis

### Load Cases

Load Cases	Load	Model 4 & 5	Units	axis
01 -0- Prestress	$F_{p,L}$	1.39e+06	N	x-axis
	$F_{p,R}$	-1.39e+06	N	x-axis
	$M_{p,L}$	6.08e+08	Nmm	$M_y$
	$M_{p,R}$	-6.08e+08	Nmm	$M_y$
02 -G- SW Beams	Deadweight	Dead weight	-	z-axis
	$q_{sw,cor.}$	-9.78e-02	N/mm	z-axis
03 -G-SW SUP	$Q_{sw,SUP}$	-2.50e-02	N/mm <sup>2</sup>	z-axis
04 -P- Perm. Load	$Q_{sw,RD}$	-0.35e-02	N/mm <sup>2</sup>	z-axis
05 -Qki- TL q1	q1	-0.90e-02	N/mm <sup>2</sup>	z-axis
06 -Qki- TL q2	q2	-0.25e-02	N/mm <sup>2</sup>	z-axis
07 -Qki- TL F	F1	4 x -3.00e05	N	z-axis
	F2	4 x -2.00e05	N	z-axis
	F3	4 x -1.00e05	N	z-axis

### Analysis – Model 4&5 – Non-Linear Static Analysis

	Load steps	Non-Linear effects	Equilibrium iterations
Phase I – Prestress Forces & Self-weight Beams			
Prestress Forces	Prestress	Physical nonlinear	Newton-Raphson
	Steps (1.00)		Modified (100 steps)
			Displ. & Force
			Line search - ON
Self-weight SUP.	SW Beam	Physical nonlinear	Newton-Raphson
	Steps (1.00)		Modified (100 steps)
			Displ. & Force
			Line search - ON
Phase II – Self-weight SUP. & Traffic Loads			
Start step I	Previous phase	Physical nonlinear	Newton-Raphson
	Steps (1.00)		Regular (10 steps)
			Displ. & Force
			Line search - ON
Self-weight SUP.	SW SUP.	Physical nonlinear	Newton-Raphson
	Steps (1.00)		Modified (100 steps)
			Displ. & Force
			Line search - ON
			Line search - ON
Perm. + Traffic Load	TF comb.	Physical nonlinear	Newton-Raphson

	Steps (0.05(20))		Modified (1000 steps)
			Displ. & Force
			Line search - ON

*Analysis – Model 4&5 – Non-Linear Static Analysis - ULS*

	Load steps	Non-Linear effects	Equilibrium iterations
<b>Phase I – Prestress Forces &amp; Self-weight Beams</b>			
Prestress Forces	Prestress ULS	Physical nonlinear	Newton-Raphson
	Steps (1.00)		Modified (100 steps)
			Displ. & Force
			Line search - ON
Self-weight SUP.	SW Beam ULS	Physical nonlinear	Newton-Raphson
	Steps (1.00)		Modified (100 steps)
			Displ. & Force
			Line search - ON
<b>Phase II – Self-weight SUP. &amp; Traffic Loads</b>			
Start step I	Previous phase	Physical nonlinear	Newton-Raphson
	Steps (1.00)		Regular (100 steps)
			Displ. & Force
			Line search - ON
Self-weight SUP.	SW SUP. ULS	Physical nonlinear	Newton-Raphson
	Steps (1.00)		Modified (100 steps)
			Displ. & Force
			Line search - ON
			Line search - ON
Perm. + Traffic Load	TF comb. ULS	Physical nonlinear	Newton-Raphson
	Steps (0.01(100))		Modified (1000 steps)
			Displ. & Force
			Line search - ON

*Analysis – Model 4&5 – Non-Linear Static Analysis – ULS (till Failure)*

	Load steps	Non-Linear effects	Equilibrium iterations
<b>Phase I – Prestress Forces &amp; Self-weight Beams</b>			
Prestress Forces	Prestress ULS	Physical nonlinear	Newton-Raphson
	Steps (1.00)		Modified (100 steps)
			Displ. & Force
			Line search - ON
Self-weight SUP.	SW Beam ULS	Physical nonlinear	Newton-Raphson
	Steps (1.00)		Modified (100 steps)
			Displ. & Force
			Line search - ON
<b>Phase II – Self-weight SUP. &amp; Traffic Loads</b>			
Start step I	Previous phase	Physical nonlinear	Newton-Raphson
	Steps (1.00)		Regular (100 steps)
			Displ. & Force
			Line search - ON
Self-weight SUP.	SW SUP. ULS	Physical nonlinear	Newton-Raphson
	Steps (1.00)		Modified (100 steps)
			Displ. & Force
			Line search - ON

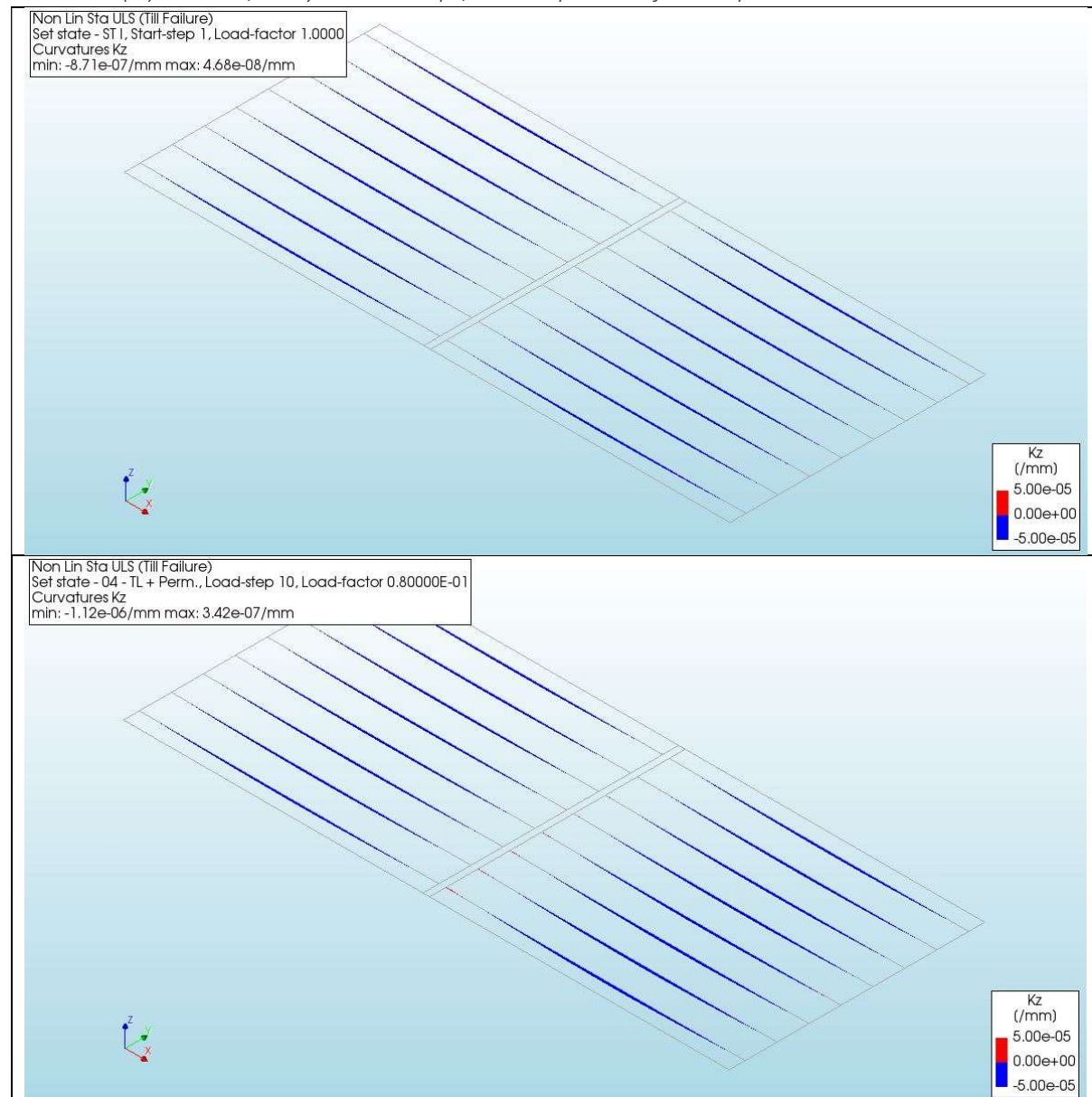
			Line search - ON
Perm. + Traffic Load	TF comb. ULS	Physical nonlinear	Newton-Raphson
	Steps (0.01(200))		Modified (1000 steps)
			Displ. & Force
			Line search - ON

*Output*

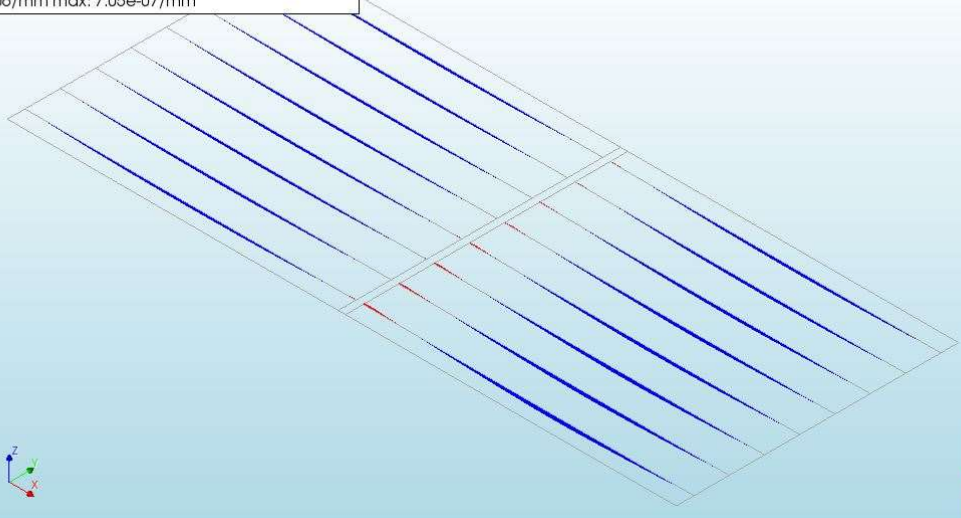
Model 3, 4 & 5	DISPLACEMENT	TOTAL	TRANSLATION	GLOBAL
Model 3	FORCE	TOTAL	TRANSLATION	GLOBAL
Model 3, 4 & 5	STRESS	TOTAL	MOMENT	LOCAL
Model 3, 4 & 5	STRAIN	REACTION	MOMENT	LOCAL

## Appendix IVc

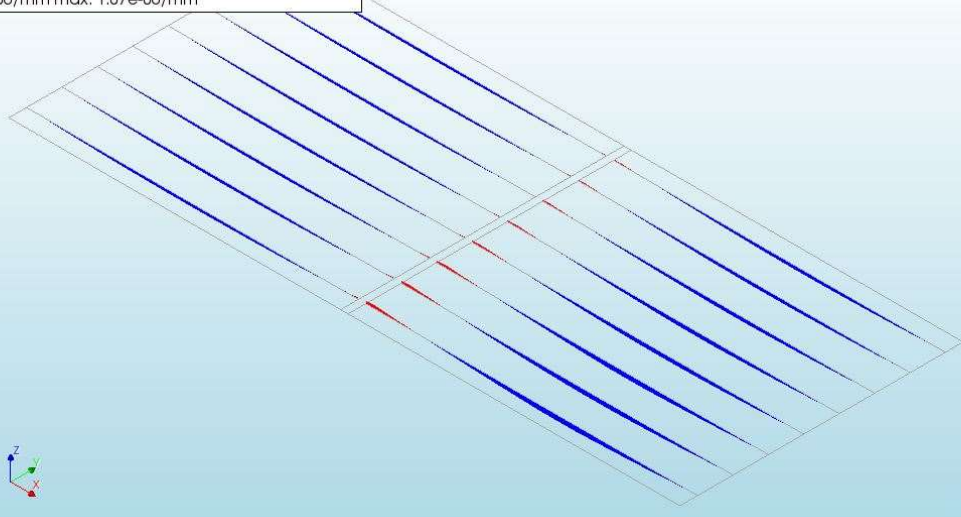
Curvature ( $\kappa_z$ ) Model 4, every 10 load steps, load step 1.00 & final step



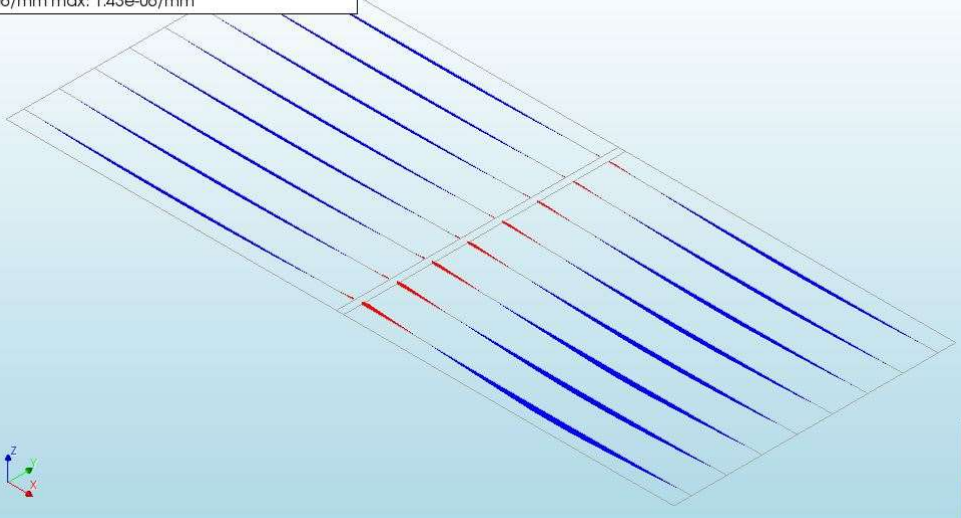
Non Lin Sta ULS (Till Failure)  
Set state - 04 - TL + Perm., Load-step 20, Load-factor 0.18000  
Curvatures Kz  
min: -1.43e-06/mm max: 7.05e-07/mm



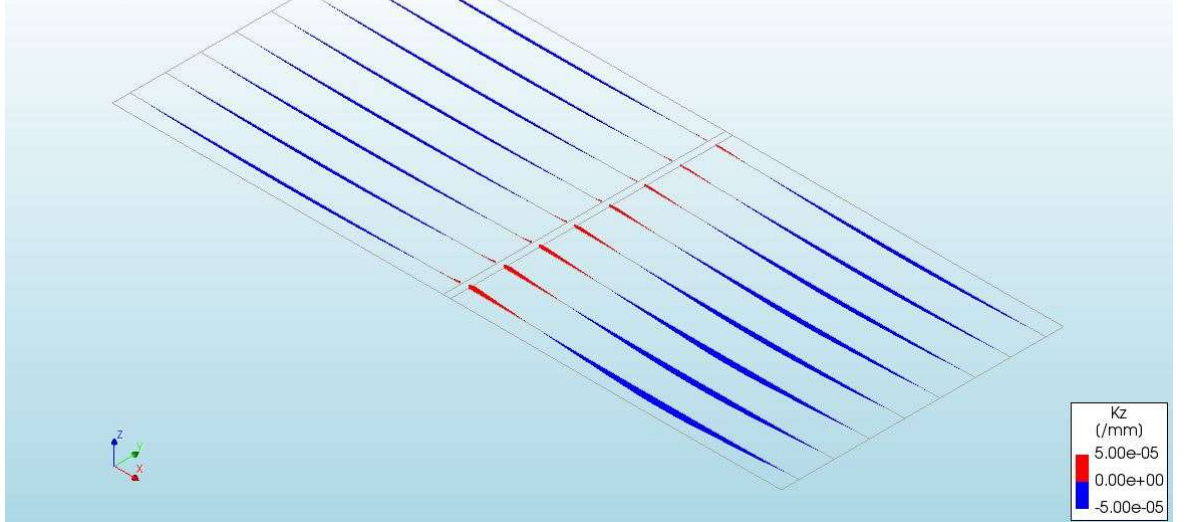
Non Lin Sta ULS (Till Failure)  
Set state - 04 - TL + Perm., Load-step 30, Load-factor 0.28000  
Curvatures Kz  
min: -1.75e-06/mm max: 1.07e-06/mm



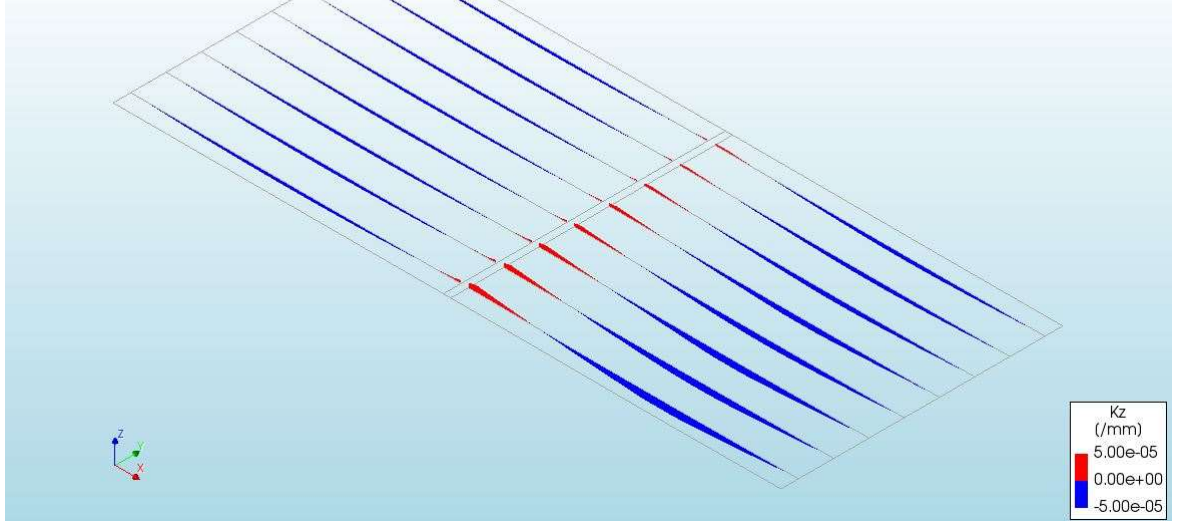
Non Lin Sta ULS (Till Failure)  
Set state - 04 - TL + Perm., Load-step 40, Load-factor 0.38000  
Curvatures Kz  
min: -2.07e-06/mm max: 1.43e-06/mm



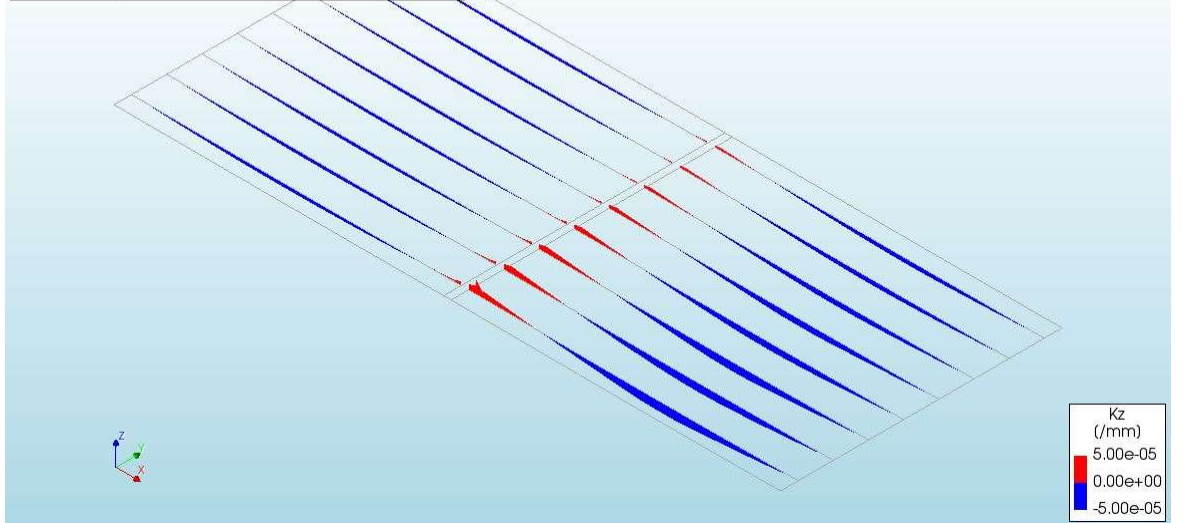
Non Lin Sta ULS (Till Failure)  
Set state - 04 - TL + Perm., Load-step 50, Load-factor 0.48000  
Curvatures Kz  
min: -2.40e-06/mm max: 1.79e-06/mm



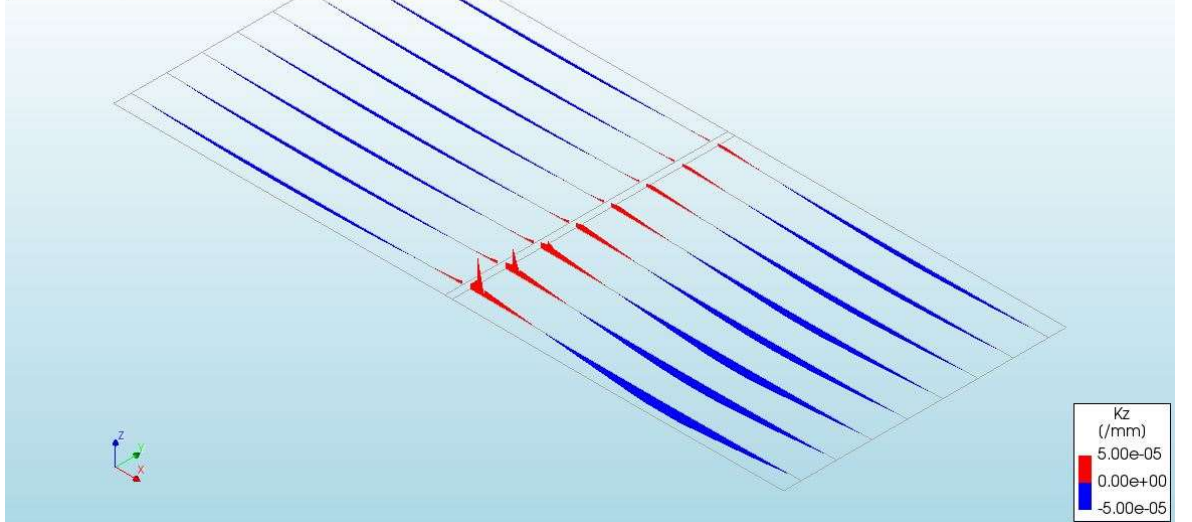
Non Lin Sta ULS (Till Failure)  
Set state - 04 - TL + Perm., Load-step 60, Load-factor 0.58000  
Curvatures Kz  
min: -2.74e-06/mm max: 2.15e-06/mm



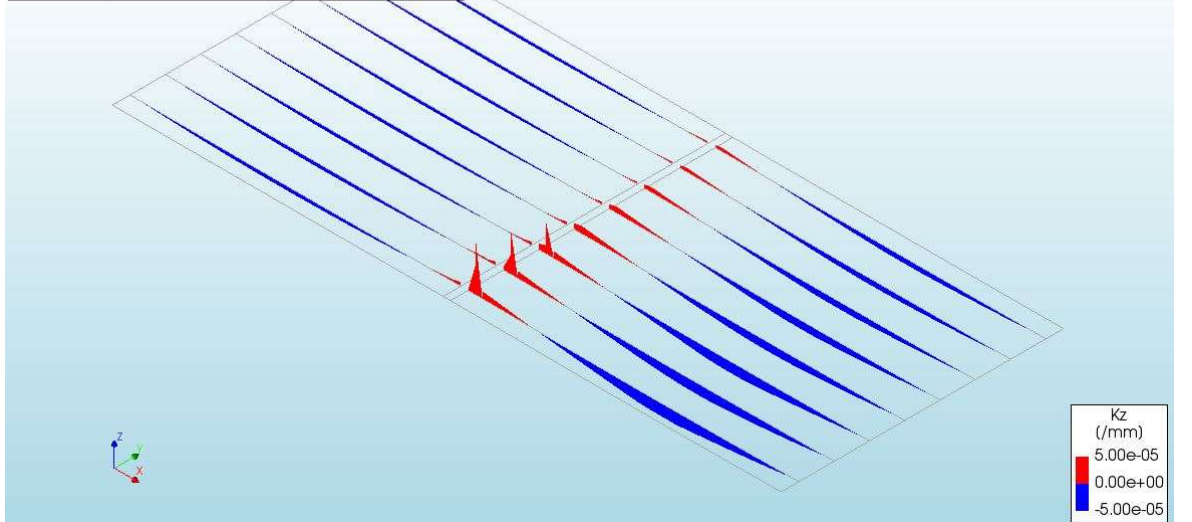
Non Lin Sta ULS (Till Failure)  
Set state - 04 - TL + Perm., Load-step 70, Load-factor 0.68000  
Curvatures Kz  
min: -3.05e-06/mm max: 4.39e-06/mm



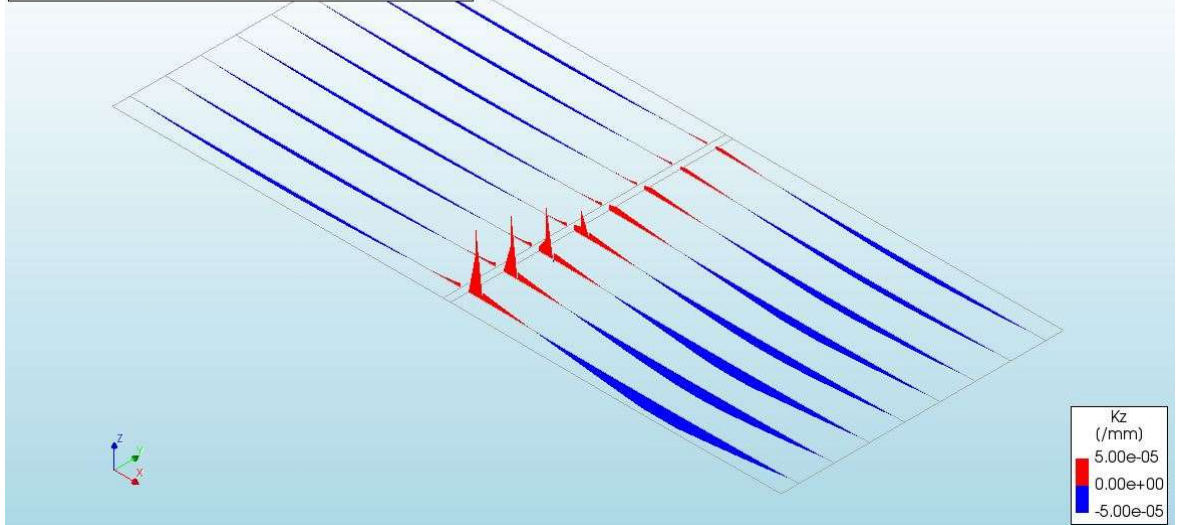
Non Lin Sta ULS (Till Failure)  
Set state - 04 - TL + Perm., Load-step 80, Load-factor 0.78000  
Curvatures Kz  
min: -3.46e-06/mm max: 1.16e-05/mm



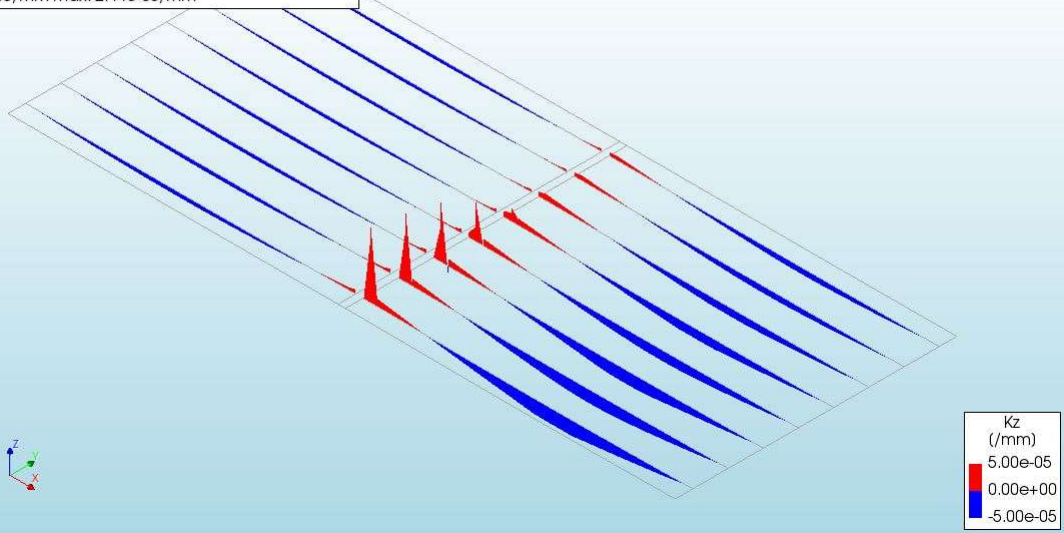
Non Lin Sta ULS (Till Failure)  
Set state - 04 - TL + Perm., Load-step 90, Load-factor 0.88000  
Curvatures Kz  
min: -3.86e-06/mm max: 1.69e-05/mm



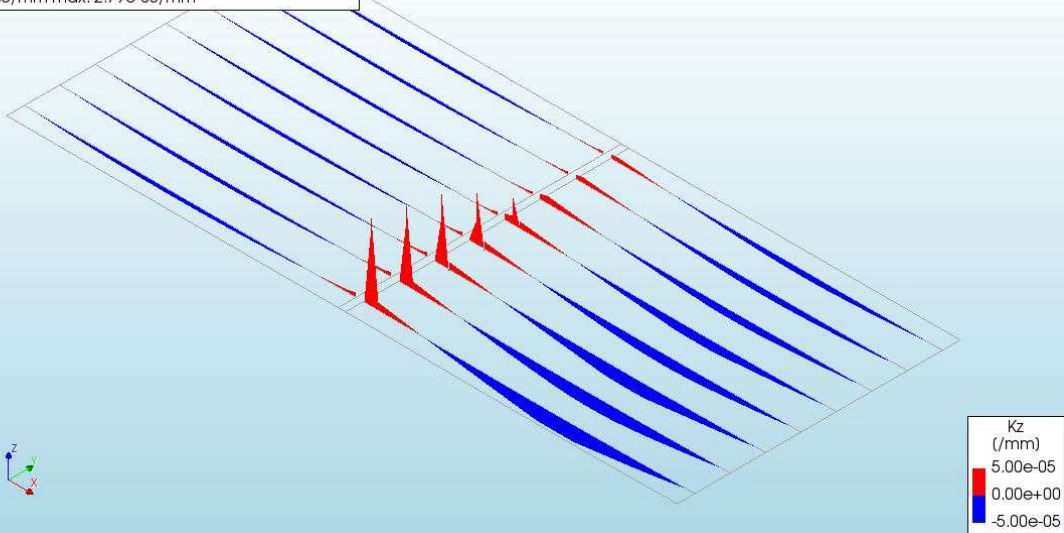
Non Lin Sta ULS (Till Failure)  
Set state - 04 - TL + Perm., Load-step 100, Load-factor 0.98000  
Curvatures Kz  
min: -4.27e-06/mm max: 2.17e-05/mm



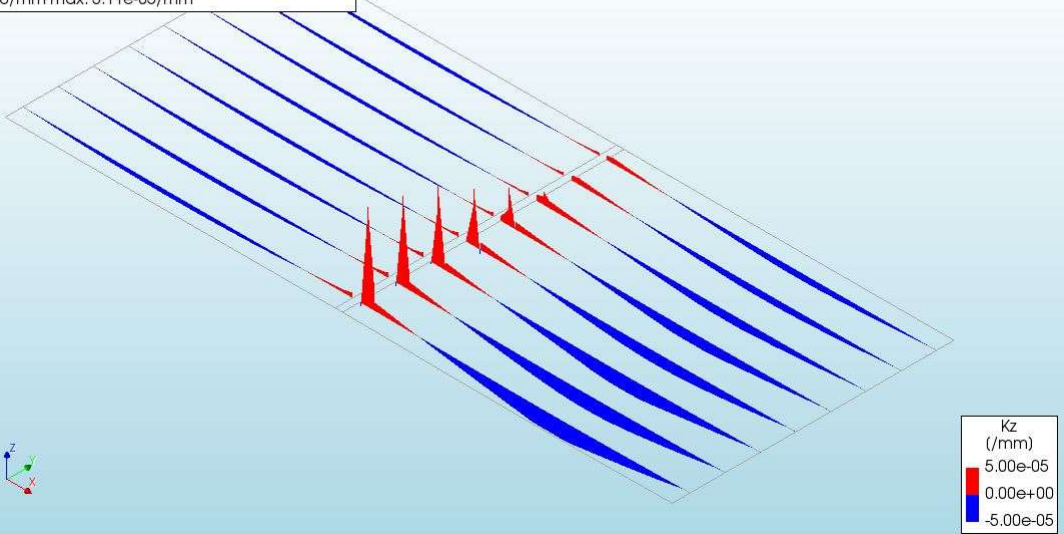
Non Lin Sta ULS (Till Failure)  
Set state - 04 - TL + Perm., Load-step 110, Load-factor 1.0800  
Curvatures Kz  
min: -4.69e-06/mm max: 2.44e-05/mm



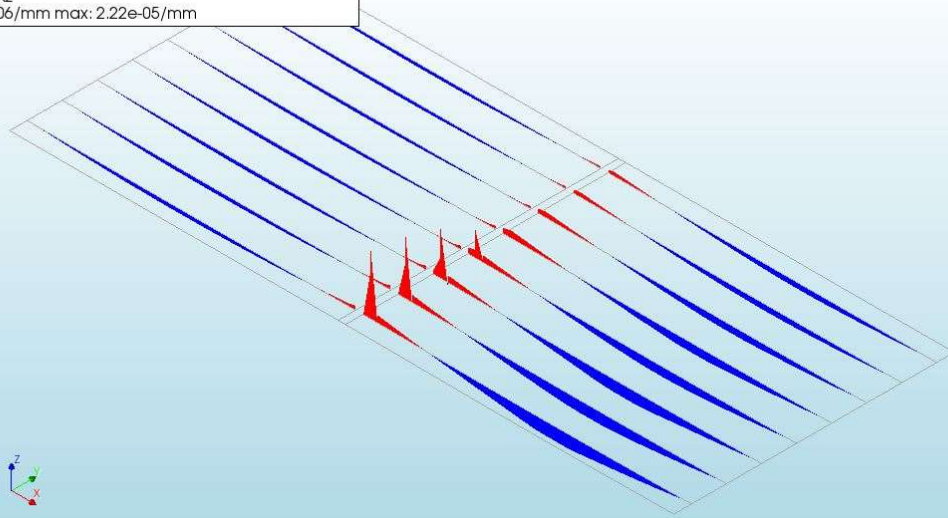
Non Lin Sta ULS (Till Failure)  
Set state - 04 - TL + Perm., Load-step 120, Load-factor 1.1800  
Curvatures Kz  
min: -5.11e-06/mm max: 2.79e-05/mm



Non Lin Sta ULS (Till Failure)  
Set state - 04 - TL + Perm., Load-step 130, Load-factor 1.2800  
Curvatures Kz  
min: -5.56e-06/mm max: 3.11e-05/mm

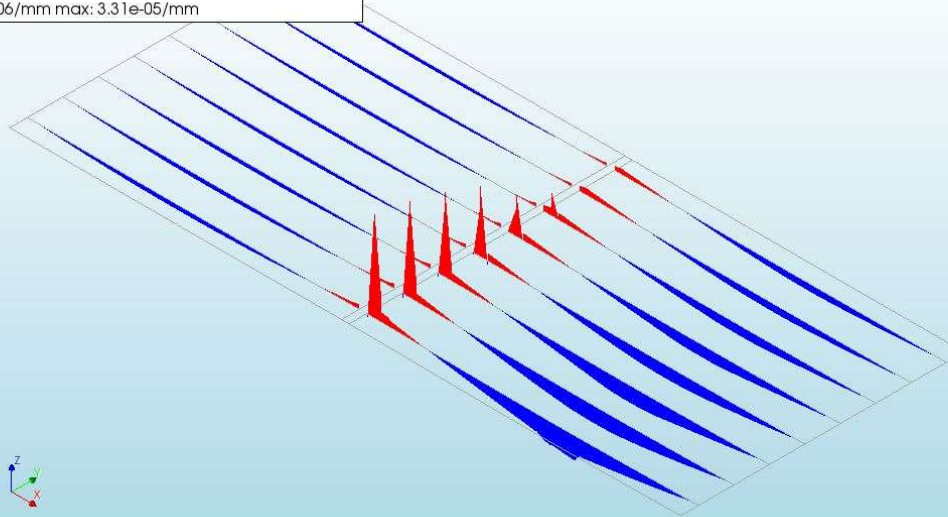


Non Lin Sta ULS (Till Failure)  
Set state - 04 - TL + Perm., Load-step 102, Load-factor 1.0000  
Curvatures Kz  
min: -4.35e-06/mm max: 2.22e-05/mm



Kz  
(/mm)  
5.00e-05  
0.00e+00  
-5.00e-05

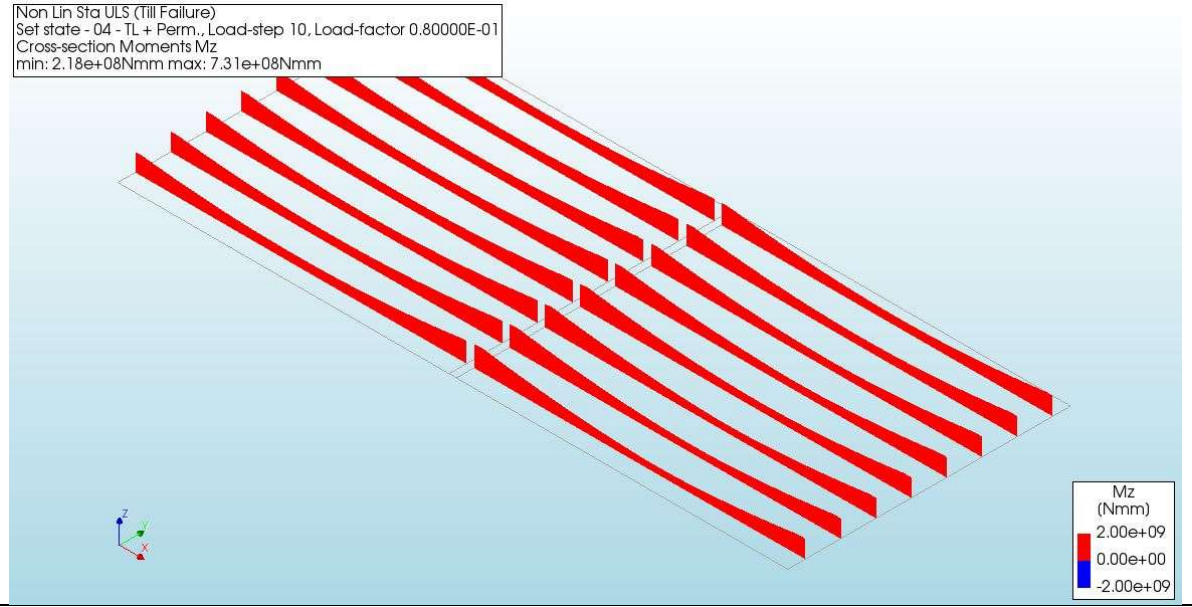
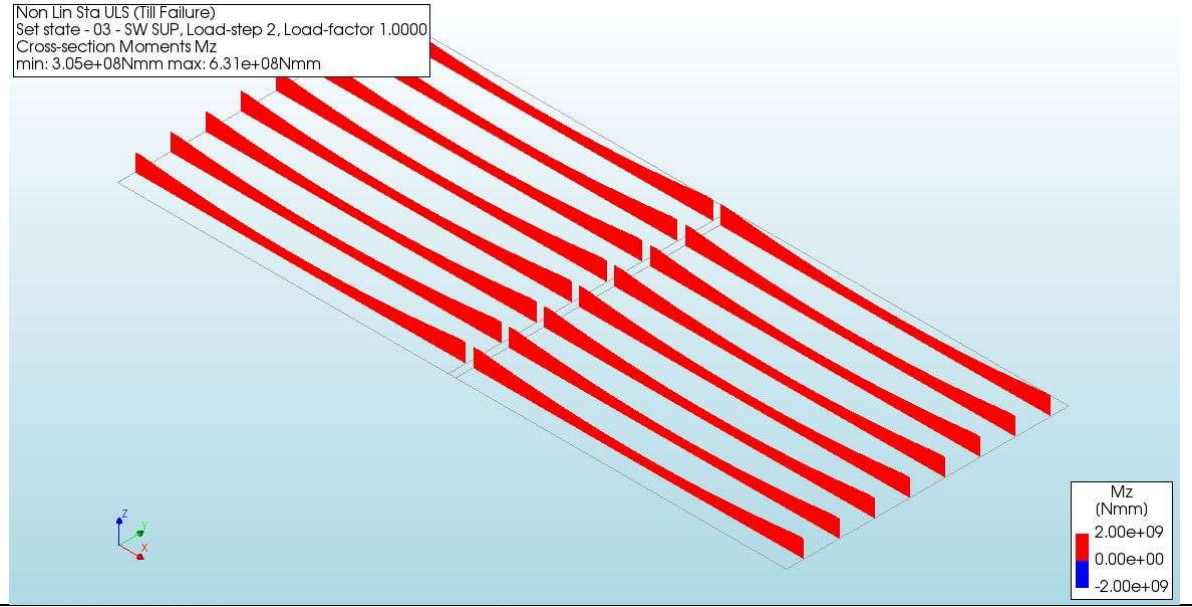
Non Lin Sta ULS (Till Failure)  
Set state - 04 - TL + Perm., Load-step 137, Load-factor 1.3500  
Curvatures Kz  
min: -7.78e-06/mm max: 3.31e-05/mm



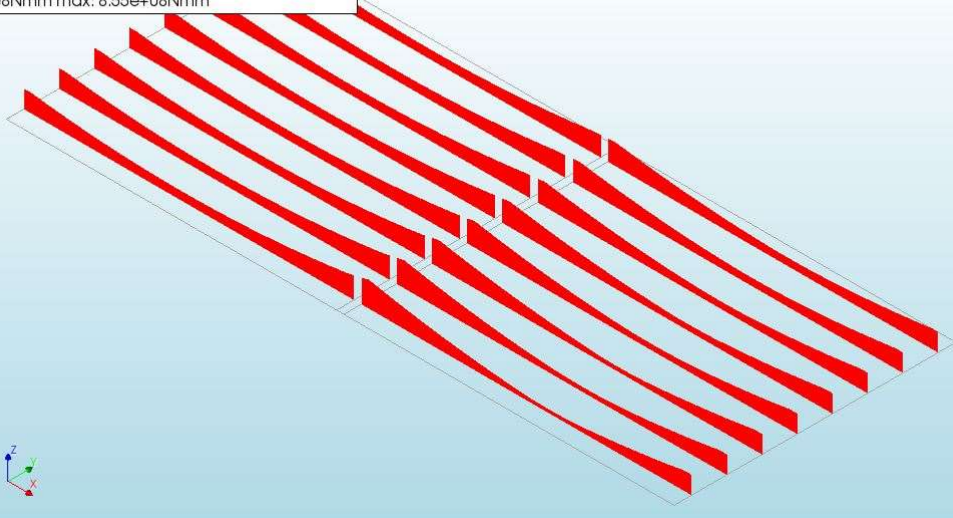
Kz  
(/mm)  
5.00e-05  
0.00e+00  
-5.00e-05

# Appendix IVd

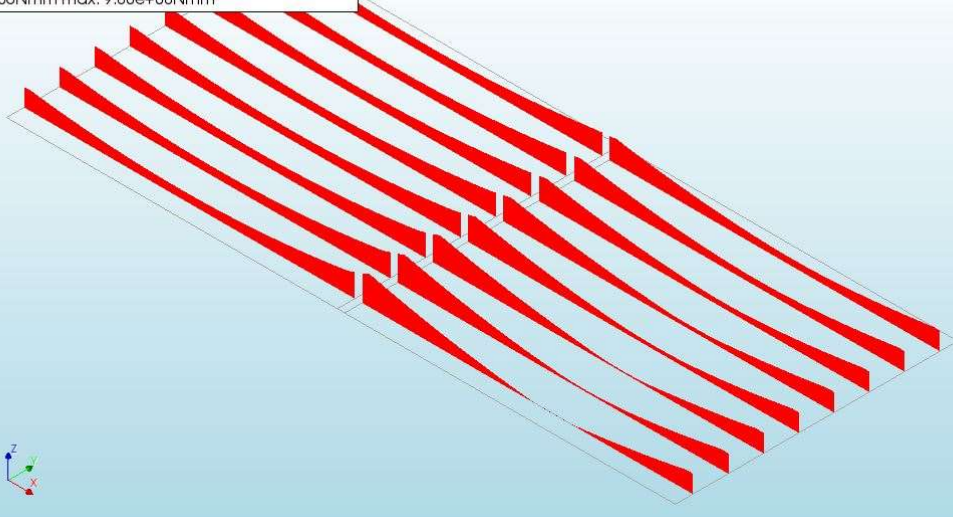
Moment ( $M_z$ ) Model 4, every 10 load steps, load step 1.00 & final step



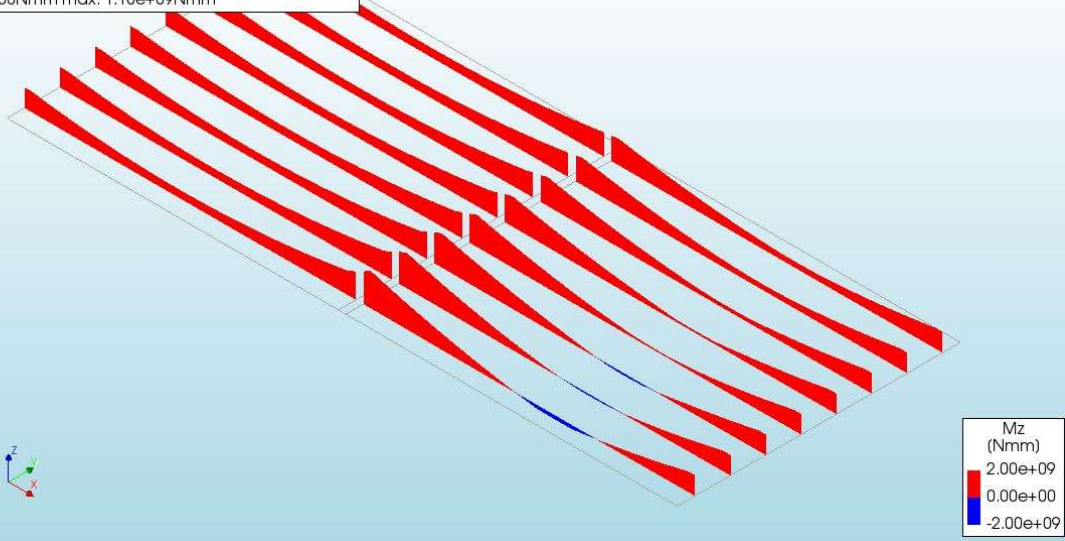
Non Lin Sta ULS (Till Failure)  
Set state - 04 - TL + Perm., Load-step 20, Load-factor 0.18000  
Cross-section Moments Mz  
min: 1.07e+08Nmm max: 8.55e+08Nmm



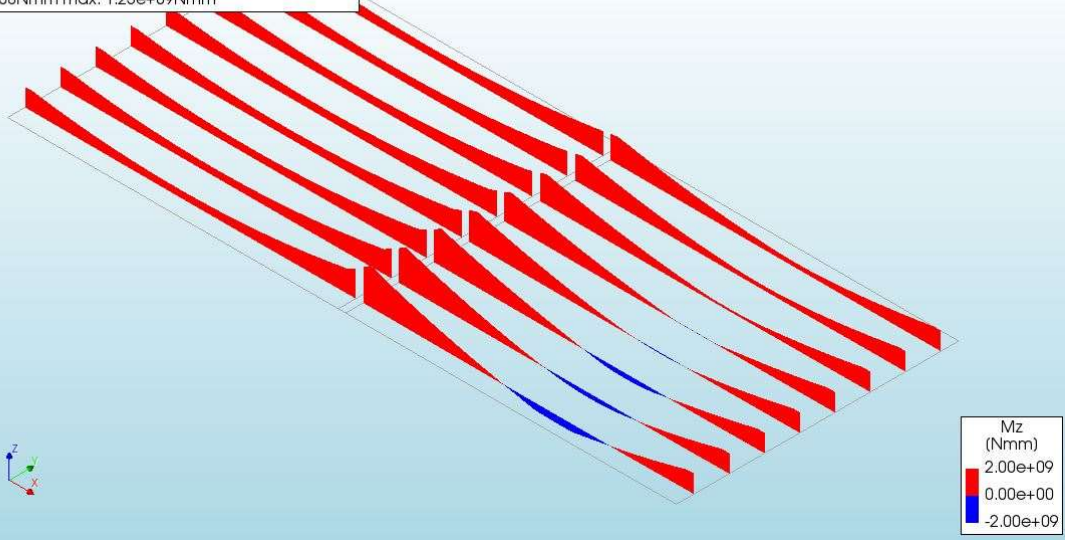
Non Lin Sta ULS (Till Failure)  
Set state - 04 - TL + Perm., Load-step 30, Load-factor 0.28000  
Cross-section Moments Mz  
min: -5.10e+06Nmm max: 9.80e+08Nmm



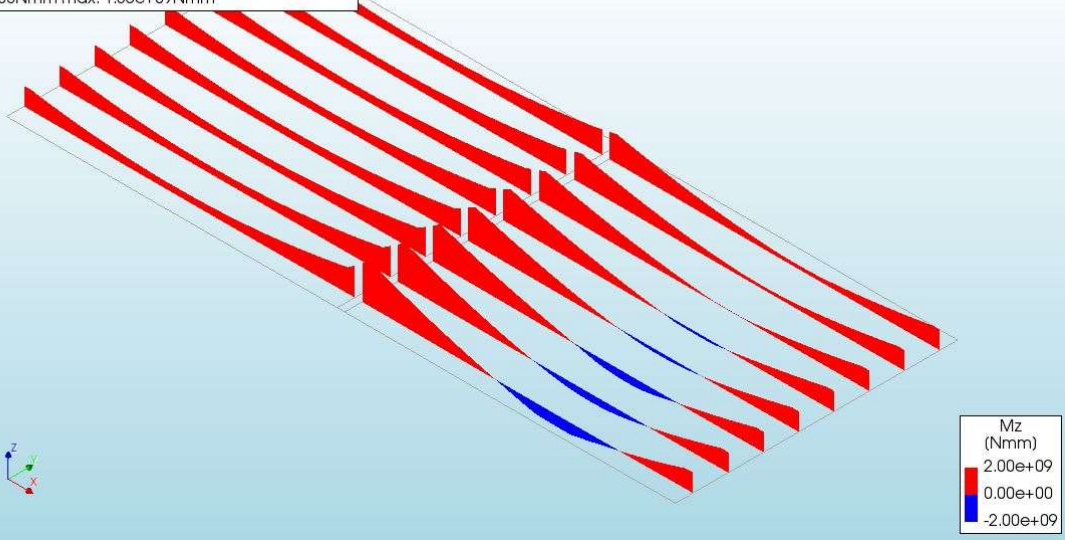
Non Lin Sta ULS (Till Failure)  
Set state - 04 - TL + Perm., Load-step 40, Load-factor 0.38000  
Cross-section Moments Mz  
min: -1.20e+08Nmm max: 1.10e+09Nmm



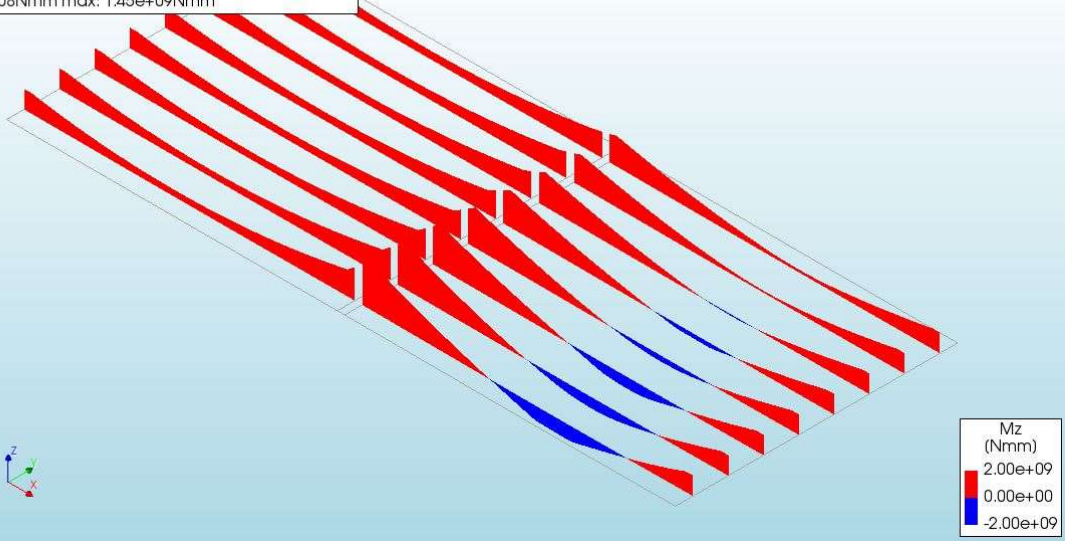
Non Lin Sta ULS (Till Failure)  
Set state - 04 - TL + Perm., Load-step 50, Load-factor 0.48000  
Cross-section Moments Mz  
min: -2.37e+08Nmm max: 1.23e+09Nmm



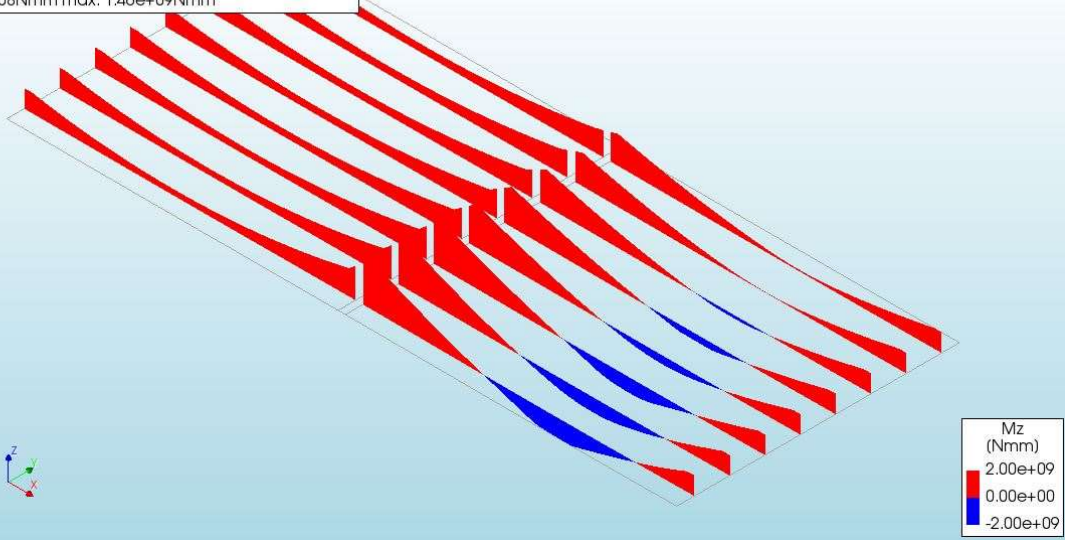
Non Lin Sta ULS (Till Failure)  
Set state - 04 - TL + Perm., Load-step 60, Load-factor 0.58000  
Cross-section Moments Mz  
min: -3.53e+08Nmm max: 1.35e+09Nmm



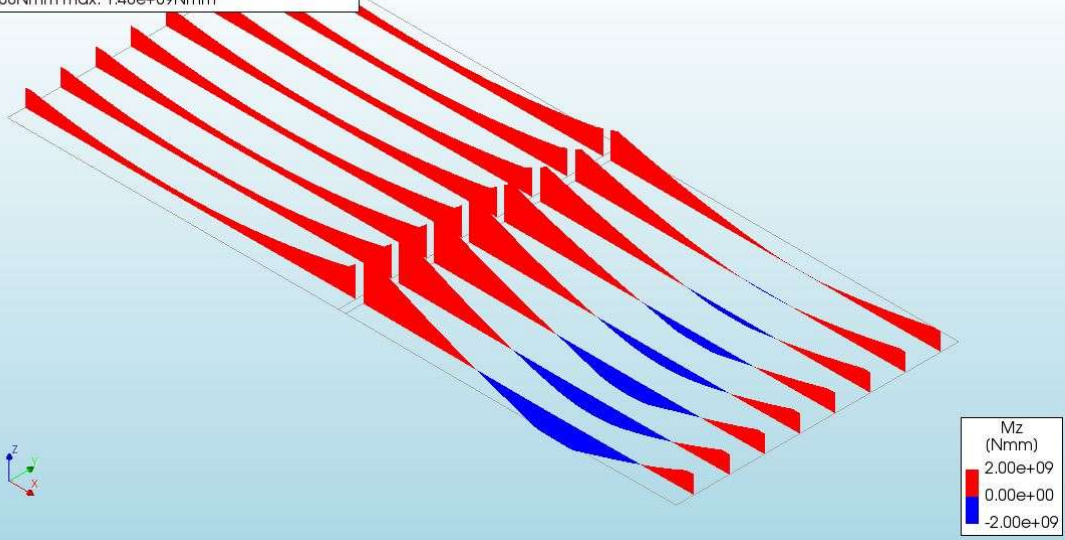
Non Lin Sta ULS (Till Failure)  
Set state - 04 - TL + Perm., Load-step 70, Load-factor 0.68000  
Cross-section Moments Mz  
min: -4.62e+08Nmm max: 1.45e+09Nmm



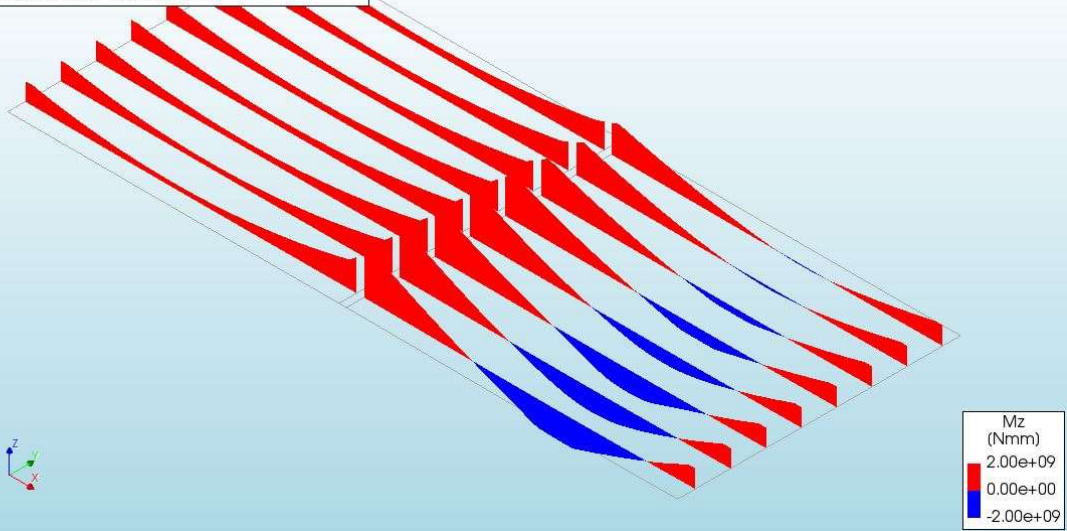
Non Lin Sta ULS (Till Failure)  
Set state - 04 - TL + Perm., Load-step 80, Load-factor 0.78000  
Cross-section Moments Mz  
min: -6.01e+08Nmm max: 1.46e+09Nmm



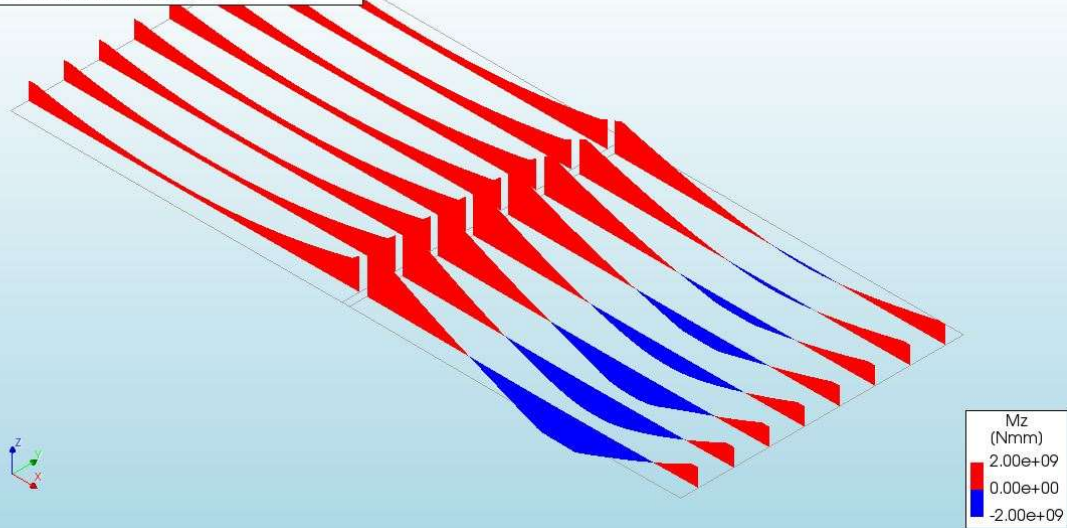
Non Lin Sta ULS (Till Failure)  
Set state - 04 - TL + Perm., Load-step 90, Load-factor 0.88000  
Cross-section Moments Mz  
min: -7.39e+08Nmm max: 1.48e+09Nmm



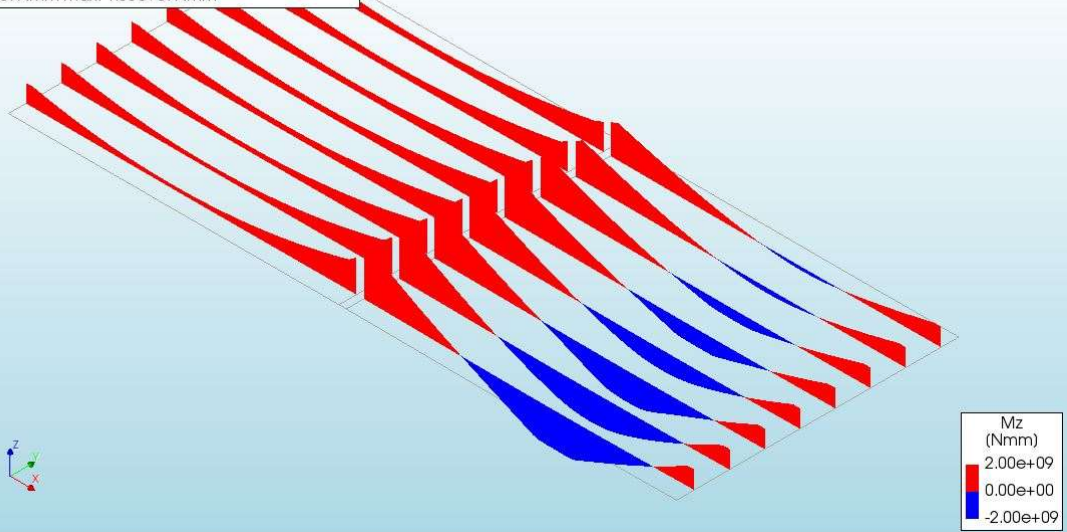
Non Lin Sta ULS (Till Failure)  
Set state - 04 - TL + Perm., Load-step 100, Load-factor 0.98000  
Cross-section Moments Mz  
min: -8.80e+08Nmm max: 1.50e+09Nmm



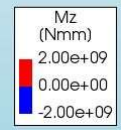
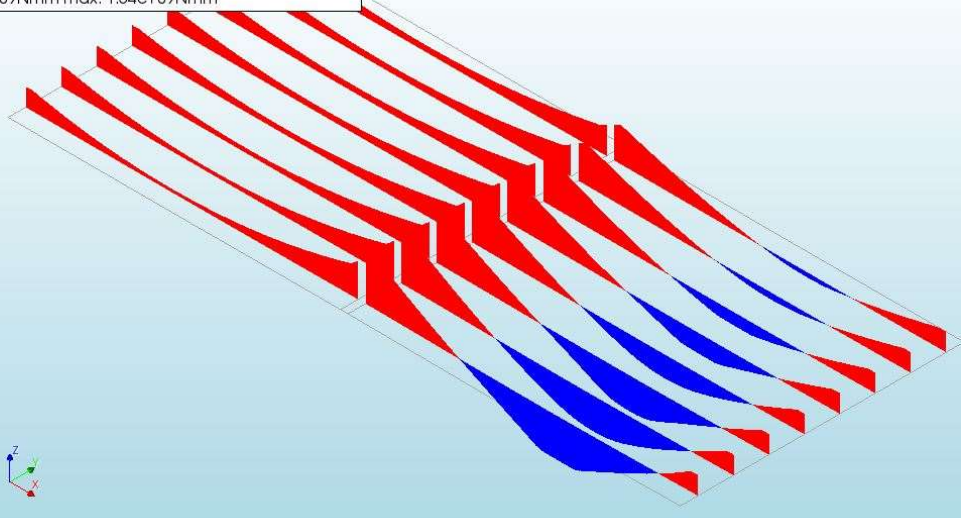
Non Lin Sta ULS (Till Failure)  
Set state - 04 - TL + Perm., Load-step 110, Load-factor 1.0800  
Cross-section Moments Mz  
min: -1.02e+09Nmm max: 1.51e+09Nmm



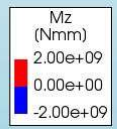
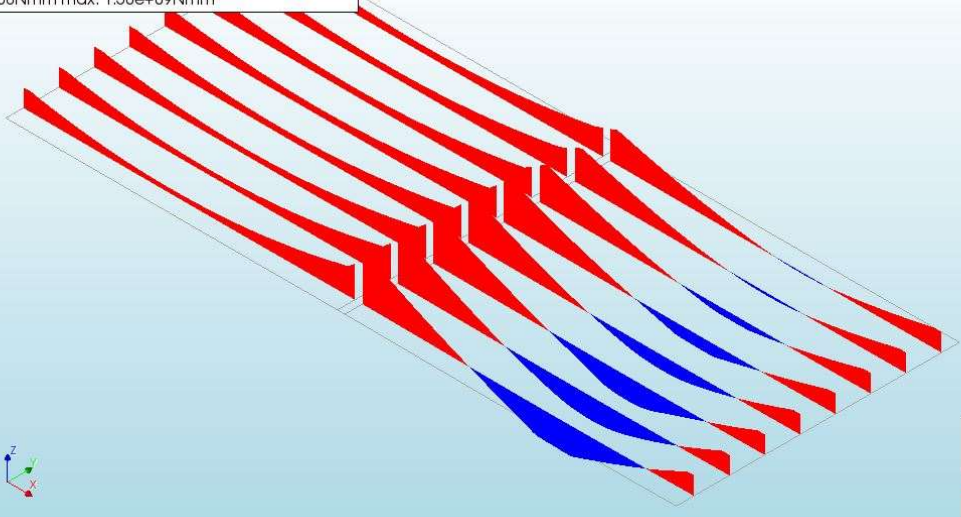
Non Lin Sta ULS (Till Failure)  
Set state - 04 - TL + Perm., Load-step 120, Load-factor 1.1800  
Cross-section Moments Mz  
min: -1.17e+09Nmm max: 1.53e+09Nmm



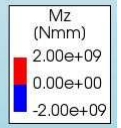
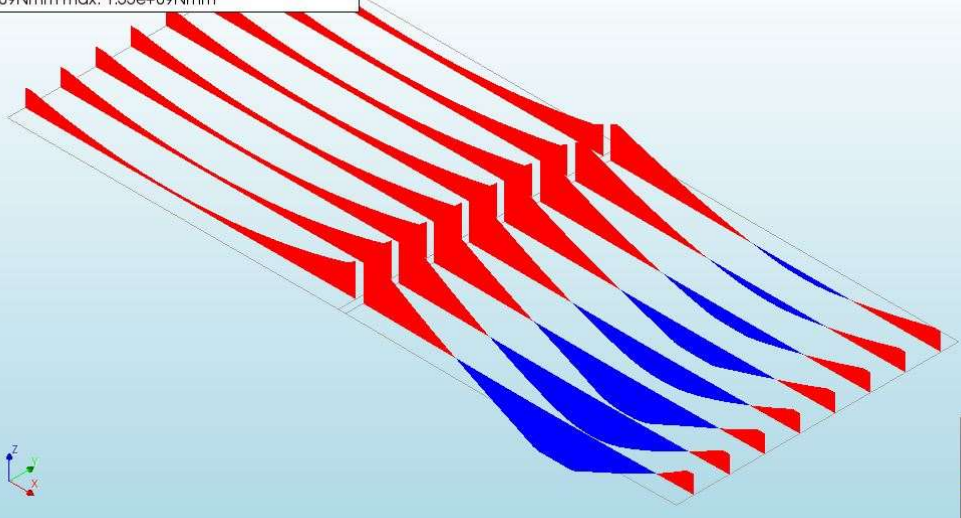
Non Lin Sta ULS (Till Failure)  
Set state - 04 - TL + Perm., Load-step 130, Load-factor 1.2800  
Cross-section Moments Mz  
min: -1.31e+09Nmm max: 1.54e+09Nmm



Non Lin Sta ULS (Till Failure)  
Set state - 04 - TL + Perm., Load-step 102, Load-factor 1.0000  
Cross-section Moments Mz  
min: -9.09e+08Nmm max: 1.50e+09Nmm



Non Lin Sta ULS (Till Failure)  
Set state - 04 - TL + Perm., Load-step 137, Load-factor 1.3500  
Cross-section Moments Mz  
min: -1.33e+09Nmm max: 1.55e+09Nmm



Appendix IVe

Curvature ( $\kappa_z$ ) development, Model 4

	SLL	SL	SLR	SRL	SR	SRR	FRM
1	0	0	0	0	0	0	0
2	-1	-1	-1	-1	-1	-1	-1
3	1	1	-1	1	1	-1	-1
4	1	1	-1	1	1	-1	-1
5	1	1	-1	1	1	0	-1
6	1	1	-1	1	1	1	-1
7	1	1	-1	1	1	1	-1
8	1	1	0	1	1	1	-1
9	1	1	0	1	1	1	-1
10	1	1	0	1	1	1	-1
11	1	1	0	1	1	1	-1
12	1	1	1	1	1	1	-1
13	1	1	1	1	1	1	-1
14	1	1	1	1	1	1	-1
15	1	1	1	1	1	1	-1
16	1	1	1	1	1	1	-1
17	1	1	1	1	1	1	-1
18	1	1	1	1	1	1	-1
19	1	1	1	1	1	1	-1
20	1	1	1	1	1	1	-1
21	1	1	1	1	1	1	-1
22	1	1	1	1	1	1	-1
23	1	1	1	1	1	1	-1
24	1	1	1	1	1	1	-1
25	1	1	1	1	1	1	-1
26	1	1	1	1	1	1	-1
27	1	1	1	1	1	1	-1
28	1	1	1	1	1	1	-1
29	1	1	1	1	1	1	-1
30	1	1	1	1	1	1	-1
31	1	1	1	1	1	1	-1
32	1	1	1	1	1	1	-1
33	1	1	1	1	1	1	-1
34	1	1	1	1	1	1	-1
35	1	1	1	1	1	1	-1
36	1	1	1	1	1	1	-1
37	1	1	1	1	1	1	-1
38	1	1	1	1	1	1	-1
39	1	1	1	1	1	1	-1
40	1	1	1	1	1	1	-1
41	1	1	1	1	1	1	-1
42	1	1	1	1	1	1	-1
43	1	1	1	1	1	1	-1
44	1	1	1	1	1	1	-1
45	1	1	1	1	1	1	-1
46	1	1	1	1	1	1	-1
47	1	1	1	1	1	1	-1
48	1	1	1	1	1	1	-1
49	1	1	1	1	1	1	-1
50	1	1	1	1	1	1	-1
51	1	1	1	1	1	1	-1
52	1	1	1	1	1	1	-1
53	1	1	1	1	1	1	-1
54	1	1	1	1	1	1	-1
55	1	1	1	1	1	1	-1
56	1	1	1	1	1	1	-1
57	1	1	1	1	1	1	-1
58	1	1	1	1	1	1	-1
59	1	1	1	1	1	1	-1
60	1	1	1	1	1	1	-1
61	1	1	1	1	1	1	-1
62	1	1	1	1	1	1	-1
63	1	1	1	1	1	1	-1

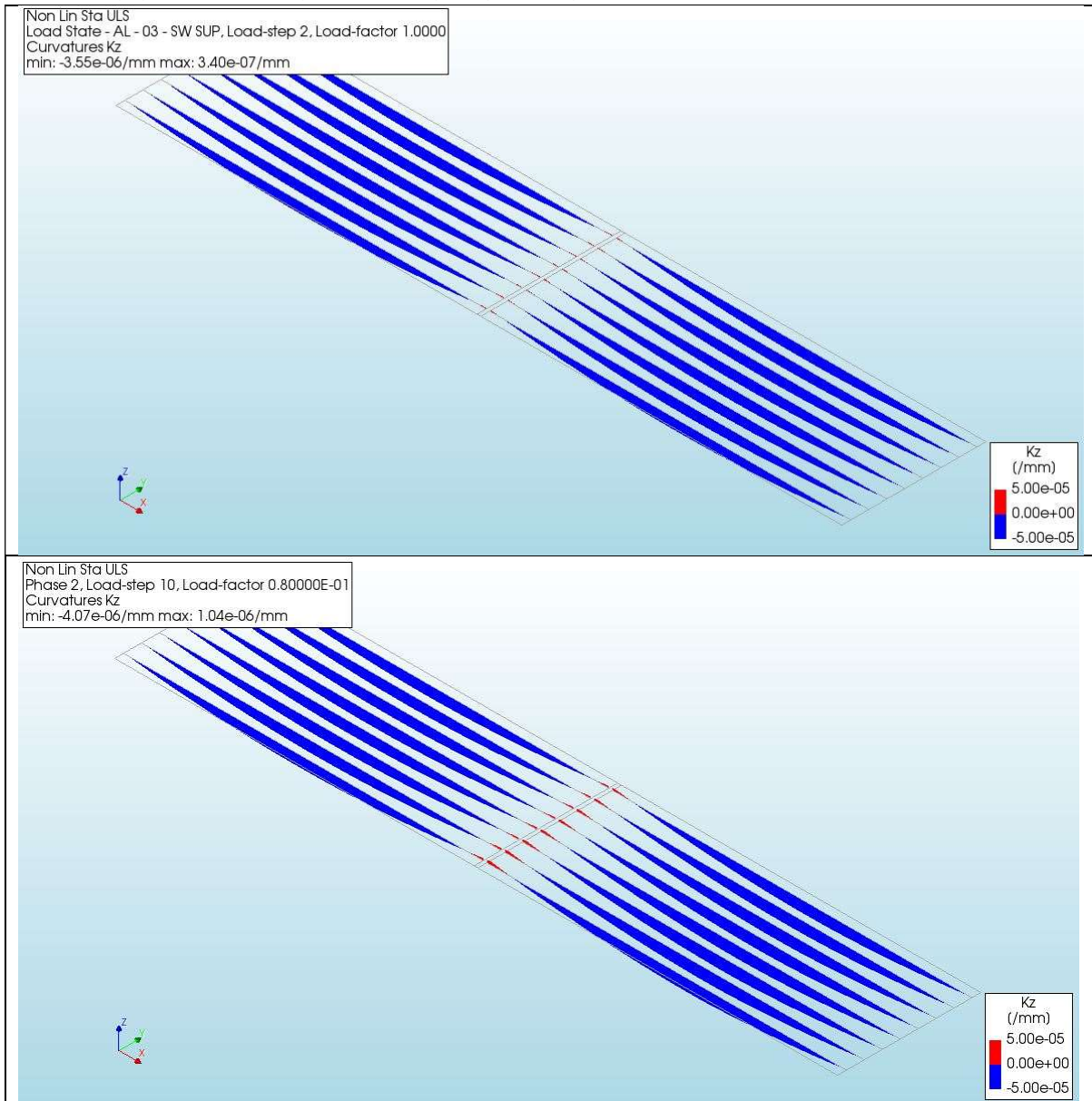
$K_{U-}$	-3,38E-05	-3
$K_{Y-}$	-5,49E-06	-2
$K_{Cr-}$	-1,00E-07	-1
$K_0$		0
$K_{Cr+}$	1,00E-07	1
$K_{Y+}$	2,32E-06	2
$K_{U+}$	4,54E-05	3

64	1	1	1	1	1	1	-1
65	1	1	1	1	1	1	-1
66	1	1	1	1	1	1	-1
67	1	1	1	1	2	1	-1
68	1	1	1	1	2	1	-1
69	1	1	1	1	2	1	-1
70	1	1	1	1	2	1	-1
71	1	1	1	1	2	1	-1
72	1	1	1	1	2	1	-1
73	1	1	1	1	2	1	-1
74	1	1	1	1	2	1	-1
75	1	1	1	1	2	1	-1
76	1	1	1	1	2	1	-1
77	1	1	1	1	2	1	-1
78	1	1	1	1	2	1	-1
79	1	1	1	1	2	1	-1
80	1	1	1	1	2	1	-1
81	1	1	1	1	2	1	-1
82	1	1	1	1	2	1	-1
83	1	1	1	1	2	1	-1
84	1	1	1	1	2	1	-1
85	1	1	1	1	2	1	-1
86	1	1	1	1	2	1	-1
87	1	1	1	1	2	1	-1
88	1	1	1	1	2	1	-1
89	1	1	1	1	2	1	-1
90	1	1	1	1	2	1	-1
91	1	1	1	1	2	1	-1
92	1	1	1	1	2	1	-1
93	1	1	1	1	2	1	-1
94	1	1	1	-1	2	1	-1
95	1	1	1	-1	2	1	-1
96	1	1	1	-1	2	-1	-1
97	1	1	1	-1	2	1	-1
98	1	1	1	-1	2	1	-1
99	1	1	1	-1	2	1	-1
100	1	1	1	-1	2	1	-1
101	1	1	1	-1	2	1	-1
102	1	1	1	-1	2	1	-1
103	1	1	1	-1	2	1	-1
104	1	1	1	-1	2	1	-1
105	1	1	1	-1	2	1	-1
106	1	1	1	-1	2	1	-1
107	1	1	1	-1	2	1	-1
108	1	1	1	-1	2	1	-1
109	1	1	1	-1	2	1	-1
110	1	1	1	-1	2	1	-1
111	1	1	1	-1	2	1	-1
112	1	1	1	-1	2	1	-1
113	1	1	1	-1	2	1	-1
114	1	1	1	-1	2	1	-1
115	1	1	1	-1	2	1	-1
116	1	1	1	-1	2	1	-1
117	1	1	1	-1	2	1	-1
118	1	1	1	-1	2	1	-1
119	1	1	1	-1	2	2	-1
120	1	1	1	-1	2	2	-1
121	1	1	1	-1	2	2	-1
122	1	1	1	-1	2	2	-1
123	1	1	1	-1	2	2	-1
124	1	1	1	-1	2	2	-1
125	1	1	1	-1	2	2	-1
126	1	1	1	-1	2	2	-1
127	1	1	1	-1	2	2	-1
128	1	1	1	-1	2	2	-1
129	1	1	1	-1	2	2	-1
130	1	1	1	-1	2	2	-1
131	1	1	1	-1	2	2	-1
132	1	1	1	-1	2	2	-1

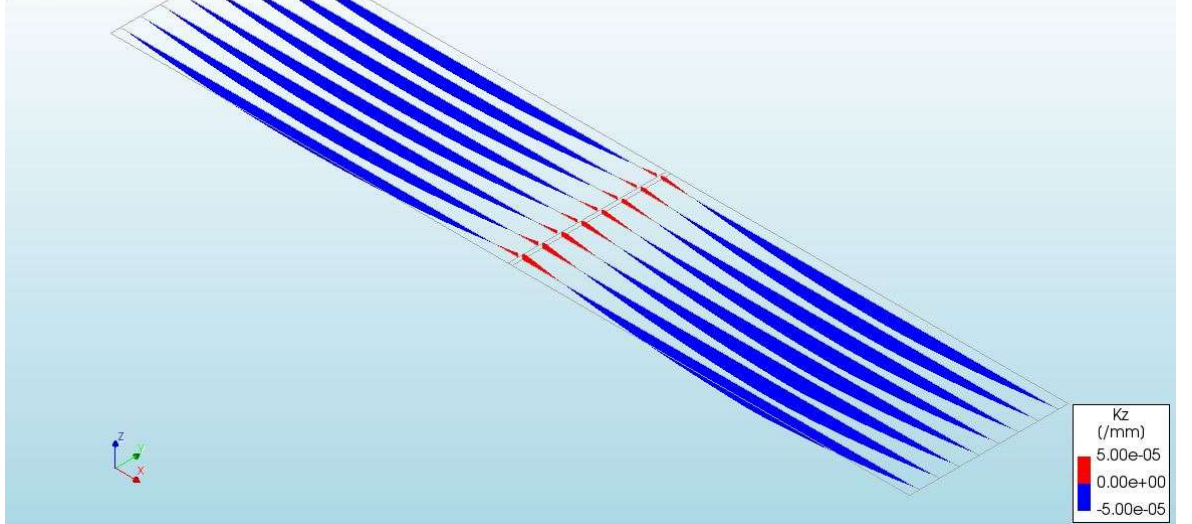
133	1	1	1	-1	2	2	-2
134	1	1	1	-1	2	2	-2
135	1	1	1	-1	2	2	-2
136	1	1	1	-1	2	2	-2
137	1	1	1	-1	2	2	-2
138	1	1	1	-1	2	2	-2
139	1	1	1	-1	2	2	-2

# Appendix IVf

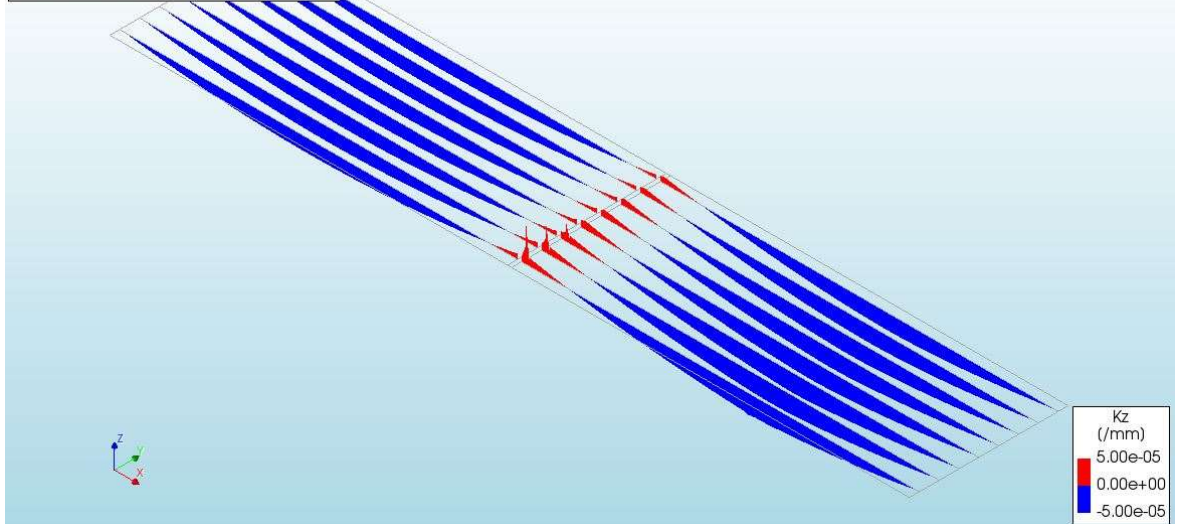
## Curvature ( $\kappa_z$ ) Model 5, every 10 load steps & final step



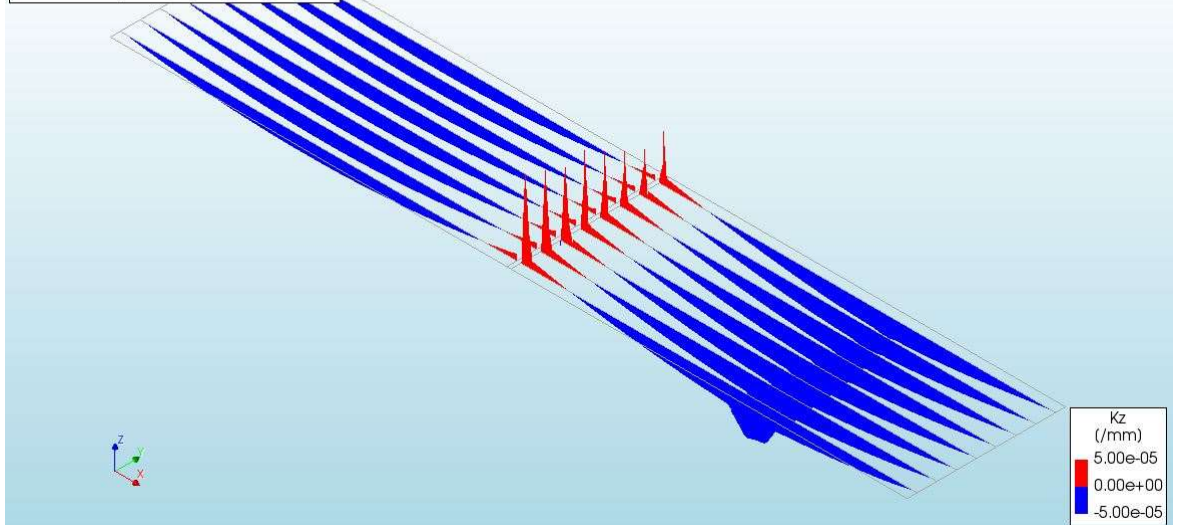
Non Lin Sta ULS  
Phase 2, Load-step 20, Load-factor 0.18000  
Curvatures Kz  
min: -4.79e-06/mm max: 1.92e-06/mm



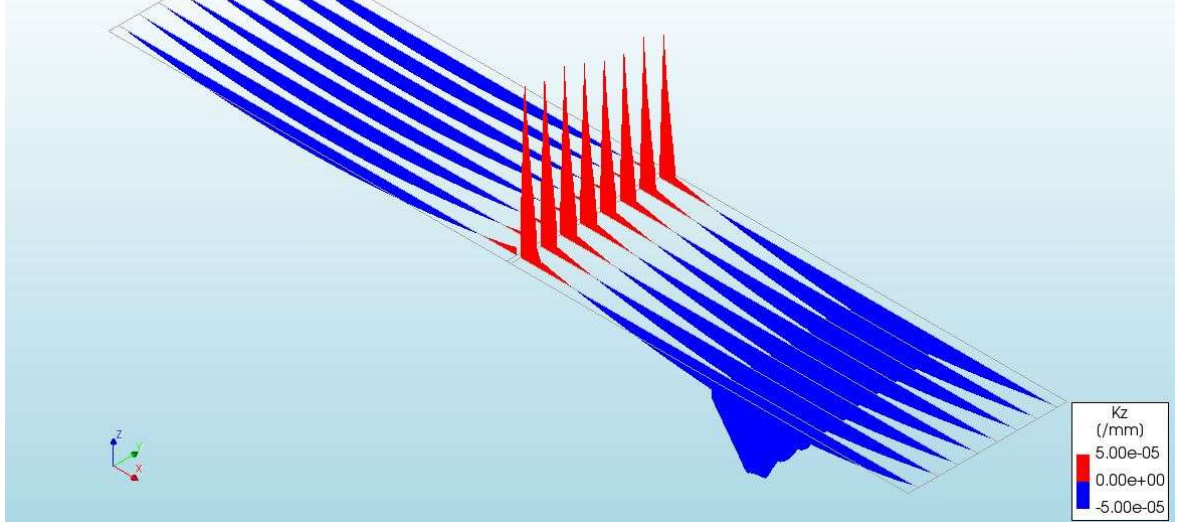
Non Lin Sta ULS  
Phase 2, Load-step 30, Load-factor 0.28000  
Curvatures Kz  
min: -5.91e-06/mm max: 1.14e-05/mm



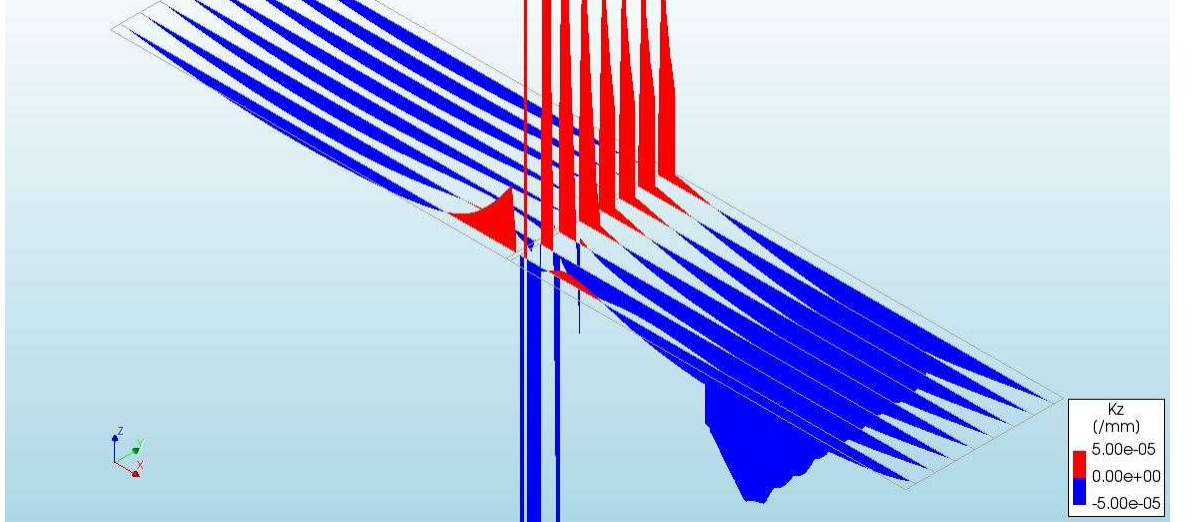
Non Lin Sta ULS  
Phase 2, Load-step 40, Load-factor 0.38000  
Curvatures Kz  
min: -1.17e-05/mm max: 2.63e-05/mm



Non Lin Sta ULS  
Phase 2, Load-step 50, Load-factor 0.48000  
Curvatures Kz  
min: -2.23e-05/mm max: 4.88e-05/mm

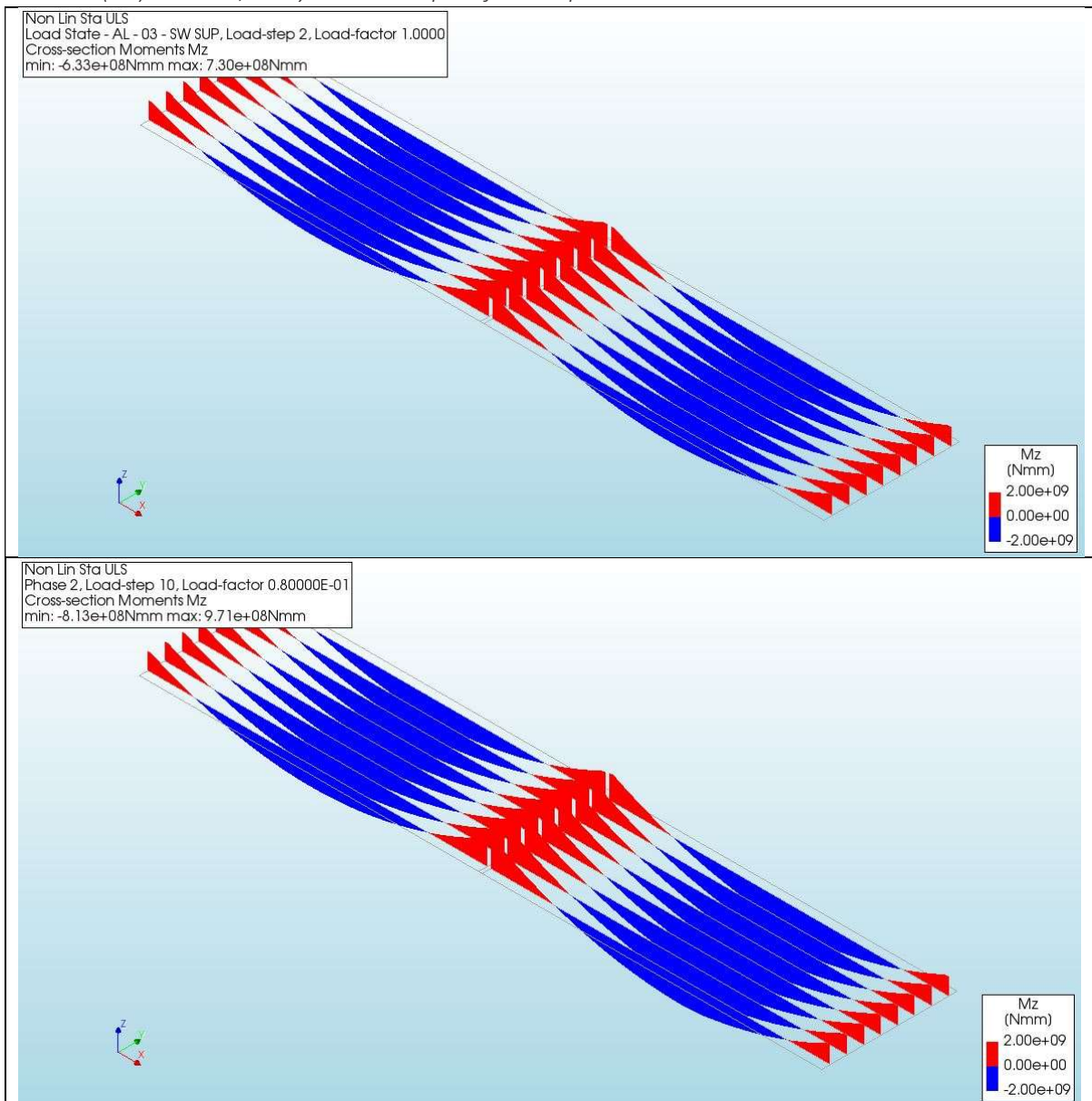


Non Lin Sta ULS  
Phase 2, Load-step 51, Load-factor 0.49000  
Curvatures Kz  
min: -4.03e-03/mm max: 8.71e-03/mm

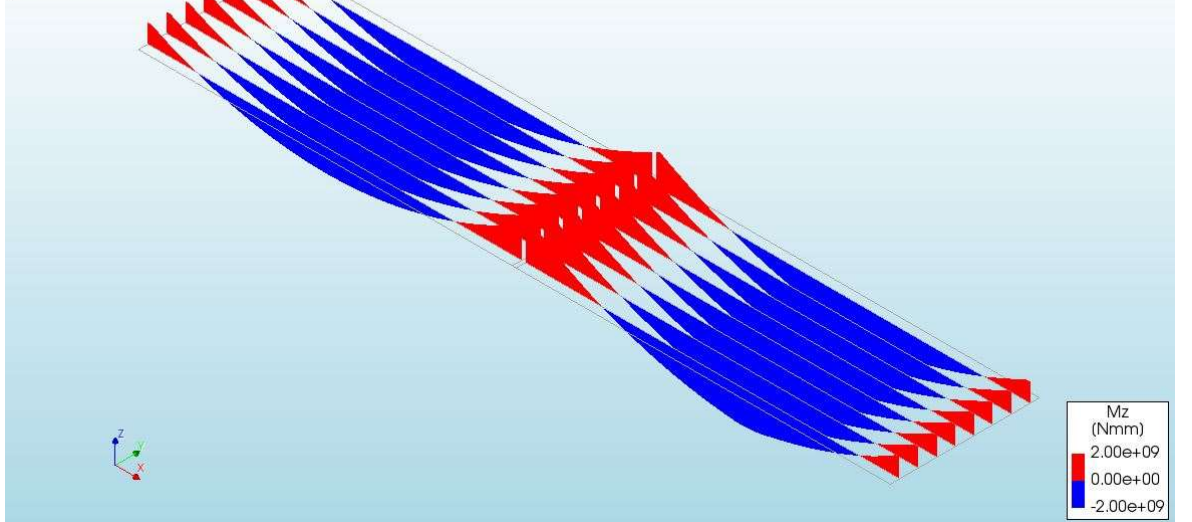


# Appendix IVg

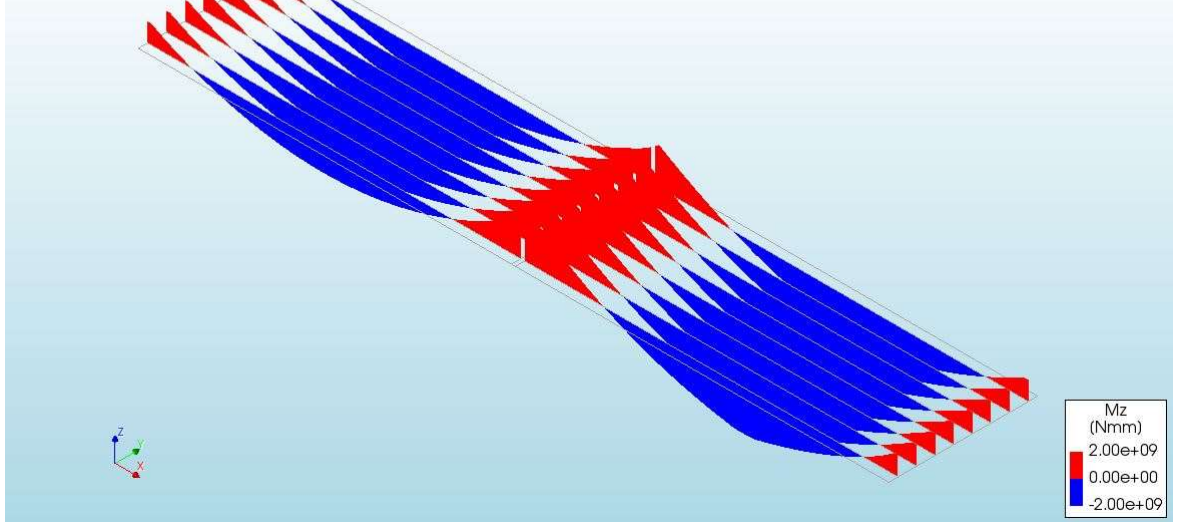
## Moment ( $M_z$ ) Model 5, every 10 load steps & final step



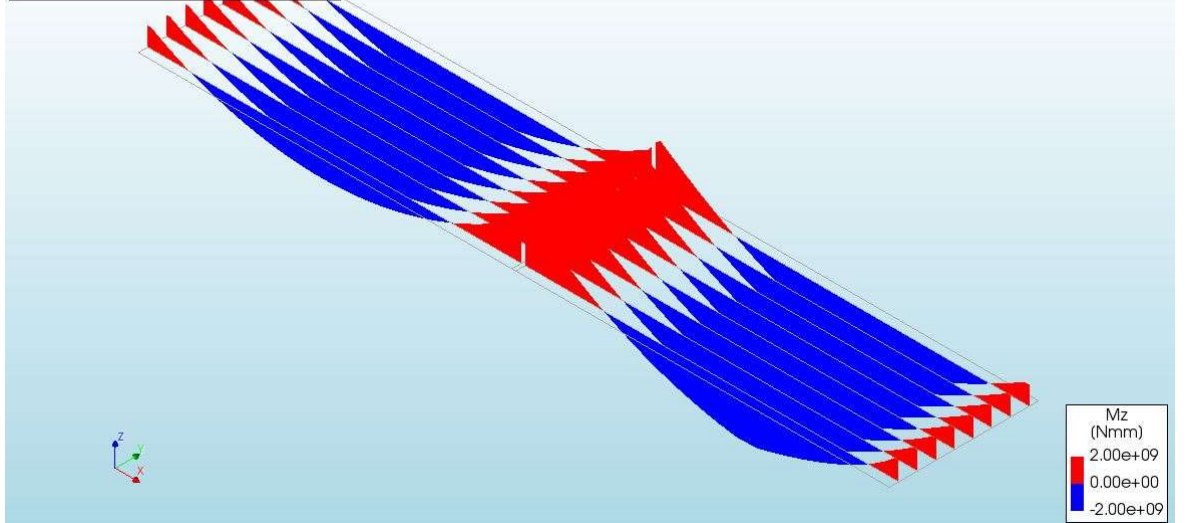
Non Lin Sta ULS  
Phase 2, Load-step 20, Load-factor 0.18000  
Cross-section Moments Mz  
min: -1.06e+09Nmm max: 1.27e+09Nmm



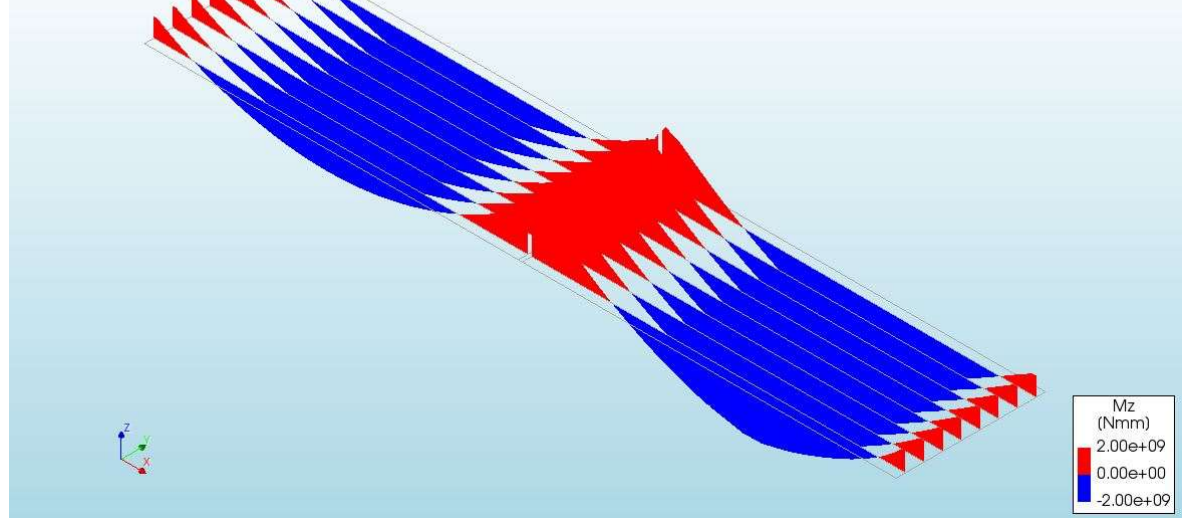
Non Lin Sta ULS  
Phase 2, Load-step 30, Load-factor 0.28000  
Cross-section Moments Mz  
min: -1.31e+09Nmm max: 1.45e+09Nmm



Non Lin Sta ULS  
Phase 2, Load-step 40, Load-factor 0.38000  
Cross-section Moments Mz  
min: -1.39e+09Nmm max: 1.52e+09Nmm



Non Lin Sta ULS  
Phase 2, Load-step 50, Load-factor 0.48000  
Cross-section Moments Mz  
min: -1.54e+09Nmm max: 1.63e+09Nmm



Non Lin Sta ULS  
Phase 2, Load-step 51, Load-factor 0.49000  
Cross-section Moments Mz  
min: -1.39e+14Nmm max: 6.54e+13Nmm

